2017

Renormalized energy momentum tensor from the Gradient Flow

Capponi, Francesco

**SUCCEED
WITH
PLYMOUTH
UNIVERSITY**

Renormalized energy momentum tensor from the Gradient Flow

by
Francesco Capponi

A thesis submitted to Plymouth University
in partial fulfilment for the degree of

DOCTOR OF PHILOSOPHY

Computing and Mathematics Doctoral Training Centre

Supervised by:

Dr. **Antonio Rago**
Dr. **Agostino Patella**

February, 2017

Copyright statement

This copy of the thesis has been supplied on condition that anyone who consults it is understood to recognise that its copyright rests with its author and that no quotation from the thesis and no information derived from it may be published without the author's prior consent.

Author's declaration

At no time during the registration for the degree of Doctor of Philosophy has the author been registered for any other University award without prior agreement of the Graduate Sub-Committee.
Work submitted for this research degree at the Plymouth University has not formed part of any other degree either at Plymouth University or at another establishment.
This study was financed with the aid of a studentship from Plymouth University.
Relevant scientific seminars and conferences were regularly attended at which work was often presented; papers have been prepared for publication.

Publications:

- Claudio Bonati, Francesco Capponi, Massimo D'Elia, Francesco Negro:
  on the Phase Diagram of Yang-Mills Theories in presence of a Θ parameter.
  http://inspirehep.net/record/1297674

- Francesco Capponi, Antonio Rago, Luigi Del Debbio, Susanne Ehret, Roberto Pellegrini:
  renormalisation of the energy-momentum tensor in scalar field theory using the Wilson flow.
  http://inspirehep.net/record/1408885

- Francesco Capponi, Luigi Del Debbio, Agostino Patella, Antonio Rago:
  renormalization constants of the lattice energy momentum tensor using the gradient flow.
  http://inspirehep.net/record/1409503

- Francesco Capponi, Luigi Del Debbio, Susanne Ehret, Roberto Pellegrini, Antonin Portelli, Antonio Rago:
  renormalisation of the scalar energy-momentum tensor with the Wilson flow.
  http://inspirehep.net/record/1505605

Presentation and Conferences Attended:

- LATTICE 2015: the 33rd International Symposium on Lattice Field Theory, held at the Kobe International Conference Center, Kobe, Japan.
  https://indico2.riken.jp/indico/sessionDisplay.py?sessionId=12&confId=1805#20150718

- LATTICE 2016: the 34rd International Symposium on Lattice Field Theory, held at Southampton university, Southampton, United Kingdom.
  https://conference.ippp.dur.ac.uk/event/470/session/16/contribution/68/author/0

Word count of main body of thesis: 57213

Signed:...

Date: ....
16/02/17

Acknowledgements

This work is the product of a titanic effort, lasted three long years. If I managed to bring this project to an end, it's just because of all the wonderful people that helped and supported me during my PhD.

The first thank goes, without any doubt, to my supervisors, Antonio Rago and Agostino Patella, for bearing with me all these 3 years. It must have been a hard task!!!
Thanks for sharing your time and your knowledge with me and for teaching me how to behave in this scientific world.

A sincere thank goes also to Roberto Pellegrini, for having faced and overcome with me the difficulties of a seemingly easy project, which turned out to be really hard and mentally draining.

I would like also to thank David Preti, for all the interesting discussions we had during these years. I whish you all the best.

There are not enough meaningful words to show my family the gratitude they deserve. Thank you for all the unconditioned support you gave me. As Leda said, you are the best *Ohana* I could ever had.

A special thank goes to Camilla, my partner. Thank you for being the wonderful girl you are, for always encouraging me, especially in the hard moments. Thank you for having been braver than me, leaving your family to follow me in this crazy adventure...you are the best!

Abstract

Renormalized energy momentum tensor from the Gradient Flow

by

Francesco Capponi.

Strongly coupled systems are elusive and not suitable to be described by conventional perturbative approaches. However, they are ubiquitous in nature, especially in particle physics.

The lattice formulation of quantum field theories provided a unique framework in which the physical content of these systems could be precisely determined. Combined with numerical techniques, the lattice formalism allowed to precisely determined physical quantities describing the thermodynamics, as well as the spectroscopy of strongly interacting theories.

In this work, the lattice formulation has been employed to probe the effectiveness of a recently proposed method, which aims at determining the renormalized energy-momentum tensor in non perturbative regimes. The latter plays a fundamental role to quantitatively describe the thermodynamics and fluid-dynamics of hot, dense systems, or to characterize theories that enlarge the actual standard model. In all these aspects, only a non perturbative approach provides physically reliable results: hence a non perturbative determination of the energy momentum tensor is fundamental.

The new method consists in defining suitable lattice Ward identities probed by observables built with the gradient flow. The new set of identities exhibits many interesting qualities, arising from the UV finiteness of such probes, and allows to define a numerical strategy for estimating the renormalization constants of the lattice energy-momentum tensor.

In this work the method has been tested within two different quantum theories, with the purpose of understanding its effectiveness and reliability.

Contents

List of Figures

List of Tables

Introduction

Quantum field theory (QFT) is recognised as the natural theoretical framework for describing the dynamics of fundamental particles and their interactions. Since its inception [1], it has been subjected to a continuous evolution process, characterized by several significant phases. Among these, one could recollect the formulation of Fermi theory of beta decay, the adoption of Feynman path integral formalism in perturbation theory, or, last but not less important, the establishment of the Standard Model.

Along this evolution path, one of the most important landmarks is surely represented by the emergence of the renormalization group (RG) apparatus. Its first appearance is dated back to the works of Stueckelberg and Petermann [2], Gell-Mann and Low [3], who studied the ambiguities in the regularization procedures of divergences that plague perturbative quantum field theory. They realized that, in renormalizable field theories, the ambiguities in the energy scale, introduced during the renormalization procedure, can be used to relate the behaviour of the theory at small and large energies. In this scenario, the parameters of the renormalized theory depend on the energy scale according to a set of identities called *renormalization group equations*, the most famous one being the well known β function [4, 5]. The RG machinery has been successfully applied to Quantum Chromodynamics (QCD): in this case, the integration of the QCD β function showed how the renormalized coupling tends to zero at short distances (asymptotic freedom [6]), while it increases at the large ones. This theoretical result allowed to explain the famous scaling phenomenon that Bjorken observed in deep inelastic experiments, as well as making plausible the idea that the quarks would be confined inside hadrons. At the same time, it also limited the applicability of perturbative methods to the high energy regime, pointing out that new strategies had to be employed to probe low energy properties of the theory from first principles.

Initially confined to renormalizable field theories [2, 3, 4, 5], the RG was then reformulated by Wilson [7, 8, 9, 10], opening the way for applications also in condensed matter and statistical mechanics. The Wilsonian RG was based on the concept of a scale-dependent effective action, obtained by integrating out degrees of freedom at energies above a given cut-off Λ. In this setting, as long as the theory is studied at energies well below Λ, the correctly normalized correlation functions should be independent on its value. From this assumption, one can derive a set of RG equations describing how the effective couplings vary with the cut-off in order to leave the physics of the system unchanged. The behaviour of the theory at small and large scales is totally determined by analyzing the possibly existing RG fixed points and the cut-off value at which they occur. Since the all apparatus can be constructed without making any strong assumption on the structure of the theory (such as renormalizability), it has a more general use than its original version. Through the concepts of *universality* and *universality class*, it has allowed to understand why different high energy theories flow to look the same in the infrared (IR) regime, showing how it is possible to study a physical problem, at a given scale, without worrying about what the degrees of freedom at much higher energies are doing. This result had important consequences in the study and characterization of critical phenomena in statistical physics. Similarly, the same concepts have been the premise for

the definition of a continuum limit in quantum field theory, a fundamental prerequisite for proving the existence of continuum, renormalized interacting theories.

Along with the Wilsonian RG, another important step has been its effective representation within the framework of lattice field theory [11]. The lattice regulator enabled to efficiently apply Wilson's idea of RG, and became an essential device for studying quantum theories non perturbatively. For example, it has allowed to consistently verify the triviality of the $O(n)$ models with quartic interaction in four dimensions [12, 13, 14], leaving little doubt that the current Standard Model can only be interpreted as an effective theory bounded by a cut-off. On the other hand, lattice QCD has made possible to tackle several problems characterizing hadron phenomenology, like quark confinement, spontaneous chiral symmetry breaking, hadrons spectroscopy, running of couplings and thermodynamics. All these theoretical issues characterize the low energy regime of the theory, where quantitative results, based on perturbation theory, are not reliable: the lattice regularization, combined with the application of numerical methods, allowed to quantitatively investigate them, bringing new insights about the world of strongly interacting particles. Nowadays, the lattice formalism is widely recognized as an essential tool for investigating non perturbative properties of quantum field theories.

In this work, the lattice regularization has been the technical framework for studying a well known, hot topic of quantum field theory: the renormalization of composite operators. The main goal of this procedure is to render Green's functions containing the insertion of some local operators, which are not in the action, finite as the cut-off is removed. These operator insertions are usually related to order parameters, like the chiral condensate, or physical observables, like the energy density: their renormalization then plays a crucial role for quantitatively describing the physical properties of a system.

Usually, the whole procedure can be performed writing the renormalized operator as a sum over local terms, with mass dimension less or equal than the original operator. With respect the latter, each of these terms has to share the same symmetry properties. In the sum, each operator is multiplied by a possibly divergent coefficient, called renormalization constant [15]. The renormalization constants encode the divergences that have to be subtracted to make insertions of the renormalized operator finite, and are determined using some specific local conditions (e.g. Ward identities). In perturbation theory, the all method can be carried out using analytic calculations, giving the renormalization constants as a power expansion in the couplings of the theory, up to a given order. Non perturbatively, the same procedure can be implemented only imposing a renormalization condition for the original operator, and then solving it with numerical methods: in this case, the lattice formulation represents the perfect candidate for the execution of this task.

Here, all the interest has been focused on the non-perturbative renormalization of the energy momentum tensor. It is important to determine the renormalized form of such operator in many aspects of quantum field theory. In thermodynamics, it is needed to correctly measure the energy, pressure and entropy density of a system at thermal equilibrium, or the shear viscosity of a fluid medium. It can also be used as an order parameter for probing fundamental properties of a theory, like translational and conformal invariance, the latter being particularly relevant when beyond Standard Model (BSM) theories are under investigation.

The energy momentum tensor is related to the Noether current of translational symmetry: in quantum field theory, the invariance of a physical system under this symmetry results in a collection of Ward identities that can be used to define the corresponding renormalized operator [16, 17, 18]. In the continuum formulation, Poincaré invariance and, if any, other internal symmetries, play an important role in limiting the number of possible operators that come into play during the renormalization process. However, when a lattice regulator is adopted, Poincaré invariance is broken and its restoration is only guaranteed in the continuum limit. For this reason, at finite lattice spacing, the correctly renormalized energy momentum tensor is obtained as a mixing of all

operators allowed by the lattice symmetries [19, 20], i.e. those of the hypercubic group. This is not an insignificant detail, since the lost of Poincaré symmetry could cause an impressive growth in the number of operators to be added, and this would make definitely more difficult the all renormalization procedure, as well as affect its outcome. The assumption that Poincaré invariance is recovered in the continuum implies that it is possible to tune the renormalization constants in such a way that translation Ward identities are satisfied up to terms that vanish when the lattice spacing goes to zero. Unfortunately, the main problem of all this approach is that local Ward identities are plagued by additional divergences (contact terms) which make the numerical extraction of the coefficients incredibly challenging.

A possible strategy to overtake this obstacle can be the definition of a new kind of observables, whose employment for probing the Ward identities does not give rise to contact terms, and then allows to get a better signal from numerical simulations. The fulfilment of such a strategy is possible thanks to a particular, exact-smearing procedure, firstly introduced in the framework of strongly interacting theories [21, 22, 23, 24], and then extended to other interesting cases [25, 26]: the gradient flow. Starting from an initial field configuration, the gradient flow evolves the field as a function of a parameter $t \geq 0$ that is referred to as the flow time. The nature of the evolution is governed by the gradient of a "flow action", whose form depends on the theory under study. The outstanding property of this evolution procedure is to render the renormalization of correlation functions, built with flowed fields, really simple, if not totally absent. During the last year, the nice features of the gradient flow have been employed in many different fields, like the study of running couplings [21, 27, 28, 29, 30], thermodynamics [31, 32, 33], and the emergence of topological sectors in gauge theories [21, 22]. For what concerns the renormalization of the energy momentum tensor, the smoothing properties of the flow can be used to formulate a set of (local) translation Ward identities that are probed by observables built along the flow, following the methodology proposed in [34]. The new set of identities is characterized by the total absence of contact terms, and then represents an appealing solution to the numerical issues encountered in the past. The purpose of this research work is to test the efficiency of this new method, applying it to different physical models, and reporting the numerical results.

It should be said that, in addition to the above mentioned method, other two alternative strategies have been proposed.

The first one is based on an interesting property that characterizes composite operators built along the flow: the so-called *small flow time expansion*. It has been shown [23] that, for sufficiently small flow times, operators composed with flowed fields allow an expansion in terms of renormalized operators, at zero flow time, coupled with coefficients that encode the remnant flow dependence. Once the value of this *small flow time coefficients* is known, it is possible to setup a set of identities from which the numerical value of a given renormalized operator can be extracted. The small flow time coefficients can be determined analytically in the perturbative regime. However, the method has been applied very far from this regime, to study the thermodynamic of pure $SU(3)$ gauge theory, close to the scale of the critical temperature[31, 32, 35, 36].

The second strategy is totally orthogonal to the previous ones and employs a different paradigm to renormalize the energy momentum tensor. In this case, the lattice theory is formulated on a finite box, with shifted boundary conditions along the temporal direction, the value of the shift given by a free parameter ξ. Requiring that rotational invariance is restored in the thermodynamic limit, it is possible to derive a set of thermal Ward identities, parametrized with ξ, from which the renormalization constants of the energy momentum tensor can be extracted [37, 38]. The advantage of this strategy relies in the possibility to determine the renormalization constants using one-point correlators, which usually can be numerically well measured. The method has been successfully applied for measuring thermodynamic quantities in $SU(3)$ pure gauge theory.

This work is structured as follows.

In the first chapter, the Wilsonian RG is presented in a quite generic manner. Then, it is effectively integrated within the lattice formulation of a simple scalar ϕ^4 theory, with the aim of focusing on all the fundamental details of the lattice regularization.

The second chapter is centred on the definition of the energy momentum tensor in the classical theory, and the renormalization of its continuum, quantum counterpart. Then, the lattice formulation is considered, as well as the additional difficulties that arise during the renormalization procedure.

The third and fourth chapter constitute the core of this research work, and study the renormalization procedure for two different models

- A $SU(3)$ Yang-Mills theory in four dimensions. This represents a first test bench for physically interesting, strongly interacting theories, with the idea of including matter fields in the future.

- A scalar $\lambda\phi^4$ theory in three dimensions, a good playground for testing both the method and its possible applications in BSM theories. In this case, the existence of an infrared fixed point (also known as the Wilson-Fisher fixed point), would allow to probe dilatation invariance using the renormalized energy momentum tensor.

In these chapters, the gradient flow, its properties, and applications in the definition of the new Ward Identities is explained in detail. The method for measuring the renormalization constants is explained and numerical results are reported and discussed.

In the last chapter all the interesting results of the project are resumed, and conclusions, along with possible future applications, formulated.

Chapter 1

Wilsonian RG and lattice field theory

1.1 Introduction

This chapter is dedicated to the lattice regularization of quantum field theory and its interpretation in terms of Wilson's idea of RG. In the first section, the Wilsonian RG is presented for a generic quantum field theory, with the purpose of underlining its main features. The concepts of RG flows, critical points, and universality, as well as their importance in the definition of a continuum limit, are explained. Here, the exposition closely follows the approach of [39]. The second section aims at including Wilson's ideas within the lattice formulation of quantum field theory. Firstly, the basic notions and formalism are introduced, then a simple lattice $\lambda\phi^4$ theory is considered, and its phase structure explained. In the third section, the perturbative analysis of the theory is carried out, and then the lattice renormalization group equations are written: here an effective application of the perturbative Wilsonian RG is shown.

1.2 Wilsonian RG

1.2.1 Effective action

The starting point for the formulation of the Wilsonian RG consists in defining a euclidean QFT, governed by the action

$$S_{\Lambda_0}[\varphi] = \int d^d x \left[\frac{1}{2} \partial_\mu \varphi \partial_\mu \varphi + \sum_i \Lambda_0^{d-d_i} g_{i0} \mathcal{O}_i(x) \right]. \tag{1.1}$$

Here, local operators $\mathcal{O}_i(x)$ have all dimension $d_i > 0$, and can be $SO(d)$ invariant monomials involving n_i powers of the fundamental field and their derivatives

$$\mathcal{O}_i(x) \sim (\partial\varphi)^{r_i} \varphi^{s_i} \quad r_i + s_i = n_i. \tag{1.2}$$

Explicit factors of some energy scale Λ_0 are included in (1.1) to make the coupling constants g_{i0} dimensionless, for later convenience.

After having summed over all the possible terms allowed by the symmetry of the system, the obtained action is totally general: it can be used to define a regularized path integral

$$\mathcal{Z}_{\Lambda_0}(g_{i0}) = \int_{C^\infty(M)_{\leq \Lambda_0}} \mathcal{D}\varphi e^{-S_{\Lambda_0}[\varphi]}, \tag{1.3}$$

where the integral is taken over the space $C^\infty(M)_{\leq \Lambda_0}$ of smooth functions on M whose energy is at most Λ_0. The integral in equation (1.3) makes sense, since it describes a regularized theory, with a momentum cut-off given by Λ_0 [1].

The integral can be performed in different ways: for example, one could first integrate out modes with energy between Λ_0 and $\Lambda < \Lambda_0$. The space $C^\infty(M)_{\leq \Lambda_0}$ is naturally a vector space with addition just being point-wise addition on M. Hence, a general field $\varphi(x)$ can be split as

$$\varphi(x) = \int_{|p| \leq \Lambda_0} \frac{d^d p}{(2\pi)^d} e^{ipx} \tilde{\phi}(p) \tag{1.4}$$

$$= \int_{|p| \leq \Lambda} \frac{d^d p}{(2\pi)^d} e^{ipx} \tilde{\phi}(p) + \int_{\Lambda < |p| \leq \Lambda_0} \frac{d^d p}{(2\pi)^d} e^{ipx} \tilde{\phi}(p) \tag{1.5}$$

$$=: \phi(x) + \xi(x), \tag{1.6}$$

with $\phi \in C^\infty(M)_{\leq \Lambda}$ and $\xi \in C^\infty(M)_{(\Lambda, \Lambda_0]}$ being the corresponding low and high-energy part of the field φ. The path integral measure on $C^\infty(M)_{\leq \Lambda_0}$ likewise factorizes as

$$\mathcal{D}\varphi = \mathcal{D}\phi \mathcal{D}\xi. \tag{1.7}$$

Performing the integral over the ξ modes provides an *effective action* at scale Λ

$$S_\Lambda^{\text{eff}}[\phi] := -\log \left[\int_{C^\infty(M)_{(\Lambda, \Lambda_0]}} \mathcal{D}\xi \exp(-S_{\Lambda_0}[\phi + \xi]) \right], \tag{1.8}$$

that actually depends only on the low energy modes. This process of integrating out modes is called *changing the cut-off* of the theory, and it can be iterated, providing a new effective action, defined at a scale Λ'

$$S_{\Lambda'}^{\text{eff}}[\phi] := -\log \left[\int_{C^\infty(M)_{(\Lambda', \Lambda]}} \mathcal{D}\xi \exp(-S_\Lambda[\phi + \xi]) \right], \tag{1.9}$$

whit $\Lambda' < \Lambda$. Equation (1.8) is known as the *renormalization group (RG) equation* for the effective action: its successive iterations describe how the effective action used to describe the regularized theory changes as the cut-off is lowered.

1.2.2 Running couplings and βunctions

The original path integral, $\mathcal{Z}_{\Lambda_0}(g_{i0}; \Lambda_0)$, is the same as the one rewritten in terms of the effective action (1.8)

$$\mathcal{Z}_\Lambda(g_i(\Lambda)) = \int_{C^\infty(M)_{\leq \Lambda}} \mathcal{D}\varphi e^{-S_\Lambda^{\text{eff}}}, \tag{1.10}$$

the difference among the two being just how the integration over the entire range of momenta up to Λ_0 is performed. For this reason, the following identity holds

$$\mathcal{Z}_\Lambda(g_i(\Lambda)) = \mathcal{Z}_{\Lambda_0}(g_{i0}; \Lambda_0). \tag{1.11}$$

---

[1] All the difficulties in defining a QFT reside in the definition of the path integral measure $\mathcal{D}\varphi$. Since a classical field has an infinite number of degrees of freedom, it is a non trivial issue to integrate over such an infinity. In perturbation theory, this difficulty is mirrored by the high momenta divergences that occur in loop integrals. Regularization procedures, like sharp momentum cut-off or lattice discretization, provide a method to well define the integration measure, and make radiative corrections finite.

Beside this issue, on a non-compact space-time manifold M, IR divergences could occur. This is a separated issue, not related with renormalization. It can be avoided if the theory is considered in a large box of side L, with periodic or reflecting boundary conditions on fundamental degrees of freedom. In this case, momentum gets quantized in units of $2\pi/L$, and the space $C^\infty(M)_{\leq \Lambda_0}$ is finite dimensional.

Allowing the scale to be lowered infinitesimally, the following differential equation is obtained

$$\Lambda \frac{d\mathcal{Z}_\Lambda(g)}{d\Lambda} = \left(\Lambda \frac{\partial}{\partial \Lambda} + \Lambda \left. \frac{\partial g_i(\Lambda)}{\partial \Lambda} \frac{\partial}{\partial g_i} \right|_\Lambda \right) \mathcal{Z}_\Lambda(g) = 0, \tag{1.12}$$

where repeated indices obey Einstein's summation rule. Equation (1.12) is known as the RG equation for the path integral, and is an example of *Callan-Symanzik equation* [4, 5]. It says that, by integrating out modes, the couplings of the effective action S_Λ^{eff} vary to account for the change in the degrees of freedom over which the path integral is taken. In this way, the path integral is independent on the scale at which the theory is defined, provided such a scale is below the original cut-off Λ_0.

Starting from a generic initial action, the effective action will also take the general form

$$S_\Lambda^{\mathrm{eff}} = \int d^d x \left[\frac{Z_\Lambda}{2} \partial_\mu \phi \partial_\mu \phi + \sum_i \Lambda^{d-d_i} Z_\Lambda^{n_i/2} g_i(\Lambda) \mathcal{O}_i(x) \right], \tag{1.13}$$

where the *wave function renormalization factor* Z_Λ takes into account quantum corrections to the kinetic term coefficient, arising from integrating out modes. At any given scale, it is always possible to define a *renormalized field*

$$\varphi := Z_\Lambda^{1/2} \phi, \tag{1.14}$$

in terms of which the kinetic contribution is canonically normalized (powers of Z_Λ have been also included in the definition of the other couplings. In this way, when the action is rewritten in terms of renormalized fields, this renormalization factor cancels out.).

The running of the couplings is clearly an important feature of the theory, and is given a particular name through the definition of the so-called β *function* [4, 5]

$$\beta_i = \Lambda \frac{\partial g_i}{\partial \Lambda}, \tag{1.15}$$

which is the derivative of the couplings g_i with respect the logarithm of the scale. For dimensionless couplings, it takes the form

$$\beta_i(g_j(\Lambda)) = (d_i - d)g_i(\Lambda) + \beta_i^{\mathrm{quant}}(g_j), \tag{1.16}$$

where the first term compensates the variation of the explicit power of Λ in front of the coupling in (1.13). The second term in equation (1.16) represents the quantum effects arising from integrating out high-energy modes. To actually compute this contribution requires to perform the path integral. This will generally introduce dependence on all the other couplings that appear in the original action (1.1), so that the β function for g_i is a function of all the couplings $\beta_i(g_j(\Lambda))$.

Likewise, even if at any given scale it is possible to remove the wave function renormalization factor, moving to a lower scale will usually cause it to re-emerge. Then one can define a sort of β function for Z_Λ as

$$\gamma_\phi := -\frac{1}{2} \Lambda \frac{\partial \ln Z_\Lambda}{\partial \Lambda}, \tag{1.17}$$

which is called the *anomalous dimension* of the field ϕ. Besides the difference of definition with respect (1.15), γ_ϕ really expresses the variation of the "kinetic term coupling" with the energy scale. The reason for such a name comes from the behaviour of correlation functions under scale transformations and will be more clear in the next section. If the theory contains more than one type of field, then there are a wave function renormalization and a corresponding anomalous dimension for each field [2]

---

[2]More generally, one would have a matrix of wave function renormalization factors, allowing different fields (with same symmetry properties) to mix their identities as modes get integrated out.

1.2.3 Anomalous dimension

The wave function renormalization plays an important role in the definitions of correlation functions. Suppose to compute the n-point correlator

$$\langle\phi(x_1)...\phi(x_n)\rangle := \frac{1}{\mathcal{Z}} \int_{C^\infty(M)_{\leq\Lambda}} \mathcal{D}\phi e^{-S_\Lambda^{\text{eff}}[Z_\Lambda^{1/2}\phi;g_i(\Lambda_0)]}\phi(x_1)...\phi(x_n) \tag{1.18}$$

using the scale Λ theory, with field insertions at points $\phi(x_1)...\phi(x_n)$, without having canonically normalized the field in the effective action. In terms of the renormalized field (1.14), the following identity holds

$$\langle\phi(x_1)...\phi(x_n)\rangle = Z_\Lambda^{-n/2}\langle\varphi(x_1)...\varphi(x_n)\rangle, \tag{1.19}$$

and, performing the path integral over φ[3], one evaluates the r.h.s. correlator as some function $\Gamma_\Lambda^{(n)}(x_1,...,x_n;g_i(\Lambda))$ that depends on the scale Λ, the couplings and the fixed points x_i. In principle, the field in coordinate space always involves all modes. However, when large distances with respect to Λ^{-1} are considered, it is reasonable to assume that only low-modes contribute. Then it should be possible to compute the same correlator using just a lower scale theory: the operator insertions will be unaffected as one integrates out modes in a range $(\Lambda/s, \Lambda]$ for some factor $s > 1$. Taking into account the wave function renormalization, one obtains

$$Z_{\Lambda/s}^{-n/2}\Gamma_{\Lambda/s}^{(n)}(x_1,...,x_n;g_i(\Lambda/s)) = Z_\Lambda^{-n/2}\Gamma_\Lambda^{(n)}(x_1,...,x_n;g_i(\Lambda)). \tag{1.20}$$

For infinitesimal lowering $(s = 1 + \delta s, \quad \delta s \ll 1)$, one finds

$$\Lambda\frac{d}{d\Lambda}\Gamma_\Lambda^{(n)}(x_1,...,x_n;g_i(\Lambda)) = \left(\Lambda\frac{\partial}{\partial\Lambda} + \beta_i\frac{\partial}{\partial g_i} + n\gamma_\phi\right)\Gamma_\Lambda^{(n)}(x_1,...,x_n;g_i(\Lambda)) = 0, \tag{1.21}$$

which is the generalized Callan-Symanzik [4, 5] equation for correlation functions. As in the case of equation (1.12), it simply states that couplings and wave function renormalization change with the scale in order to render correlation functions unaltered.

If the theory is Poincaré invariant, correlation functions depend on the distance between pairs of insertion points. The typical size of these separations defines a new scale, quite apart from any choice of Λ. The former can be used to obtain another interpretation of the renormalization group. One could in principle integrate out the modes in the range $(\Lambda/s, \Lambda]$, and then apply a scale transformation

$$x'^\mu := x^\mu/s \tag{1.22}$$

$$\phi'(x) := s^{(d-2)/2}\phi(x) \tag{1.23}$$

$$\Lambda' := s\Lambda \tag{1.24}$$

according to which the form of the effective action does not change, the couplings are not touched (since rescaling does not have anything to do with integrating out modes), and the energy scale Λ/s is restored to its original value Λ. Under these combined operations, one finds

$$\Gamma_\Lambda^{(n)}(x_1,...,x_n;g_i(\Lambda)) = \left[\frac{Z_\Lambda}{Z_{\Lambda/s}}\right]^{n/2}\Gamma_{\Lambda/s}^{(n)}(x_1,...,x_n;g_i(\Lambda/s)) \tag{1.25}$$

$$= \left[s^{d-2}\frac{Z_\Lambda}{Z_{\Lambda/s}}\right]^{n/2}\Gamma_\Lambda^{(n)}(x_1/s,...,x_n/s;g_i(\Lambda/s)), \tag{1.26}$$

---

[3]The change in the integration measure cancels out since the correlator is given in terms of a normalized path integral.

where the wave function renormalization and the couplings g_i in the last line are taken at the scale Λ/s, since their value is not affected by the previous rescaling.

Equation (1.25) admits the following, interesting interpretation. If one would have started with insertions at points sx_i, then one could equivalently write

$$\Gamma_\Lambda^{(n)}(sx_1, ..., sx_n; g_i(\Lambda)) = \left[s^{d-2}\frac{Z_\Lambda}{Z_{\Lambda/s}}\right]^{n/2}\Gamma_\Lambda^{(n)}(x_1, ..., x_n; g_i(\Lambda/s)). \tag{1.27}$$

The *l.h.s.* of (1.27) shows a correlator computed with the Λ scale effective theory that probes separations $s|x_i - x_j|$. So, as $s \to \infty$, this correlator is is testing the long distance, or *infra-red* properties of the theory. On the other hand, the *r.h.s.* tells that the same correlator could be obtained studying correlation functions where the insertions points are held fixed, but the effective theory employed runs over different values of $g_i(\Lambda/s)$. This makes perfect sense: the IR properties of the theory are governed by the low-energy modes that survive as more and more high-energy modes are integrated out.

Equation (1.26) also yields insights into the meaning of the anomalous dimension γ_ϕ. Looking at the *r.h.s.* of (1.26), one could recognize the factor $s^{n(d-2)/2}$ as the classical scaling behaviour for a correlation function with dimension $n(d-2)/2$. However, this classical scaling is modified by the factor $[Z_\Lambda/Z_{\Lambda/s}]^{n/2}$ that arises when high-energy modes gets integrated out. To quantify such departures from the classical behaviour, one could look for the effect of an infinitesimal scaling transformation, parametrized as $s = 1 + \delta s$, with $0 < \delta s \ll 1$. Expanding (1.26) up to $O(\delta s)$ gives

$$\left[s^{d-2}\frac{Z_\Lambda}{Z_{\Lambda/s}}\right]^{n/2} = n\left\{1 + \left[\frac{d-2}{2} + \gamma_\phi\right]\delta s + ...\right\}, \tag{1.28}$$

with γ_ϕ given by (1.17). From equation (1.28) seems that correlation functions behaves as if the fundamental field scaled with the following mass dimension

$$\Delta_\phi = (d-2)/2 + \gamma_\phi, \tag{1.29}$$

rather than the classically expected value. Δ_ϕ is known as the *scaling dimension* of the fundamental field, and the anomalous dimension γ_ϕ represents the difference between the scaling dimension and the naïve classical dimension.

1.2.4 RG flows

To better understand what happens under renormalization, it is important to study the RG equations of the couplings g_i. The easiest way to do this is by starting from a theory, whose initial couplings g_{i0} are defined such that all the β functions vanish

$$g_{i0} = g_i^* \quad , \quad \beta_j\big|_{g_j=g_i^*} = 0. \tag{1.30}$$

Hence the couplings do not depend on the scale. This theory represents a particular configuration in the evolution described by the RG equation, and is defined as a *critical point* of the RG flow. The most simple example of critical point is given by the prescription

$$g_i^* = 0, \tag{1.31}$$

where all the operators but the mass-less kinetic term are zero. This theory is know as the *Gaussian critical point*, and has clearly vanishing β functions since it has no interaction responsible for the emergence of vertices as the cut-off is lowered. Nonetheless, with a proper tuning of the initial couplings, it should be possible to induce quantum corrections to cancel precisely the classical

rescaling term in (1.16) and let the β functions vanish. Hence, even if not so easily, other critical points, beside the gaussian one, could be defined.

The independence of the couplings g_i^* on the scale yields important implications for the correlation functions of the theory. The first thing to note is that, being γ_ϕ a dimensionless function of the other couplings, it is scale independent at the critical point. Then the Callan-Symanzik equation (1.21) for the two-point correlator becomes

$$\Lambda\frac{\partial\Gamma_\Lambda^{(2)}(x,y)}{\partial\Lambda} = -2\gamma_\phi^*\Gamma_\Lambda^{(2)}(x,y),\tag{1.32}$$

with $\gamma_\phi^* = \gamma_\phi(g_i^*)$. Equation (1.32) tells that $\Gamma^{(2)}$ is a homogeneous function of the scale: because of $SO(d)$ invariance, it can only depend on the insertion points through $|x-y|$. Using dimensional analysis, one shows that

$$\Gamma_\Lambda^{(2)}(x,y) = \Lambda^{d-2}G(\Lambda|x-y|,g_i^*),\tag{1.33}$$

with $G(\Lambda|x-y|,g_i^*)$ being a dimensionless function of the dimensionless combination $\Lambda|x-y|$ and couplings g_i^*. Plugging this formula in equation (1.32) results in

$$\Gamma_\Lambda^{(2)}(x,y) = \Lambda^{d-2-2\Delta_\phi}\frac{c(g_i^*)}{|x-y|^{2\Delta_\phi}} \sim \frac{c(g_i^*)}{|x-y|^{2\Delta_\phi}},\tag{1.34}$$

where Δ_ϕ is the scaling dimension defined in (1.29). The power law described by (1.34) is typical of correlation functions of a scale-invariant theory, i.e. a theory with zero mass gap and infinite correlation length. Well known examples of this kind of behaviour can be found in the theory of second order phase transitions, where actually the Wilsonian RG was originally formulated[7, 8].

The next step to characterize RG flows is to study small deviations from the critical point: starting from a neighbourhood of $g_i = g_i^*$ and linearizing around it, one gets

$$\Lambda\left.\frac{\partial g_i}{\partial\Lambda}\right|_{g_j^*+\delta g_j} = B_{ij}\delta g_j + \mathcal{O}(\delta g^2),\tag{1.35}$$

with $\delta g_i = g_i - g_i^*$, and B_{ij} being a constant (infinite dimensional) matrix. Equation (1.35) can be better studied working with a vector basis that diagonalizes the matrix B_{ij}. Let σ_i be one of the eigenvectors [4], then equation (1.35) becomes

$$\Lambda\frac{\partial\sigma_i}{\partial\Lambda} = (\Delta_i - d)\sigma_i + \mathcal{O}(\sigma^2),\tag{1.36}$$

$\Delta_i - d$ being the eigenvalue of σ_i. Naïvely, one would expect the coupling to scale with a power of Λ given by the classical dimension of the operator coupled to σ_i, so one should have $\Delta_i = d_i$. However, quantum corrections modify the scaling behaviour close to the critical point, the deviations being given by the eigenvalues of the linearized β function matrix B. In total analogy with the definition of γ_ϕ, an anomalous dimension for the operator σ_i can be defined

$$\gamma_i = \Delta_i - d_i,\tag{1.37}$$

where Δ_i represents the scaling dimension of the operator. At this order in perturbations away from the critical point, the solution of equation (1.36) provides the following RG flow

$$\sigma_i(\Lambda) = \left(\frac{\Lambda}{\Lambda_0}\right)^{\Delta_i-d}\sigma_i(\Lambda_0).\tag{1.38}$$

---

[4]To be precise, σ_i is a linear combination of couplings associated to operators with classical dimension d_i. It should be also stressed that the matrix B is generally not normal. If this is the case, then σ_i represents a left eigenvector of B.

The above equation is the starting point for characterizing a quantum theory in the IR, as well as in the UV energy regime.

Starting from eigenvectors σ_i with $\Delta_i > d$, equation (1.38) states that, as the theory gets probed in the infrared, these deformations shrink to zero. So, as the scale is lowered, the theory flows back to the critical point along the directions identified by σ_i. Couplings, and corresponding eigenoperators, that behave in this fashion are called *irrelevant*. The condition $\Delta_i > d$ can be easily fulfilled by operators with higher and higher mass dimension (all of them included in the original action): for this reason, the critical point g_i^* is expected to sit on an infinite dimensional surface $\mathcal{C}$ of the couplings space, such that, turning on any combination of operators that moves along $\mathcal{C}$, the RG flow will make the theory flow back at the critical point. $\mathcal{C}$ is known as the *critical surface* and the couplings of irrelevant operators can be thought of as provided coordinates on $\mathcal{C}$, at least in the neighbourhood of g_i^* (figure 1.1). On this infinite dimensional subspace of theories, the mass gap vanishes, and the fixed point represents a non trivial IR limit at which only the massless degrees of freedom survive. [5]
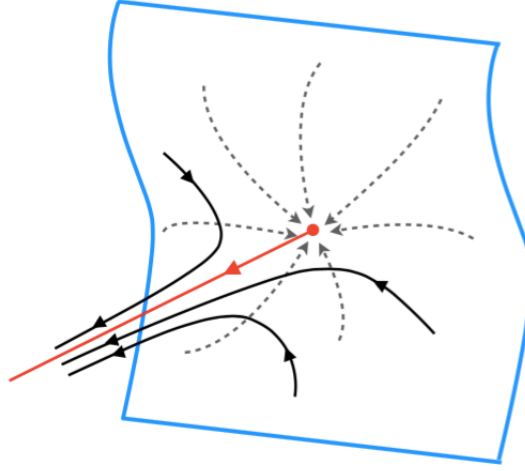
Figure 1.1: Schematic plot of the RG flows, taken from [40]. The region within the blue contour represents the critical surface, on which the RG acts driving a given theory towards the fixed point g_i^*. All the quantum theories that lie on this surface have been obtained switching on only irrelevant couplings. The red line emanating from the fixed point represents the renormalized trajectory, whose evolution is obtained only by deforming the relevant couplings from their critical value. Black solid lines are lines of constant physics starting somewhere off the critical surface, and then driven away by the relevant operators.

Conversely, eigenvectors with $\Delta_i < d$ grows as the scale is lowered, so their separation from the critical point increases as the theory is probed in the IR. For this reason they are called *relevant* couplings. Starting exactly from the critical point and then deforming only relevant operators generates a particular flow called the *renormalized trajectory*. As one investigates the theory deeper and deeper in the IR, the latter evolves according to the flow described by the renormalized trajectory[6]. Since every power of field or derivative of the field increases the classical dimension of an operator, at fixed space-time dimension d there will be just a finite number of relevant operators. This implies that the critical surface has finite codimension.

---

[5]In statistical physics, the critical surface identifies a region of the coupling space where a second order phase transition takes place: in this case, the study of the linearized RG transformation around the IR fixed point provides quantitative knowledge of the critical exponents of the theory. The latter are intimately related to the eigenvalues of the relevant couplings. Knowledge of such exponents allows to determine how correlation length, correlation functions and other physical observables behave as the phase transition is approached.

[6]When more than one relevant operator is deformed, infinite renormalized trajectories are created.

The other possible case is the one described by *marginal* operators, whose eigenvalue is zero and then do not evolve under the action of the RG. At the Gaussian point, where no interaction occurs, the scaling dimension of these operators just equals their engineered dimension, so one would expect $d_i = d$. Close to a critical point, higher quantum corrections could result in weak (usually logarithmic) dependence to a classically marginal operator, turning it to *marginally relevant* or *marginally irrelevant*. If the value of the eigenvalues is sufficiently small, one would expect that the size of nearly marginal couplings could stay unchanged for long "RG flow times", and then finally turn to relevant or irrelevant. From a phenomenological point of view these operators play a really important role.

The final possibility is represented by couplings whose eigenvalue is zero at all orders: this is the case of a *truly marginal* coupling, for which the original fixed point is actually part of a whole line of fixed points.

The most general QFT is characterized by several different types of operators, and then could be represented by a specific point, in couplings space, positioned somewhere off the critical surface. As one turns on the RG machinery, the theory starts to evolve, the irrelevant couplings converge to the fixed point, while the relevant ones depart from it as the scale is lowered. Thus, the flow line of a generic theory will strongly focus around the renormalized trajectory, and in the IR a generic theory will resemble the theory emanating from the critical point, characterized only by relevant operators. Hence, many different high energy theories will look all the same in the IR: this phenomenon is called *universality*, and it guarantees that only a finite set of couplings, the relevant ones, is needed to study the properties of a theory at the large scales. Theories whose RG flows focus around the same renormalized trajectory[7] are said to belong the same *universality class*[8]. Theories in a given universality class could look very different at the microscopical level, but they will all end up looking the same at large distances. This is not a trivial fact, since it explains why is it possible to study a physical problem, at a given scale, without worrying about what higher energy degrees of freedom are doing.

1.2.5   Continuum limit

The original action (1.1) is characterized by an explicit cut-off Λ_0, which guarantees the meaningfulness of the path integral (1.3) and the finiteness of the correlation functions of the theory. Up to now, it has been showed how the couplings, starting from their initial value g_{i0}, evolve as the theory is probed at a lower scale Λ. For a theory described by the effective action (1.8), this evolution results in an independence of the correlation functions from the cut-off Λ. The remaining question is: what about the dependence on the cut-off Λ_0? In QFT this is an important question, since ideally one would like to send Λ_0 to infinity, allowing the field to fluctuate on arbitrarily small length scales, without affecting the value of physical observables. This procedure is called *taking the continuum limit* of the theory and plays a fundamental role in the definition of renormalized quantum field theories. To better examine this issue, it could be useful to start from a given low-energy, effective theory (whose validity could have been probed by the results of some experiment) and wonder how is it possible to remove the cut-off without affecting what the theory predicts for low-energy phenomena.

In taking the continuum limit, the concept of universality of RG flows plays a key role. The easiest way to study this procedure is first looking at a theory defined on the critical surface, within the domain of attraction of the critical point g_i^*. In this case, only irrelevant couplings have been deformed from their critical value and, as can be seen from equation (1.36), as Λ_0 is sent to infinity

---

[7]When more than one relevant operator is deformed, a surface of relevant trajectories has to be considered.

[8]In statistical physics, a universality class is usually identified by a specific set of critical exponents. These exponents are related to the RG eigenvalues of the relevant operators that parametrize the renormalized trajectory.

while keeping Λ fixed, such deformations goes to zero, driving the theory back to the critical point. Here, the theory is scale invariant, and then the cut-off can be easily removed. To be precise, given a theory S_{Λ_0} on the critical surface, the following limit

$$\lim_{\Lambda_0 \to \infty} \left[\int_{C^\infty(M)_{(\Lambda,\Lambda_0]}} \mathcal{D}\xi \exp(-S_{\Lambda_0}[\phi + \xi]) \right] \tag{1.39}$$

exists, provided the cut-off is removed after having computed the integral. The critical surface has finite codimension, so one just needs to tune a finite number of coefficients, i.e. those of the relevant operators, in order to guarantee that the set g_{i0} belongs to $\mathcal{C}$.

Physically interesting theories, like Yang-Mills theory or QCD are not scale invariant, but their actions rather have relevant and marginally relevant operators. In this case, the continuum limit can be understood through the concept of universality. This kind of theories have a starting point that lies somewhere off the critical surface. The RG flow moves them towards the critical point for a while, and then drives them away, close to the renormalized trajectory (1.1). The theory will pass close to g_i^* at an energy scale μ, whose value is determined by the initial conditions of the RG flow. Using dimensional arguments, one could write

$$\mu = \Lambda_0 f(g_{i0}), \tag{1.40}$$

with $f(g_{i0})$ a dimensionless function of the initial couplings satisfying the condition

$$f(g_{i0}) = 0, \quad g_{i0} \in \mathcal{C}. \tag{1.41}$$

If one wants a theory with relevant or marginally relevant operators at the scale μ, then the initial couplings g_{i0} have to be tuned in order to keep μ finite as $\Lambda_0 \to \infty$. If this is possible, then the set of couplings $\{g_{i0}(\Lambda_0 = \infty)\}$ will define a UV fixed point of the RG, that lies on the critical surface. The question is: how many couplings have to be tuned to get the correct continuum limit? The UV fixed point will be characterized by an infinite number of irrelevant couplings and a finite subset of relevant and marginally relevant ones: these are the couplings that need to be tuned in order to remove the cut-off and leave the IR physics unchanged. These couplings will equal in number exactly the parameters that describes the physics of the system at the IR scale μ. The corresponding RG flow emanating from the UV fixed point will be a renormalized trajectory that defines a theory on all length scales. Both how the IR physics is fixed and how the irrelevant couplings of the UV fixed point behave in the UV can be chosen in different ways. As a consequence, there can be many "RG schemes" to take the continuum limit, which all lead to the same continuum theory.

The tuning procedure of the relevant UV couplings is usually achieved adding a counterterm $S_{\mathrm{CT}}[\varphi, \Lambda_0]$ to the original action, characterized by and explicit dependence on the field as well as the cut-off.

$$S_{\Lambda_0}[\varphi] \to S_{\Lambda_0}[\varphi] + S_{\mathrm{CT}}[\varphi, \Lambda_0]. \tag{1.42}$$

In principle, $S_{CT}[\varphi, \Lambda_0]$ does not add anything new, since, in eq (1.1), all the possibly allowed interacting terms have been included. The reason of making S_{CT} explicit is to make contact with the familiar picture of perturbation theory, where the values of the counterterm couplings are tuned, order by order, with the purpose of render the path integral, and its correlation functions, finite when the cut-off is removed [9]. So the following limit

$$e^{-S^{\mathrm{eff}_\Lambda}[\varphi]} = \lim_{\Lambda_0 \to \infty} \left[\int_{C^\infty(M)_{(\Lambda,\Lambda_0]}} \mathcal{D}\xi \exp[-(S_{\Lambda_0}[\phi + \xi] + S_{\mathrm{CT}}[\phi + \xi, \Lambda_0])] \right] \tag{1.43}$$

---

[9]From this requirement, one can extract the dependence for the original couplings, also-called *bare couplings*, on the cut-off Λ_0: this dependence is again described by an RG flow.

exist. Here again, one should stress that the limit has to be taken after having performed the field integration. If the limit defined in equation (1.43) exists, then the procedure of sending Λ_0 to infinity will define a *renormalized* QFT with *renormalized* relevant couplings at scale Λ.

When it is not possible to send Λ_0 to infinity, without affecting the IR physics, then the theory is not renormalizable, and it does not have a continuum limit. This could happen when, in order to explain some experimental result, some UV irrelevant operators need to be included. When the cut-off is removed, these operators will be arbitrarily suppressed at any finite energy scale. Their presence then indicates that the theory cannot be valid up to arbitrarily high energies. However, this does not imply that such a theory is useless for study the physics of a system, but only that its applicability is limited to a definite energy range, upper bounded by a cut-off Λ_0^*. In order to go deeper in the UV regime, new physical input is needed.

1.2.6 RG flows and perturbation theory

The RG flows of a theory can be determined in several different ways. When the analytic approach is preferred, approximation methods are usually needed to get some insights about the theory under study. These approximation could depend also on the regulator adopted, whose choice, usually, depends on the symmetries characterizing the quantum theory. In this chapter, for example, a sharp momentum cut-off has been applied to regularize the theory: this regulator is usually quite good for study the RG flows of scalar theories. For a generic d-dimensional scalar theory, the Lagrangian density is

$$\mathcal{L} = \frac{1}{2}\partial_\mu\varphi\partial_\mu\varphi + V(\varphi), \tag{1.44}$$

where

$$V(\varphi) = \sum_n \Lambda^{n-n(d-2)}\frac{g_{2n}}{2n!}\varphi^{2n}, \tag{1.45}$$

is what is called the *effective potential*, and a Z_2 symmetry has been assumed. Equation (1.45) represents a first level of approximation: using classical scaling arguments, derivative couplings gets ruled out. This procedure is called the *local potential approximation*, and it tells the shape of the effective potential experienced by a slowly varying field. Within this formulation, Wilson's RG approach can be straightforwardly applied: one has to first split the field in *fast* and *slow* modes, as in equation (1.6), and then apply equation (1.8) for an infinitesimal RG transformation.

$$S[Z(\Lambda-\delta\Lambda)^{1/2}\phi; \Lambda-\delta\Lambda, g_{2n}(\Lambda-\delta\Lambda)] := -\log\left[\int_{C^\infty(M)_{(\Lambda-\delta\Lambda,\Lambda]}} \mathcal{D}\xi \exp(-S[\phi+\xi; \Lambda, g_{2n}(\Lambda)])\right]. \tag{1.46}$$

Expanding the action on the r.h.s. of the above equation gives

$$S[\phi+\xi; \Lambda, g_{2n}(\Lambda)] = S[\phi; \Lambda, g_{2n}(\Lambda)] + \int d^d\left[\frac{1}{2}(\partial\xi)^2 + \frac{1}{2}\xi^2 V''(\phi) + \frac{\xi^3}{3!}V'''(\phi) + ...\right]. \tag{1.47}$$

Now the *fast* modes ξ need to be integrated out. The Feynman diagrams that contributes to the path integral (1.46) have only ξ on internal lines, contributing with propagator

$$\xi \text{ -------- } \xi \quad \sim \quad \frac{1}{p^2 + g_2\Lambda^2} \tag{1.48}$$

and only ϕ on external lines (but with no propagators). The interaction vertices are provided by the expansion (1.47) in powers of ϕ and ξ. As an example, there will be a vertex of the form

$$\sim \quad \frac{g_6}{4!2!}\phi^4\xi^2 \tag{1.49}$$

Each loop involves an integral over the momentum of ξ in a shell between radii Λ and $\Lambda + \delta\Lambda$ in momentum space

$$\int_{\Lambda-\delta\Lambda<|p|\leq\Lambda} \frac{d^dp}{(2\pi)^2}(...) = \frac{\Lambda^{d-1}\delta\Lambda}{(2\pi)^d}\int_{S^{d-1}} d\Omega(...), \tag{1.50}$$

where S^{d-1} is the $d-1$ dimensional unit sphere. Here a second level of approximation has to be done: since each loop integral contributes with a factor $\delta\Lambda$, then, to lowest non trivial order, only 1-loop diagrams have to be considered. It can be shown that, in order to keep track just of 1-loop diagrams, only vertices with 2 ξ fields have to be retained in equation (1.47), which becomes

$$S[\phi+\xi; \Lambda, g_{2n}(\Lambda)] = S[\phi; \Lambda, g_{2n}(\Lambda)] + \int d^d \left[\frac{1}{2}(\partial\xi)^2 + \frac{1}{2}\xi^2 V''(\phi)\right]. \tag{1.51}$$

The path integral (1.46) can now be evaluated, giving as result

$$\delta_\Lambda S[\phi] = a\Lambda^{d-1}\delta\Lambda \int d^dx \log[\Lambda^2 + V''(\phi)], \tag{1.52}$$

where $a = \mathrm{Vol}(S^{d-1})/[2(2\pi)^d] = (4\pi)^{-d/2}/\Gamma(d/2)$ and

$$\delta_\Lambda S[\phi] = S[\phi; \Lambda - \delta\Lambda, g_{2n}(\Lambda - \delta\Lambda)] - S[\phi; \Lambda, g_{2n}(\Lambda)]. \tag{1.53}$$

Notice that no wave function renormalization has been generated in this case[10]. Expanding the l.h.s. of (1.52) to order $\delta\Lambda$, one obtains

$$\left(\frac{\partial}{\partial\lambda} + \frac{dg_{2n}}{d\lambda}\frac{\partial}{\partial\Lambda}\right) S[\phi; \Lambda, g_{2n}(\Lambda)] = -a\Lambda^{d-1}\int d^dx \log[\Lambda^2 + V''(\phi)], \tag{1.54}$$

and expanding the r.h.s. in powers of ϕ allows to extract the beta functions for the couplings directly

$$\Lambda\frac{dg_{2n}}{d\Lambda} = (n(d-2)-d)g_{2n} - a\Lambda^{n(d-2)}\frac{d^{2n}}{d\phi^{2n}}\log[\Lambda^2 + V''(\phi)]\bigg|_{\phi=0}. \tag{1.55}$$

From (1.55), the first beta functions in the hierarchy can be easily written down

$$\Lambda\frac{dg_2}{d\Lambda} = -2g_2 - \frac{ag_4}{1+g_2}, \tag{1.56}$$

$$\Lambda\frac{dg_4}{d\Lambda} = (d-4)g_4 + \frac{3ag_4^2}{(1+g_2)^2} - \frac{ag_6}{1+g_2}, \tag{1.57}$$

$$\Lambda\frac{dg_6}{d\Lambda} = (2d-6)g_6 - \frac{30ag_4^3}{(1+g_2)^3} + \frac{15ag_4g_6}{(1+g_2)^2} - \frac{ag_8}{1+g_2}. \tag{1.58}$$

It should be noticed that, with this renormalization scheme, quantum contributions involve inverse powers of $1 + g_2$, which physically is $1 + (m/\Lambda)^2$, m being the mass of the field. These factors are generated by the propagators of the fast modes inside the loops: when $\Lambda \ll m$, quantum contributions gets suppressed, as one wold expect on the basis of decoupling.

---

[10]In this theory, at 1-loop order, the only Feynman diagram with two external legs has no external momentum dependence, so it cannot give rise to terms like $(\partial\phi)^2$.

The method used above for the scalar, Z_2-invariant theory is one of the possible strategies that could be employed to get quantitative knowledge about the RG flows. RG ideas can be also implemented in the context of perturbation theory, using regularization schemes different from the sharp momentum cut-off[11]. In this case, only relevant (and marginally relevant) couplings for the UV fixed point are considered, since they play a fundamental role in determining the continuum limit of the theory, while the irrelevant ones can be set to zero. Writing down the path integral as a power series in the relevant couplings, one evaluates correlation functions up to a given order in the couplings: in principle, this correlation functions will depend on the external momenta, the parameters of the theory and the adopted regulator. The perturbative expansion can be carried out in terms of the *bare parameters* of the theory, those defined at the cut-off scale Λ_0 in the Wilsonian formulation. However, this is not the only possible choice: in principle, one could also expand the theory in terms of the "renormalized" couplings, defined at a physically relevant scale Λ. In this case, one has simply to write the original action as

$$S[\phi_b; \Lambda_0, g_b(\Lambda_0)] = S[\phi_R; \Lambda, g_R(\Lambda)] + S_{CT}[Z(\Lambda)^{-1/2}\phi_R; \Lambda_0, \Lambda, g_R(\Lambda)], \qquad (1.59)$$

where the subscripts b and R mean bare and renormalized. The l.h.s. of equation (1.59) is independent on the scale Λ, and this is ensured by the appropriate dependence of $g_R(\Lambda)$ and $Z(\Lambda)$ on Λ according to the RG flows. The role of the counterterm action on the r.h.s. is to render (renormalized) correlation functions finite as the regulator (the cut-off Λ_0 in this representation) is removed. This is mirrored in $S[\phi_b; \Lambda_0, g_b(\Lambda_0)]$ by the appropriate tuning of $g_b(\Lambda_0)$ (as described in equation (1.42)), but, at this point, adding also a counterterm for the bare action sounds only redundant). Both representations allow to extract quantitative knowledge about the RG flows, the difference being simply the way these flows are obtained. Whichever formulation has been chosen, it is necessary to check the consistency of perturbation theory, making certain that the parameters adopted for the expansion are actually small at their proper energy scale.

As already mentioned, tuning the bare parameters (or adding counterterms) is fundamental to render correlation functions finite and regulator independent, as the latter gets removed: this procedure is usually accomplished imposing specific *renormalization conditions* on renormalized correlation functions. There are several ways this conditions can be formulated: for example, one could use the following tower of equations

$$\Gamma_R^{(2)}(p) = -(p^2 + m^2),$$
$$\left.\frac{d\Gamma_R^{(2)}(p)}{dp^2}\right|_{p^2=-m^2} = -1,$$
$$\Gamma_R^{(3)}(p_1, p_2, p_3) = g_3^*,$$
$$......$$
$$\Gamma_R^{(n)}(p_1, p_2, ..., p_n) = g_n^*,$$

that fixes the physical mass and couplings in terms of the renormalized two, three and n-point vertex functions, at some specific momentum scale μ, such that $p_i^2 = \mu^2$. Using the r.h.s. representation of (1.59) one finds counterterms explicitly depending on the scale μ (which is now the physically relevant scale) and, once divergences have been removed, the Callan-Symanzik equation (1.12) can be used to determine RG flows of the couplings g_R as a function of μ. Nonetheless, one can also use the l.h.s. representation in (1.59), write $\phi_b = Z^{1/2}\phi_R$, and impose renormalized correlation

---

[11]This kind of formulation is usually very useful to introduce the concepts of the RG flow. However, it has also its frailties. When gauge theories are under investigation, it is not obvious how to make the sharp momentum cut-off consistent with gauge invariance.

functions to be regulator independent up to violations that reduce to zero when the regulator is removed: from this condition one determines the RG flows of the bare parameters as functions of the regulator itself.[12] What is really important is that, independently on the specific "RG scheme" adopted, the first two coefficients of the perturbative expansion of the beta function will be universal. Therefore, one can study the nature of perturbative RG flows choosing the method he prefers.

In this work, the lattice regularization has been adopted, the role of the regulator being performed by the lattice spacing, usually called a in the literature. From the Wilsonian point of view, it allows to define a theory with an effective action at a cut-off $\Lambda_0 \sim a^{-1}$: within this formulation, Wilson's ideas of RG can be straightforwardly applied, both in perturbative and non perturbative regimes. As a proof for that, the perturbative study of the RG flows of a scalar $\lambda\phi^4$ theory will be described in the next sections.

1.3 Lattice formulation

In this section, the structure of a scalar quantum field theory on a lattice is presented, with the aim of defining the basic formalism to be then employed in the next sections. The geometry of the system consists of a flat, four-dimensional, euclidean space-time, discretized as a hypercubic lattice

$$\mathbf{\Lambda} = \{x \in a\mathbb{Z}^4 | 0 \le x_\mu \le a(L_\mu - 1)\}, \tag{1.60}$$

where a is the lattice spacing, $L = L_i \quad i = 0, ..., 3$, $\Omega = \prod_{i=0}^{3} L_i$ is the total number of lattice points. Functions defined on the lattice satisfy periodic boundary conditions

$$f(x + a\hat{\mu}L_\mu) = f(x). \tag{1.61}$$

In analogy to the continuous case, it is possible to define a scalar product in Hilbert space as

$$(f, g) = a^4 \sum_x f(x)g(x)^*, \tag{1.62}$$

and a discretized derivative operator, using, e.g., the *forward* representation

$$\partial_{\mu F}g(x) = \frac{1}{a}[f(x + a\hat{\mu}) - f(x)], \tag{1.63}$$

where $\hat{\mu}$ is a unit four-vector along the direction μ. A possible alternative is given by the *backward* formulation

$$\partial_{\mu B}g(x) = \frac{1}{a}[f(x) - f(x - a\hat{\mu})], \tag{1.64}$$

the two being related by the following relation

$$(\partial_{\mu F}g(x), h(x)) = -(g(x), \partial_{\mu B}h(x)), \tag{1.65}$$

from which one deduces that

$$(\partial_{\mu F})^\dagger = -\partial_{\mu B}, \tag{1.66}$$

and

$$\Box = \sum_{\mu=0}^{3} \partial_{\mu F}\partial_{\mu B}. \tag{1.67}$$

---

[12]This is true for renormalization schemes like lattice, sharp momentum cut-off and Pauli Villard, where the regulator has the dimension of an energy. Things are slightly different in dimensional regularization. When the latter is employed, the coordinate integration measure changes dimension and a scale parameter (usually called μ) has to be introduced to keep the action dimensionless. In this case, the dependence on μ is encoded only in the renormalized parameters of the theory.

A function defined on the lattice can be expanded in Fourier modes as

$$f(x) = \frac{1}{a^4\Omega} \sum_p e^{ipx} \tilde{f}(p),$$

(1.68)

where the allowed lattice momenta are constrained inside the Brillouin zone

$$p_\mu = \frac{2\pi}{aL_\mu} n_\mu, \quad n_\mu = 0, 1, ..., L_\mu - 1,$$

(1.69)

and the Fourier transform of $f(x)$ is

$$\tilde{f}(p) = a^4 \sum_x e^{-ipx} f(x).$$

(1.70)

The theory is described by a scalar field $\phi(x)$ whose action has the following form

$$S[\phi, a] = S_0[\phi] + S_I[\phi],$$

(1.71)

where $S_0[\phi]$ represents the free field contribution to the global action

$$S_0[\phi] = \frac{1}{2}(\phi, (\Box + m_0^2)\phi),$$

(1.72)

while $S_I[\phi]$ is the interacting contribution [13]

$$S_I[\phi] = a^4 \sum_x \sum_{j\neq 2, k, m}^\infty \frac{g_{jk}}{j!k!} \phi(x)^j (\partial_{\mu F}\phi(x)\partial_{\mu F}\phi(x))^k (\Box\phi)^m.$$

(1.73)

In four space-time dimensions, keeping only relevant or marginal operators, the interaction simply becomes

$$S_I[\phi] = a^4 \sum_x \frac{\lambda_0}{4!} \phi(x)^4,$$

(1.74)

with $\lambda_0 = g_{40}$. The generating functional for this theory is given by the following path integral

$$Z_0[J, a] = \frac{1}{Z_0(a)} \int D[\phi] \exp\left\{-\left[\frac{1}{2}(\phi, (\Box + m_0^2)\phi) + S_I[\phi]\right] + (J, \phi)\right\},$$

(1.75)

where J represents the usual source term, and

$$Z_0(a) = \int D[\phi] \exp\left\{-\left[\frac{1}{2}(\phi, (\Box + m_0^2)\phi) + S_I[\phi]\right]\right\},$$

(1.76)

is the vacuum normalization. With this formulation, a generic, lattice connected correlation function is obtained as

$$\langle\phi(x_1)\phi(x_2)...\phi(x_n)\rangle_c = \frac{\delta}{\delta J(x_1)}\frac{\delta}{\delta J(x_2)}...\frac{\delta}{\delta J(x_n)} \ln Z_0[J, a]\bigg|_{J=0}.$$

(1.77)

At finite lattice spacing, the integration measure

$$D[\phi] = \prod_{x\in\Lambda} d\phi(x),$$

(1.78)

is well defined, so the path integral (1.75) and the expectation value (1.77) can be evaluated either analytically, in perturbation theory, or, since the integrand e^{-S} is strictly positive, numerically in the non perturbative case. Before going on with the perturbative analysis of the theory, it is better to stop for a moment and take a look at its phase structure.

---

[13] According to the notation of the previous sections, $g_2 = a^2 m_0^2$

1.3.1 $\lambda\phi^4$ theory: phase structure

The $\lambda\phi^4$ theory is characterized by two different phases, yielding two different minimum configurations of the field. Writing down the action

$$S = \int d^d x \left[\frac{1}{2} \partial_{\mu_F} \phi \partial_{\mu_F} \phi + U(\phi) \right],$$

$$U(\phi) = \frac{m_0^2}{2}\phi^2 + \frac{\lambda_0}{4!}\phi^4,$$

one identifies the ground state of the theory as the field configuration with lowest energy. This corresponds to

$$\partial_{\mu_F}\phi^* = 0,$$
$$\left.\frac{\partial U}{\partial \phi}\right|_{\phi^*} = 0, \tag{1.79}$$

where obviously $\lambda_0 > 0$, so S is bounded from below for all values of ϕ. The constraints in (1.79) are satisfied by a constant-field configuration that takes the value

$$\phi^* = 0, \quad U(\phi^*) = 0, \qquad\qquad m_0^2 > 0; \tag{1.80}$$

$$\phi^* = \pm v, \quad U(\pm v) = -\frac{3(m_0^2)^2}{2\lambda_0}, \quad v^2 = -\frac{6m_0^2}{\lambda_0}, \qquad m_0^2 < 0;. \tag{1.81}$$
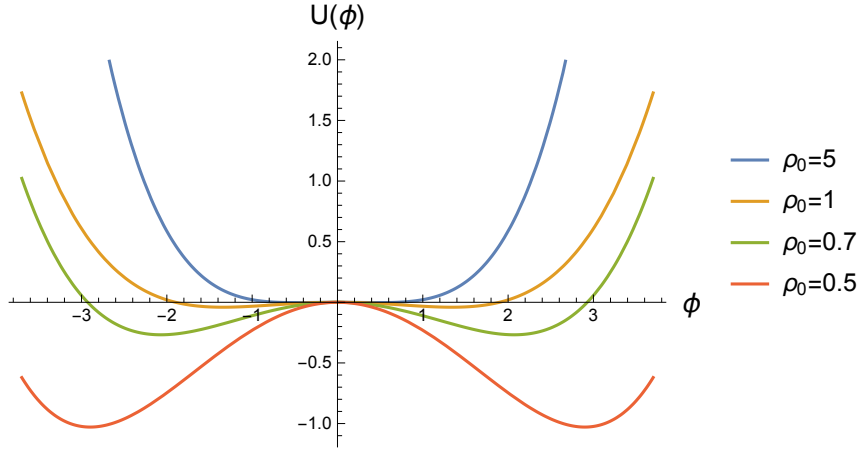
Figure 1.2: Values of $U(\phi)$ as a function of ϕ when $m_0^2 < 0$. Here different theories, characterized by the ratio $\rho_0 = \lambda_0/m_0$ have been considered. It can be seen how the theory exhibit two degenerate minima at $\phi = \pm\sqrt{\frac{6}{\lambda_0}}|m_0|$

The case in (1.81) leads to a doubly degenerate ground state. When the theory chooses one of the two minima, the Z_2 symmetry of the action $(\phi(x) \to -\phi(x))$ is broken, and one speaks of *spontaneous symmetry-breaking*. Hence the theory is characterized by two different phases, one in which Z_2 symmetry is conserved, and one in which is broken: the action characterizing each phase will be

$$S = a^4 \sum_x \left(\sum_{\mu=0}^{3} \partial_{\mu_F}\phi\partial_{\mu_F}\phi + \frac{m_0^2}{2}\phi^2 + \frac{\lambda_0}{4!}\phi^4 \right) \qquad \text{unbroken,} \tag{1.82}$$

$$S = a^4 \sum_x \left(\sum_{\mu=0}^{3} \partial_{\mu_F}\xi\partial_{\mu_F}\xi - m_0^2\xi^2 + \frac{v\lambda_0}{6}\xi^3 + \frac{\lambda_0}{4!}\xi^4 \right) \qquad \text{broken.} \tag{1.83}$$

When $m_0^2 < 0$, the transition between the two phases occurs at a specific value of the couplings of the theory: in the (m_0, λ_0) plane the subset of values (m_{0c}, λ_{0c}) represents a critical line at which the phase transition takes place.
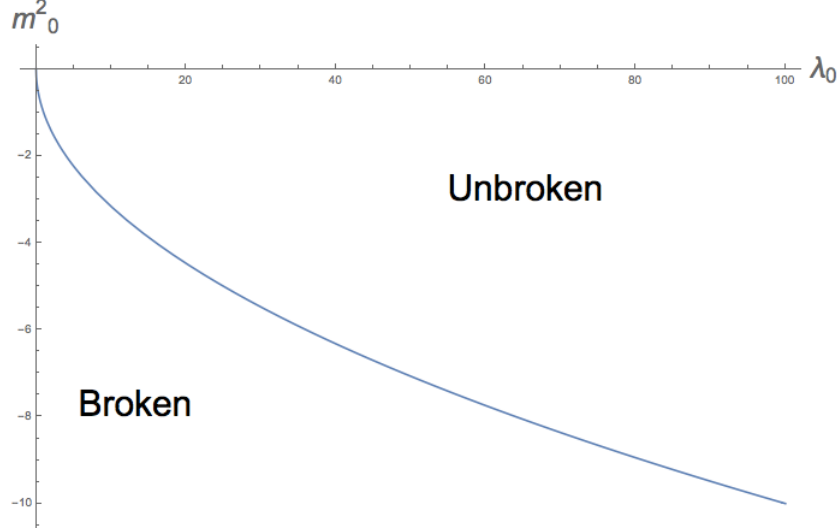
Figure 1.3: Schematic plot of the phase diagram in the (m_0, λ_0) plane. The symmetric phase comprises the $m_0^2 > 0$ and part of the $m_0^2 < $ regions.

To better understand this fact, the original lattice action has to be rewritten in the following way (lattice units, $a = 1$ have been adopted)

$$S = -\frac{1}{2} \sum_x \sum_{\mu=\pm0}^{\pm3} \phi(x)\phi(x+\hat{\mu}) + \sum_x \left[\frac{1}{2}(8+m_0^2)\phi^2 + \frac{\lambda_0}{4!}\phi^4 \right]. \tag{1.84}$$

Then, the following parametrization

$$\phi = \sqrt{2k}\varphi, \quad m_0^2 = \frac{1-2\lambda}{\kappa} - 8, \quad \lambda_0 = \frac{6\lambda}{\kappa^2}, \tag{1.85}$$

brings the original action into the new form

$$S = -\kappa \sum_x \sum_{\mu=\pm0}^{\pm3} \varphi(x)\varphi(x+\hat{\mu}) + \sum_x [\varphi^2 + \lambda(\varphi^2 - 1)^2], \tag{1.86}$$

and the path integral becomes

$$Z = \int D\mu(\varphi) \exp\left(\kappa \sum_x \sum_{\mu=\pm0}^{\pm3} \varphi(x)\varphi(x+\hat{\mu}) \right). \tag{1.87}$$

The integration measure

$$D\mu(\varphi) = \prod_x d\mu(\varphi(x)), \quad d\mu(\varphi) = d\varphi \exp(-\varphi^2 - \lambda(\varphi^2 - 1)^2) \tag{1.88}$$

sets a constraint on the magnitude of φ as a function of λ, which has to be positive in order to make the integration $\int d\mu(\varphi)$ meaningful. Equation (1.87) shows the path integral as the partition function of a generalized Ising model[14]. When $\lambda \to \infty$ the distribution $d\mu(\varphi)$ peaks at $\varphi^2 = 1$

$$\frac{\int d\mu(\varphi) f(\varphi)}{\int d\mu(\varphi)} \to \frac{1}{2}[f(1) + f(-1)] \tag{1.89}$$

Hence, for infinite λ, one gets precisely the Ising model in 4 dimensions. The representation of the theory given by (1.87) allows to better understand the transition between the two phases. For a fixed λ, the system could be in a ferromagnetic (broken) or in a paramagnetic (unbroken) phase, such that, in the infinite volume limit,

$$\langle \varphi \rangle = v, \quad k > k_c(\lambda),$$
$$\langle \varphi \rangle = 0, \quad k < k_c(\lambda).$$

The critical line $k_c(\lambda)$ represents the boundary between the two phases in the $\lambda - \kappa$ plane. It is possible to give a mean field estimate of the critical coupling κ_c using the following approximation

$$\kappa \sum_x \sum_{\mu=\pm 0}^{\pm 3} \varphi(x)\varphi(x + \hat{\mu}) = \tag{1.90}$$

$$= \kappa \sum_x \sum_{\mu=\pm 0}^{\pm 3} [(v + (\varphi(x) - v))(v + (\varphi(x + \hat{\mu}) - v))] \tag{1.91}$$

$$\simeq -2kVdv^2 + 4d\kappa \sum_x \varphi(x) + \mathcal{O}(\delta\varphi^2) \tag{1.92}$$

$$= -8k(L_0 L_1 L_2 L_3)v^2 + 16\kappa \sum_x \varphi(x), \quad d = 4, \tag{1.93}$$

$$\tag{1.94}$$

where higher powers in the variation $\delta\varphi = (\varphi - v)$ have been ignored. Within this approximation, the mean value of $\varphi(x)$ becomes

$$\varphi = \frac{\int d\mu(\varphi)\varphi \exp(16\kappa v\varphi)}{\int d\mu(\varphi) \exp(16\kappa v\varphi)}. \tag{1.95}$$

One now impose $\langle \varphi \rangle = v$ and uses the path integral formalism to get

$$\langle \varphi \rangle = \frac{1}{z(J)} \frac{\partial}{\partial J} z(J) \bigg|_{J=16kv},$$
$$z(J) = \int d\mu(\varphi) \exp(J\varphi).$$

The integral $z(J)$ can be evaluated analytically in various limits, numerically otherwise: the two extreme cases are

- $\lambda = 0$: this case is called the gaussian limit, the integral defining $z(J)$ can be easily done

$$z(J) = \sqrt{\pi} \exp(64k^2 v)$$

  and the corresponding critical value is $\kappa_c(0) = 1/8$

---

[14]This is true because all the four directions have been compactified.

- $\lambda = \infty$: this is the Ising limit, where one obtains

$$z(J) = z(0)\cosh(J),$$
$$v = \tanh(16kv).$$

As κ approaches κ_c from above, $v \to 0$, then the following expansion is legitimate

$$v \simeq 16kv - \frac{1}{3}(16kv)^3 + ...,$$

from which one get

$$\kappa_c(\infty) = \frac{1}{16}$$
$$v^2 \propto (\kappa - \kappa_c)$$
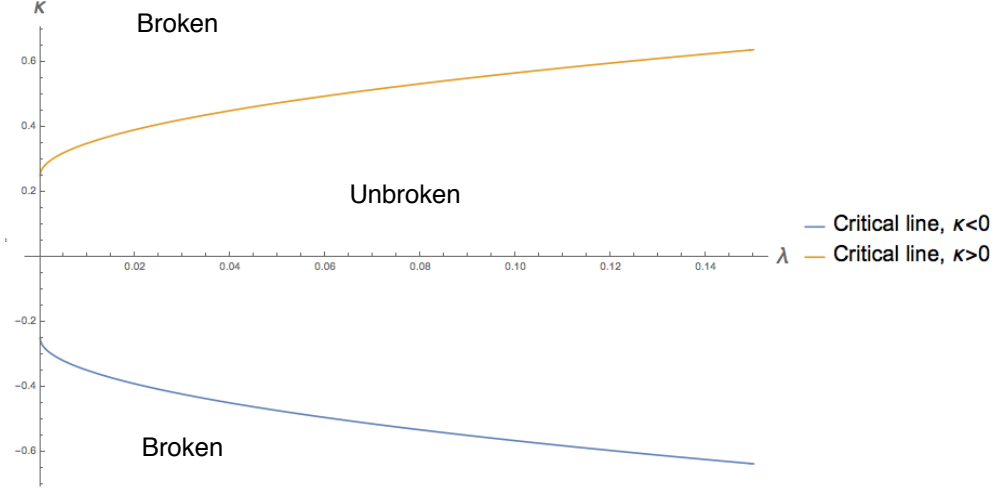
Figure 1.4: Schematic plot of the phase diagram in the (κ, λ) plane.

Close to the critical line, the behaviour of $v \propto (\kappa - \kappa_c(\lambda))^\beta$ is typical of a second order phase transition, with $\beta = 1/2$ representing a critical exponent in the mean field approximation. As the critical line is approached, the correlation length of the system will diverge with $(\kappa - \kappa_C(\lambda))$, according to another critical exponent. In the language of the RG, the critical line represents the intersection of the critical surface with the theories subspace (m_0, λ_0). As can be seen from (1.55) in $d = 4$ dimensions, there exists only one fixed point that lies on such a surface, and this is the Gaussian fixed point. For the statistical theory represented by (1.87), the full critical exponents (which in general are different from their mean field approximation counterparts) are determined by the RG eigenvalues of the relevant couplings around the Gaussian fixed point.

Since only the Gaussian fixed point is available, a continuum limit for the interacting theory, if existing, can only be represented by a renormalized trajectory emanating from such a point in the

(m_0, λ_0) plane. To check for this possibility, a perturbative study of the theory can be performed to determine the nature of the perturbative RG flows. The analysis can be carried out both in the broken and in the unbroken phase. For simplicity, only the symmetric phase will be considered.

1.4 Perturbation theory

The perturbative study of a QFT is performed by expanding the path integral in powers of the bare parameter λ_0 and then evaluating correlation functions like in (1.77). The expansion can be represented in terms of Feynman diagrams both in coordinate and momentum space. From now on, the momentum space representation will be adopted, focussing on the determination of the (connected) two and four-point vertex functions at leading order in the coupling.

1.4.1 Perturbative expansion

The two fundamental pieces for constructing the diagrammatic expansion are the free theory propagator

$$\tilde{G}(p) = \frac{1}{m_0^2 + \hat{p}^2} = \underline{\qquad\qquad}_{p} \tag{1.96}$$

and the tree level four vertex function

$$\Gamma^{(4)}(p_1, p_2, p_3, p_4) = -\lambda_0 = \tag{1.97}$$

Where lattice unit $a = 1$ have been assumed and

$$\hat{p}^2 = 2 \sum_{\mu=0}^{3} (1 - \cos p_\mu).$$

The leading contribution to the two-point function is given by the following diagrams

$$\tilde{G}^{(2)}(p) = \underline{\qquad}_{p} + \underline{\qquad}_{p}\bullet_{p} \; . \tag{1.98}$$

The corresponding two-vertex function is obtained taking the (negative) inverse propagator

$$\Gamma^{(2)}(p) = - \left[m_0^2 + p^2 + \frac{\lambda_0}{2} I(m_0) \right] . \tag{1.99}$$

On the other hand, the leading contribution to the four-point vertex function is given by

$$\Gamma^{(4)}(p_1, p_2, p_3, p_4) =$$

$$\Gamma^{(4)}(p_1, p_2, p_3, p_4) = -\left\{ \lambda_0 - \frac{\lambda_0^2}{2} \left[J(m_0, p_1 + p_2) + (p_2 \leftrightarrow p_3) + (p_2 \leftrightarrow p_4) \right] \right\}, \tag{1.101}$$

where the functions I and J are given by

$$I(m_0) = \int_{-\pi}^{\pi} \frac{d^4 l}{(2\pi)^4} \frac{1}{m_0^2 + \hat{l}^2}, \tag{1.102}$$

$$J(m_0, p) = \int_{-\pi}^{\pi} \frac{d^4 l}{(2\pi)^4} \frac{1}{\left[m_0^2 + \hat{l}^2 \right] \left[m_0^2 + 2\sum_\mu (1 - \cos(l + p)_\mu) \right]}. \tag{1.103}$$

Here the infinite volume limit $\sum_l \to \int d^4 l/(2\pi)^4$ has been assumed. The integrals $I(m_0)$ and $J(m_0, p)$ diverge quadratically and logarithmically with the cut-off a^{-1}. To determine how the bare parameters get tuned, one has simply to retain the divergent and non vanishing terms arising from the expansion of $I(m_0)$ and $J(m_0, p)$ as $a \to 0$. There are several ways this procedure can be carried out [41, 42], here only the final results are reported

$$I(m_0) = \frac{C_0}{a^2} - C_2 m_0^2 + \frac{1}{16\pi^2} \log(a^2 m_0^2) + \mathcal{O}(a^2),$$

$$J(m_0, p) = -\frac{1}{16\pi^2} \int_0^1 dx \log[a^2(m_0^2 + x(1-x)p^2)] + C_2 - \frac{1}{16\pi^2} + \mathcal{O}a^2,$$

$$C_0 = 0.154933...,$$

$$C_2 = 0.0303457...$$

The two and four vertex functions are then given by

$$\Gamma^{(2)}(p) = -\left\{ m_0^2 + p^2 + \frac{\lambda_0}{2} \left[\frac{C_0}{a^2} - C_2 m_0^2 + \frac{1}{16\pi^2} m_0^2 \log(a^2 m_0^2) \right] \right\}, \tag{1.104}$$

$$\Gamma^{(4)}(p_1, p_2, p_3, p_4) = -\lambda_0 + \frac{\lambda_0^2}{2} \left\{ C_2 - \frac{1}{16\pi^2} \right.$$

$$\left. -\frac{1}{16\pi^2} \int_0^1 dx \log[a^2(m_0^2 + x(1-x)(p_1 + p_2)^2)] \right] + (p_2 \leftrightarrow p_3) + (p_2 \leftrightarrow p_4) \right\}. \tag{1.105}$$

1.4.2 Renormalization

To determine the perturbative RG flows, the Callan-Symanzik equations for renormalized two and four-point vertex functions have to be solved. This can be done after having specified a

renormalization condition for correlation functions[15]. One possible choice could be represented by

$$\lim_{a \to 0} Z(\lambda_0, \hat{m}_0) \Gamma^{(2)}(p; \lambda_0, \hat{m}_0, a) = -(m_R^2 + p^2 + \mathcal{O}(p^4)),$$

$$\lim_{a \to 0} Z(\lambda_0, \hat{m}_0) \Gamma^{(4)}(0, 0, 0, 0; \lambda_0, \hat{m}_0, a) = -\lambda_R, \tag{1.106}$$

where, following the notation adopted in (1.2), correlation functions have been written in terms of the cut-off $1/a$ and dimensionless couplings $\lambda_0, \hat{m}_0 = m_0 a$. The above conditions state that the bare parameters have to be tuned with the lattice spacing to make the renormalized correlation functions finite and cut-off independent as continuum limit is approached. The quantities m_R and λ_R are defined as the *renormalized mass* and *renormalized coupling* of the theory. These are physical observables that define a specific interacting theory in the continuum. More precisely, m_R fixes the scale for all the dimensionful quantities[16], and λ_R the strength of the interaction at zero momentum. At leading order in λ_0, no divergences proportional to p^2 have been introduced, hence

$$Z(\lambda_0, m_0 a) = 1 + \mathcal{O}(\lambda_0^2) \tag{1.107}$$

From the set of equations (1.106), one infers

$$m_R^2 = \frac{\hat{m}_0^2}{a^2} + \frac{\lambda_0}{2} \left[\frac{C_0}{a^2} - C_2 \frac{\hat{m}_0^2}{a^2} + \frac{\hat{m}_0^2}{16\pi^2 a^2} \log(\hat{m}_0^2) \right], \tag{1.108}$$

$$\lambda_R = \lambda_0 + \frac{3\lambda_0^2}{32\pi^2} \left[\log(\hat{m}_0^2) - C_2 + \frac{1}{16\pi^2} \right]. \tag{1.109}$$

Using λ_R as an expansion parameter, the set of equations (1.106) allows to rewrite the bare couplings as functions of the renormalized ones

$$\hat{m}_0^2 = (am_R)^2 - \frac{\lambda_R}{2} \left[C_0 - C_2 (am_R)^2 + \frac{(am_R)^2}{16\pi^2} \log(a^2 m_R^2) \right] + \mathcal{O}(\lambda_R^2), \tag{1.110}$$

$$\lambda_0 = \lambda_R - \frac{3\lambda_R^2}{32\pi^2} \left[\log(a^2 m_R^2) - C_2 + \frac{1}{16\pi^2} \right] + \mathcal{O}(\lambda_R^3). \tag{1.111}$$

With this definitions, one determines the renormalized vertex functions in terms of λ_R and m_R

$$\Gamma_R^{(2)}(p; \lambda_R, m_R) = -(m_R^2 + p^2) + \mathcal{O}(\lambda_R^2), \tag{1.112}$$

$$\Gamma_R^{(4)}(p_1, p_2, p_3, p_4; \lambda_R, m_R) = -\lambda_R - \frac{\lambda_R^2}{2} \left\{ \frac{1}{16\pi^2} \int_0^1 dx \log \left[\frac{m_R^2 + x(1-x)(p_1 + p_2)^2}{m_R^2} \right] + \right.$$

$$\left. (p_2 \leftrightarrow p_3) + (p_2 \leftrightarrow p_4) \right\} + \mathcal{O}(\lambda_R^3), \quad (1.113)$$

which are, indeed, independent on the lattice spacing a. It has to be noticed that the constants C_0 and C_2 are absent: all reference to the lattice has disappeared from the renormalized vertex functions. Quantitative knowledge of the RG flows can be obtained studying the behaviour of the bare couplings: one has simply to require renormalized vertex functions to be independent on the cut-off. At finite lattice space, one should write

$$Z(\lambda_0, \hat{m}_0) \Gamma^{(n)}(p_1, ..., p_n; \lambda_0, \hat{m}_0, a) = \Gamma_R^{(n)}(p_1, ..., p_n; \lambda_R, m_R, a), \tag{1.114}$$

---

[15]In the following, the momentum space version of the Callan-Symanzik equations will be adopted.

[16]It should be noticed that m_R, in principle, does not represent the physical mass of a particle, which is usually identified with the pole of the propagator, or the zero of $\Gamma^{(2)}(p)$. In the low momentum expansion defined in (1.106) the two quantities coincide only at tree level.

where, from a detailed analysis in perturbation theory [43], it can be shown that

$$\Gamma_R^{(n)}(p_1, ..., p_n; \lambda_R, m_R, a) = \Gamma_R^{(n)}(p_1, ..., p_n; \lambda_R, m_R, 0) + \mathcal{O}(a^2(\log a)^k), \qquad (1.115)$$

i.e. the renormalized vertex functions differ from their continuum limits by terms $\mathcal{O}(a^2(\log a)^k)$ in k-loop order. Consequently, the Callan-Symanzik equation for these correlation functions will be

$$a\frac{d}{da}\Gamma_R^{(n)}(p_1, ..., p_n; \lambda_R, m_R, a) = \mathcal{O}(a^2(\log a)^k). \qquad (1.116)$$

The terms on the r.h.s. are the so called *scaling violations*: close to the continuum limit, these contributions are small and then can be neglected[17], and then it is possible to set the r.h.s equal to zero. Writing the renormalized vertex functions in (1.116) in terms of the bare ones, one obtains[18]

$$\left(a\frac{\partial}{\partial a} + \beta_{m_0}(\lambda_0, \hat{m}_0)\frac{\partial}{\partial \hat{m}_0} + \beta_{\lambda_0}(\lambda_0, \hat{m}_0)\frac{\partial}{\partial \lambda_0} + n\gamma_\phi\right)\Gamma^{(n)}(p_1, ..., p_n; \lambda_0, \hat{m}_0, a) = 0, \qquad (1.117)$$

where

$$\beta_{m_0}(\lambda_0, \hat{m}_0) = a\frac{d\hat{m}_0}{da},$$

$$\beta_{\lambda_0}(\lambda_0, \hat{m}_0) = a\frac{d\lambda_0}{da},$$

$$\gamma_\phi = \frac{1}{2}a\frac{d\log Z}{da},$$

are the β functions for the dimensionless couplings and field renormalization in terms of the cut-off scale a^{-1}. Equation (1.117) is a sort of Callan Symanzik equation for the bare vertex function.[19] Since Z is 1 at leading order, the contribution from the anomalous dimension γ_ϕ in (1.117) can be removed, and one can solve the following system of equations.

$$\left(a\frac{\partial}{\partial a} + \beta_{\hat{m}_0}(\lambda_0, \hat{m}_0)\frac{\partial}{\partial \hat{m}_0} + \beta_{\lambda_0}(\lambda_0, \hat{m}_0)\frac{\partial}{\partial \lambda_0}\right)\Gamma^{(2)}(p; \lambda_0, \hat{m}_0, a) = 0, \qquad (1.118)$$

$$\left(a\frac{\partial}{\partial a} + \beta_{\hat{m}_0}(\lambda_0, \hat{m}_0)\frac{\partial}{\partial \hat{m}_0} + \beta_{\lambda_0}(\lambda_0, \hat{m}_0)\frac{\partial}{\partial \lambda_0}\right)\Gamma^{(4)}(0, 0, 0, 0; \lambda_0, \hat{m}_0, a) = 0, \qquad (1.119)$$

with respect $\beta_{\hat{m}_0}$ and β_{λ_0}. Plugging equations (1.104) and (1.105) in the above system, one finds

$$\left(\lambda_0 - \frac{\beta_{\lambda_0}}{2}\right)\left(\frac{C_2\hat{m}_0^2}{a^2} - \frac{C_0}{a^2} - \frac{\hat{m}_0^2\log\left(\hat{m}_0^2\right)}{16\pi^2 a^2}\right) - \frac{2\hat{m}_0^2}{a^2} \qquad (1.120)$$

$$+ \beta_{\hat{m}_0}\left[\lambda_0\left(-\frac{C_2\hat{m}_0}{a^2} + \frac{\hat{m}_0\log\left(\hat{m}_0^2\right)}{16\pi^2 a^2} + \frac{\hat{m}_0}{16\pi^2 a^2}\right) + \frac{2\hat{m}_0}{a^2}\right] = 0, \qquad (1.121)$$

$$\beta_{\lambda_0}\left[\lambda_0\left(C_2 - \frac{3\log\left(\hat{m}_0^2\right)}{16\pi^2} - 16\pi^2\right) - 1\right] - \frac{3\lambda_0^2\beta_{\hat{m}_0}}{16\pi^2\hat{m}_0} = 0. \qquad (1.122)$$

The system can be solved using brute force, and at leading order in λ_0 gives

$$\beta_{\hat{m}_0} = \hat{m}_0 + \left(\frac{C_0}{2\hat{m}_0} - \frac{\hat{m}_0}{32\pi^2}\right)\lambda_0 + O\left(\lambda_0^2\right), \qquad (1.123)$$

$$\beta_{\lambda_0} = -\frac{3\lambda_0^2}{(4\pi)^2} + O\left(\lambda_0.^3\right) \qquad (1.124)$$

---

[17]In the previous perturbative analysis, this is mirrored by ignoring terms that vanish when $a \to 0$.

[18]In principle, equation (1.117) holds only when contributions from irrelevant couplings are also included, otherwise violations appear. To a first level of approximation, these violations can be neglected, and equation (1.117) used just to determine the running of relevant and marginal couplings.

[19]As a matter of fact, the real Callan Symanzik equation involves renormalized couplings and vertex functions
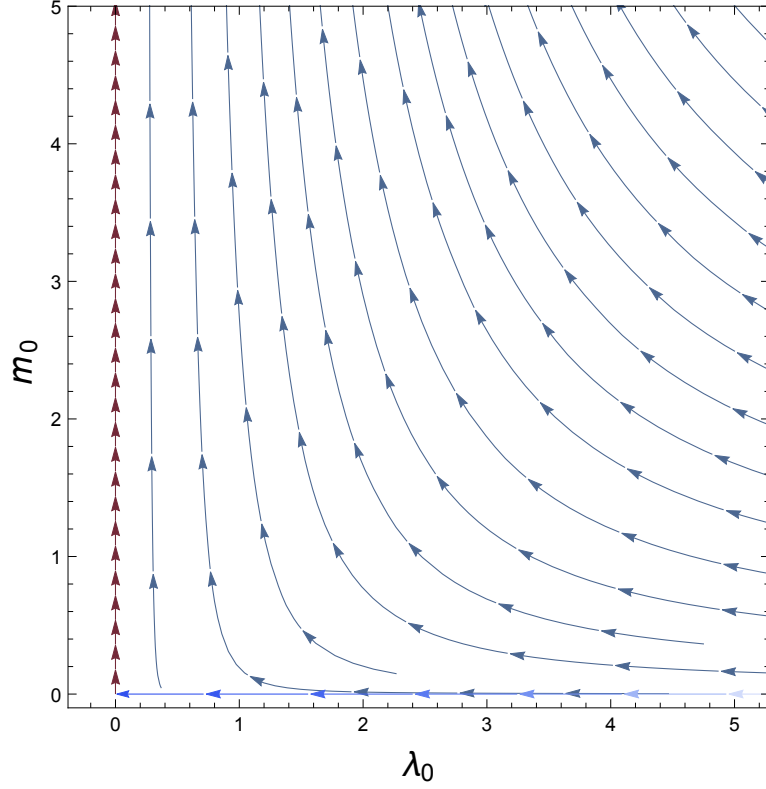
Figure 1.5: Qualitative plot of the RG flows in the (m_0, λ_0) plane. The arrows describes the vector field associated to RG trajectories evolving towards the infrared (increasing lattice spacing). As can be seen, the mass parameter is a relevant coupling for the Gaussian fixed point (as one could have expected on the basis of classical scaling), while the quartic coupling λ_0 is marginally irrelevant.

The above set of differential equations can be solved: ignoring the subleading $\mathcal{O}(\lambda_0)$ contribution to $\beta_{\hat{m}_0}$, the following identities are obtained

$$\hat{m}_0(a_1) = \frac{a_1}{a_2}\hat{m}_0(a_2), \tag{1.125}$$

$$\lambda_0(a_1) = \frac{\lambda_0(a_2)}{1 + \frac{3}{16\pi^2}\lambda_0(a_2)\log\frac{a_1}{a_2}}, \quad a_1 < a_2 \tag{1.126}$$

$$\tag{1.127}$$

which describes the perturbative RG flows of the dimensioless couplings.[20] From figure (1.5) one could see that the direction identifying λ_0 is "UV-repulsive" to the Gaussian fixed point: following the RG flows backward, it is impossible to reach the fixed point, because the bare coupling diverge. The only possible theory emanating from the Gaussian fixed point is represented by the free field one. This means that scalar theories in 4 dimensions are *trivial*. Looking at the RG group equations (1.125-1.126), one could estimate the value of the cut-off at which λ_0 diverges

$$a_1^* = a_2 e^{-\frac{(4\pi)^2}{3\lambda_0(a_2)}} \tag{1.128}$$

the value of a_1^* is called a *Landau Pole* for the coupling λ_0: the name is due to Landau, who first observed the triviality problem studying the QED coupling. Equation (1.128) tells that the only

---

[20]This result could have also been obtained in an easier way imposing $\hat{m}_0 = am_R$ in the $\mathcal{O}(\lambda_0)$, $\mathcal{O}(\lambda_0^2)$ terms of equations (1.104),(1.105)

possible way to let a_1 vanish is setting $\lambda_0(a_2)$ equal to zero, which effectively means to rule out the quartic interaction. However, the perturbative analysis shows a flaw in one aspect: as the lattice space is lowered down, the value of λ_0 increases: this means that perturbation theory will lose its reliability at a certain point. To gain a better knowledge of the RG flows in the non perturbative regime, other methods have to be employed.

Numerical investigations of the $\lambda\phi^4$ triviality have been performed by Lüscher and Weisz, who determined the RG flows of $O(n)$ scalar models both in perturbative and non perturbative regimes. The authors addressed the problem for $n = 1$ component fields [12, 13] and the general n case [14]. Combining results from the *high temperature expansion* with numerical integration of the Callan-Symanzik equations, the authors determined the renormalized trajectories (where λ_R is fixed) in the entire (m_0, λ_0) plane[21]. The outcome of their numerical study is that the only available RG fixed point is the Gaussian one, and is UV-repulsive. This implies that $O(n)$ scalar models with quartic interaction do not have a continuum limit, and can only be regarded as effective theories, bounded by a cut-off.

---

[21]Renormalized trajectories have been initially determined in the unbroken phase of the theory. Extensions to the broken phase have been done using mass perturbation theory.

Chapter 2

Renormalization of the energy momentum tensor

2.1 Introduction

This chapter focuses on the renormalization of the energy momentum tensor in QFT. The procedure is described using both continuum and lattice formulations. First, the definition of the conserved energy momentum tensor is given through the Ward Takahashi identities. Then, its renormalization is discussed and a continuum example is given. Finally, the lattice formulation of the problem, along with its related issues, is introduced. Some known results in lattice perturbation theory are presented and then a strategy for a non perturbative determination of the renormalized energy momentum tensor is discussed.

2.2 Ward-Takahashi Identities

Consider the following path integral in the continuum formulation

$$Z[J] = \int D[\phi] e^{-S + \int d^d y J_a \phi_a}, \tag{2.1}$$

where the index a could in principle represent a Lorentz index, or an internal index (like color in QCD), or a collection of both. The value of the path integral is clearly invariant under a change of the variable of integration $\phi_a(x) \to \phi_a(x) + \delta\phi_a(x)$. If the integration measure is left unchanged by the infinitesimal deformation $\delta\phi_a(x)$[1], the following identity holds

$$0 = \delta Z(J)$$

$$= \int D[\phi] e^{-S + \int d^d y J_a \phi_a} \int d^d y \left(-\frac{\delta S}{\delta\phi_b(y)} + J_b(y) \right) \delta\phi_b(y).$$

One now can take n functional derivatives with respect to $J_{a_j}(x_j)$ and set $J = 0$, to get

$$0 = \int D[\phi] e^{-S} \int d^d y \left[-\frac{\delta S}{\delta\phi_b(y)} \phi_{a_1}(x_1)...\phi_{a_n}(x_n) \right.$$

$$\left. + \sum_{j=1}^{n} \phi_{a_1}(x_1)...\delta_{b,a_j}\delta^d(y - x_j)...\phi_{a_n}(x_n) \right] \delta\phi_b(y). \tag{2.2}$$

---

[1]This point is crucial. If this condition is not fulfilled, then other terms appear, usually defined as *quantum anomalies*. A quite famous example is given by the $U(1)_A$ anomaly for chiral theories [44, 45, 46]

Differentiating both sides with respect $\delta\phi_a(x)$, one finally gets

$$\langle \frac{\delta S}{\delta\phi_a(x)}\phi_{a_1}(x_1)...\phi_{a_n}(x_n)\rangle = \sum_{j=1}^{n}\langle\phi_{a_1}(x_1)...\delta_{a,a_j}\delta^d(x-x_j)...\phi_{a_n}(x_n)\rangle. \tag{2.3}$$

These are the *Schwinger-Dyson equations* for the quantum theory: they simply state that classical equations of motions are satisfied by a quantum field inside correlation functions, as long as its space-time argument differs from those of all other fields

$$\langle \frac{\delta S}{\delta\phi_a(x)}\phi_{a_1}(x_1)...\phi_{a_n}(x_n)\rangle = 0 \quad \text{for} \quad x \neq x_{1,...,n}. \tag{2.4}$$

If this is not the case, extra *contact terms* arise, whose nature will be explained later. More information can be extracted from (2.2) when $\delta\phi_a(x)$ is a symmetry transformation of the classical theory. In this case, the Noether theorem has to be recalled: "To every differentiable symmetry generated by local actions, there corresponds a conserved current"

$$\delta\phi_a(x)\frac{\delta S}{\delta\phi_a(x)} = -\partial_\mu J_\mu. \tag{2.5}$$

If the field $\phi_a(x)$ satisfies the classical equation of motions, then the current J_μ is a conserved quantity. However, in the quantum theory, not only classical configurations contribute to the path integral. So, from equation (2.2), one infers

$$\langle\partial_\mu J_\mu(x)\phi_{a_1}(x_1)...\phi_{a_n}(x_n)\rangle = -\sum_{j=1}^{n}\langle\phi_{a_1}(x_1)...\delta\phi_{a_j}(x)\delta^d(x-x_j)...\phi_{a_n}(x_n)\rangle, \tag{2.6}$$

which are defined as the *Ward-Takahashi identities (WI)*. At the quantum level, the conservation of the Noether current holds inside correlation functions up to contact terms[2]. The specific form of these violations depends on the details of the infinitesimal (local) transformations. A different version of (2.6) is obtained by integrating both terms of the identity over a space-time volume Ω

$$\langle\int_{\partial\Omega} d\sigma_\mu J_\mu(x)\phi_{a_1}(x_1)...\phi_{a_n}(x_n)\rangle = -\sum_{j=1}^{n}\langle\phi_{a_1}(x_1)...\delta\phi_{a_j}(x_j)...\phi_{a_n}(x_n)\rangle, \tag{2.7}$$

where, on the left hand side, a surface integral over the boundary of Ω is obtained.[3] Equation (2.7) represents the global version of the Ward-Takahashi identities. A more general form of the WI can be derived coupling the source term in (2.1) to a generic operator $O_a(x) = O(\phi(x))_a$: in this case one gets

$$\langle\partial_\mu J_\mu(x)O_{a_1}(x_1)...O_{a_n}(x_n)\rangle = -\sum_{j=1}^{n}\langle O_{a_1}(x_1)...\delta_x O_{a_j}(x_j)...Oa_n(x_n)\rangle, \tag{2.8}$$

where

$$\delta_x O_{a_j}(x_j) = \int d^d z \frac{\delta O_{a_j}(x_j)}{\delta\phi_b(z)}\delta\phi_b(z)\delta^d(x-z). \tag{2.9}$$

The main feature of equation (2.8) is that composite operators enter in the definition of correlation functions. Such operators are built with fields coalescing at the same point, so they could generate contact terms too.

---

[2] Said in another way, the Ward-Takahashi identities probe the response of the theory under ultra-local infinitesimal diffeomorphism $\delta\phi_a(x)\delta^d(x-y)$.

[3] Usually, one requires fields to vanish at spatial infinity and sends $\Omega \to \infty$ in order to obtain an equation for the Noether charge $Q = \int d^{d-1}x J_0$.

At the quantum level, it is important to understand under which conditions the identities (2.6-2.8) hold. These equations involve correlation functions of fields and other complicated operators and will generate divergences in the bare theory. After having rewritten everything in terms of renormalized fields and parameters, one obtains

$$\langle \partial_\mu J_\mu(x) \phi_{R,a_1}(x_1)...\phi_{R,a_n}(x_n)\rangle \;\; = \;\; -\sum_{j=1}^{n} \langle \phi_{R,a_1}(x_1)...\delta\phi_{R,a_j}(x)\delta^d(x - x_j)...\phi_{R,a_n}(x_n)\rangle, \quad (2.10)$$

which is an expression that still contains divergences arising from the insertion of $J_\mu(x)$ and $\delta\phi_{R,a_j}(x)$: these operators usually represent vertices that are not present in the action of the theory, and whose divergences need to be subtracted.

Both sides of (2.10) can be proved to be finite, if the following conditions are satisfied:

1. the regularized action and path integral measure are invariant under the transformation described by $\delta\phi_{R,a_j}(x)$;

2. the symmetry transformation $\delta\phi_{R,a_j}(x)$ is linear in the fundamental fields.

If this two conditions are satisfied, then, integrating equation (2.10) over a small sphere Ω centered around one of the fields, the following identity holds

$$\int_{\partial\Omega_{x_j}} d\sigma_\mu \langle J_\mu(x)\phi_{R,a_1}(x_1)...\phi_{R,a_n}(x_n)\rangle \;\; = \;\; -\langle \phi_{R,a_1}(x_1)...\delta\phi_{R,a_j}(x_j)...\phi_{R,a_n}(x_n)\rangle \quad j = 1,...,n,$$

$$(2.11)$$

In the above equation, none of the fields but $\phi_{R,a_j}(x_j)$ are contained in the sphere Ω_{x_j}. On the r.h.s. no divergence can be produced, since the variation $\delta\phi_{R,a_j}(x_j)$ is proportional to the renormalized field. This is true for all the field inserted. Hence the r.h.s. of (2.10) is finite and, as a consequence, also $\partial_\mu J_\mu$[4].

Whenever the conditions (1-2) do not hold, then the insertion of $J_\mu(x)$ and $\delta\phi_{R,a_j}(x)$ generate divergences that need to be subtracted. In this case, a set of counterterms, to make both sides of (2.10) finite, is needed. The role of these counterterms will be that of defining new *renormalized operators* $(J_\mu)_R$ and $(\delta\phi_{R,a_j}(x_j))_R$, whose insertions in the Ward-Takahashi identities are free from any UV divergence. The process of determining the right counter terms is called *renormalization of composite operators* and it will be discussed in the following section.

It should be stressed that the whole procedure works if the field insertions in (2.10) are taken at separate space-time points. If this is not the case, then the arising contact terms produce further divergences. This is a situation that is better to avoid, since it makes the renormalization of the operator J_μ and $\delta\phi_{R,a_j}(x_j)$ harder.

In this work, a specific composite operator has been studied: the Energy Momentum Tensor (EMT) of the quantum theory.

Classically, the EMT is the generator of infinitesimal translations, and is related to the Noether current J_μ by

$$\alpha_\mu T_{\mu\nu} = J_\nu, \quad (2.12)$$

where α_μ is a vector parametrizing the direction of an infinitesimal translation. More generally, the EMT is related to a larger class of fundamental space-time symmetries. The latter, for a non-zero

---

[4]J_μ can still contain a divergent contribution K_μ with vanishing total divergence $\partial_\mu K_\mu$.

spin field theory, are described by

$$\delta_\alpha \phi_a(x) = \alpha_\mu \partial_\mu \phi_a(x) \qquad\qquad \text{translations,} \quad (2.13)$$

$$\delta_\alpha \phi_a(x) = \frac{\alpha_{\mu\nu}}{2}[(x_\mu \partial_\nu - x_\nu \partial_\mu)\delta_{ab} + (S_{\mu\nu})_{ab}]\phi_b(x) \qquad\qquad SO(d), \quad (2.14)$$

$$\delta_\alpha \phi_a(x) = \alpha(d_\phi + x_\rho \partial_\rho)\phi_a(x) \qquad\qquad \text{dilatation,} \quad (2.15)$$

$$\delta_\alpha \phi_a(x) = \alpha_\mu[(x^2 \partial_\mu - 2x_\mu x_\nu \partial_\nu - 2d_\phi x_\mu)\delta_{ab} - 2x_\nu (S_{\mu\nu})_{ab}]\phi_b(x) \qquad \text{special conformal,} \quad (2.16)$$

where ϕ_a transforms according to a given representation of $SO(d)$, spanned by the index a. The matrices $(S_{\mu\nu})_{ab}$ are the generators of the group in such representation.

To each of the previous symmetries corresponds a (canonical) Noether current[5], given by [16]

$$(T_{\mu\nu})_c = \frac{\partial \mathcal{L}}{\partial(\partial_\mu \phi_a)}\partial_\nu \phi_a - \delta_{\mu\nu}\mathcal{L}., \qquad (2.17)$$

$$(\mathcal{M}_{\nu\mu\lambda})_c = [x_\nu(T_{\mu\lambda})_c - x_\lambda(T_{\mu\nu})_c] + (\Pi_\mu)_b(S_{\nu\lambda})_{bc}\phi_c(x), \qquad (2.18)$$

$$(D_\mu)_c = x_\rho(T_{\rho\mu})_c + d_\phi(\Pi_\mu)_b\phi_b(x), \qquad (2.19)$$

$$(K_{\lambda\mu})_c = [2x_\lambda x_\nu - \delta_{\lambda\nu}x^2](T_{\mu\nu})_c + 2x_\nu(\Pi_\mu)_b[\delta_{\nu\lambda}\delta_{bc}d_\phi - (S_{\nu\lambda})_{bc}]\phi_c(x) - 2\sigma_{\lambda\mu}, \qquad (2.20)$$

$$\partial_\beta \sigma_{\alpha\beta} = (\Pi_\beta)_b[\delta_{\alpha\beta}\delta_{bc}d_\phi - (S_{\alpha\beta})_{bc}]\phi_c(x), \qquad (2.21)$$

where

$$(\Pi_\mu)_a = \frac{\partial \mathcal{L}}{\partial(\partial_\mu \phi_a)}, \qquad (2.22)$$

and $(T_{\mu\nu})_c$ represents the canonical EMT. Unless spin-zero fields are concerned, the canonical EMT (2.17) is usually not symmetric under the exchange of indices. A corresponding symmetrized form can be obtained using the fact that the EMT is always defined up to terms with vanishing four-divergence

$$(T_{\mu\nu})_{imp} = (T_{\mu\nu})_c + O_{\mu\nu}, \qquad (2.23)$$

$$\partial_\mu O_{\mu\nu} = 0, \qquad (2.24)$$

where on the l.h.s an *improved* EMT has been defined. When a theory with non zero spin field is considered, the following tensor

$$(T_{\mu\nu})_B = (T_{\mu\nu})_c + \partial_\beta X_{\beta\mu\nu}, \qquad (2.25)$$

$$X_{\beta\mu\nu} = \frac{1}{2}\left[(\Pi_\beta)^a(S_{\mu\nu})^{ab}\phi^b - (\Pi_\mu)^a(S_{\beta\nu})^{ab}\phi^b - (\Pi_\nu)^a(S_{\beta\mu})^{ab}\phi^b\right] \qquad (2.26)$$

is symmetric and defines an improved conserved current for $SO(d)$ rotations

$$\mathcal{M}_{\nu\mu\lambda} = [x_\nu(T_{\mu\lambda})_B - x_\lambda(T_{\mu\nu})_B]. \qquad (2.27)$$

Here $(T_{\mu\nu})_B$ is defined as the *Belinfante* tensor [47]. In terms of (2.27), the generators of the $SO(d)$ group can be easily determined

$$M_{\mu\lambda} = \int d^{d-1}x \mathcal{M}_{0\mu\lambda}. \qquad (2.28)$$

Another improved version of the EMT is obtained when invariance under dilatations is studied. Rewriting the canonical current (2.19) in terms of the Belinfante EMT, one obtains

$$D_B^\mu = x_\nu(T^{\mu\nu})_B + V^\mu, \qquad (2.29)$$

$$V_\mu = \Pi_\rho^a\left[\delta^{ab}\delta_{\rho\mu}d_\phi - (S_{\rho\mu})^{ab}\right]\phi^b, \qquad (2.30)$$

---

[5]In literature, Noether currents are defined disregarding the infinitesimal parameters that define the symmetry transformation.

up to terms whose four-divergence vanishes. The term on the second line is called *field virial*. An improved EMT can be defined provided the field virial can be rewritten as a total divergence

$$V_\mu = \partial_\alpha \sigma_{\mu\alpha}. \tag{2.31}$$

If the above condition is verified, the improved EMT is given by the following definition

$$T_{\mu\nu} = (T_{\mu\nu})_B + \frac{1}{2}\partial_\rho\partial_\lambda X^{\lambda\rho\mu\nu}, \tag{2.32}$$

where

$$X^{\lambda\rho\mu\nu} = \delta_{\lambda\rho}\sigma_+^{\mu\nu} - \delta_{\lambda\mu}\sigma_+^{\rho\nu} - \delta_{\lambda\nu}\sigma_+^{\mu\rho} + \delta_{\mu\nu}\sigma_+^{\lambda\rho} - \frac{1}{3}\delta_{\lambda\rho}\delta_{\mu\nu}\sigma_+^{\beta\beta} + \frac{1}{3}\delta_{\lambda\mu}\delta_{\rho\nu}\sigma_+^{\beta\beta} \tag{2.33}$$

and

$$\sigma_+^{\mu\nu} = \tfrac{1}{2}(\sigma^{\mu\nu} + \sigma^{\nu\mu}), \tag{2.34}$$

$$\sigma_-^{\mu\nu} = \tfrac{1}{2}(\sigma^{\mu\nu} - \sigma^{\nu\mu}). \tag{2.35}$$

This new EMT is symmetric and defines improved currents both for dilatations and conformal transformations

$$D_\mu = x_\rho T_{\rho\mu}, \tag{2.36}$$

$$K_{\lambda\mu} = [2x_\lambda x_\nu - \delta_{\lambda\nu}x^2]T_{\mu\nu}. \tag{2.37}$$

In section (2.4), an example of improved EMT will be given for a $\lambda\phi^4$ scalar theory. The interesting feature of equations (2.36-2.37) is that the conservation of dilatation and conformal currents is related to the trace of the EMT [6]

$$\partial_\mu D_\mu = T_{\mu\mu}, \tag{2.38}$$

$$\partial_\mu K_{\lambda\mu} = 2x_\lambda \partial_\mu D_\mu. \tag{2.39}$$

When theories with local internal symmetries are considered, the Belinfante improvement is not sufficient to define a symmetric EMT satisfying such symmetries. The same statement holds also for the improvement related to dilatations. A conserved current with the correct symmetry properties can be obtained by requiring invariance under a more general transformation. The latter is a composition of a local space-time transformation and internal symmetry transformations that leaves the action unchanged. A clear example will be given in section (2.6.2), where the EMT for gauge theories is considered[7].

When derived from the path integral, the WIs for space-time symmetries involve the Noether currents written in terms of the canonical EMT. With some manipulation, it is always possible to rewrite these identities in terms of the classically improved operator. For example, the Dilatation Ward identities (DWI) take the following form [16]

$$\delta_{\mu\nu}\langle T_{\mu\nu}(x)\phi_{a_1}(x_1)...\phi_{a_n}(x_n)\rangle$$

$$= \langle T_{\mu\mu}(x)\phi_{a_1}(x_1)...\phi_{a_n}(x_n)\rangle - d_\phi \sum_{j=1}^{n}\delta^d(x - x_j)\langle\phi_{a_1}(x_1)...\phi_{a_n}(x_n)\rangle, \tag{2.41}$$

---

[6]Indeed, it can be shown [16] that the condition for expressing the dilatation current as in (2.36) also guarantees conformal invariance.

[7]There is also an easier way to obtain the improved energy momentum tensor. If the original QFT is coupled to gravity, then the EMT can be found varying the action with respect the metric $g_{\mu\nu}(x)$

$$\Theta_{\mu\nu} = \frac{\delta S}{\delta g_{\mu\nu}(x)}. \tag{2.40}$$

The resulting $\Theta_{\mu\nu}$ will be symmetric by construction and will also preserve all the internal symmetries of the theory (like gauge invariance, for example). This happens because the variation in (2.40) acts on the geometry of the system, leaving the internal symmetries unchanged.

where the first insertion on the r.h.s. includes terms that could violate the symmetry at the classical level. These terms are identified by having dimensionful couplings[8].

From a classical point of view, a EMT with vanishing trace describes a scale invariant theory, as can be seen from equation (2.38). At the quantum level, this is not true anymore. Even if dimensionful couplings are absent, a scale dependence on dimensionless couplings is induced by the renormalization of the quantum theory.

In the perturbative regime, this is quantitatively described by the so-called *trace anomaly*, which directly relates the renormalized trace of the EMT to the beta functions of the quantum theory. A simple example of trace anomaly can be found in non abelian gauge theories

$$(T_{\mu\mu})_R = \frac{\beta(g_R)}{g_R(\mu)^3}(\text{tr}\{F_{\mu\rho}F_{\mu\rho}\})_R, \tag{2.42}$$

where g_R denotes the renormalized coupling of the theory. Equation (2.42) tells that the trace of the EMT yields information about possibly existing RG fixed points. Indeed, the latter could be identified by a theory whose renormalized EMT has vanishing trace.

Non perturbatively, the above statement does not hold, since equation (2.42) loses its validity. However, RG fixed points could still be determined by studying the space-time symmetries of the system. Indeed, RG fixed points denote theories which are invariant under scale transformations. Such invariance should be mirrored in the corresponding DWI. Non perturbative studies of the latter can be performed only if the fully renormalized EMT has been previously determined. Hence, knowledge of the renormalized EMT is crucial to probe a fundamental property of quantum theories, both in perturbative and non perturbative regimes.

Moreover, the renormalized EMT can also be used for other physical applications. For example, it is fundamental for the determination of extensive quantities, like[9]

- pressure density
$$\langle \epsilon - 3p \rangle_T = - \langle T_{\mu\mu} \rangle_T. \tag{2.43}$$

- entropy density
$$\langle s \rangle_T = \left(- \langle T_{00} \rangle_T + \sum_{i=1}^{3} \langle T_{ii} \rangle_T \right) /T. \tag{2.44}$$

These observables enter in the equations of state of a thermodynamic system, and their numerical determination is important, especially in non perturbative regimes.

Another physical application consists in the determination of the shear viscosity

$$\eta = \pi \lim_{\omega \to 0} \text{Im} \left\{ \left[i \int_0^\infty dt e^{i\omega t} \int d^3x \left\langle T_{12}(t,x)T^{12}(0,0) \right\rangle_T \right] \right\}, \tag{2.45}$$

which expresses the resistance of a fluid to shearing flows, where adjacent layers move parallel to each other with different speeds. This quantity is crucial in describing the dynamic of hot, dense matter (Quark Gluon Plasma) in heavy ion collisions.

These few examples should have made quite clear why the renormalized EMT plays a key role in different aspects of QFT. The latter can be quantitatively determined only if a proper renormalization procedure has been established. As it will become clear in the following, the renormalization of this operator can be performed using the WI for space-time symmetries.

---

[8]Equation (2.41) shows that the trace operation does not commute with taking expectation values. This is because the regularized theory *is not* scale invariant, even if dimensionful couplings are excluded.

[9]All these quantities are defined subtracting the expectation value of the EMT at zero temperature.

2.3   Renormalization of composite operators

As already mentioned, a composite operator consists of a product of elementary fields (and their derivatives) at the same space-time point. At tree level, its insertion can be seen as a new kind of vertex that, in principle, is not present in the action of the theory. For example, the operator ϕ^2 can be described by the following Feynman graph

$$\frac{1}{2}\langle\phi(x)\phi^2(0)\phi(y)\rangle = \qquad\qquad\qquad\qquad (2.46)$$

at tree level, in coordinate space. When loop corrections are included, UV divergences arise. In principle, these divergences are not the same that appear in the Green's functions of elementary fields. To make expectation values of ϕ^2 finite, an *ad hoc* renormalization is needed. This is performed looking for appropriate counterterms for the insertion of ϕ^2. In the perturbative regime, this procedure can be carried out order by order in the couplings of the theory. For example, the 1-loop renormalization of $\frac{1}{2}\phi^2$ for a $g\phi^3$ theory in 6 dimensions [15] is given by

$$\frac{1}{2}(\phi^2)_R = \left[1 - \frac{g^2}{64\pi^3\epsilon}\right]\frac{1}{2}\phi^2 - \frac{g\mu^{-\epsilon/2}}{64\pi^3\epsilon}(m^2 + \frac{1}{6}\Box)\phi + \mathcal{O}(g^3), \qquad (2.47)$$

where dimensional regularization ($d = 6 - \epsilon$) has been adopted. The renormalized operator is represented by a sum of bare operators coupled to divergent coefficients. The first thing to note is that the operators that enter in the definition of ϕ_R^2 have dimension smaller than or equal to the original operator ϕ^2. Moreover, the only operators of such dimension are those actually appearing in (2.47). The renormalization (2.47) can also be written as a matrix equation

$$\begin{pmatrix} \frac{1}{2}(\phi^2)_R \\ \phi_R \\ \Box\phi_R \end{pmatrix} = \begin{pmatrix} Z_a & \mu^{-\epsilon/2}Z_b m^2 & \mu^{-\epsilon/2}Z_c \\ 0 & Z_\phi & 0 \\ 0 & 0 & Z_\phi \end{pmatrix} \times \begin{pmatrix} \frac{1}{2}(\phi^2) \\ \phi \\ \Box\phi \end{pmatrix}, \qquad (2.48)$$

where the values of $Z_{a,b,c}$ can be read off from equation (2.47). In this case, the operators ϕ, $\Box\phi$ are said to mix with ϕ^2 under renormalization, because the matrix (2.48) is not diagonal. In a more general form, a renormalized composite operator A_R is given by

$$A_R = \sum_B Z_{AB} B, \qquad (2.49)$$

the sum running over all the operators that

- have dimension $d_B \leq d_A$

- have the same $SO(d)$ structure of A

- transform as A under the action of a given internal symmetry

The (possibly divergent) entries of the matrix Z_{AB} are called the renormalization constants of the operator A_R. In perturbation theory, these constants are determined from the renormalization of the operator insertions, at a given order in the couplings. Non perturbatively, their determination is achieved through the imposition of specific renormalization conditions.

The role of symmetries is crucial to constrain the operators that could mix with A and then minimize their number. However, these symmetries are usually derived from the regularized theory; some of these could be broken by a specific regularization, and will be restored only after the regulator has

been removed. As a consequence, the number of mixing operators could increase in the regularized theory. A clear example is given by the lattice regulator and space-time symmetries, as it will be explained later. Other interesting properties of renormalized composite operators are [10]

- *Linearity*

$$aA_R + bB_R = (aA + bB)_R. \tag{2.50}$$

The above equation has to be intended inside Green's functions.

$$a\langle A_R X \rangle + b\langle B_R X \rangle = \langle (aA + bB)_R X \rangle, \tag{2.51}$$

where X is a product of fields and their derivatives.

- *Differentiation is distributive.* Suppose A is a composite operator

$$A = \prod_{j=1}^{n} \phi_j(x), \tag{2.52}$$

where $\phi_j(x)$ is an elementary field or one of its derivative. Then

$$\frac{\partial}{\partial x_\mu} A_R = \left(\frac{\partial}{\partial x_\mu} A \right)_R, \tag{2.53}$$

where, again, the equation makes sense only inside correlation functions.

- *Ward Identities.* If the Noether current, as well as classical violation terms, are rewritten in terms of their renormalized counterparts, then the renormalized WI hold

$$\partial_\mu \langle (J_\mu^b)_R X \rangle_R = \langle (\Delta^b)_R T \rangle + \left\langle \delta_b \phi(x) \frac{\delta X}{\delta \phi(x)} \right\rangle_R, \tag{2.54}$$

where the subscript b means that transformations of the bare action are considered. The above equation plays a fundamental role in the definition of renormalized Noether currents. It can be used to determine the renormalization constants of J_μ both in perturbative and non perturbative regimes.

- *Non renormalization of current.* Under certain assumptions, it can be proved that Noether currents do not renormalize at all.
  To show this, let consider a quantum theory, whose bare action is invariant under a given symmetry transformation. To the latter a classically conserved Noether current corresponds. Then, two basic conditions need to be satisfied (cfr. (1)-(2)):

  1. the symmetry is preserved by the regularized theory;

  2. the symmetry transformation is linear in the fundamental fields.

If these two conditions are verified, then it can be proved that $\partial_\mu J_\mu$ is finite (cfr. section (2.2)): however, nothing guarantees the finiteness of J_μ. The latter could still be defined up to a divergent term K_μ whose total derivative vanishes. The form of K_μ depends on the symmetry under study and on the dimensions of the system. In the following, the case of four space-time dimensions is considered.

---

[10] The proofs of the above properties can be found in [15].

– *Internal symmetry*: in this case K_μ is an operator with mass dimension 3, and takes the following form

$$K_\mu = \alpha_\nu[\partial_\mu\partial_\nu - \Box\delta_{\mu\nu}]O(x), \tag{2.55}$$

with α_ν a dimensionless vector. The operator $O(x)$ contains only matter fields. Since K_μ has dimension 3, $O(x)$ can only be proportional to a single scalar field

$$K_\mu = \alpha_\nu[\partial_\mu\partial_\nu - \Box\delta_{\mu\nu}]\phi(x), \tag{2.56}$$

where ϕ is complex or real. Noether currents for internal symmetries are hermitean, and always invariant under phase transformations, being quadratic in the matter fields. For complex scalar fields, these properties cannot be satisfied by (2.56): for real fields, the same statement holds if the Z_2 symmetry is used. Hence, J_μ cannot mix with divergent terms with zero total derivative, and the following identity holds

$$(J_\mu)_R = J_\mu. \tag{2.57}$$

– *Space-time symmetry*: the operator K_μ has the same form as in (2.55). However, it has mass dimension 4, a fact that allows different types of fields to be included

$$K_\mu = \alpha_\nu[\partial_\mu\partial_\nu - \Box\delta_{\mu\nu}]O(x), \tag{2.58}$$
$$O(x) = \phi^2(x), \phi^\dagger\phi... \qquad\qquad \text{matter fields}, \tag{2.59}$$
$$O(x) = A_\rho A_\rho \qquad\qquad \text{gauge fields}, \tag{2.60}$$
$$O(x) = \bar{c}c \qquad\qquad \text{ghost fields}. \tag{2.61}$$

Combinations described by (2.59-2.60-2.61) provide a K_μ with the same properties of the usual Noether currents of space-time symmetries, and cannot be ruled out. A clear example will be given in section (2.4), where the renormalization of the EMT for a $\lambda\phi^4$ theory is considered.

The term described by (2.60) and (2.61) are in principle allowed when theories with a gauge fixing are investigated. In this case, one can still use BRST symmetry to check if some of these contributions can be excluded.

When gauge invariant theories are considered, a gauge invariant EMT can be formulated using a properly generalized symmetry transformation. In this case, the terms in (2.59-2.60-2.61) can be ruled out and the corresponding bare Noether current does not renormalize[11].

Coming back to the EMT, it should be clear that a renormalized form of this operator can be obtained imposing equation (2.54). Given the renormalized EMT as[12]

$$(T_{\mu\nu})_R = \sum_{i=1}^{n} Z_i(T_{\mu\nu}^{(i)} - \langle T_{\mu\nu}^{(i)}\rangle), \tag{2.62}$$

then, if the space-time symmetries are exact and not broken by the regulator, the renormalization constants can be obtained by imposing space-time WI. For example, the WI for translation invariance can be applied

$$\langle\partial_\mu\sum_{i=1}^{n} Z_i T_{\mu\nu}^{(i)}\phi_{R,a_1}(x_1)...\phi_{R,a_n}(x_n)\rangle =$$
$$= -\sum_{j=1}^{n}\langle\phi_{R,a_1}(x_1)...\partial_\nu\phi_{R,a_j}(x)\delta^d(x-x_j)...\phi_{R,a_n}(x_n)\rangle. \tag{2.63}$$

---

[11] The corresponding VEV needs always to be subtracted.

[12] When the renormalized operator is defined, also a possible mixing with the identity has to be considered.

In this case, one would need just a set of n TWIs, as many as the mixing operators, and could solve the system with respect the renormalization constants Z_i. It should be stressed that this procedure can be performed only if

- The arguments of each field insertion are separated, otherwise contact terms arise. In the latter case, one has to take care separately of the divergences related to $T_{\mu\nu}$ and those related to fields coalescing in the same point. From the point of view of equation (2.8), this means that each operator $O_a(x_i)$ has to be substituted by its renormalized counterpart, as well as the variation $\delta_x O_{a_j}(x_j)$. After this, the renormalization of the EMT can be take into account.

- The arguments of each field (or operator, if one is using (2.8)) have to be different from that of the EMT. If this is not the case, then another kind of contact term appears. One will have to renormalize the operator given by the product of the EMT and a collection of fields (or operators). A possible example is represented by

$$O(x)_{\mu\nu} = T_{\mu\nu}(x)\phi^2(x).\tag{2.64}$$

This is an operator of dimension $d_T + 2d_\phi$, defined by a different mixing with respect $T_{\mu\nu}$. Clearly this is not the operator that one wants to renormalize.

In the following section, an example of renormalized EMT, using continuum formulation, is provided.

2.4   Renormalized EMT: a continuum example

To give an idea of how the renormalization of the EMT has been implemented, an example in the continuum will be rapidly shown. The theoretical framework is a $\lambda\phi^4$ theory in 4 space-time dimensions. For this theory, the renormalization of the EMT has been addressed by Coleman, Callan and Jackiw [17]. They provided an improved version of the energy momentum tensor that does not need any kind of renormalization, beside the ones coming from the underlying theory. The Lagrangian density of the theory is

$$\mathcal{L} = \frac{1}{2}\partial_\mu\phi\partial_\mu\phi + \frac{m_0^2}{2}\phi^2 + \frac{\lambda_0}{4!}\phi^4.\tag{2.65}$$

The improved operator is given by

$$\Theta_{\mu\nu} = (T_{\mu\nu})_c - \frac{1}{6}(\partial_\mu\partial_\nu - g_{\mu\nu}\square)\phi^2, \quad \Theta_{\mu\nu} = \Theta_{\nu\mu},\tag{2.66}$$

where $(T_{\mu\nu})_c$ is the canonical EMT, given by equation (2.17). The first thing to note is that the extra term on the l.h.s of (2.66) does not violate the conservation of the current. The second detail to appreciate, is that the dilatation current can be written elegantly as

$$D_\mu = x_\nu\Theta_{\mu\nu}.\tag{2.67}$$

This is a consequence of a general result: the canonical dilatation current is

$$(D_\mu)_c = x_\nu(T_{\mu\nu})_c + V_\mu,\tag{2.68}$$
$$V_\mu = \Pi_\mu(x)\phi(x),\tag{2.69}$$
$$\Pi_\mu = \frac{\partial\mathcal{L}}{\partial(\partial_\mu\phi)}.\tag{2.70}$$

The term V_μ is called the *field virial*. The reason behind this nomenclature is that V_μ consists of the product between the field momentum Π_μ and the field ϕ, a structure analogous to the virial in non-relativistic Lagrangian theory[13]. It can be easily proved that the vanishing of the trace of $(T_{\mu\nu})_c$ does not ensure scale invariance

$$\partial_\mu D_\mu = (T_{\mu\mu})_c + \partial_\mu V_\mu, \tag{2.71}$$

however, if the field virial is a total divergence

$$V_\mu = \partial_\xi \sigma_{\xi\mu}, \tag{2.72}$$

further simplifications can be obtained. The following substitution has to be adopted

$$\Theta_{\mu\nu} = (T_{\mu\nu})_c + \frac{1}{2}\partial_\rho\partial_\lambda X^{\lambda\rho\mu\nu}, \tag{2.73}$$

where

$$X^{\lambda\rho\mu\nu} = \delta_{\lambda\rho}\sigma_+^{\mu\nu} - \delta_{\lambda\mu}\sigma_+^{\rho\nu} - \delta_{\lambda\nu}\sigma_+^{\mu\rho} + \delta_{\mu\nu}\sigma_+^{\lambda\rho} - \frac{1}{3}\delta_{\lambda\rho}\delta_{\mu\nu}\sigma_+^{\beta\beta} + \frac{1}{3}\delta_{\lambda\mu}\delta_{\rho\nu}\sigma_+^{\beta\beta} \tag{2.74}$$

and

$$\sigma_+^{\mu\nu} = \tfrac{1}{2}(\sigma^{\mu\nu} + \sigma^{\nu\mu}), \tag{2.75}$$
$$\sigma_-^{\mu\nu} = \tfrac{1}{2}(\sigma^{\mu\nu} - \sigma^{\nu\mu}). \tag{2.76}$$

Substituting for $(T_{\mu\nu})_c$, one finds

$$D_\mu = x_\nu\Theta_{\mu\nu} - \frac{1}{2}\partial_\rho\partial_\lambda(X^{\lambda\rho\mu\nu}x_\nu) + \partial_\beta\sigma_-^{\mu\beta}. \tag{2.77}$$

Since the last two terms have zero divergence, they can be dropped, allowing to recover equation (2.67). What is really interesting is that the condition (2.72) is also the one that allows the theory to be conformal invariant [16]. In their work, Coleman, Callan and Jackiw proved that the space-time WI are fully satisfied (i.e. free from any divergence) only if the renormalized EMT is represented by $\Theta_{\mu\nu}$. This means that the canonical EMT, $(T_{\mu\nu})_c$, which is derived from a variation of the basic action, does not suffice to make all the possible insertions finite when the cut-off is removed. This is exactly one of the cases that has been presented in (2.59).[14] They proved the finiteness of $\Theta_{\mu\nu}$ using a combination of translation and dilatation Ward Identities:

$$\partial_\mu\langle\Theta_{\mu\nu}(x)\phi_{a_1}(x_1)...\phi_{a_n}(x_n)\rangle = -\sum_{j=1}^n \delta^d(x-x_j)\langle\phi_{a_1}(x_1)...\partial_\mu\phi_{a_j}(x_j)...\phi_{a_n}(x_n)\rangle, \tag{2.78}$$

$$\delta_{\mu\nu}\langle\Theta_{\mu\nu}(x)\phi_{a_1}(x_1)...\phi_{a_n}(x_n)\rangle$$
$$= \langle\Theta_{\mu\mu}(x)\phi_{a_1}(x_1)...\phi_{a_n}(x_n)\rangle - \sum_{j=1}^n \delta^d(x-x_j)\langle\phi_{a_1}(x_1)...\phi_{a_n}(x_n)\rangle, \tag{2.79}$$

In momentum space, these identities take the following form

$$k_\mu\Gamma_{\mu\nu}^{(n)}(k;p_1,...,p_n) = -\sum_P (p_1+k)_\nu G^{(n)}(p_1+k,p_2,...,p_n), \tag{2.80}$$

$$\delta_{\mu\nu}\Gamma_{\mu\nu}^{(n)}(k;p_1,...,p_n) = \Gamma^{(n)}(k;p_1,...,p_n) - \sum_P G^{(n)}(p_1+k,p_2,...,p_n), \tag{2.81}$$

---

[13]When non-zero spin fields are included, the field virial acquires also a contributions from the Lorentz generators,as can be seen in eqs (2.18-2.19-2.20).

[14]Said in another way, the canonical EMT can only renormalize the translation WI, but not the identities related to dilatation invariance.

where $\Gamma_{\mu\nu}^{(n)}$ is the insertion of the EMT, $\Gamma^{(n)}$ the insertion of its trace and $G^{(n)}$ is the n-point correlation function. The sum in the above equations is on the ciclic permutations of the indices 1 to n. Another equation that has been used is the following corollary

$$\Gamma_{\mu\nu}^{(n)}(0; 0, ..., 0) = -(n-1)\delta_{\mu\nu}G^{(n)}(0, ..., 0), , \tag{2.82}$$

which can be obtained deriving (2.80) with respect k_μ and then setting all momenta to zero. Using the BPH approach [48], the authors started from the analysis of the trace term whose form is, using the equation of motion

$$\Theta_{\mu\mu} = m^2\phi^2. \tag{2.83}$$

One of the advantages of using the operator $\Theta_{\mu\nu}$ is that the violation of scale invariance is characterized by a single operator, which is close under renormalization[15], i.e.

$$(\Theta_{\mu\mu})_R = Z_0\Theta_{\mu\mu}. \tag{2.84}$$

The renormalization constant can be fixed imposing

$$\Gamma^{(2)}(0; 0, 0) = Z_0, \tag{2.85}$$

however, from equations (2.81-2.82) follows

$$\Gamma^{(2)}(0; 0, 0) = -2G^{(2)}(0, 0). \tag{2.86}$$

Since $G^{(2)}(0, 0)$ is finite, then also c is. This means that all the insertions of $\Theta_{\mu\mu}$ are finite. For the non-diagonal components, the operator mixing is defined by

$$\{\delta_{\mu\nu}\phi^2, \delta_{\mu\nu}\partial_\lambda\phi\partial_\lambda\phi, \delta_{\mu\nu}\phi\Box\phi, \partial_\mu\phi\partial_\nu\phi, \phi\partial_\nu\partial_\mu\phi, \delta_{\mu\nu}\phi^4\} \tag{2.87}$$

which represents a closed set under renormalization. The bare operator $\Theta_{\mu\nu}$ is just a linear combination of these operators. Therefore, a proper counterterm for it could be given by

$$(\Theta_{\mu\nu})_{CT} = \sum_{i=1}^{6} Z_i O_{\mu\nu}^{(i)}. \tag{2.88}$$

According to the BPH procedure, the Z_i can be chosen in order to cancel the first relevant terms[16] in the Taylor expansion of divergent diagrams about the point zero (which is identified by zero external momenta). This means that the coefficients Z_i could be, in principle, divergent. The renormalized operator could then be given by

$$(\Theta_{\mu\nu})_R = \Theta_{\mu\nu} + \sum_{i=1}^{6} Z_i O_{\mu\nu}^{(i)} = \sum_{i=1}^{6} \tilde{Z}_i O_{\mu\nu}^{(i)} \tag{2.89}$$

To show the finitess of $\Theta_{\mu\nu}$, the key point is to prove that the coefficients $\tilde{Z}_i$ are finite. The counterterms can be chosen such that the two and four point insertions obey

$$\Gamma_{\mu\nu}^{(2)}(k; p_1, p_2) = \delta_{\mu\nu}(\tilde{Z}_1 + \tilde{Z}_2 q^2 + \tilde{Z}_3 k^2) + \tilde{Z}_4(k_\mu k_\nu - \delta_{\mu\nu}k^2) + \tilde{Z}_5 q_\mu q_\nu + ... \tag{2.90}$$

$$\Gamma_{\mu\nu}^{(4)}(0; 0, 0, 0, 0) = \tilde{Z}_6\delta_{\mu\nu}, \tag{2.91}$$

with triple dots indicating higher terms and $q = p_1 - p_2$. Equation (2.80) tells that $k_\mu\Gamma_{\mu\nu}^{(n)}$ is finite, since the r.h.s. does not diverge when everything is written in terms of renormalized fields. As a consequence, one has that

$$(\tilde{Z}_1 + \tilde{Z}_2 q^2 + \tilde{Z}_3 k^2)k_\mu + \tilde{Z}_5(qk)q_\mu, \quad \tilde{Z}_6 k_\mu, \tag{2.92}$$

---

[15]Disconnected contributions can be avoided defining $\Theta_{\rho\rho} = \Theta_{\rho\rho} - \langle\Theta_{\rho\rho}\rangle$.

[16]The number of these terms is given by the superficial degree of divergence of the diagram

have to be finite. Working on the coefficients multiplying k_μ and q_μ, it is possible to show that all the Z's are finite, with the exception of Z_4. Since the trace is finite, then the dilatation identities can be used to write

$$4(\tilde{Z}_1 + \tilde{Z}_2 q^2 + \tilde{Z}_3 k^2) - 3\tilde{Z}_4 k^2 + \tilde{Z}_5 q^2 \tag{2.93}$$

The finiteness of $\delta_{\mu\nu}\Gamma^{(n)}_{\mu\nu}$ automatically implies the finiteness of Z_4. Hence, no counterterms are really needed to renormalize $\Theta_{\mu\nu}$. The bare operator is already the renormalized one. As a consistency check, Coleman, Callan and Jackiw probed the space-time WI at 1-loop level, finding that the above result is correct.

2.5 Renormalized EMT: lattice regularization

When a lattice regulator is adopted, the renormalization procedure becomes more cumbersome. The main problem is that fundamental space-time symmetries are broken at finite lattice spacing[17]. Starting from the simplest symmetry, i.e. translations, one finds

$$\partial_\mu \hat{T}^{naive}_{\mu\nu} = -\frac{\delta\hat{S}}{\delta\hat{\phi}}\partial_\nu\hat{\phi} + \hat{X}_\nu, \tag{2.94}$$

where

- $\hat{T}^{naive}_{\mu\nu}$ is the naïve discretization of the classical energy momentum tensor[18].

- $\hat{X}_\nu$ is a dimension 5 operator that vanishes in the continuum limit, when translational invariance is restored.

At the quantum level, the corresponding TWI becomes

$$\langle(\partial_\mu \hat{T}_\mu + \hat{X}_\nu)(x)\hat{\Phi}_{a_1}(x_1)...\hat{\Phi}_{a_n}(x_n)\rangle = -\sum_{j=1}^n \langle\hat{\Phi}_{a_1}(x_1)...(\hat{\delta}_{x,\nu}\hat{\Phi}_{a_j}(x_j))...\hat{\Phi}_{a_n}(x_n)\rangle, \tag{2.95}$$

Here the representation in terms of a generic, renormalized operator $\hat{\Phi}_a(x)$[19] has been preferred, the reason to become clear in the next chapter. In the above representation, the operator $\hat{\delta}_{x,\nu}$ produces (discretized) local translations on fields or composite probes. For the latter, the action of $\hat{\delta}_{x,\nu}$ can be syntetized by the following formula

$$\hat{\delta}_{x,\nu}\hat{\Phi}_{a_j}(x_j) = a^d \sum_z \frac{\delta\hat{\Phi}_{a_j}(x_j)}{\delta\hat{\phi}_b(z)}\hat{\delta}_{x,\nu}\hat{\phi}_b(z), \tag{2.96}$$

where $\hat{\delta}_{x,\nu}\hat{\phi}_b(z)$ is the discretized form of a local translation applied to elementary lattice fields. For the theories considered in this work, it will be described by the following equations

$$\hat{\delta}_{x,\nu}\hat{\phi}(z) = \delta_{x,z}\hat{\partial}_\mu\phi(z) \qquad\qquad \text{scalar field,} \tag{2.97}$$

$$\hat{\delta}_{x,\nu}U_\mu(z) = \delta_{x,z}\hat{F}_{\nu\mu}U_\mu(z) \qquad\qquad \text{gauge field.} \tag{2.98}$$

The set of transformations described by (2.97-2.98) represents one of the possible discretized forms that can be employed on the lattice. In principle, any formulation of $\hat{\delta}_{x,\nu}\hat{\phi}_b(z)$ which converges to the correct transformation in the continuum can be adopted. This is not a trivial fact, since the

---

[17]Said in another way, the Leibniz rule does not hold.

[18]From now on, lattice operators will be denoted with a $\hat{}$ symbol.

[19]The subscript $_R$ for renormalized operators $\hat{\Phi}_a(x)_R$ is omitted to lighten the formulation.

renormalization of $\hat{\delta}_{x,\nu}\hat{\Phi}_{a_j}(x_j)$ depends both on the choice of the composite probe $\hat{\Phi}_{a_j}(x_j)$ and the specific form of $\hat{\delta}_{x,\nu}\hat{\phi}_b(z)$ adopted on the lattice.

The operator $\hat{X}_\nu$ that appears in equation (2.94) vanishes at tree level when $a \to 0$. However, radiative corrections can make its insertion to produce finite and divergent contributions to the WI. These contributions need to be subtracted if one wants to recover the correct WI in the continuum. This implies that the naïvely discretized EMT will not suffice to render the WI finite when the regulator is removed. To remove divergences (and finite contributions) generated by the lattice regularization, a properly renormalized form of $\hat{T}_{\mu\nu}$ has to be determined. For the latter, a mixing with operators with mass dimension ≤ 4 has to be considered. Their classification is accomplished by taking into account the internal symmetries of the action and the remnants of Poincaré invariance, i.e. hyper-cubic symmetry. It comes out that the possible mixing takes the form

$$\hat{X}_\nu \approx \partial_\rho \hat{O}_{\rho\nu}, \tag{2.99}$$

the approximate identity to be understood inside Green's functions. Then a renormalized energy momentum tensor could be devised imposing

$$(\hat{T}_{\mu\nu})_R = \hat{T}_{\mu\nu}^{naive} - \hat{O}_{\mu\nu} = \sum_{i=1}^{n} Z_i \hat{T}_{\mu\nu}^{(i)}, \tag{2.100}$$

and the lattice WI can be written as

$$\langle [\partial_\mu (\hat{T}_{\mu\nu})_R + R_\nu](x)\hat{\Phi}_{a_1}(x_1)...\hat{\Phi}_{a_n}(x_n)\rangle = -\sum_{j=1}^{n}\langle \hat{\Phi}_{a_1}(x_1)...(\delta_{x,\nu}\hat{\Phi}_{a_j}(x_j))...\hat{\Phi}_{a_n}(x_n)\rangle, \tag{2.101}$$

where the quantity R_ν is a finite operator whose insertion vanishes in the continuum limit. The above equation does still not represent the correct form of renormalized lattice WI. Renormalizations coming from the term

$$\hat{\delta}_{x,\nu}\hat{\Phi}_{a_j}(x_j), \tag{2.102}$$

have also to be taken into account. The operator mixing that defines the renormalized version of $\hat{\delta}_{x,\nu}\hat{\Phi}_{a_j}(x_j)$ depends on:

- the specific lattice formulation of $\hat{\delta}_{x,\nu}\hat{\Phi}_{a_j}(x_j)$;

- the choice of composite probe $\hat{\Phi}_{a_j}(x_j)$.

Once these two conditions have been specified, the renormalized form of $\hat{\delta}_{x,\nu}\hat{\Phi}_{a_j}(x_j)$ can be written as a sum of bare lattice operators coupled to specific renormalization constants[20]. Collecting all the pieces together, one can write down a proper lattice WI, which converges to the expected continuum form, when $a \to 0$

$$\langle [\sum_{i=1}^{n} Z_i \partial_\mu \hat{T}_{\mu\nu}^{(i)} + R_\nu](x)\hat{\Phi}_{a_1}(x_1)...\hat{\Phi}_{a_n}(x_n)\rangle = -\sum_{j=1}^{n}\langle \hat{\Phi}_{a_1}(x_1)...(\hat{\delta}_{x,\nu}\hat{\Phi}_{a_j}(x_j))_R...\hat{\Phi}_{a_n}(x_n)\rangle. \tag{2.103}$$

It is important to clearly explain what does it mean to recover the correct continuum limit. The renormalization constants of $(\hat{T}_{\mu\nu})_R$ and $(\hat{\delta}_{x,\nu}\hat{\Phi}_{a_j}(x_j))_R$ can be expressed in terms of the bare couplings of the theory, the lattice spacing and logarithms of dimensionless combinations like $(am_0)^2$ or similar. These constants encode all the subtractions needed to render equation (2.103) finite and

---

[20] At finite lattice spacing, these operators will be non vanishing only in a small region of the spacetime, defined by a radius $\delta = |x - x_j|$.

lattice independent in the $a \to 0$ limit. As a consequence, when correlation functions are written in terms of the renormalized parameters and fields of the theory

$$\langle [\sum_{i=1}^{n} c_i \partial_\mu \hat{T}_{\mu\nu}^{(i)} + R_\nu](x) \hat{\Phi}_{a_1}(x_1)...\hat{\Phi}_{a_n}(x_n) \rangle \underset{a \to 0}{\to} \langle \partial_\mu (T_{\mu\nu})_R(x) \Phi_{a_1}(x_1)...\Phi_{a_n}(x_n) \rangle + \mathcal{O}(a),$$

$$\sum_{j=1}^{n} \langle \hat{\Phi}_{a_1}(x_1)...(\hat{\delta}_{x,\nu} \hat{\Phi}_{a_j}(x_j))_R...\hat{\Phi}_{a_n}(x_n) \rangle \underset{a \to 0}{\to} \sum_{j=1}^{n} \langle \Phi_{a_1}(x_1)...(\delta_{x,\nu} \Phi_{a_j}(x_j))...\Phi_{a_n}(x_n) \rangle + \mathcal{O}(a).$$

So, continuum TWI are recovered up to lattice artefacts that vanish, at least, with a[21]. This is the result of the so-called *Symanzik improvement program* [43] and plays an important role both in perturbative and non perturbative lattice field theory. Taking a look at the previous chapter, it exactly corresponds to what has been shown in section (1.4) for the renormalized vertex functions of $\lambda\phi^4$ theory.

Even if only the case of translations has been treated, the renormalization procedure can be straightforwardly extended to the case of $SO(d)$ rotations and dilatations. In the following, an application of the method in perturbation theory is provided.

2.6 Lattice Perturbative EMT

The perturbative renormalization of the lattice EMT has been pioneered by S. Caracciolo, G. Curci, P. Menotti and A. Pelissetto, who studied the problem for different kind of theories and defined a method for a systematic renormalization of this operator[22]. In the following, two examples will be given. The first will be the, now well known, lattice $\lambda\phi^4$ theory [19] , while the second one is the case of lattice gauge theory [20, 49, 50].

2.6.1 Scalar lattice EMT

Scalar field theory represents the best laboratory for studying the restoration of space-time symmetries broken by the lattice. In this case, the attention was focused on the recover of translational invariance, studying the TWI. In the continuum, these identities are satisfied by the canonical EMT

$$T_{\mu\nu}(x) = \partial_\mu \phi(x) \partial_\nu \phi(x) - \delta_{\mu\nu} \left[\frac{1}{2} \partial_\rho \phi \partial_\rho \phi + \frac{1}{2} m_0^2 \phi^2(x) + \frac{\lambda_0}{4!} \phi^4(x) \right]. \tag{2.104}$$

The interest, in this case, was to determine a lattice-renormalized EMT, at one loop, satisfying the Ward identity up to $\mathcal{O}(a)$.

To perform this task, a specific strategy, based on the *local effective lagrangian*, has been adopted.

Given the $\lambda\phi^4$ lattice action (1.82), and the corresponding generating functional (1.75), lattice correlation functions can be computed in weak coupling perturbation theory. At small lattice spacing, they admit the following expansion

$$G^n(p_1, ..., p_n; \lambda_0, \hat{m}_0, a) = \sum_{j=0}^{\infty} \sum_{k=0}^{\infty} a^j (\log a)^k K_{jk}^{(n)}(p_1, ..., p_n, \lambda_0, \hat{m}_0). \tag{2.105}$$

The same expansion can be obtained in terms of a *local effective Lagrangian* [51] defined in the continuum, at scale $1/a$

$$\mathcal{L}^{eff} = \mathcal{L}_{cont} + \sum_{j=1}^{\infty} a^j \mathcal{L}_j \tag{2.106}$$

---

[21] This is a general result that could be modified according to the theory under study. For example, the TWI in Yang Mills theory are supposed to converge $\mathcal{O}(a^2)$ for symmetry reasons.

[22] Actually, they devised the renormalization procedure presented in the previous section.

Each term in the equation above contain continuum operators coupled to a specific low energy constant. The value of the latter can be fixed by double expanding lattice correlation functions with respect a and λ_0 and requiring the following identity

$$G^n(p_1, ..., p_n; \lambda_0, \hat{m}_0, a) = G^n(p_1, ..., p_n; \lambda_0, \hat{m}_0, a)_{eff}$$
$$= \sum_{j=0}^{\infty} \sum_{k=0}^{\infty} a^j (\log a)^k K_{jk}^{(n)}(p_1, ..., p_n, \lambda_0, \hat{m}_0). \qquad (2.107)$$

to be valid up to a given order in a and λ_0. On the r.h.s, continuum correlation functions are computed using dimensional regularization, the value of the arbitrary scale μ having been fixed to $1/a$.

Hence, the identity (2.107) defines a mapping between two different regularizations, one that violates translational invariance and one that preserves it.

In this case, only the leading order terms in the expansion in a have been considered, disregarding contributions which vanish as $a \to 0$. As a consequence, the identity (2.107) becomes

$$G_{latt}^{(N)}(p_1, ..., p_n, \lambda_0, a, m_0) \approx G_{continuum}^{(N)}(p_1, ..., p_n, \lambda_0, m_0)_{1/a} \qquad (2.108)$$

where $G_{continuum}^{(N)}(p_1, ..., p_n, \lambda_0, m_0)_{1/a}$ is computed using the continuum Lagrangian $\mathcal{L}_{cont}$. The latter is given by

$$\mathcal{L}_{cont} \approx \frac{1}{2} Z_\phi \partial_\mu \phi \partial_\mu \phi + \frac{1}{2} m_0^2 Z_m \phi^2 + \frac{\lambda_0}{4!} Z_{\lambda_0} \phi^4, \qquad (2.109)$$

where the factors $Z_i(\lambda_0)$ are finite renormalizations that link the two different regularizations, and have been determined at one loop [19].

With this identification, at one loop order in perturbation theory and at leading order in the expansion in a, the lattice EMT is given by

$$T_{\mu\nu}^{eff} = Z_\phi N[\partial_\mu \phi \partial_\nu \phi] - \delta_{\mu\nu} N[\mathcal{L}], \qquad (2.110)$$

where the operation $N[]$ represents the renormalization procedure in a continuum scheme. Then, the whole procedure is reduced to define a lattice form of $\hat{T}_{\mu\nu}$ such that[23]

$$\hat{T}_{\mu\nu} \approx T_{\mu\nu}^{eff}. \qquad (2.111)$$

At tree level, a possible lattice discretization of (2.104) is given by

$$\hat{T}_{\mu\nu}^{naive}(x) = \partial_{\mu S}\phi \partial_{\nu S}\phi - \delta_{\mu\nu} \left[\frac{1}{2} \partial_{\rho S}\phi \partial_{\rho S}\phi + \frac{1}{2}(m^2 + \delta m^2)\phi^2 + \frac{\lambda_0}{4!}\phi^4 \right]. \qquad (2.112)$$

where δm^2 is an additive renormalization of the form $a^{-2} f(\lambda)$. The value of this term can be read off from the set of equations (1.110), in section (1.4)

$$\delta m^2 = -\frac{\lambda_R}{2a^2} C_0,$$
$$C_0 = 0.15493...$$

and can be determined requiring the self energy to vanish at zero mass and momentum. This kind of renormalization is motivated by the possibility to relate m^2 to a physical correlation length ξ, such that the $\xi \to \infty$ limit represents a massless theory. The operator $\partial_{\mu S}$ represents the symmetric derivative, as described in section (1.3). This choice allows to preserve the hermiticity of the tensor, and ensure $\mathcal{O}(a^2)$ corrections to physical quantities in the continuum limit. When

---

[23]The approximate equality has to be intended inside correlation functions.

radiative corrections are included, the tree-level operator $T^{naive}_{\mu\nu}$ does not suffice to absorb all the divergencies, and it has to be modified with a proper operator mixing. Following the strategy explained in the previous section, one has

$$\hat{T}_{\mu\nu} = \hat{T}^{naive}_{\mu\nu} - \hat{O}_{\mu\nu} \approx T^{eff}_{\mu\nu}, \tag{2.113}$$

where

$$\hat{O}_{\mu\nu}(x) = b_1 \partial_{\mu S}\phi\partial_{\nu S}\phi + \delta_{\mu\nu}\left[\frac{b_2}{2}\partial_{\rho S}\phi\partial_{\rho S}\phi + \frac{b_3}{2}\phi^2 + \frac{b_4}{4!}\phi^4 + \frac{b_5}{2}\partial_{\mu S}\phi\partial_{\mu S}\phi\right]. \tag{2.114}$$

In this way, all the b's are at least $\mathcal{O}(\lambda_0)$. Note that the last term on the r.h.s of the equation is not $SO(4)$ covariant, since the index μ is not summed. This is a simple example of how breaking the $SO(4)$ symmetry induces new contributions in the mixing which are not expected in the continuum. The renormalization of $T_{\mu\nu}$ is now established imposing the WI for translations. The structure of $T_{\mu\nu}$ suggests that the restoration of continuum WI has to be checked just for two and four-point functions. The renormalization constants have been determined imposing the WI for 1PI (fully propagator amputated) vertex functions at zero momenta: for the four vertex function one gets

$$\Gamma^{naive(4)}_{\mu\nu}(0;0,0,0,0) - O^{(4)}_{\mu\nu}(0;0,0,0,0) = -\delta_{\mu\nu}\Gamma^{(4)}(0,0,0,0), \tag{2.115}$$

the insertion on the r.h.s being the four-vertex function of the theory. The above equation serves to fix the value of the constant b_4: the relevant diagrams for the insertion of $T^{naive}_{\mu\nu}$ are

$$= \lambda_0\left\{-\delta_{\mu\nu} + 3\lambda_0\int\frac{d^4l}{(2\pi)^4}\left[\frac{2\bar{l}_\mu\bar{l}_\nu - \delta_{\mu\nu}(\bar{l}^2+m^2)}{(\hat{l}^2+m^2)^3} + \frac{\delta_{\mu\nu}}{(\hat{l}^2+m^2)^2}\right]\right\},$$

and exhibit just a logarithmic divergence[24]. The value of b_4 is set to

$$b_4 = \frac{3}{2}\lambda_0^2\frac{1}{(4\pi)^2}(2\pi^2 Z_{0000} - 1) \tag{2.117}$$

$$Z_{0000} = 4.369... \tag{2.118}$$

The same procedure is done for the two-point function. In this case, the contributing diagrams

$$= -3\lambda_0^2\delta_{\mu\nu}\int\frac{d^4l}{(2\pi)^4}\left[\frac{a^2\hat{l}^2}{16(\hat{l}^2+m^2)^2} + \frac{\bar{l}^2-\hat{l}^2}{(\hat{l}^2+m^2)^3}\right],$$

---

[24]In this case

$$\bar{l}_\mu = \frac{1}{a}\sin l_\mu a, \quad \hat{l}_\mu = \frac{2}{a}\sin\frac{l_\mu a}{2} \tag{2.116}$$

are quadratically divergent, then two subtractions would need to be done, in the spirit of the BPH approach. Since the renormalization is carried out at zero external momentum, no dependence on external momenta is generated, so the constants $b_{1,2,5}$ will be determined only at two loop level[25]. This leaves only b_3 to be determined. The final result for $T_{\mu\nu}$ is given by the following equation.

$$\hat{T}_{\mu\nu}(x) = \partial_{\mu S}\phi\partial_{\nu S}\phi - \delta_{\mu\nu}\left\{ \frac{1}{2}\partial_{\rho S}\phi\partial_{\rho S}\phi + \left[m^2\left(1 + \frac{\lambda_0}{2(4\pi)^2}(2\pi^2 Z_{0000} - 1)\right) - \frac{\lambda_0}{16a^2} \right]\frac{\phi^2}{2} \right.$$
$$\left. + \left[1 + \frac{3\lambda_0}{2(4\pi)^2}(2\pi^2 Z_{0000} - 1)\right]\frac{\lambda_0}{4!}\phi^4 \right\} \quad (2.119)$$

An analogous calculation has been carried out using the continuum effective theory at scale $1/a$. The renormalized operators defined in (2.110) have been transcribed in terms of lattice operators imposing the equality $\mathcal{O}(a)$ of the Green functions computed in the two different regularization schemes. Then the transcription has been applied to equation (2.110). The result obtained is the same as equation (2.119), showing that the $\hat{T}_{\mu\nu}$ is the correctly renormalized operator on the lattice. As a proof of consistency, the authors investigated the form of the trace identities, showing that the trace of (2.119) exhibit the correctly expected anomaly.

2.6.2 Gauge lattice EMT

The lattice gauge theory presents some additional difficulties arising from the necessity of defining an EMT that could be symmetric and gauge invariant. The canonical EMT, defined from the variation of the action under canonical translations of the field, is neither symmetric nor gauge invariant. In pure Yang-Mills theory, a tensor that satisfies such symmetries can be obtained from the following transformation

$$A_\mu \to \alpha_\rho(x)F_{\rho\mu}, \quad (2.120)$$

which is simply the composition of a (local) canonical translation and a gauge transformation parametrized with the gauge field [52]. Equation (2.120) can be also generalized to gauge invariant theories that comprise matter fields.

A more general method consists in defining the theory on a curved manifold and varying the action with respect the metric, holding the other fields fixed[26]. A simple example can be given by considering a pure gauge theory. Disregarding the gauge fixing term for a moment, the action on a curved manifold is described by

$$S = \int d^4x\sqrt{-g}\frac{1}{2}\text{tr}\{F_{\lambda\tau}F_{\gamma\delta}\}g^{\lambda\gamma}g^{\tau\delta}, \quad (2.125)$$

---

[25]The tree-level contributions of the counterterms coupled to $b_{1,2,5}$ are polynomial in the external momenta. If the latters are set to zero, then these counterterms can contribute only at two-loop order. From the BPH point of view, this means that only the zeroth order in the Taylor expansion of the loop integral has to be subtracted.

[26]There is an easy way to understand this. On a curved manifold, the action is invariant under local coordinate transformations. These transformations induce local deformations both of the metric tensor, as well as of the other fields. For the latter, a generic local diffeomorphism can be described by

$$\delta\phi = -\xi^\nu\partial_\nu\phi, \qquad \text{spin zero}, \quad (2.121)$$
$$\delta A_\mu = -\xi^\nu\partial_\nu A_\mu - \partial_\mu\xi^\nu A_\nu \qquad \text{spin one}, \quad (2.122)$$
$$\dots \qquad \dots \quad (2.123)$$

For a constant vector ξ, the set of transformations (2.121-2.122), reduces to a global infinitesimal translation, whose generator is exactly the EMT of the theory. This result can be used to trade variations with respect the fields, from which the EMT is usually derived, with variations with respect the metric.

$$-\frac{\delta S}{\delta g_{\mu\nu}}\delta g_{\mu\nu} = \sum_{i=1}^n \frac{\delta S}{\delta B_i}\delta B_i \quad (2.124)$$

The variation of the action with respect the metric brings

$$\frac{\delta S}{\delta g^{\mu\nu}} = \sqrt{-g}\frac{1}{2}\text{tr}\{F_{\lambda\tau}F_{\gamma\delta}\}(4\delta^\lambda_\mu\delta^\gamma_\nu g^{\tau\delta} - g_{\mu\nu}g^{\lambda\gamma}g^{\tau\delta}),\tag{2.126}$$

from which one infers $(g_{\mu\nu} \to \delta_{\mu\nu})$

$$T_{\mu\nu} = \frac{1}{\sqrt{-g}}\frac{\delta S}{\delta g^{\mu\nu}} = 2\text{tr}\left[F_{\mu\tau}F_{\nu\tau} - \frac{\delta_{\mu\nu}}{4}F_{\lambda\tau}F_{\lambda\tau}\right].\tag{2.127}$$

The above EMT is clearly gauge invariant and symmetric, and its trace is zero, as it would be *classically* expected from a theory with massless particles[27].

When matter fields are included, a similar approach can be followed. In this case the action on the manifold is given by

$$S = \int d^4x\sqrt{-g}\left[\bar{\psi}\gamma^c e_c^\lambda\left(D_\lambda + \frac{1}{2}\sigma^{ab}\omega_\lambda^{ab}\right)\psi + m\bar{\psi}\psi + \frac{1}{4}\text{tr}\{F_{\lambda\tau}F_{\gamma\delta}\}g^{\lambda\gamma}g^{\tau\delta}\right.$$
$$\left. + \frac{1}{2\xi}\text{tr}\{\nabla_\rho A^\rho\nabla_\mu A^\mu\} + g^{\mu\nu}\partial_\mu\bar{c}D_\nu c\right],\quad(2.128)$$

where also gauge fixing terms have been included. The operator D_μ is the covariant derivative for gauge transformations

$$D_\mu = \partial_\mu + ig_0 A_\mu \qquad\qquad \text{fundamental,}$$
$$D_\mu = \partial_\mu + ig_0[A_\mu,] \qquad\qquad \text{adjoint,}$$

for fundamental and adjoint representation. ∇_μ represents the covariant derivative in the metric $g^{\mu\nu}$

$$\nabla_\mu V^{\nu...}_{\alpha...} = \partial_\mu V^{\nu...}_{\alpha...} + \Gamma^\nu_{\mu\lambda}V^{\lambda...}_{\alpha...} - \Gamma^\lambda_{\mu\alpha}V^{\nu...}_{\lambda...}\tag{2.129}$$

where $\Gamma^\nu_{\mu\lambda}$ is the Christoffel symbol and σ^{ab} is the γ-matrix commutator divided by four. The vierbein field e^a_μ are related to the metric by the following relations

$$e^a_\mu e^a_\nu = g_{\mu\nu},$$
$$e = \sqrt{-g} = \det(e^a_\mu)$$

They represent a coordinate transformation on the tangent space that diagonalyze the scalar product

$$x_\nu y^\nu = g_{\mu\nu}x^\mu y^\nu = \delta_{ab}(e^a_\mu x^\mu)(e^b_\gamma x^\gamma).\tag{2.130}$$

On the other hand, the spin connection ω_μ^{ab} is given by

$$\omega_\mu^{ab} = e_\nu^a\Gamma^\nu_{\sigma\mu}e^{\sigma b} + e_\nu^a\partial_\mu e^{\nu b} = e_\nu^a\Gamma^\nu_{\sigma\mu}e^{\sigma b} - e^{\nu a}\partial_\mu e_\nu^b\tag{2.131}$$

and is necessary to construct a generally covariant Dirac equation.

To derive the EMT, the following quantity has to be defined[28]

$$\Theta^\mu_\nu = -\frac{1}{e}e^a_\nu\frac{\delta S}{\delta e^a_\mu}.\tag{2.132}$$

---

[27]This method can be adopted also when theories with gauge fixing are studied: in this case, clearly, the corresponding EMT will no be gauge invariant.

[28]Variations with respect the metric are here traded with variations with respect the vierbein field.

Then, the invariance of the action under the following reparametrization

$$\delta B = -\xi^\nu \partial_\nu B, \quad B = \{c, \bar{c}, \psi, \bar{\psi}\}, \tag{2.133}$$

$$\delta A_\mu = -\xi^\nu \partial_\nu A_\mu - \partial_\mu \xi^\nu A_\nu, \tag{2.134}$$

$$\delta e_\mu^a = -\xi^\nu \partial_\nu e_\mu^a - \partial_\mu \xi^\nu e_\nu^a \tag{2.135}$$

is employed to write

$$e\Theta_{;\mu}^{\mu\nu} - e e_\rho^a e_\mu^{a;\nu} \frac{\Theta^{\mu\rho} - \Theta^{\rho\mu}}{2} = -\left[\frac{\delta S}{\delta c} \partial^\nu c + \partial^\nu \bar{c} \frac{\delta S}{\delta \bar{c}} + \frac{\delta S}{\delta \psi} \partial^\nu \psi + \partial^\nu \bar{\psi} \frac{\delta S}{\delta \bar{\psi}} \right]$$
$$+ \sqrt{-g} \left(\frac{A^\nu}{\sqrt{-g}} \frac{\delta S}{\delta A_\mu} \right)_{;\mu} - A_\mu^{;\nu} \frac{\delta S}{\delta A_\mu}. \tag{2.136}$$

Further simplifications can be obtained exploiting the invariance under internal local $SO(4)$ rotations

$$\delta e_\mu^a = \epsilon_{ab} e_\mu^b, \tag{2.137}$$

$$\delta \psi = \frac{1}{2} \sigma^{ab} \epsilon_{ab} \psi, \tag{2.138}$$

$$\delta \bar{\psi} = -\bar{\psi} \epsilon_{ab} e_\mu^b, \tag{2.139}$$

from which it can be shown that

$$e(\Theta^{\mu\rho} - \Theta^{\rho\mu}) = \bar{\psi} \sigma^{\mu\rho} \frac{\delta S}{\delta \bar{\psi}} - \frac{\delta S}{\delta \psi} \sigma^{\mu\rho} \psi. \tag{2.140}$$

Defining the energy momentum tensor as

$$T^{\mu\nu} = \frac{1}{2} (\Theta^{\mu\nu} + \Theta^{\nu\mu}) \tag{2.141}$$

and using equation (2.140), one finally finds

$$T_{;\mu}^{\mu\nu} = -\frac{1}{\sqrt{-g}} \left[\frac{\delta S}{\delta c} \partial^\nu c + \partial^\nu \bar{c} \frac{\delta S}{\delta \bar{c}} + \frac{\delta S}{\delta \psi} \partial^\nu \psi + \partial^\nu \bar{\psi} \frac{\delta S}{\delta \bar{\psi}} + A_\mu^{;\nu} \frac{\delta S}{\delta A_\mu} \right]$$
$$+ \sqrt{-g} \left(\frac{A^\nu}{\sqrt{-g}} \frac{\delta S}{\delta A_\mu} \right)_{;\mu} - \left[\frac{1}{2\sqrt{-g}} \left(\bar{\psi} \sigma^{\mu\nu} \frac{\delta S}{\delta \bar{\psi}} - \frac{\delta S}{\delta \psi} \sigma^{\mu\nu} \psi \right) \right]_{;\mu}$$
$$+ \frac{e_\rho^a e_\mu^{a;\nu}}{2\sqrt{-g}} \left(\bar{\psi} \sigma^{\mu\nu} \frac{\delta S}{\delta \bar{\psi}} - \frac{\delta S}{\delta \psi} \sigma^{\mu\nu} \psi \right). \tag{2.142}$$

On a flat manifold, the above equation reduces to

$$\partial_\mu T^{\mu\nu} = -\left(\frac{\delta S}{\delta c} \partial^\nu c + \partial^\nu \bar{c} \frac{\delta S}{\delta \bar{c}} \right) - \left(\frac{\delta S}{\delta \psi} \partial^\nu \psi + \partial^\nu \bar{\psi} \frac{\delta S}{\delta \bar{\psi}} \right)$$
$$- \left[\partial_\nu A_\mu \frac{\delta S}{\delta A_\mu} - \partial_\mu \left(A^\nu \frac{\delta S}{\delta A_\mu} \right) \right] - \frac{1}{2} \partial_\mu \left(\bar{\psi} \sigma^{\mu\nu} \frac{\delta S}{\delta \bar{\psi}} - \frac{\delta S}{\delta \psi} \sigma^{\mu\nu} \psi \right). \tag{2.143}$$

The r.h.s of the equation is proportional to the equation of motion, and tells that the symmetrized $T^{\mu\nu}$ is conserved at the classical level. Using the explicit formula for the EMT, one finds

$$T_{\mu\nu} = T_{\mu\nu}^F + T_{\mu\nu}^\gamma + T_{\mu\nu}^{g.f.} + T_{\mu\nu}^{ghost}, \tag{2.144}$$

where (sum over color indices is intended)

$$T^F_{\mu\nu} = \frac{1}{4}(\bar{\psi}\gamma_\mu \overset{\leftrightarrow}{D}_\nu \psi + \bar{\psi}\gamma_\nu \overset{\leftrightarrow}{D}_\mu \psi) - \delta_{\mu\nu}(\frac{1}{2}\bar{\psi}\gamma_\rho \overset{\leftrightarrow}{D}_\rho \psi + m\bar{\psi}\psi),\tag{2.145}$$

$$T^\gamma_{\mu\nu} = F_{\mu\tau}F_{\nu\tau} - \frac{\delta_{\mu\nu}}{4}F_{\lambda\tau}F_{\lambda\tau},\tag{2.146}$$

$$T^{g.f.}_{\mu\nu} = \frac{1}{\xi}\left\{-(A_\mu\partial_\nu + A_\nu\partial_\mu)\partial_\lambda A_\lambda + \delta_{\mu\nu}\left[\frac{1}{2}\partial_\rho A_\rho \partial_\lambda A_\lambda + A_\lambda \partial_\lambda \partial_\rho A_\rho\right]\right\},\tag{2.147}$$

$$T^{ghost}_{\mu\nu} = \partial_\mu\bar{c}D_\nu c + \partial_\nu\bar{c}D_\mu c - \delta_{\mu\nu}\partial_\lambda\bar{c}D_\lambda c\tag{2.148}$$

The operator described by (2.144) is symmetric, gauge invariant, but only the first two terms are BRS invariant. However, one can writes the sum $T^{g.f.}_{\mu\nu} + T^{ghost}_{\mu\nu}$ as a BRS variation of an operator $\Omega_{\mu\nu}$

$$T^{g.f.}_{\mu\nu} + T^{ghost}_{\mu\nu} = \delta_{BRS}\Omega_{\mu\nu},$$

$$\Omega_{\mu\nu} = A_\mu\partial_\nu\bar{c} + A_\nu\partial_\mu\bar{c} - \delta_{\mu\nu}\left[\frac{1}{2}\partial_\lambda A_\lambda\bar{c} + A_\lambda\partial_\lambda\bar{c}\right]$$

so that

$$\delta_{BRS}(\delta_{BRS}\Omega_{\mu\nu}) = \frac{\lambda}{\xi}[(A_\nu\partial_\mu + A_\mu\partial_\nu)\partial_\rho D_\rho c - \delta_{\mu\nu}\partial_\rho(A_\rho\partial_\rho D_\rho c)],\tag{2.149}$$

where λ is the parameter related to the BRS transformation. Since the above equation is proportional to the ghosts' equation of motion, then the EMT in (2.144) is BRS invariant modulo the equation of motion of the ghost fields [29]. This tensor is already finite [18], i.e. its insertions in the WI do not generate further divergences beside the ones of the elementary theory [30].

On the lattice, the naïvely discretized version of (2.144) does not allow to recover the right WI in the continuum, and a proper renormalization procedure is needed. Starting from the naïve operator, the authors chose a discretization that could preserve

- hyper-cubic symmetry;

- locality;

- hermiticity;

- BRS invariance modulo equation of motions.

The different terms contributing to this operator, which will be defined as $T^{tree}_{\mu\nu}$ from now on, are

- Gluonic term (sum over colors is intended)

$$\hat{T}^{\gamma tree}_{\mu\nu} = \sum_\rho F_{\mu\rho}F_{\nu\rho} - \frac{\delta_{\mu\nu}}{4}\sum_{\rho\lambda}F_{\lambda\rho}F_{\lambda\rho},\tag{2.150}$$

where the *Clover* definition of the operator $F^a_{\mu\nu}$ has been adopted

$$F^a_{\mu\nu}(x) = \frac{1}{4a^2}\text{tr}\{[P(x;\mu,\nu) + P(x;-\mu,-\nu) + P(x;\nu,-\mu) + P(x;-\nu,\mu)$$
$$- P(x;\nu,\mu) - P(x;-\nu,-\mu) - P(x;\mu,-\nu) - P(x;-\mu,\nu)]T^a\}.\tag{2.151}$$

---

[29]It has to be stressed that such a tensor cannot be obtained just through the Belinfante symmetrization procedure.
[30]The authors verified this property for the simplest case of continuum QED at 1-loop level [20].

Here $P(x; \mu, \nu)$ is the Plaquette operator defined in terms of the gauge links $U_\mu(x)$

$$U_\mu(x) = e^{iagT^c A_\mu^c(x)},$$

$$\text{tr}\{T^a T^b\} = \frac{\delta^{ab}}{2},$$

$$P(x; \mu, \nu) = U_\mu(x) U_\nu(x + a\hat{\nu}) U_\mu^\dagger(x + \hat{\nu}) U_\nu^\dagger(x).$$

- Fermionic term

$$\hat{T}_{\mu\nu}^{ftree} = \frac{1}{8a} \bar{\psi}(x) \gamma_\mu [U_\nu(x) \psi(x + a\hat{\nu}) - U_\nu^\dagger(x) \psi(x - a\hat{\nu})] \tag{2.152}$$

$$+ \frac{1}{8a} [\bar{\psi}(x + a\hat{\nu}) U_\nu(x) - \bar{\psi}(x - a\hat{\nu}) U_\nu^\dagger(x)] \gamma_\mu \psi(x) \tag{2.153}$$

$$+ \frac{1}{8a} \bar{\psi}(x) \gamma_\nu [U_\mu(x) \psi(x + a\hat{\mu}) - U_\mu^\dagger(x) \psi(x - a\hat{\mu})] \tag{2.154}$$

$$+ \frac{1}{8a} [\bar{\psi}(x + a\hat{\mu}) U_\mu(x) - \bar{\psi}(x - a\hat{\mu}) U_\mu^\dagger(x)] \gamma_\nu \psi(x) \tag{2.155}$$

$$- \delta_{\mu\nu} \mathcal{L}^F, \tag{2.156}$$

where $\mathcal{L}^F$ is the Wilson Lagrangian for fermion fields on the lattice.

- Gauge fixing and ghost terms, given as a BRS variation of

$$\hat{\Omega}_{\mu\nu} = \frac{1}{2} \partial_{\mu B} A_\mu \partial_{\nu S} \bar{c}(x) + \partial_{\nu B} A_\nu \partial_{\mu S} \bar{c}(x) - \delta_{\mu\nu} \sum_\lambda \left[\frac{a}{4} \partial_{\lambda S} \partial_{\lambda B} A_\lambda(x) \bar{c}(x) \right]. \tag{2.157}$$

In this theory, the renormalized lattice EMT mixes with 7 operators

$$\hat{T}_{\mu\nu}^{(1)} = \left[\bar{\psi} \gamma_\mu D_\nu \psi - D_\nu \bar{\psi} \gamma_\mu \psi + (\mu \leftrightarrow \nu) \right]_L, \tag{2.158}$$

$$\hat{T}_{\mu\nu}^{(2)} = \delta_{\mu\nu} \left(\mathcal{L}^F \right)_L, \tag{2.159}$$

$$\hat{T}_{\mu\nu}^{(3)} = \delta_{\mu\nu} \bar{\psi} \psi, \tag{2.160}$$

$$\hat{T}_{\mu\nu}^{(4)} = \delta_{\mu\nu} \left(\bar{\psi} \gamma_\mu D_\mu \psi - D_\mu \bar{\psi} \gamma_\mu \right)_L, \tag{2.161}$$

$$\hat{T}_{\mu\nu}^{(5)} = \left(\sum_\rho F_{\mu\rho} F_{\nu\rho} - \frac{\delta_{\mu\nu}}{4} \sum_{\rho\lambda} F_{\lambda\rho} F_{\lambda\rho} \right)_L, \tag{2.162}$$

$$\hat{T}_{\mu\nu}^{(6)} = \delta_{\mu\nu} \left(\sum_{\rho\lambda} F_{\lambda\rho} F_{\lambda\rho} \right)_L, \tag{2.163}$$

$$\hat{T}_{\mu\nu}^{(7)} = \delta_{\mu\nu} \left(\sum_\rho F_{\mu\rho} F_{\mu\rho} \right)_L, \tag{2.164}$$

the subscript L meaning the proper discretization of the operator inside brackets. As in the previous section, it is important to stress the presence of terms

$$\hat{T}_{\mu\nu}^{(4)} = \delta_{\mu\nu} \left(\bar{\psi} \gamma_\mu D_\mu \psi - D_\mu \bar{\psi} \gamma_\mu \right)_L,$$

$$\hat{T}_{\mu\nu}^{(7)} = \delta_{\mu\nu} \left(\sum_\rho F_{\mu\rho} F_{\mu\rho} \right)_L,$$

that are manifestly $SO(4)$ non-covariant in the continuum limit. The renormalized EMT has been determined at 1-loop level for the QED case [20] and the QCD case [49, 50] imposing the translation

WI for two-photon and two-fermion Green's functions. As an example, here are reported the relevant diagrams for the latter

$$\langle \hat{T}_{\mu\nu}(0)\psi(p)\bar{\psi}(-p)\rangle^{irr} =$$

$+$

$+ \qquad\qquad +$

$+ \qquad\qquad +$

$+$

The gauge dependence of $\hat{T}_{\mu\nu}$ and its renormalization constants has been studied in detail for the QED case, with the possibility to extend the results to QCD. The outcome is that all the dependence on the R_ξ parameter is confined on the $1/\xi$ factor multiplying the gauge-fixing term and in the renormalization constant coupled to $\hat{T}_{\mu\nu}^{(2)}$. As in the scalar case, a consistency check for the trace anomaly has been carried out. Moreover, the authors provided a method for a non perturbative determination of the renormalization constants has been proposed. This will be the subject of the next section.

2.7   Lattice non perturbative EMT

In principle, a strategy for a non perturbative determination of the lattice EMT can be devised using the WI. Starting from the form of $\hat{T}_{\mu\nu}$ described by (2.158), the renormalization constants coupled to each $\hat{T}_{\mu\nu}^{(i)}$ could be determined using the TWI

$$\langle \sum_{\mu} \partial_\mu \hat{T}_{\mu\nu}(0)\hat{\Lambda}_1(x_1)...\hat{\Lambda}_n(x_n)\rangle = 0 \quad x_i \neq 0. \tag{2.165}$$

Here, the $\hat{\Lambda}_i(x_i)$ are gauge invariant, *renormalized*, composite operators. Since no gauge fixing is required in non perturbative studies, the gauge fixing and ghost term will not contribute to the above expectation values. For the same reason, the contribution from the operator $\hat{T}_{\mu\nu}^{(2)}$ vanishes, since no dependence on a gauge fixing parameter ξ can be generated.
With this setup, the renormalization of the operator $\hat{\delta}_{x,\rho}\hat{\Lambda}_j(x_j)$ cannot be determined, since the EMT and the probe do not coalesce on the same point. Hence, six renormalization constants have to be determined.

It should be noted that TWI for non coalescing operators provide the renormalized $\hat{T}_{\mu\nu}$ up to an overall multiplicative factor. The latter has to be determined using another renormalization condition.

The numerical strategy can be described in few steps: starting from the renormalized lattice EMT

$$(\hat{T}_{\mu\nu})_R = \sum_{i \neq 2}^{7} Z_i \hat{T}_{\mu\nu}^{(i)}, \tag{2.166}$$

a first simplification is done fixing the renormalization of $\hat{T}_{\mu\nu}^{(1)}$ to 1

$$(\hat{T}_{\mu\nu})_R = Z_1 \sum_{i \neq 2}^{7} \tilde{Z}_i \hat{T}_{\mu\nu}^{(i)}, \tag{2.167}$$

$$\tilde{Z}_1 = 1, \tag{2.168}$$

$$\tilde{Z}_{3,4,5,6,7} = Z_{3,4,5,6,7}/Z_1. \tag{2.169}$$

Then, the lattice TWI can be used to determine the five coefficients $\tilde{Z}_{3,4,5,6,7}$. One just needs a set of five, gauge invariant probes such that the matrix

$$A^{ij} = \langle \sum_{\mu} \partial_{\mu} \hat{T}_{\mu\nu}^{(i)}(0) \hat{\Lambda}^{(j)}(x) \rangle, \quad x \neq 0, \quad i = \{3,4,5,6,7\} \quad ; j = 1,...,5 \tag{2.170}$$

is not degenerate. For the following set of probes

$$\hat{\Lambda}^{(1)} = \bar{\psi}(x)\psi(x), \tag{2.171}$$

$$\hat{\Lambda}^{(2)} = \bar{\psi}(x)\gamma_{\nu}[U_{\nu}(x)\psi(x+a\hat{\nu}) - U_{\nu}^{\dagger}(x)\psi(x-a\hat{\nu})] \tag{2.172}$$

$$+ [\bar{\psi}(x+a\hat{\nu})U_{\nu}(x) - \bar{\psi}(x-a\hat{\nu})U_{\nu}^{\dagger}(x)]\gamma_{\nu}\psi(x), \tag{2.173}$$

$$\hat{\Lambda}^{(3)} = g \left[\sum_{\sigma} \bar{\psi}(x)\gamma_{\sigma} T^a F_{\rho\sigma}^a(x)\psi(x) \right]_L, \tag{2.174}$$

$$\hat{\Lambda}^{(4)} = \left(\sum_{\rho,\nu} F_{\nu\rho}(x)F_{\nu\rho}(x) \right)_L, \tag{2.175}$$

$$\hat{\Lambda}^{(5)} = \left(\sum_{\rho} F_{\nu\rho}(x)F_{\nu\rho}(x) \right)_L, \tag{2.176}$$

it has been proved [20] that the matrix A has a non vanishing determinant, and thus allow to determine $\tilde{Z}_{3,4,5,6,7}$. The remaining renormalization Z_1 can be determined equating the expectation value of

$$H = \int d^3x\, T_{00}(\vec{x}, 0) \tag{2.177}$$

on a state of known mass.

The strategy presented seems apparently a good one for determining the fully renormalized EMT[31]. A set of field configurations can be numerically generated with a Monte Carlo algorithm, and then expectation values defining the matrix A can be obtained averaging over these configurations. However, it is at the numerical level that the strategy shows its drawbacks. Indeed, the system defined by (2.170) can be solved only keeping the probe $\hat{\Lambda}^j$ and the operator $\hat{T}_{\mu\nu}$ at physically separated points, otherwise contact terms arises. The matrix elements of A can be represented by correlators depending on the distance $x = |x_T - x_{\Lambda}|$. The signal arising from these euclidean

---

[31]It should be stressed that the renormalization of the TWI requires also the Z_{δ} factor.

correlators decrease rapidly as the distance x increases. So there is a serious probability that the signal-to-noise ratio could be not big enough to numerically solve (2.170).

What is needed is a strategy in which probe and the EMT could coalesce without generating divergences. Clearly, composite operators built from elementary fields do not represent the right candidate for devising such a strategy. In the next chapter, a powerful mathematical tool, called *gradient flow*, will be introduced, with which well behaving probes can be created. The latter will forbid the appearance of contact terms, even when they coalesce with the EMT, proving to be the right candidates to numerically solve translation WI.

Chapter 3

Energy momentum tensor and Gradient flow

3.1 Introduction

The present and the following chapters represent the core of this work. In section (3.2), a detailed description of the Gradient Flow (or Wilson Flow in lattice theory) is provided. The description follows the lines of the paper written by Lüscher and Weisz [23], where dimensional regularization has been adopted. Then, in section (3.3), the gradient flow is used to define a new strategy for renormalizing the EMT. The strategy consists in probing WI for space-time symmetries using operators evolved along the flow. As will become clear in the following, the main advantage of this specific method is the total absence of contact terms.

3.2 Gradient flow in Yang Mills theory

The fundamental properties of the Gradient Flow are here explained. The attention is focused on the perturbative study of correlation functions made with *flowed fields*, the meaning of this definition to become clear later. The outcome of the perturbative analysis is that composite operators built along the flow do not need to be renormalized.

3.2.1 Gradient Flow prescription

In this subsection, the gradient flow is presented as an evolution equation for gauge fields over a new temporal extensions. The evolution can be graphically represented in terms of directed tree diagrams.

The starting point is a generic $SU(N)$ Yang Mills theory, with a gauge field $A_\mu(x)$ normalized

so that its action takes the form [1]

$$S = -\frac{1}{2g_0^2} \int d^D x \, \text{tr}\{F_{\mu\nu}(x)F_{\mu\nu}(x)\}, \qquad (3.4)$$

$$F_{\mu\nu} = \partial_\mu A_\nu - \partial_\nu A_\mu + [A_\mu, A_\nu]. \qquad (3.5)$$

The Gradient flow is then described by the following differential equation [23]

$$\partial_t B_\mu = D_\nu G_{\nu\mu}, \qquad\qquad B_\mu|_{t=0} = A_\mu, \qquad (3.6)$$

$$G_{\mu\nu} = F_{\mu\nu}|_{A_\mu=B_\mu}, \qquad\qquad D_\nu = \partial_\nu + [B_\nu, ...], \qquad (3.7)$$

where the fictitious parameter t will be referred to as the *flow time*. The form of the equation (3.6) resembles that of the Langevin equation for gauge theories [53]

$$\partial_t A_\mu = D_\nu F_{\nu\mu} + \eta_\mu(t,x), \qquad (3.8)$$

$$\langle \eta_\mu(t,x) \rangle = 0, \qquad (3.9)$$

$$\langle \text{tr}\{\eta_\mu(t,x)\eta_\nu(s,y)\} \rangle = 2\delta_{\mu\nu}\delta^D(x-y)\delta(t-s), \qquad (3.10)$$

In this case, correlation functions of the field A_μ can be averaged over the stochastic field η_ν and, when $t \to \infty$, they coincide with those of the Euclidean field theory described by the Yang Mills action. This is the main result of the so-called *stochastic quantization* process. Equation (3.6) differs from the Langevin equation for two points

1. The stochastic term is absent.

2. The initial distribution of the gauge field is not ignored, as usually happens when (3.8) is solved.

Nonetheless, perturbative properties, like the renormalization of the field B_μ can be studied following the same approach applied to the case of the Langevin equation. The renormalization of the latter has been thoroughly studied by Zinn-Justin and Zwanziger [54]. The first important result coming from their analysis is that some technicalities can be avoided if a *gauge damping* term is

---

[1] In this formulation, the generators of the Lie algebra $\mathfrak{su}(N)$ of $SU(N)$ are identified with antihermitean, traceless $N \times N$ matrices. Their normalization is fixed by

$$\text{tr}\{T^a T^b\} = -\frac{\delta^{ab}}{2}, \qquad (3.1)$$

The algebra is closed under the following commutation relations

$$[T^a, T^b] = f^{abc}T^c, \qquad (3.2)$$

and any element Y of $\mathfrak{su}(N)$ is given by

$$Y = Y^a T^a. \qquad (3.3)$$

added[2].

$$\partial_t B_\mu = D_\nu G_{\nu\mu} + \alpha_0 D_\mu \partial_\nu B_\nu, \tag{3.14}$$

$$B_\mu|_{t=0} = A_\mu. \tag{3.15}$$

This procedure does not affect the evolution of gauge-invariant observables. Indeed, equation (3.14) and (3.6) can be connected by a (time-dependent) gauge transformation

$$B_\mu = \Lambda(B_\mu|_{\alpha=0})\Lambda^{-1} + \Lambda\partial_\mu\Lambda^{-1}, \tag{3.16}$$

$$\dot{\Lambda}(t,x) = -\alpha_0\partial_\nu B_\nu \Lambda(t,x), \quad \Lambda|_{t=0} = 1. \tag{3.17}$$

Any gauge-invariant observable, built with the field B_μ, does not change under (3.16), hence it does not depend on α_0. This means that the perturbative study of the flow equation can be done using (3.14) without affecting gauge-invariant correlation functions.

Flow equation: analytic solution

The solution of equation (3.14) is obtained separating the linear part in the gauge field from the non-linear one.

$$\dot{B}_\mu = \mathfrak{L}_{\mu\nu}B_\nu + R_\mu, \tag{3.18}$$

$$\mathfrak{L}_{\mu\nu} = \Box\delta_{\mu\nu} + (\alpha_0 - 1)\partial_\nu\partial_\nu, \tag{3.19}$$

$$R_\mu = 2[B_\nu, \partial_\nu B_\mu] - [B_\nu, \partial_\mu B_\nu] + (\alpha_0 - 1)[B_\mu, \partial_\nu B_\nu] + [B_\nu, [B_\nu, B_\mu]]. \tag{3.20}$$

The linear part of the flow equation can be solved using the following heat kernel[3]

$$K_t(z)_{\mu\nu} = \int_p e^{ipz}\tilde{K}_t(p) = \int_p \frac{e^{ipz}}{p^2}\left[(\delta_{\mu\nu}p^2 - p_\mu p_\nu)e^{-tp^2} + p_\mu p_\nu e^{-\alpha_0 tp^2}\right]. \tag{3.22}$$

Taking into account the boundary condition in (3.14), the solution can be represented by the following integral form

$$B_\mu(t,x) = \int d^d y \left[K_t(x-y)_{\mu\nu}A_\nu(y) + \int_0^t ds K_{t-s}(x-y)_{\mu\nu}R_\nu(s,y)\right]. \tag{3.23}$$

It should be noted the retarded character of the above equation. The solution allows an expansion in terms of the fundamental gauge field, obtained by recursively inserting the equation on the right

---

[2]Basically, the free gluon propagator, obtained from the solution of (3.8), takes the following form

$$\tilde{\Delta}(k) = \left[(\delta_{\mu\nu} - k_\mu k_\nu/k^2) + t(k_\mu k_\nu)\right]/k^2. \tag{3.11}$$

The longitudinal part of $\tilde{\Delta}(k)$ is of order k^0 and gives a contribution that is not renormalizable by naïve power counting. The term coupled to α_0 in (3.14) is meant to suppress such longitudinal part. A similar problem arises when the renormalizability of the Standard Model in unitary gauge is concerned [55]. In this case, the gauge propagator

$$\tilde{\Delta}(k) = (\delta_{\mu\nu} + k_\mu k_\nu/M^2)/(k^2 + M^2). \tag{3.12}$$

scales like M^{-2} at high momenta and power counting cannot be used to study the divergence of diagrams. The problem is solved using the R_ξ gauge fixing

$$\tilde{\Delta}(k) = \frac{(\delta_{\mu\nu} - k_\mu k_\nu/k^2)}{k^2 + M^2} + \frac{\xi k_\mu k_\nu}{k^2(k^2 + \xi M^2)} \tag{3.13}$$

[3]From now on

$$\int_p = \int \frac{d^d p}{(2\pi)^d} \tag{3.21}$$

of itself. In momentum space, it becomes

$$\tilde{B}_\mu^a(t,p) = \tilde{K}_t(p)_{\mu\nu}\tilde{A}_\nu^a(t,p)$$

$$+ \sum_{n=2}^{3}\frac{1}{n!}\int_0^t ds\,\tilde{K}_{t-s}(p)_{\mu\nu}\int_{q_1}...\int_{q_n}(2\pi)^d\delta^d\left(p+\sum_{i=1}^{n}q_i\right)$$

$$\times X^{(n,0)}(p,q_1,...,q_n)_{\nu\nu_1...\nu_n}^{ab_1...b_n}\tilde{B}_{\nu_1}^{b_1}(t,-q_1)...\tilde{B}_{\nu_n}^{b_n}(t,-q_n). \quad (3.24)$$

Here, the flow-vertices $X^{(2,0)}$, $X^{(3,0)}$ can be worked out writing R_μ in momentum space [23]: they are totally symmetric only under the exchange of index-momentum combinations $(q_1,\nu_1,a_1)...(q_n,\nu_n,a_n)$, (p,ν,a) excluded.

Flow equation: diagrammatic solution

The expansion of (3.24) at a given order in the fundamental gauge field can be obtained through graphical methods. One just need to organize a small set of Feynman rules

- Flow line: this represents the heath kernel $\tilde{K}_{t-s}(p)$, that drives from a time s to a time $t > s$.

$$= \quad \delta^{ab}\theta(t-s)\tilde{K}_{t-s}(p)_{\mu\nu} \qquad (3.25)$$

The arrow points toward increasing flow time. It has to be noted the step function, introduced in order to keep manifest the retarded nature *flow propagator*.

- One-point vertex: this graphical element represents the boundary field A_μ.

$$= \quad \tilde{A}_\mu^a(p) \qquad (3.26)$$

- Flow-vertices: these terms come from the non-linear contribution R_μ.

$$= \quad \tilde{X}^{(2,0)}(p,q_1,q_2)_{\mu\nu_1\nu_2}^{ab_1b_2} \qquad (3.27)$$

$$= \quad \tilde{X}^{(3,0)}(p,q_1,q_2,q_3)_{\mu\nu_1\nu_2\nu_3}^{ab_1b_2b_3} \qquad (3.28)$$

Each flow vertex is integrated with respect the flow time, from zero to infinity: the range of integration is then bounded by the step functions in the flow propagator (3.25).

At a given order n in the fundamental field, the general contribution to $\tilde{B}_\mu^a(t,p)$ is given by the sum of all diagrams with up to n one-point vertices

$$+ \, ... \tag{3.29}$$

All the diagrams contributing are directed tree graphs with a single external line (denoted by the little square at the end of such line). As can be seen from the example above, flow lines can start at a one-point vertex, or a flow vertex, but can end only at another flow vertex (unless the line considered is the external one). Each flow vertex has an outgoing line that brings the combination (p, μ, a). The complete solution (3.24) can then be represented as a sum over an infinite set of tree-diagrams.

3.2.2 Perturbation theory

Gauge fields satisfying the flow equation can be used to define a new type of correlation function. The latter can be analytically studied when perturbation theory applies. In this subsection, a set of diagrammatic rules will be given to make the perturbative analysis easy to perform.

A n-point correlation function of B fields can be evaluated using the expansion (3.29) and then averaging over the fundamental gauge fields. However, it can also be obtained directly from a set of Feynman rules defined in a $(D+1)-$dimensional theory.

The flow equation is invariant under the following infinitesimal transformation

$$\delta B_\mu(t,x) = D_\mu \omega(t,x), \tag{3.30}$$

$$\dot{\omega} = \alpha_0 D_\mu \partial_\mu \omega, \tag{3.31}$$

$$\omega(t,x) \in \mathfrak{su}(N). \tag{3.32}$$

It has to be noted that the initial value of ω is not constrained, so it can generate the full gauge group at $t=0$ and extend the $SU(N)$ gauge symmetry to the *bulk theory* (the theory at positive flow time). To allow a perturbative expansion, a gauge fixing procedure has to be applied: this is usually achieved through the Faddevv-Popov procedure [56], which results in adding a gauge fixing and a ghost action.

$$S_{gf} = -\frac{\lambda_0}{g_0^2} \int d^d x \, \text{tr}\{\partial_\nu A_\nu(x) \partial_\mu A_\mu(x)\}, \tag{3.33}$$

$$S_{gh} = -\frac{2}{g_0^2} \int d^d x \, \text{tr}\{\partial_\nu \bar{c}(x) D_\mu c(x)\}. \tag{3.34}$$

$$\tag{3.35}$$

It should be clear that gauge-invariant correlation functions built with B fields are independent on the gauge fixing parameter λ_0.

$(D + 1)$ dimensional Feynman rules

To derive a new set of diagrammatic rules, the flow-line diagrams that describe the B field need to be combined with the Feynman rules of the underlying theory. This can be easily done by computing the two-point function of flow-evolved fields. At leading order, this corresponds to contract two terms like the first diagram on the r.h.s. of (3.29)

$$\langle \tilde{B}^a_\mu(t,p)\tilde{B}^b_\nu(s,q)\rangle = (2\pi)^d \delta^d(p+q)g_0^2 \delta^{ab}\tilde{D}_{t+s}(p)_{\mu\nu} + \mathcal{O}(g_0^4), \tag{3.36}$$

$$\tilde{D}_t(p)_{\mu\nu} = \frac{1}{(p^2)^2}\left[(\delta_{\mu\nu}p^2 - p_\mu p_\nu)e^{-tp^2} + \frac{p_\mu p_\nu}{\lambda_0}e^{-\alpha_0 tp^2}\right] \tag{3.37}$$

$$= \delta^{ab}g_0^2\tilde{D}_{t+s}(p)_{\mu\nu} \tag{3.38}$$

The nice property of this two-point function is that the same analytic expression for AA and AB contractions can be obtained just turning off the dependence on flow times in $\tilde{D}_{t+s}(p)_{\mu\nu}$. For this reason, the same graphical symbol will be used to indicate the three different contractions. It should be noted that contraction of one-point vertices always converts flow lines to gauge-field (wiggly) lines. As an example, the contraction of the following diagram

transforms flow lines in gauge-field lines and couples them with elementary ($t = 0$) and flow vertices. This should clarify enough how the flow line diagrams combine with the Feynman rules of the underlying theory.

Then, one has to consider the flow time as an additional coordinate, and the $(D+1)$ dimensional space as a half-space with a D-dimensional boundary (only positive flow times are allowed). The $SU(N)$ gauge theory lies on the boundary, while the B fields, generated by the flow equation, belong to the $(D+1)-$dimensional bulk. The ordinary and flow vertices represents boundary and bulk interaction terms, while the propagation in the $(D+1)$ dimensions is described by (3.38) and (3.25). The ghost propagator

$$\langle \tilde{c}^a(p)\tilde{\bar{c}}^b(q)\rangle = (2\pi)^d \delta^d(p+q)g_0^2\tilde{D}(p), \tag{3.40}$$

$$= \delta^{ab}g_0^2\tilde{D}(p) = \delta^{ab}g_0^2 p^{-2}, \tag{3.41}$$

propagates only on the boundary. The n-point correlation functions built with flowed fields are then given by Feynman diagrams in $(D+1)$ dimensions. Some special features, however, need to be pointed out.

1. Flow vertices have always one outward-directed flow line. This line corresponds to the first momentum-index combination of the vertices $X^{(2,0)}$, $X^{(3,0)}$, as given by (3.27). The other attached lines can be gauge-field lines or flow lines. Here is given the example of $X^{(2,0)}$

$$\tag{3.42}$$

2. Flow lines can only start at a flow vertex and are either external or end at another flow vertex. The situation is different for gauge-field lines, which can start and end at both flow vertices and ordinary vertices.

3. Ordinary vertices are clearly defined at zero flow time, while flow vertices are inserted at some intermediate time, which is integrated up to infinity. The time dependence of propagators is given by the flow times that label the end points.

4. Diagrams with closed flow line loops are set to zero. This happens because flow-line diagrams are tree diagrams, and the contraction of n-point vertices never leads to new flow lines. This point is crucial when the renormalization of the $(D+1)$-dimensional theory is concerned.

$(D+1)$ dimensional field theory

The Feynman diagrams of the previous subsection can be considered as a set of graphic rules for a *local* $(D+1)$-dimensional field theory. To prove this, an action describing the evolution of the B field has to be introduced. Moreover, this field has to be considered as an independent degree of freedom (with exception of the boundary condition at zero flow time). All this can be achieved introducing a Lagrange multiplier $L_\mu(t,x) = L_\mu^a(t,x)T^{a}$[4]. The total action is given by

$$S_{tot} = S + S_{gf} + S_{gh} + S_{fl}, \tag{3.43}$$

$$S_{fl} = -2\int_0^\infty dt \int d^dx \mathrm{tr}\{L_\mu(t,x)(\dot{B}_\mu - D_\nu G_{\nu\mu} - \alpha_0 D_\mu \partial_\nu B_\nu)(t,x)\}, \tag{3.44}$$

and the path integral is given by

$$\mathcal{Z} = \int D[A]D[B]D[L]\exp\left(-S_{tot}\right). \tag{3.45}$$

The integration over the field L_μ automatically impose the validity of the flow equation. It should be noted that no particular boundary condition has been applied on the Lagrange multiplier. The next step is to define which kind of propagators characterizes the theory. From the previous subsection, it should be clear that contractions like AA, AB, BB are naturally included in the theory (3.43). One has still to deal with LB and LA contractions. The former is evident from the form of the flow action S_{fl}, while the latter arises from the boundary condition $B_\mu(0,x) = A_\mu(x)$. Things can be simplified rewriting the field B_μ as

$$B_\mu(t,x) = \int d^dy K_t(x-y)_{\mu\nu} A_\nu(y) + b_\mu(t,x), \tag{3.46}$$

$$b(t,x)_\mu|_{t=0} = 0. \tag{3.47}$$

If now one considers just the quadratic part of S_{fl}

$$\int_0^\infty dt \int d^dx \mathrm{tr}\{L_\mu(\partial_t\delta_{\mu\nu} - \mathfrak{L}_{\mu\nu})B_\nu\}(t,x), \tag{3.48}$$

it comes out that the Lagrange multiplier and the gauge field A_μ decouple, leaving only a constraint for the field $b_\mu(t,x)$. This result is important since leaves the form of the gauge field and ghost propagators unchanged, and condense the information of LB contractions in the bL propagator. The latter can be determined from the solution of

$$(\partial_t\delta_{\mu\nu} - \mathfrak{L}_{\mu\nu})H(t,x;s,y)_{\nu\rho} = \delta_{\mu\rho}\delta(t-s)\delta^d(x-y), \tag{3.49}$$

$$H(t,x;s,y)_{\nu\rho}|_{t=0,s>0} = 0, \tag{3.50}$$

---

[4]The component $L_\mu^a(t,x)$ is purely imaginary.

where

$$\langle b_\mu^a(t,x)L_\nu^b(s,y)\rangle|_{l.o.} = \delta^{ab}H(t,x;s,y)_{\nu\rho}. \tag{3.51}$$

It is easy to show that

$$H(t,x;s,y)_{\nu\rho} = \theta(t-s)K_{t-s}(x-y)_{\mu\nu}, \tag{3.52}$$

which implies that the b field has to be *delayed* with respect the L field. The retarded Green function above equals exactly the flow propagator (3.25), which now will be identified as a bL contraction. As far the propagation in the $(D+1)$-theory is concerned, the main results are

- On the boundary, only AA and $\bar{c}c$ propagators exist. The former can be regarded as BB propagators at zero flow times

- In the bulk, only BB and BL propagators exists, the former represented by gauge-field lines, the latter by directed flow lines.

What is missing now is the inclusion of flow vertices (3.42) inside the $(D+1)$-dimensional theory. These are generated by the non linear component of the flow equation and can be recast in the interacting part of S_{fl}

$$S_{fl,Int} = 2\int_0^\infty dt \int d^dx \operatorname{tr}\{L_\mu(r,x)R_\mu(t,x)\}. \tag{3.53}$$

Hence, all the vertices and propagators of the previous subsection have been recovered. Keeping in mind the structure of B_μ (3.46), it is now possible to derive any correlation function using the Feynman rules of the $(D+1)$-dimensional theory.

A final remark has to be done about flow-lines and flow-line loops. The first thing to recall is that flow-lines can start and end at flow vertices, but never are attached to boundary vertices. Given the structure of (3.52), one identifies outward- and inward-directed external lines with B and L external fields respectively. The same rule applies to closed flow lines. However, because of the retarded nature of (3.52) and of the fact that no flow loops are generated in the tree expansion of B_μ, diagrams with closed flow lines are totally absent. Two simple examples can be displayed

- Closed loop on single flow vertex.

$$\tag{3.54}$$

    This kind of diagrams vanishes because dimensional regularization sets the loop momentum integral to zero[5].

- Closed loops on multiple flow vertices

$$\tag{3.55}$$

    In this case, the diagram vanishes because of time integration. Indeed, the retarded nature of the flow propagator forces the flow time at each vertex to be squeezed to a interval of measure zero.

---

[5]If a lattice regulator is adopted, this result may not be guaranteed. However, it is always possible to include a ghost field in the action that cancel these flow loops algebraically [57]

3.2.3   1-loop non-renormalization

It is interesting to study the renormalization properties of the new *bulk* correlation functions. To do so, a detailed analysis of their leading divergences has to be carried out.

A simple example of one-loop calculation has been done for BB propagator [23]: here, only the divergent diagrams are presented, followed by their related ϵ^{-1} singularities.

$$\langle B_\mu(t,x)B_\nu(s,y)\rangle = \tag{3.56}$$

The first three diagram represent the one-loop contribution to the gauge AA vertex function. These terms arise from the boundary theory. The fourth diagram is a contribution to the LA contraction, which arises only at 1-loop order. The fifth and sixth diagrams are correction to the LB (note that only flow vertices appear) while the seventh is the contribution to the LL vertex function. The divergences arising from the boundary loops are already known from standard perturbation theory: here is reported their contribution[6]

$$\Gamma_{AA}^{(1)}(p)_{\mu\nu}^{ab}(p)|_{pole} = \delta^{ab}(p^2\delta_{\mu\nu} - p_\mu p_\nu)\frac{N}{16\pi^2\epsilon}\left(\frac{13}{6} - \frac{1}{2\lambda_0}\right). \tag{3.57}$$

Diagrams involving flow vertices are finite for $d = 4$ as long as the flow time is positive. The only source of divergence can arise from the integration on t attached to flow vertices, where the flow time goes from 0 up to an upper limit imposed by the external flow propagator. The divergent part can be extracted taking the asymptotic series of the time integral at large loop momentum and retaining the leading terms [23]. For the LA and LB contribution, the divergences are

$$\Gamma_{LA}^{(1)}(t,p)_{\mu\nu}^{ab}|_{pole} = g_0^2\delta^{ab}\delta(t)\delta_{\mu\nu}\frac{N}{16\pi^2\epsilon}\left(\frac{3}{4} + \frac{3}{4\lambda_0}\right), \tag{3.58}$$

$$\Gamma_{LB}^{(1)}(t,sp)_{\mu\nu}^{ab}|_{pole} = g_0^2\delta^{ab}\delta(t)\delta(s)\delta_{\mu\nu}\frac{N}{16\pi^2\epsilon}\left(-\frac{1}{2\lambda_0}\right). \tag{3.59}$$

On the other hand, the last diagram does not produce divergences, implying that the LL vertex function is finite for $d = 4$. It has to be noted that divergences are localized on the boundary of the 5D theory, their localization being established by flow time delta functions .

---

[6]In this notation, $\Gamma|_{pole}$ represents the divergent part of the 1PI two-vertex function

It is interesting to check whether or not the BB propagator actually renormalizes. To do this, first bare parameters and fields need to be rewritten in terms of their renormalized counterparts

$$g_0^2 = \mu^{2\epsilon} g_R^2 Z, \tag{3.60}$$

$$\lambda_0 = \lambda_R Z_3^{-1}, \tag{3.61}$$

$$A_\mu^a = \sqrt{Z Z_3}(A_R)_\mu^a, \tag{3.62}$$

$$c^a = \tilde{Z}_3 \sqrt{Z Z_3}(c_R)_\mu^a, \tag{3.63}$$

$$\bar{c}^a = \sqrt{\frac{Z}{Z_3}}(\bar{c}_R)_\mu^a, \tag{3.64}$$

where Z, Z_3 and $\tilde{Z}_3$ are the renormalization constants of the coupling, the gauge field and the ghost field in the standard representation of the Yang Mills action. Here, A_μ takes also a contribution from Z due to the specific normalization chosen in this case. The asymmetric renormalization of the fields c and $\bar{c}$ has been chosen for reason that will become clear in the following. At leading order, the renormalization constants one needs are

$$Z = 1 - \frac{b_0}{\epsilon} g_R^2 + \mathcal{O}(g_R^4), \quad b_0 = \frac{N}{16\pi^2} \frac{11}{3}, \tag{3.65}$$

$$Z_3 = 1 + \frac{c_0}{\epsilon} g_R^2 + \mathcal{O}(g_R^4), \quad c_0 = \frac{N}{16\pi^2}\left(\frac{13}{6} - \frac{1}{2\lambda_R}\right), \tag{3.66}$$

Then, the propagator has to be expressed in terms of its $SO(4)$ invariant parts $\mathcal{A}$ and $\mathcal{B}$

$$\langle \tilde{B}_\mu^a(t,p)\tilde{B}_\nu^b(s,q)\rangle = (2\pi)^d \delta^d(p+q)\frac{\delta^{ab}}{(p^2)^2}\{(\delta_{\mu\nu}p^2 - p_\mu p_\nu)\mathcal{A}(t,s,p^2) + p_\mu p_\nu \mathcal{B}(t,s,p^2)\} \tag{3.67}$$

All the self-energy diagrams displayed in (3.56) contributes to $\mathcal{A}$ and $\mathcal{B}$. Once bare couplings are expressed in terms of the renormalized ones, these functions admit an expansion of the form

$$\zeta = \mu^{2\epsilon}\sum_{l=0}^{\infty} g_R^{2l+2}\zeta, \quad \zeta = \mathcal{A} \text{ or } \mathcal{B} \tag{3.68}$$

At leading order, one has

$$\mathcal{A} = g_R^2\left(1 - g_R^2 \frac{b_0}{\epsilon}\right)e^{(t+s)p^2}, \tag{3.69}$$

$$\mathcal{B} = g_R^2\left(1 + g_R^2 \frac{c_0 - b_0}{\epsilon}\right)e^{\alpha_0(t+s)p^2}. \tag{3.70}$$

On the other hand, contributions coming all the diagrams listed in (3.56) have to be included. The boundary contribution is obtained sandwiching $\Gamma_{AA}|_{pole}$ between two gauge propagators at time t and s

$$g_R^4 \tilde{D}_t^{ac}(p)_{\mu\rho}\Gamma_{AA}(p)_{\rho\lambda}^{cd}|_{pole}\tilde{D}_s^{db}(p)_{\lambda,\nu} = g_R^4 \frac{c_0}{\epsilon}\frac{\delta^{ab}}{(p^2)^2}(\delta_{\mu\nu}p^2 - p_\mu p_\nu)e^{-(s+t)p^2} \tag{3.71}$$

A similar procedure can be done for $\Gamma_{LA}|_{pole}$, $\Gamma_{LB}|_{pole}$ with few details to be specified:

1. Both vertex functions must be multiplied by the appropriate flow/gauge propagator and integrated over the flow time. One integration is sufficient for $\Gamma_{LA}|_{pole}$, two for $\Gamma_{LB}|_{pole}$. The role of the delta functions is then to locate the divergences on the boundary of the theory.

2. Diagrams with flow vertices brings two contributions, due to the difference in the external legs.

Taking into account these simple details, one obtains

$$g_R^2 \int_0^\infty d\tau \tilde{H}^{ac}_{t-\tau}(p)_{\mu\rho} \left(\Gamma_{LA}(p,\tau)^{cd}_{\rho\lambda}|_{pole} + \int_0^\infty d\sigma \Gamma_{LA}(p,\tau,\sigma)^{cd}_{\rho\lambda}|_{pole} \right) \tilde{D}^{db}_s(p)_{\lambda,\nu} + (s \leftrightarrow t)$$

$$= g_R^4 \frac{(b_0 - c_0)}{\epsilon} \frac{\delta^{ab}}{(p^2)^2} \left[(\delta_{\mu\nu}p^2 - p_\mu p_\nu)e^{-(s+t)p^2} + \frac{1}{\lambda_R}p_\mu p_\nu e^{-\alpha_0(s+t)p^2} \right] \quad (3.72)$$

Adding (3.71) and (3.72) to the expansion (3.69) and (3.70) results in a cancellation of all divergences at leading order in g_R. This means that the fields B_μ and L_μ do not need to be renormalized. The cancellation of divergences can be easily proved also for BL and BA_R contractions. The case of LA_R and LL is even easier to prove: since there cannot be diagrams with only in-going and not outgoing flow lines, LA_R and LL contractions must be identically zero.

Since the field B_μ and L_μ do not renormalize, any kind of correlation function of the $(D+1)$-dimensional theory can be evaluated, its finiteness being guaranteed by the counterterms of the boundary $SU(N)$ gauge theory. The statement is strictly true only at one-loop in perturbation theory. However it is possible to extend its validity to all orders in the gauge coupling

3.2.4 BRS symmetry

To prove the finiteness of flowed correlation functions, the BRS symmetry [58] has to be extended from the boundary theory to the bulk one. The boundary theory

$$S + S_{gf} + S_{gh} \quad (3.73)$$

as well as the integration measure of fields A_μ, c and $\bar{c}$ can be proved to be invariant under the following BRS variation (also called Slavnov transformation)

$$\delta A_\mu = D_\mu c, \quad (3.74)$$

$$\delta c = -c^2, \quad (3.75)$$

$$\delta\bar{c} = \lambda_0 \partial_\mu A_\mu. \quad (3.76)$$

From this invariance, a set of WI arises, called Slavnov-Taylor identities. These identities can be used to generate a certain number of constraints on the possible counterterms of the theory.
Studying the renormalization of the $(D+1)$-dimensional theory means to classify the counterterms needed to make correlation functions finite at all order in perturbation theory. Extending the BRS symmetry to the $t > 0$ bulk will make this work easier. Since the B fiels are non local in the fundamental gauge degrees of freedom, it seems really difficult to generalize, in a *local* way, the BRS transformation at positive flow times. However, it has been shown [54] that this problem can be overcome adding a new kind of ghost fields.

Ghost fields in the bulk

The additional ghost fields can be generated by the following term

$$S_{d\bar{d}} = -2 \int_0^\infty dt \int d^dx \, \text{tr}\{\bar{d}(t,x)(\dot{d} - \alpha_0 D_\mu \partial_\mu d)(t,x)\}, \quad (3.77)$$

$$d|_{t=0} = c, \quad (3.78)$$

where no boundary condition has been imposed on the $\bar{d}$ field, which plays a role of a Lagrange multiplier[7]. Two new propagators can be introduced,

---

[7]Note that the field $d(t,x)$ satisfy the same differential equation of the transformation $\omega(t,x)$ that extends the gauge symmetry to the bulk theory.

- $d\bar{d}$ propagator. This contraction is the analogue of the BL propagator, and its momentum space representation is given by

$$\langle \tilde{d}^a(t,p)\tilde{\bar{d}}^a(t,p)\rangle = (2\pi)^d \delta^d(p+q)\delta^{ab}\theta(t-s)\tilde{K}_{t-s}(p) + \mathcal{O}(g_0^2), \tag{3.79}$$

$$= \quad \delta^{ab}\theta(t-s)\tilde{K}_{t-s}(p) = \delta^{ab}\theta(t-s)e^{-\alpha_0(t-s)p^2} \tag{3.80}$$

- $d\bar{c}$ propagator. This is a mixed contraction that reduces to the boundary ghost propagator at $t=0$.

$$\langle \tilde{d}^a(t,p)\tilde{\bar{c}}^a(t,p)\rangle = (2\pi)^d \delta^d(p+q)\delta^{ab}\tilde{D}_t(p) + \mathcal{O}(g_0^2), \tag{3.81}$$

$$\tilde{D}_t(p) = \frac{1}{p^2}e^{-\alpha_0 tp^2} \tag{3.82}$$

As for the gauge field, this mixed contraction is symbolically represented as a ghost propagator. The arrow has to flow from the barred field to the unbarred one. No $c\bar{d}$ contractions are allowed. From the non linear component of (3.77) a flow vertex is generated

$$S_{d\bar{d},Int} = -\int_0^\infty dt \int_{p,q,r} (2\pi)^d \delta^d(p+q) \times X^{(1,1)}(p,q,r)_\mu^{abc}\tilde{B}_\mu^a(t,-p)\tilde{\bar{d}}^b(t,-q)\tilde{d}^c(t,-r), \tag{3.83}$$

where it can be easily shown that

$$X^{(1,1)}(p,q,r)_\mu^{abc} = \alpha_0 f^{abc}r_\mu. \tag{3.84}$$

It is possible to prove that closed $d\bar{d}$ lines vanish as in the case of flow loops in the previous section. Moreover, loops with mixed propagators cannot exist, since the propagation $c \leftarrow \bar{d}$ is not allowed. Then the only possible loops are the usual ones of the theory at flow time zero.

BRS symmetry in the bulk

According to [54], a set of BRS transformations for the bulk theory can be represented by

$$\delta B_\mu = D_\mu d, \tag{3.85}$$

$$\delta L_\mu = [L_\mu, d], \tag{3.86}$$

$$\delta d = -d^2, \tag{3.87}$$

$$\delta \bar{d} = D_\mu L_\mu - \{d, \bar{d}\}. \tag{3.88}$$

The nice feature of equations (3.85) and (3.87) is that they reproduces the exact BRS variation for boundary fields at $t=0$. It is possible to show that the bulk action $S_{fli} + S_{d\bar{d}}$ is invariant under the above symmetry transformations [8]. As a consequence, a set of Slavnov-Taylor identities can be

---

[8]An easy way to show this is by introducing the following fields

$$E_\mu(t,x) = \dot{B}_\mu - D_\nu G_{\nu\mu} - \alpha_0 D_\mu \partial_\nu B_\nu, \tag{3.89}$$

$$e(t,x) = \dot{d} - \alpha_0 D_\mu \partial_\mu d, \tag{3.90}$$

which obey the following BRS variations
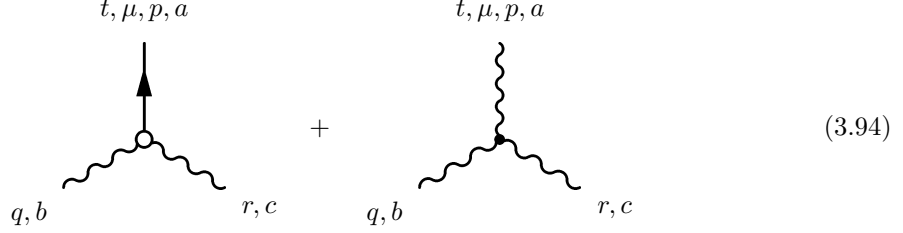
$$\delta E_\mu = [E_\mu, d] + D_\mu e, \tag{3.91}$$

$$\delta e = -\{e, d\}. \tag{3.92}$$

written down and used to impose constraints on the renormalization constants of the theory. One of these identities will be really important in the following

$$\lambda_0 \langle B_\mu^a(t,x)\partial_\nu A_\nu^b(y)\partial_\rho A_\rho^b(z)\rangle = -\langle (D_\mu d)^a(t,x)\bar{c}^b(y)\partial_\nu A_\nu^b(z)\rangle, \tag{3.93}$$

which involves three-point vertices and non-trivial cancellations among the various contributions. The identity can be proved at tree level setting $\alpha_0 = \lambda_0 = 1$ [9]: the relevant diagrams for the l.h.s. are

$$\tag{3.94}$$

The first diagram is represented by the following formula[10]

$$g_0^4 \int_0^\infty d\tau\,\theta(t-\tau)\tilde{K}_{t-\tau}(p)_{\mu\mu'}X^{(2,0)}(p,q,r)_{\mu'\nu'\rho'}^{abc}\tilde{D}_\tau(q)_{\nu\nu'}\tilde{D}_\tau(r)_{\rho\rho'}(iq_\nu)(ir_\rho). \tag{3.95}$$

With the above mentioned choice for the gauge fixing and gauge damping parameters, one has

$$\tilde{K}_t(p) = e^{-tp^2}, \tag{3.96}$$

$$\tilde{D}_t(p)_{\mu\nu} = \frac{\delta_{\mu\nu}}{p^2}e^{-tp^2}, \tag{3.97}$$

$$X^{(2,0)}(p,q,r)_{\mu\nu\rho}^{abc} = if^{abc}\{(r-q)_\mu\delta_{\nu\rho} + 2(q_\rho\delta_{\mu\nu} - r_\nu\delta_{\mu\rho})\}. \tag{3.98}$$

Plugging these expressions in (3.95) gives

$$g_0^4\frac{q_\nu r_\rho}{q^2 r^2}X^{(2,0)}(p,q,r)_{\mu\nu\rho}^{abc}\left(\frac{e^{-(q^2+r^2)t} - e^{-p^2 t}}{q^2 + r^2 - p^2}\right) =$$

$$= \frac{ig_0^4 f^{abc}}{q^2 r^2}\frac{1}{2}(q-r)_\mu\left(e^{-(q^2+r^2)t} - e^{-p^2 t}\right)$$

$$= -\frac{ig_0^4 f^{abc}}{p^2 q^2 r^2}C_{\mu,1}, \tag{3.99}$$

where

$$C_{\mu,1} = \frac{1}{2}(q-r)_\mu p^2\left(e^{-(q^2+r^2)t} - e^{-p^2 t}\right). \tag{3.100}$$

The second diagram results in a similar structure, with a coefficient

$$C_{\mu,2} = \left[\frac{1}{2}(q-r)_\mu p^2 + \frac{1}{2}(q^2 - r^2)p_\mu\right]e^{-p^2 t}. \tag{3.101}$$

---

[9]It should be stressed that any value of λ_0 and α_0 satisfy (3.93). This is not surprising, since BRS symmetry is intimately related with gauge invariance.

[10]A global $(2\pi)^d\delta^d(p+q+r)$ has been factored out

The r.h.s is characterized by three different diagrams

$$= -\frac{ig_0^4 f^{abc}}{p^2 q^2 r^2} \underbrace{\left(-p^2 r_\mu e^{-(q^2+r^2)t}\right)}_{C_{\mu,3}} \tag{3.102}$$

$$\tag{3.103}$$

$$+ \qquad = -\frac{ig_0^4 f^{abc}}{p^2 q^2 r^2} \underbrace{\left[-\frac{p^2}{2} p_\mu \left(e^{-(q^2+r^2)t} - e^{-p^2 t}\right)\right]}_{C_{\mu,4}} \tag{3.104}$$

$$\tag{3.105}$$

$$+ \qquad = -\frac{ig_0^4 f^{abc}}{p^2 q^2 r^2} \underbrace{\left[-(qr+r^2) p_\mu e^{-p^2 t}\right]}_{C_{\mu,5}} \tag{3.106}$$

It is then easy to show that

$$C_{\mu,1} + C_{\mu,2} = C_{\mu,3} + C_{\mu,4} + C_{\mu,5} \tag{3.107}$$

Finiteness of the renormalized perturbation expansion

To show that correlation functions of bulk fields are finite, it is necessary to reorganize the perturbation expansion in terms of renormalized parameters and fields. The expansion is generated by an action $S_0 + \Delta S$, organized in the following way

$$S_{tot} = S + S_{gf} + S_{c\bar{c}} + S_{fl} + S_{d\bar{d}}, \tag{3.108}$$

$$S_0 = S_{tot}|_{Z=Z_3=\tilde{Z}_3=1}, \tag{3.109}$$

$$\Delta S = S_{tot} - S_0 + \Delta S_{bc}. \tag{3.110}$$

In this way, ΔS contains counterterms of the underlying $SU(N)$ theory and an additional countertem

$$\Delta S_{bc} = 2 \int d^d x \text{tr}\{(\sqrt{ZZ_3} - 1) L_\mu(0, x)(A_R)_\mu(x) + (\sqrt{ZZ_3 \tilde{Z}_3} - 1)\bar{d}(0, x) c_R(x)\} \tag{3.111}$$

The boundary conditions for renormalized fields then become

$$B_\mu|_{t=0} = (A_R)_\mu, \quad d|_{t=0} = c_R. \tag{3.112}$$

These conditions differ from those applied on boundary bare fields, since multiplicative factors are missing. The role of ΔS_{bc} is to correct for this difference.

The next step is to classify the possible, *local* counterterms, which can in principle belong to both the boundary or the bulk. For the theory under study, bulk counterterms are excluded. The statement is supported by the following arguments

1. At large flow times, correlation functions containing bulk fields $(B_\mu, L_\mu, d, \bar{d})$ are generated only by Feynman diagrams containing only flow lines and flow vertices. These are directed trees diagrams, or products of such trees. Each tree ends at one of the B or d field contained in the correlation function, while the starting point will correspond to L and $\bar{d}$ fields.

2. Directed tree diagrams do not generate loops, so the corresponding correlation functions are not singular. Even if one ore more bulk fields coalesce on the same point, no divergence arises, since no loops are generated.[11]

The above result implies that any divergent part of correlation functions, if existing, should be matched by the insertion of a counterterm localized on the boundary. The boundary counterterms of the underlying theory are already included, so contractions of A_R, c_R and $\bar{c}_R$ fields are finite to all orders. Divergences can arise only from diagrams with at least one flow vertex, attached to an external flow line. As a consequence, the new counterterms should contain L_μ and $\bar{d}$ fields. The available operators should have mass dimension not larger than 4, and respect $SO(4)$ symmetry, as well as ghost number conservation.

This reduces the choice to countertems of the form[12]

$$2g_R^{2l} \int d^d x \, \mathrm{tr}\{y_1 L_\mu(0,x)(A_R)_\mu(x) + y_2 \bar{d}(0,x)c_R(x)\}, \tag{3.113}$$

where the coefficients y_1 and y_2 are singular in ϵ[13]. It is now that the Slavnov-Taylor identity (3.93) plays a key role. In terms renormalized quantities, the identity becomes

$$\lambda \langle B_\mu^a(t,x)\partial_\nu(A_R)_\nu^b(y)\partial_\rho(A_R)_\rho^b(z)\rangle = -\langle (D_\mu d)^a(t,x)(\bar{c}_R)^b(y)\partial_\nu(A_R)_\nu^b(z)\rangle, \tag{3.114}$$

where now the asymmetric renormalization of ghost fields find its motivation (all renormalization factors drop out).

The equation above holds only if no divergence arises. All the fields appearing in the identity are renormalized, and cannot receive further renormalizations.

If the correlation functions of the theory are singular at a given loop order l, then singularities must be cancelled by a counterterm of the form (3.113). The contribution of the latter to the identity (3.114) is obtained by inserting the corresponding two-point vertices into the tree diagrams (3.2.4-3.2.4). The effect of these insertions is to multiply the values of the diagrams by g^{2l} and then redefine the identity as

$$2y_1 C_{\mu,1} + y_1 C_{\mu,2} = (y_1 + y_2)(C_{\mu,3} + C_{\mu,4}) + y_2 C_{\mu,5} \tag{3.115}$$

Written in this form, the above equation is valid only if $y_{1,2} = 0$. This means that insertions of the operator (3.113) are not compatible with the BRS identity (3.114). Since BRS symmetry has to be preserved, the addition to the action of a counterterm of the form (3.113) has to be ruled out. Hence, correlation functions appearing in (3.114) must therefore be finite at l-loop order: the same statement holds for all the other (renormalized) correlation functions of the theory.

This suffices to say that the $(D+1)$-dimensional theory generated by the flow does not need to be renormalized.

3.2.5 Concluding remarks

The finiteness of correlation functions built along the flow can be proved using different types of regulators. In particular, the same results hold when the theory is regularized with the lattice.

---

[11]This point will be crucial for the strategy adopted to renormalize the lattice EMT.

[12]It has to be kept in mind that $[L_\mu] = [\bar{d}] = 3$

[13]In principle, also LB and $\bar{d}d$ terms could be included. However, these terms are not independent due to (3.112), and their inclusion will end up simply in a redefinition of y_1 and y_2

In this case, a possible choice for the flow evolution could be given by the gradient of the Wilson action[14]

$$\dot{V}_t(x,\mu) = -g_0^2 \{\partial_{x,\mu} S_W(V_t)\} V_t(x,\mu), \tag{3.116}$$

$$V_t(x,\mu)|_{t=0} = U(x,\mu), \tag{3.117}$$

$$S_W(U) = \frac{1}{g_0^2} \sum_p \mathrm{Re}\left[\mathrm{tr}\{1 - U(p)\}\right], \tag{3.118}$$

$V_t(x,\mu)$ representing the flow of lattice gauge fields. The link differential operator is given by the Lie derivative

$$\partial_{x,\mu}^a f(U) = \frac{d}{ds} f(e^{sX} U)|_{s=0}, \quad X(y,\nu) = \begin{cases} T^a & \text{if } (y,\nu) = (x,\mu) \\ 0 & \text{otherwise} \end{cases}$$

with its basis-independent form given by

$$\partial_{x,\mu} f(U) = \partial_{x,\mu}^a f(U) T^a. \tag{3.119}$$

The above formulation is not unique. Every kind of lattice discretization whose continuum classical limit reproduces the correct form of the gradient flow is a good candidate. Except for artefacts proportional to a positive power of the lattice spacing, the correlation functions of bulk fields will not depend on the discretization adopted. Even if the fundamental space-time symmetries are not fulfilled, the remaining ones suffice to exclude counterterms that are not present in the continuum formulation. So, correlation functions of time-dependent fields do not need to be renormalized, and their value in the continuum limit will be regulator-independent[15]. This is an important results, since allows to exploit the properties of the gradient flow in lattice numerical studies.

Indeed, the gradient flow covers a wide spectrum of applications.

- It can be used to define a running coupling

$$g_{WF}^2 \propto t^2 \langle \mathrm{tr}\{G_{\mu\nu} G_{\mu\nu}\}\rangle, \tag{3.120}$$

  as shown in [21]. This *Wilson Flow* coupling has been employed for systematic scale-setting studies in lattice simulations, using different types of boundary conditions [21, 27, 28, 29, 30].

- Reparametrizing the path integral in terms of evolved fields[16]

$$\mathcal{Z} = \int D[V] e^{-\tilde{S}(V)} \tag{3.122}$$

  improved the understanding of how topological sectors gets divided on the lattice as continuum limit is approached [21].

- The asymptotic study of flowed quantities in the $t \to 0$ can be performed through a *small flow time expansion*. In its general form, this expansion relates composite, flowed operator to renormalized quantities

$$\mathcal{O}(x,t) - \langle \mathcal{O}(x,t)\rangle = \sum_{i=1}^{n} c_i(t) (\mathcal{U})_R^i(x), \tag{3.123}$$

---

[14]This is why the lattice version of the gradient flow is also called *Wilson Flow*

[15]There could be only finite renormalizations of couplings and gauge-fixing parameters.

[16]This is allowed since the transformation

$$U \to V = V_t \tag{3.121}$$

is a diffeomorphism on the field space.

the mapping provided by the *small flow time coefficients*. The role of these coefficients is to encode the divergences that would affect the insertion of the (bare) operator $\mathcal{O}(x, t)$ at $t = 0$. Using the small flow time expansion, Suzuki et al. devised a strategy for perturbatively compute the lattice renormalized EMT [31].

Finally, it should be mentioned that the *finiteness* of the Yang Mills gradient flow remains intact when matter content is included at $t = 0$, provided that the bulk action is left unchanged. Things do not work equally well when the flow evolution is extended to matter fields[17]

3.3 Ward Identities with Wilson Flow

3.3.1 Introduction

The previous section showed the remarkable properties of the gradient flow. It could be questioned whether or not these properties could be useful to renormalize the lattice energy momentum tensor. Intuitively, an answer can be given by reminding one of the key features of the bulk theory:

> ...*flowed correlation functions do not generate divergences, even if one or more bulk fields coalesce on the same point...*

Recalling the general form of translation WI

$$\langle \partial_\mu T_{\mu\nu}(x) O_{a_1}(x_1)...O_{a_n}(x_n) \rangle = -\sum_{j=1}^{n} \langle O_{a_1}(x_1)...\delta_{x,\nu} O_{a_j}(x_j)...O_{a_n}(x_n) \rangle, \tag{3.124}$$

it would be tempting to define a new set of identities

$$\langle \partial_\mu T_{\mu\nu}(x) O_{a_1}(x_1, t)...O_{a_n}(x_n, t) \rangle = -\sum_{j=1}^{n} \langle O_{a_1}(x_1, t)...\tilde{\delta}_{x,\nu} O_{a_j}(x_j, t)...O_{a_n}(x_n, t) \rangle, \tag{3.125}$$

where composite operators have been substituted by their flowed versions. Here, the operator $\tilde{\delta}_{x_j,\nu}$ generates a local translation on fundamental fields and propagates it at positive flow time. The first advantage of the above formulation is that each operator $O_{a_i}(x_i, t)$ is finite, and can be safely plugged inside correlation functions. The second advantage is that no contact terms arise when $x_1 = x_2 = ... = x_n = x$

$$\langle \partial_\mu T_{\mu\nu}(x) V_{a_1 a_2...a_n}(x, t) \rangle = -\langle \tilde{\delta}_{x,\nu} V_{a_1 a_2...a_n}(x, t) \rangle, \tag{3.126}$$

the only divergences being here related to the bare EMT and the variation $\tilde{\delta}_{x,\nu} V_{a_1 a_2...a_n}(x, t)$. If the latter are replaced by their renormalized counterparts, then the following identity

$$\langle \partial_\mu (T_{\mu\nu})_R(x) V_{a_1 a_2...a_n}(x, t) \rangle = -\langle (\tilde{\delta}_{x,\nu} V_{a_1 a_2...a_n}(x, t))_R \rangle, \tag{3.127}$$

will be finite. All these interesting features are consequences of the gradient flow smoothing properties. Numerically, equation (3.127) would represent the perfect candidate to measure the EMT renormalization constants. In this case, correlation functions of objects coalescing on the boundary (but not in the bulk) are involved. The smearing effect at positive flow time prevents the rise of divergences, while the coalescence on the boundary is supposed to maximize the signal coming from numerical simulations.

A priori nothing would forbid to devise a set of WI like those in (3.127). For a candidate probe

---

[17]Indeed, it has been proved that a multiplicative renormalization [24] is needed for fermionic degrees of freedom.

at positive flow time, the local translation in (3.127) should be localized at $t = 0$, and then propagated through the bulk. Due to the gradient flow, the propagation will be non-local with respect boundary fields.

This raises an issue that need to be properly addressed: the renormalization of the operator $\tilde{\delta}_{x,\nu} V_{a_1 a_2 \ldots a_n}(x,t)$.

The theory of renormalization is based on the possibility of adding local counterterms to make correlation functions finite. However $\tilde{\delta}_{x,\nu} V_{a_1 a_2 \ldots a_n}(x,t)$ depends on boundary fields in a non local way. Hence, its renormalization could require the presence of non local boundary counterterms. Loss of locality dramatically affects the outcome of the renormalization program. The presence of non local counterterms undermines the validity of the expansion

$$a \frac{d}{da} \Gamma_R^{(n)}(p_1, \ldots, p_n; \lambda_R, m_R, a) = \mathcal{O}(a^2 (\log a)^k), \tag{3.128}$$

for renormalized correlation functions. This in turn would also affect the so-called Symanzik improvement program. As a consequence, numerical studies of renormalized quantities could not be carried out. Needless to say that this would be a total disaster.

Being locality a fundamental property of renormalizable quantum theories, it shouldn't be lost.

This problem has been addressed, and solved, by Del Debbio, Patella and Rago [34], for the specific case of Yang Mills theory[18]. In their work, the authors proved that the operator $\tilde{\delta}_{x,\nu} V_{a_1 a_2 \ldots a_n}(x,t)$ renormalizes only multiplicatively, ruling out any kind of unwanted non-local monster. In addition to that, they also shown how equation (3.127) can be derived from a generalized version of TWI, extended to the $(D+1)$-dimensional theory.

In the following subsections, it will be explained in detail how these results have been obtained.

3.3.2 Translations: boundary theory

Before proceeding, it is better to recall some of the results shown at the beginning of (2.6.2). The first is the gauge-covariant translation of gauge fields [52]

$$\delta_\alpha A_\mu(x) =$$
$$= \int d^d y \, \alpha_\rho(y) \delta_{y,\rho} A_\mu(x)$$
$$= \int d^d y \, \alpha_\rho(y) \delta^d(x-y) F_{\rho\mu}(x)$$
$$:= \alpha_\rho(x) F_{\rho\mu}(x), \tag{3.129}$$

which allows to determine a gauge-invariant EMT in pure Yang-Mills theory [19]

$$S = -\frac{1}{2g_0^2} \int d^d x \, \mathrm{tr} F_{\sigma\tau} F_{\sigma\tau}, \tag{3.130}$$

$$\delta_\alpha S = -\int d^d x \, \alpha_\rho \partial_\mu T_{\mu\rho}, \tag{3.131}$$

$$T_{\mu\rho} = -\frac{2}{g_0^2} \mathrm{tr} \left\{ F_{\mu\nu} F_{\rho\nu} - \frac{\delta_{\mu\rho}}{4} F_{\sigma\nu} F_{\sigma\nu} \right\}. \tag{3.132}$$

For a uniform α, equation (3.129) reduces to a composition of a global translation and a field-dependent gauge transformation

$$\delta_\alpha A_\mu(x) := \alpha_\rho \partial_\rho A_\mu - D_\mu(\alpha_\rho A_\rho). \tag{3.133}$$

---

[18] A similar strategy has been developed by Capponi, Del Debbio, Ehret, Pellegrini and Rago for the case of scalar field theories (5).

[19] Here, the same notation of (3.2) will be adopted for the generators of the $\mathfrak{su}(N)$ algebra.

Then, for a gauge-invariant observable, the transformation (3.133) acts effectively as a canonical translation. The diffeomorphism (3.129) can be generalized to the case of a generic probe P

$$
\begin{aligned}
\delta_\alpha P &= \int d^d x \alpha_\rho(x) \delta_{x,\rho} P \\
&:= \int d^d x \alpha_\rho(x) \frac{\delta P}{\delta A_\mu^a(x)} F_{\rho\mu}^a(x),
\end{aligned}
\tag{3.134}
$$

and a corresponding translation WI can be written as

$$
\langle \delta_{x,\rho} P \rangle = -\langle P \partial_\mu T_{\mu\rho} \rangle.
\tag{3.135}
$$

In the following subsections, it will be shown how these formulae can be adapted for probes evolved with the gradient flow.

3.3.3 Translations: probes at positive flow time

The effect of a local translation on a probe at positive flow time can be written in the following way

$$
\begin{aligned}
\delta_{x,\rho} P_T &= \\
&= \int d^d y \frac{\delta P_T}{\delta B_\nu^c(T,y)} \frac{\delta B_\nu^c(T,y)}{\delta A_\mu^a(x)} F_{\rho\mu}^a(x) \\
&:= \int d^d y \frac{\delta P_T}{\delta B_\nu^c(T,y)} J_{\nu\mu}^{ca}(T,y;0,x) F_{\rho\mu}^a(x),
\end{aligned}
\tag{3.136}
$$

where the simple chain rule has been applied. $J_{\nu\mu}^{ca}(T,y;0,x)$ is the Jacobian associated with the map between field configurations at different flow times [59]

$$
J_{\mu\nu}^{ab}(t,x;s,y) = \theta(t-s) \frac{\delta B_\mu^a(t,x)}{\delta B_\nu^b(s,y)},
\tag{3.137}
$$

where only forward propagation has been considered. The Jacobian can be determined from the following linearized equation

$$
\delta \dot{B}_\mu(t,x) = [G_{\mu\rho}, \delta B_\rho] + D_\rho D_\rho \delta B_\mu - D_\rho D_\mu \delta B_\rho + \alpha_0 D_\mu \partial_\rho \delta B_\rho - \alpha_0 [\partial_\rho B_\rho, \delta B_\mu],
\tag{3.138}
$$

which is obtained applying a field deformation to (3.6). A flow equation for the Jacobian is generated by taking a functional derivative with respect $B_\nu(s,y)$

$$
\partial_t J_{\mu\nu}^{ab}(t,x;s,y) = \mathcal{D}^{ac}(t,x)_{\mu\rho} J_{\rho\nu}^{bc}(t,x;s,y),
\tag{3.139}
$$

$$
\mathcal{D}(t,x)_{\mu\rho} \delta B(t,x)_\rho := [G_{\mu\rho}, \delta B_\rho] + D_\rho D_\rho \delta B_\mu - D_\rho D_\mu \delta B_\rho + \alpha_0 D_\mu \partial_\rho \delta B_\rho - \alpha_0 [\partial_\rho B_\rho, \delta B_\mu].
\tag{3.140}
$$

Forward propagation is ensured by the following boundary conditions

$$
J_{\mu\nu}^{ab}(t^+,x;t,y) = \delta_{ab} \delta_{\mu\nu} \delta^d(x-y),
\tag{3.141}
$$

$$
J_{\mu\nu}^{ab}(t,x;s,y) = 0 \quad t < s.
\tag{3.142}
$$

It has to be noticed that (3.141) allows to recover the correct variation of a probe P at flow time zero

$$
\lim_{T\to 0^+} \delta_{x,\rho} P_T = \frac{\delta P}{\delta A_\mu^a(x)} F_{\rho\mu}^a(x).
\tag{3.143}
$$

The solution of (3.139) is obtained with the same method adopted for the flow equation (3.6)

- Detach linear and non-linear terms of the differential operator $\mathcal{D}$

$$\mathcal{D}_{\mu\nu} := \delta_{\mu\nu}\partial_\rho\partial_\rho + (\alpha_0 - 1)\partial_\nu\partial_\mu + \mathcal{R}_{\mu\nu}. \tag{3.144}$$

- Find the kernel for the linear component of $\mathcal{D}$

$$K_t(x)_{\mu\nu} = \int_p \frac{e^{ipx}}{p^2}\left[(\delta_{\mu\nu} - p_\mu p_\nu)e^{-tp^2} + p_\mu p_\nu e^{-\alpha_0 t p^2}\right]. \tag{3.145}$$

This is exactly the flow propagator (3.25).

- Recast the solution of the linearized flow equation into the following integral form

$$J_{\mu\nu}^{ab}(t,x;s,y) = \delta^{ab}K_{t-s}(x-y)_{\mu\nu} + \int_s^t d\tau \int d^d z\, K_{t-\tau}(x-z)_{\mu\lambda}\mathcal{R}^{ac}(\tau,z)_{\lambda\rho}J_{\rho\nu}^{cb}(\tau,z;s,y). \tag{3.146}$$

The complete solution is obtained iterating the l.h.s on the r.h.s of the above identity, provided $\mathcal{R}$ is written in terms of fields that satisfy the flow equation.

For $\alpha_0 = 1$, the leading term in the expansion (3.146) is given by

$$J_{\mu\nu}^{ab}(t,x;s,y) = \delta_{\mu\nu}\delta^{ab}\theta(t-s)\frac{e^{-\frac{|x-y|^2}{4(t-s)}}}{[4\pi(t-s)]^{d/2}} + ..., \tag{3.147}$$

where the dots stand for $\mathcal{O}(g_0^2)$ terms and contributions that decouple from gauge invariant observables. Combined with (3.147), equation (3.136) tells that local translations at $t = 0$ can be *smoothly* propagated at $t > 0$, integrating boundary fields over a smearing radius of $\sqrt{8t}$.

The representation in terms of the Jacobian allows to precisely describe the renormalization properties of the operator $\delta_{x,\rho}P_T$. In the next subsection it will be shown how this happens.

3.3.4 Renormalization of $\delta_{x,\rho}P_T$

In the $(D+1)$-dimensional theory, the expectation value of a probe at positive flow time is given by

$$\langle P_T \rangle = \mathcal{Z}^{-1} \int D[A]e^{-S}\int D[B]D[L]P_T e^{-S_{fl}}, \tag{3.148}$$

the definition of S and S_{fl} being described by (3.4) and (3.44) respectively. It is interesting to study how the expectation value P_T changes under an infinitesimal transformation of the bulk fields

$$(B')_\mu^a(t,x) = B_\mu^a(t,x) + \int_0^t ds \int d^d y\, J_{\mu\nu}^{ab}(t,x;s,y)\alpha(s,y)X_\nu^b(s,y), \tag{3.149}$$

where α is a generic infinitesimal function that vanishes on the boundaries. The operator $X_\nu^b(s,y)$ and the gauge-invariant probe P_T depend on B fields and their derivatives. Under the transformation (3.149) the path integral becomes

$$\langle P_T \rangle = \mathcal{Z}^{-1} \int D[A]e^{-S}\int D[B']D[L]\det\left[\frac{\delta B'}{\delta B}\right]^{-1}(P_T + \delta P_T)\,e^{-S_{fl}-\delta S_{fl}} \tag{3.150}$$

The elements of the Jacobian matrix have the following form

$$\frac{\delta(B')_\mu^a(t,x)}{\delta B_\rho^b(s,y)} = \delta^{ab}\delta_{\mu\rho}\delta(t-s)\delta^d(x-y)$$

$$+ \int_0^t d\sigma \int d^d z \left[\frac{\delta J_{\mu\nu}^{ac}(t,x;\sigma,z)}{\delta B_\rho^b(s,y)}\alpha(\sigma,z)X_\nu^c(\sigma,z)\right.$$

$$\left. + J_{\mu\nu}^{ac}(t,x;\sigma,y)\alpha(\sigma,z)\frac{\delta X_\nu^c(\sigma,z)}{\delta B_\rho^b(s,y)}\right].$$
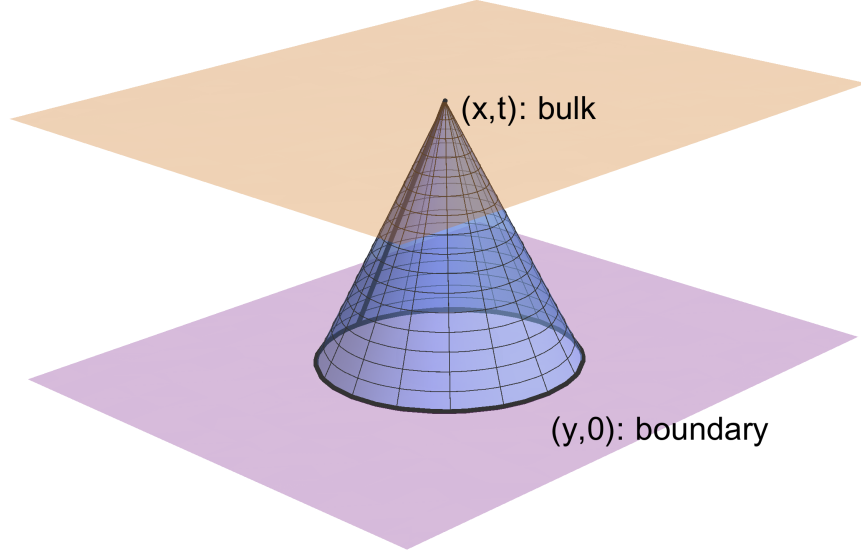
Figure 3.1: Action of the Jacobian $J_{\mu\nu}^{ab}(t, x; 0, y)$. The effect of a local translation at $t = 0$ is driven into the bulk towards a probe positioned at (x, t). The propagation is obtained integrating boundary degrees of freedom within a smearing radius $r = \sqrt{8t}$.

The determinant is then given by

$$
\begin{aligned}
\det\left[\frac{\delta B'}{\delta B}\right] = {}& 1 \\
& + \int_0^\infty dt \int_0^t d\sigma \int d^d x d^d z \left[\frac{\delta J_{\mu\nu}^{ac}(t, x; \sigma, z)}{\delta B_\mu^a(t, x)}\alpha(\sigma, z)X_\nu^c(\sigma, z)\right. \\
& \left. + J_{\mu\nu}^{ac}(t, x; \sigma, y)\alpha(\sigma, z)\frac{\delta X_\nu^c(\sigma, z)}{\delta B_\mu^a(t, x)}\right],
\end{aligned}
\tag{3.151}
$$

where the relation $\det[\mathbb{I} + M] = 1 + \text{tr}\{M\}$ has been used. The term on the second line vanishes since the Jacobian depends only on fields at flow times $\sigma < t$.

$$
\frac{\delta J_{\mu\nu}^{ac}(t, x; \sigma, z)}{\delta B_\mu^a(t, x)} = 0.
\tag{3.152}
$$

On the other hand, the variation on the third line results in

$$
\frac{\delta X_\nu^c(\sigma, z)}{\delta B_\mu^a(t, x)} := \delta^{ac}\delta_{\mu\nu}\delta^d(z - x)\delta(t - \sigma)\chi(t, x),
\tag{3.153}
$$

because $X_\nu^c(\sigma, z)$ is a local function of bulk fields and their derivatives [20]. Plugging this expression in (3.151) gives

$$\det\left[\frac{\delta B'}{\delta B}\right] = 1 + \theta(0)\delta^d(0)\int_0^\infty dt \int d^dx\,\alpha(t,x)\chi(t,x), \tag{3.154}$$

which makes sense only in a regularized theory. To preserve translation invariance, dimensional regularization is employed. With this kind of regularization, $\delta^d(0) = 0$ and

$$\det\left[\frac{\delta B'}{\delta B}\right] = 1, \tag{3.155}$$

i.e. the Jacobian determinant is trivial. Expanding $e^{-\delta S_{fl}}$ at leading order in δB allows to rewrite (3.150) as

$$\langle P_T\rangle = \langle P_T\rangle + \langle\delta P_T\rangle \tag{3.156}$$
$$- \mathcal{Z}^{-1}\int D[A]e^{-S}\int D[B]D[L]P_T e^{-S_{fl}}\left(\int_0^\infty dt \int d^dx\,L_\mu^a(t,x)\left[\delta\dot{B}_\mu^a - \mathcal{D}_{\mu\nu}^{ab}\delta B_\nu^b\right]\right). \tag{3.157}$$

The identity simplifies once the time derivative of (3.149) is written down and the Jacobian equation (3.139) is used

$$\langle\delta P_T\rangle = \langle P_T\delta S\rangle, \tag{3.158}$$
$$\delta P_T = \int_t^\infty ds \int d^dz \frac{\delta P_T}{\delta B_\mu^a(s,y)}J^{ab}(s,y;t,x)_{\mu\nu}X_\nu^b(t,x), \tag{3.159}$$
$$\delta S = L_\mu^a(t,x)X_\nu^a(t,x), \tag{3.160}$$

where the arbitrariness of the function α has been exploited. Equations (3.158-3.159-3.160) can be used to study the renormalization properties of $\delta_{x,\rho}P_T$. Indeed, the identity (3.158) holds for any kind of field transformation described by $X_\nu^a(t,x)$. For an infinitesimal translation at zero flow time, the identities above take the following form

$$\langle\delta_{x,\rho}P_T\rangle = \langle P_T\tilde{T}_{0\rho}(x)\rangle, \tag{3.161}$$
$$\delta_{x,\rho}P_T = \int d^dz \frac{\delta P_T}{\delta B_\mu^a(T,y)}J^{ab}(T,y;0,x)_{\mu\nu}F_{\rho\nu}^b(x), \tag{3.162}$$
$$\tilde{T}_{0\rho}(x) = -2\text{tr}\{L_\mu(0,x)F_{\rho\mu}(x)\}. \tag{3.163}$$

Equation (3.161) tells that the renormalization of $\delta_{x,\rho}$ can be determined by analyzing the operator $\tilde{T}_{0\rho}(x)$, a *local* operator built with A_μ and L_μ fields. Before proceeding, it is worth to stress few points

- With some adjustment, the results above hold also when a lattice regulator is adopted. In this case, a slight modification has to be applied to the following operator

$$[L_\mu^a X_\mu^a](t,x) = \lim_{\epsilon\to 0+}L_\mu^a(t,x)X_\mu^a(t-\epsilon,x), \tag{3.164}$$

  where the ϵ limit has to be taken *after* the cut-off has been removed. The insertion of (3.164) is generated by the field transformation

$$(B')_\mu^a(t,x) = B_\mu^a(t,x) + \int_0^{t-\epsilon}d\sigma \int d^dz\,J_{\mu\nu}^{ab}(t,x;\sigma,z)\alpha(\sigma,z)X_\nu^b(\sigma,z). \tag{3.165}$$

---

[20]Written in this form, $\chi(t,x)$ is obtained taking partial derivatives with respect fields and their derivatives.

This redefinition is motivated by the following argument: the variation

$$\langle \int_t^\infty ds \int d^d z \frac{\delta P_T}{\delta B_\mu^a(s,y)} J^{ab}(s,y;t,x)_{\mu\nu} X_\nu^b(t,x) \rangle = \langle P_T L_\mu^a(t,x) X_\nu^a(t,x) \rangle \qquad (3.166)$$

vanishes if P_T depends on B fields at flow times $T < t$. On the l.h.s. this is caused by the Jacobian boundary conditions. On the r.h.s. this can be understood from the perturbative analysis of the gradient flow (3.2). The $B(t,x) \leftarrow L(s,y)$ propagation is allowed only if the B field is at flow time $t \geq s$. If P_T in (3.166) is defined at flow times smaller than t, flow lines originates only from $L_\mu^a(t,x) X_\mu^a(t,x)$ contractions. This generates closed flow-loops, which vanish in dimensional regularization, but not in a lattice-regularized theory. This in turn affects the value of the determinant (3.151), since $\delta^d(0)$ is not zero at finite lattice spacing. All these problems can be easily fixed if the operator (3.164) is employed.

- The transformation (3.162) can be generalized to the case of local translations applied on a $t > 0$ hyperplane

$$\bar{\delta}_{t,x,\rho} P_T = \int d^d z \frac{\delta P_T}{\delta B_\mu^a(T,y)} J^{ab}(T,y;t,x)_{\mu\nu} G_{\rho\nu}^b(t,x), \quad t < T \qquad (3.167)$$

The above result will be important in the following, when a formulation of TWI at positive flow time shall be devised.

A generic form for the observable P_T could be given by

$$P_T = \prod_{i=1}^n \Phi_i(T, x_i), \qquad (3.168)$$

where each $\Phi_i(T, x_i)$ represents a gauge-invariant, local observable of the B fields and their derivatives. Equation (3.161) signals that the divergences of $\langle \delta_{x,\rho} P_T \rangle$ can arise from products of operators of the $(D+1)$-dimensional theory. It is already known that local operators of the bulk theory do not require renormalization[21]. The only possible divergences are related to the operator $\tilde{T}_{0\rho}(x)$, which is defined on the boundary. The latter has the following properties

- Its engineered dimension is 5.

- It is gauge invariant.

- It transforms as a four-vector under $SO(4)$ rotations.

In principle, any operator with mass dimension ≤ 5 that shares the same properties could mix with $\tilde{T}_{0\rho}(x)$. However, it is worth to make few remarks

- Since no LA contractions are admitted, insertions of $\tilde{T}_{0\rho}(x)$ with observables built from boundary gauge fields vanishes. This means that $\tilde{T}_{0\rho}(x)$ does not mix with operators made with boundary fields.

- A mix with the Lagrange multiplier could be considered, however $\tilde{T}_{0\rho}(x)$ itself is the only operator with dimension not greater than 5 and the required symmetries.

From this analysis, it can be safely assessed that $\tilde{T}_{0\rho}(x)$ renormalizes only multiplicatively[22]. Moreover, no extra divergences are generated when x hits one of the x_i's, since $\tilde{T}_{0\rho}(x)$ and $\Phi_i(T, x_i)$ are

---

[21]Note that all the points $x_1, ..., x_n$ could also coincide and no divergences would be generated.

[22]It should be stressed that this result holds also when regulators that break translational invariance (like the lattice) are employed.

always at separate points in the $(D + 1)$-dimensional theory. In terms of renormalized operators, a possible translation WI can be written as

$$Z_\delta \langle P_T \tilde{T}_{0\rho}(x) \rangle = Z_\delta \langle \delta_{x,\rho} P_T \rangle = -\langle P_T \partial_\mu (T_{\mu\rho})_R \rangle. \tag{3.169}$$

This is the main result of this chapter, and the core of this work. Equation (3.169) tells that a set of TWI with probes at positive flow time can be built and adopted to renormalize the EMT.

In dimensional regularization, Poincaré invariance is preserved, and then $Z_\delta = 1$ [46] and the operator $\delta_{x,\rho}$ does not renormalize at all. In this case, the bare EMT, with VEV subracted, is finite and the identity (3.169) holds when the cut-off is removed.

Things will be different when the lattice regulator is employed. In the following, it will be shown how a numerical strategy based on (3.169) can be setup to renormalize the lattice EMT.

Before moving to lattice numerical studies, it is still interesting to see how equation (3.169) can be actually derived from a generalized version of the TWI, where also translations along the flow time direction are considered. This will be the subject of the next subsection.

3.3.5 Translation WI at positive flow time

The flow equations are invariant under global translations. This implies the equivalence between the two following actions

- Evolve from the boundary theory and then translate the bulk fields at a given flow time t.

- Translate the boundary fields and then evolve them up to flow time t in the bulk.

This argument allows to define a family of transformations parametrized by the flow time

$$\bar{\delta}_{t,\alpha} P = \int d^d x\, \alpha_\rho(x) \bar{\delta}_{t,x,\rho} P = \int d^d x\, \alpha_\rho(x) \frac{\delta P}{\delta B_\mu^a(t,x)} G_{\rho\mu}^a(t,x), \tag{3.170}$$

where the differential operator $\bar{\delta}_{t,x,\rho}$, cfr. (3.167), depends locally on B fields that satisfy the flow equation. In analogy to (3.161), it is possible to show that

$$\langle \bar{\delta}_{t,x,\rho} P_T \rangle = \langle P_T \tilde{T}_{0\rho}(t,x) \rangle, \tag{3.171}$$

the operator $\tilde{T}_{0\rho}(t,x)$ being computed at positive flow time. For uniform α_ρ, the transformation generated by (3.167) reduces to the composition of a canonical, infinitesimal translation of the B field and a field-dependent gauge transformation. The action of the operator $\bar{\delta}_{t,x,\rho}$ assumes two different forms

$$\bar{\delta}_{t,x,\rho} \Phi(T,y) = \frac{\delta \Phi(T,y)}{\delta B_\mu^a(T,x)} G_{\rho\mu}^a(T,x) \quad \text{for } T = t, \tag{3.172}$$

$$\bar{\delta}_{t,x,\rho} \Phi(T,y) = \int d^d z\, \frac{\delta \Phi(T,y)}{\delta B_\mu^a(T,z)} J^{ab}(T,z;t,x)_{\mu\nu} G_{\rho\nu}^b(t,x) \quad \text{for } T > t, \tag{3.173}$$

These two equations clearly state that the operator $\bar{\delta}_{t,x,\rho}$ generates a local translation on hyperplanes at fixed $t > 0$. A global version of the previous transformations is given by

$$\int_V d^d x\, \bar{\delta}_{t,x,\rho} \Phi(T,y) = \partial_\rho \Phi(T,x) \quad \text{for } T = t, \tag{3.174}$$

$$\int_V d^d x\, \bar{\delta}_{t,x,\rho} \Phi(T,y) = \partial_\rho \Phi(T,x) + \mathcal{O}\left(e^{-\frac{r^2}{4(T-t)}}\right) \quad \text{for } T > t, \tag{3.175}$$

where the integration domain is a sphere V with radius r, centered in x. The result on the second line will be proved at then end of the subsection.

The interesting feature of the operator $\bar{\delta}_{t,\alpha}$ is that it only depends on bulk fields, and therefore it does not require any renormalization. Associated with it, for each flow time t, there is a new EMT and a corresponding bulk TWI can be formulated. Clearly, this new EMT will be non-local in the fundamental gauge fields. Nevertheless, it can be written in terms of local operators exploiting the space-time symmetries of the $(D+1)$-dimensional field theory. Following the example of subsection (3.3.2), a gauge-covariant translation in the bulk theory can be described as

$$
\begin{aligned}
\delta_\alpha B_M(t,x) &= \int_0^\infty ds \int d^d y \, \alpha_R(s,y) \delta_{s,y,R} B_M(t,x) \\
&= \int_0^\infty ds \int d^d y \, \alpha_R(s,y) \delta(t-s) \delta^d(x-y) G_{RM}(t,x) \\
&:= \alpha_R(t,x) G_{RM}(t,x),, \qquad (3.176) \\
\delta_\alpha L_\mu(t,x) &= \int_0^\infty ds \int d^d y \, \alpha_R(s,y) \delta_{s,y,R} L_\mu(t,x) \\
&= \int_0^\infty ds \int d^d y \, \alpha_R(s,y) \delta(t-s) \delta^d(x-y) D_R L_\mu(t,x) \\
&:= \alpha_R(t,x) D_R L_\mu(t,x), \qquad (3.177)
\end{aligned}
$$

with $\alpha_0(0,x) = 0$ and $R, M = 0, 1, ..., D,$. The direction 0 identifies the flow time extension. For a probe that does not depend on the Lagrange multiplier, the corresponding variation will be

$$
\begin{aligned}
\delta_\alpha P &= \int_0^\infty dt \int d^d x \, \alpha_R(t,x) \delta_{t,x,R} P \\
&:= \int_0^\infty dt \int d^d x \, \alpha_R(t,x) \frac{\delta P}{\delta B_M^a(t,x)} G_{RM}^a(t,x). \qquad (3.178)
\end{aligned}
$$

From equations (3.176) and (3.177), the difference between the operator $\delta_{t,x,R}$ and $\bar{\delta}_{t,x,\rho}$ should appear quite clear. However, few comments could be necessary

- $\bar{\delta}_{t,x,\rho}$ acts on fields that already satisfy the flow equation. The fields are deformed at flow time t, and the flow equation propagates the deformation at all other flow times. A peculiar example is given by the case $\delta_{x,\rho} = \bar{\delta}_{0,x,\rho}$, where the deformation is carried out on the boundary theory, and propagated to any positive flow time

- $\delta_{t,x,R}$ acts on the $(D+1)$-dimensional fields *before* the flow equation is imposed. It generates local deformations in $(D+1)$ dimensions that are not propagated in flow time. Starting from a configuration that satisfies the flow equation, its deformation will not generally satisfy the same equation. The variation of the equation is reabsorbed by the transformation of the Lagrange multiplier (3.177)

From the transformation induced by $\delta_{t,x,R}$, an EMT at any positive flow time can be defined[23]

$$\delta_\alpha S_{fl} = \int_0^\infty dt \int d^d x \tilde{T}_{MR}(t,x) \partial_M \alpha_R(t,x), \tag{3.181}$$

$$\tilde{T}_{0R} = -2\text{tr}\{L_\mu G_{R\mu}\}, \tag{3.182}$$

$$\tilde{T}_{\nu R} = 2\text{tr}\{L_\mu D_\nu G_{R\mu}\} - 2\text{tr}\{D_\nu L_\mu G_{R\mu}\} - 2\text{tr}\{D_\mu L_\mu G_{\nu R}\} + 2\delta_{R0}\text{tr}\{L_\nu D_\mu G_{\mu 0}\}, \tag{3.183}$$

up to terms proportional to the flow equation that vanish inside expectation values (see appendix A). From the set of transformations (3.176) and (3.177), the following WI can be derived

$$\langle \delta_{t,x,\rho} P \rangle = -\langle P \partial_M \tilde{T}_{MR}(t,x) \rangle. \tag{3.184}$$

For a probe P_T depending on B fields at flow time $T > t$, the l.h.s of the previous equation vanishes, leaving the identity

$$\langle P_T \partial_t \tilde{T}_{0R}(t,x) \rangle = -\langle P_T \partial_\mu \tilde{T}_{\mu R}(t,x) \rangle. \tag{3.185}$$

In the following, only the case $R = \rho$ will be considered. It has to be noticed that both sides of the equation are finite at positive flow time. Equation (3.185) leads to a set of WI for the family of transformations identified by (3.173). To verify this statement, it is necessary to integrate (3.185) with respect the flow time in an interval $(0,t)$. The problem is that, at $t = 0$, an extra contribution arises from the fact that boundary fields are transformed along with the bulk ones. Moreover equation (3.185) is valid for bare fields at finite cut-off. As long as the flow time is non-zero, this equations does not exhibit divergences in the $\epsilon \to 0$ limit. Therefore, the cut-off gets removed at positive flow time, then equation (3.185) is integrated in an interval (t_0, t)

$$\langle P_T \tilde{T}_{0\rho}(t,x) \rangle = \langle P_T \tilde{T}_{0\rho}(t_0,x) \rangle - \langle P_T \partial_\mu \int_{t_0}^t ds \tilde{T}_{\mu\rho}(s,x) \rangle, \tag{3.186}$$

and then the $t_0 \to 0^+$ limit is taken. The l.h.s. of the previous identity can be rewritten as

$$\langle P_T \tilde{T}_{0\rho}(t,x) \rangle = \langle \bar{\delta}_{t,x,\rho} P_T \rangle, \tag{3.187}$$

and can be used to take the the limit of the first term on the r.h.s.

$$\lim_{t_0 \to 0^+} \langle P_T \tilde{T}_{0\rho}(t_0,x) \rangle = \langle \delta_{x,\rho} P_T \rangle = -\langle P_T \partial_\mu T_{\mu\rho}(x) \rangle. \tag{3.188}$$

Collecting all the pieces together, a translation WI for the operator $\bar{\delta}_{t,x,\rho}$ can be written as

$$\langle \bar{\delta}_{t,x,\rho} P_T \rangle = -\langle P_T \partial_\mu \bar{T}_{\mu\rho}(t,x) \rangle, \tag{3.189}$$

$$\bar{T}_{\mu\rho}(x) = T_{\mu\rho}(x) + \int_0^t ds \tilde{T}_{\mu\rho}(s,x). \tag{3.190}$$

This TWI can be reduced to equation (3.169) at $t = 0$ only if the integral appearing in (3.190) is finite. Before setting $t = 0$, a classification of divergences arising from $\tilde{T}_{\mu\rho}(s,x)$ when $s \to 0^+$ must be done. This task can be accomplished counting the operators that could mix with $\tilde{T}_{\mu\rho}(s,x)$. The procedure can be simplified if the following arguments are taken into account

---

[23]The following flow action

$$S_{fl} = -2\int_0^\infty dt \int d^d x \text{tr}\{L_\mu(t,x)[G_{0\mu} - D_\nu G_{\nu\mu}](t,x)\}, \tag{3.179}$$

$$G_{0\mu} = \dot{B}_\mu - D_\mu B_0. \tag{3.180}$$

has been used. This formulation automatically ensures invariance under local gauge transformations in $(D + 1)$ dimensions. The original action is recovered in the $B_0 = 0$ gauge. As the measure in the path integral is invariant under the change of variables that drives to the $B_0 = 0$ gauge, the actions (3.44) and (3.179) describe the same quantum theory.

- Candidate operators must have mass dimension smaller than or equal than 6.

- Taking into account the $SO(4)$ structure of $\tilde{T}_{\mu\rho}(s,x)$, only operators with dimension 6 and 4 are allowed.

- Candidate operators must at least contain a Lagrange multiplier, whose dimension is 3.

Requiring gauge-invariance allows to rule out dimension 4 operators, stating that $\tilde{T}_{\mu\rho}(s,x)$ has at most a logarithmic divergence for $s \to 0^+$. Since this singularity is integrable, the $t \to 0^+$ limit in (3.189) can be safely taken, finally giving

$$\langle \delta_{x,\rho} P_T \rangle = -\langle P_T \partial_\mu T_{\mu\rho}(x) \rangle. \tag{3.191}$$

Which is exactly equation (3.169).

The last part of this subsection is devoted to prove equation (3.175). Starting again from equation (3.185), one can integrate the mentioned identity in the interval (t,T). This will result in the following equation

$$\langle P_T \tilde{T}_{0\rho}(T,x) \rangle = \langle P_T \tilde{T}_{0\rho}(t,x) \rangle - \langle P_T \partial_\mu \int_t^T ds \tilde{T}_{\mu\rho}(s,x) \rangle, \tag{3.192}$$

which can be rewritten as

$$\langle \bar{\delta}_{t,x,\rho} P_T \rangle = \langle \bar{\delta}_{T,x,\rho} P_T \rangle + \langle P_T \partial_\mu \int_t^T ds \tilde{T}_{\mu\rho}(s,x) \rangle. \tag{3.193}$$

The probe observable P_T is then decomposed according to

$$P_T = X_T \phi(T,x), \tag{3.194}$$

X_T being a product of probes at flow time T but different space-time positions with respect x. Equation (3.193) can be integrated on a space-time sphere V with radius r and centered in x

$$\langle X_T \int_V d^d y \bar{\delta}_{t,y,\rho} \phi(T,x) \rangle = \langle X_T \partial_\rho \phi(T,x) \rangle + \langle X_T \phi(T,x) \int_0^T ds \int_{\partial V} dS_\mu \tilde{T}_{\mu\rho}(s,x) \rangle. \tag{3.195}$$

The operator $\tilde{T}_{\mu\rho}(s,x)$ contains only terms that are linear in the Lagrange multiplier L_μ. Since the LB propagator is exponentially suppressed with the space-time separation, the contribution of the last term on the r.h.s. is exponentially suppressed if all the fields are far enough from the boundary of the sphere V. Denoting $\bar{r}$ as the distance from ∂V of the closest operator, then

$$\langle X_T \int_V d^d y \bar{\delta}_{t,y,\rho} \phi(T,x) \rangle = \langle X_T \partial_\rho \phi(T,x) \rangle + \mathcal{O}\left(e^{-\frac{\bar{r}^2}{4(T-t)}} \right). \tag{3.196}$$

3.3.6 Dilatations

In this work, all the numerical effort has been devoted to the renormalization of translation WI. However, it is interesting to see how the previous method can be extended to the case of dilatations. Also in this case, non local renormalization are ruled out, since the results of section (3.3.4) hold for local dilatations applied to probes at positive flow time. Hence, a proper set of DWI with flowed operators can be setup

$$\langle x_\rho \delta_{x,\rho} P_T \rangle = -\langle P_T \partial_\mu (x_\rho T_{\mu\rho}(x)) \rangle + \langle P_T T_{\mu\mu}(x) \rangle. \tag{3.197}$$

Similiarly to the case of translations, the above equation can be derived from a set of DWI of the $(D+1)$-dimensional theory. To discuss the latters, the operator $\bar{\delta}_{t,x,\rho}$ need to be extended, in order to include the flow-time direction

$$\bar{\delta}_{t,x,R}P := \frac{\delta P}{\delta B_\mu^a(t,x)}G_{R\mu}^a(t,x), \tag{3.198}$$

where the following relation

$$\langle \bar{\delta}_{t,x,R}P_T \rangle = \langle P_T \tilde{T}_{0R}(t,x) \rangle, \tag{3.199}$$

can always be proved using the path integral formalism. A local dilatation in the bulk is represented by

$$\delta_\alpha B_\mu(t,x) = \alpha_R(t,x)G_{RM}(t,x), \tag{3.200}$$
$$\delta_\alpha L_\mu(t,x) = \alpha_R(t,x)D_R L_\mu(t,x), \tag{3.201}$$
$$\alpha_\rho(t,x) = x_\rho \beta(t,x), \tag{3.202}$$
$$\alpha_0(t,x) = 2t\beta(t,x), \tag{3.203}$$

and its global counterpart is obtained taking β uniform. It should be noticed how local dilatations are simply a special case of local translations. For uniform β, the flow equation is invariant under the set of transformations (3.200-3.201-3.202-3.203). The variation of the bulk action is given by

$$\delta_\beta S_{fl} = -\int_0^\infty dt \int d^d x \beta(t,x) \left[\partial_M(\lambda_{RN}x_R\tilde{T}_{MN}) - \lambda_{MR}\tilde{T}_{MR} \right], \tag{3.204}$$

where the $(D+1)$-dimensional euclidean metric

$$\lambda_{MR} = \begin{pmatrix} 2 & & & & \\ & 1 & & & \\ & & 1 & & \\ & & & 1 & \\ & & & & 1 \end{pmatrix}, \tag{3.205}$$

has been introduced. From equation (3.204), the corresponding dilatation WI can be derived

$$\langle \delta_{t,x,R}P_T \rangle = -\langle P_T \left[\partial_M(\lambda_{RN}x_R\tilde{T}_{MN}) - \lambda_{MR}\tilde{T}_{MR} \right] \rangle, \tag{3.206}$$

where the l.h.s vanishes if $T > t$, since probe and variation are not coalescing at the same point. Since the r.h.s. of (3.206) is set equal to zero, the following relation is generated

$$\langle P_T\partial_t \left[2t\tilde{T}_{00} + x_\rho\tilde{T}_{0\rho} \right] \rangle = \langle P_T \left[2\tilde{T}_{00} + \tilde{T}_{\lambda\lambda} \right] \rangle - \langle P_T\partial_\mu \left[2t\tilde{T}_{\mu 0} + x_\rho\tilde{T}_{\mu\rho} \right] \rangle. \tag{3.207}$$

As for the case of boundary DWI, the trace of the bulk EMT seems to violate dilatation invariance in $(D+1)$ dimensions. However, it can be easily shown that the generalized trace in (3.207) equals a four-divergence

$$\left[2\tilde{T}_{00} + \tilde{T}_{\lambda\lambda} \right](t,x) = \partial_\mu\tilde{T}_{0\mu}(t,x), \tag{3.208}$$

up to terms proportional to the flow equation that vanish inside correlation functions. Using the relation (3.208), equation (3.207) becomes

$$\langle P_T\partial_t \left[2t\tilde{T}_{00} + x_\rho\tilde{T}_{0\rho} \right] \rangle = -\langle P_T\partial_\mu \left[2t\tilde{T}_{\mu 0} + x_\rho\tilde{T}_{\mu\rho} - \tilde{T}_{0\mu} \right] \rangle. \tag{3.209}$$

Mimicking the procedure followed for the case of translations, the above equation is integrated in the flow-time interval $(0, t)$ with $T > t$

$$\langle P_T \left[2t\tilde{T}_{00} + x_\rho \tilde{T}_{0\rho} \right] (t, x) \rangle - \lim_{t_0 \to 0^+} \langle P_T \left[2t_0\tilde{T}_{00} + x_\rho \tilde{T}_{0\rho} \right] (t_0, x) \rangle =$$

$$= -\langle P_T \partial_\mu \int_0^t ds \left[2s\tilde{T}_{\mu 0} + x_\rho \tilde{T}_{\mu\rho} - \tilde{T}_{0\mu} \right] (s, x) \rangle. \quad (3.210)$$

The first thing to notice is that

$$\lim_{t_0 \to 0^+} \langle P_T 2t_0 \tilde{T}_{00} \rangle = 0, \quad (3.211)$$

as $\tilde{T}_{00}(t_0, x)$ diverges at most logarithimcally. Using equation (3.199), the integrated DWI becomes

$$\langle \left[2t\bar{\delta}_{t,x,0} + x_\rho \bar{\delta}_{t,x,\rho} \right] P_T \rangle = -\langle P_T \partial_\mu \bar{D}_\mu(t, x) \rangle + \langle P_T T_{\mu\mu}(x) \rangle, \quad (3.212)$$

$$\bar{D}_\mu(t, x) = x_\rho T_{\mu\rho}(x) + \int_0^t ds \tilde{D}_\mu(s, x), \quad (3.213)$$

$$\tilde{D}_\mu(s, x) = \left(2s\tilde{T}_{\mu 0} + x_\rho \tilde{T}_{\mu\rho} - \tilde{T}_{0\mu} \right)(s, x). \quad (3.214)$$

The differential operator $2t\bar{\delta}_{t,x,0} + x_\rho \bar{\delta}_{t,x,\rho}$ generates dilatations on hyperplanes at fixed flow time t. As before, power counting arguments show that the integral in $\bar{D}_\mu$ is finite, so the $t \to 0^+$ limit can be safely carried out

$$\langle x_\rho \delta_{x,\rho} P_T \rangle = -\langle P_T \partial_\mu (x_\rho T_{\mu\rho}(x)) \rangle + \langle P_T T_{\mu\mu}(x) \rangle. \quad (3.215)$$

Equation (3.215) defines dilatation WI probed by observables built along the flow. As usual, the probes are observables that depend on the bulk field B_μ at flow time T. This is not the only possible relation that can be extracted from (3.212). A different outcome is generated integrating (3.212) over the space time and setting $P_T = \Phi(T, x)$

$$\langle \int d^d y \left[2t\bar{\delta}_{t,y,0} + y_\rho \bar{\delta}_{t,y,\rho} \right] \Phi(T, x) \rangle = \langle \Phi(T, x) \int d^d y T_{\mu\mu}(y) \rangle, \quad (3.216)$$

which defines the effect of a global dilatation on a probe $\Phi(T, x)$. If the probe is positioned at the origin, then the following equation holds

$$\langle \left[2T \frac{d}{dT} + d_\Phi \right] \Phi(T, x) \rangle = \langle \Phi(T, x) \int d^d y T_{\mu\mu}(y) \rangle, \quad (3.217)$$

where d_Φ is the dimension of the operator $\Phi(T, x)$. Equation (3.217) is the operatorial form of the Callan-Symanzik equation [4, 5], where $1/\sqrt{8T}$ is the energy scale and contact terms are absent. This equation is extremely interesting. It allows to probe the trace of the EMT just by looking at the evolution under gradient flow of observables. In Yang-Mills theory this result is really important, because the trace of the EMT is the source of the quantum anomaly [18]. It should be stressed that the strategy proposed above has been formulated for the specific case of pure gauge theories. However, as it will be shown in chapter (5), a similar method can be developed for scalar field theories.

3.3.7 Renormalized EMT from the gradient flow

As previously mentioned, the thesis focuses on the renormalization of the lattice EMT using the translation WI. The numerical analysis has been completely based on the following equations

$$\langle \delta_{x,\rho} P_T \rangle = -\langle P_T \partial_\mu T_{\mu\rho}(x) \rangle, \quad (3.218)$$

$$\langle X_T \int_V d^d y \bar{\delta}_{t,y,\rho} \phi(T, x) \rangle = \langle X_T \partial_\rho \phi(T, x) \rangle + \mathcal{O} \left(e^{-\frac{\bar{r}^2}{4(T-t)}} \right), \quad (3.219)$$

to determine the EMT renormalization constants and the multiplicative factor Z_δ. In the previous subsections, it has been shown that the identity

$$\langle \hat{\delta}_{x,\rho} \hat{P}_T \rangle = -2\langle \mathrm{tr}\{\hat{L}_\mu(0,x)\hat{F}_{\rho\mu}\}\hat{P}_T \rangle, \tag{3.220}$$

holds at any lattice spacing (the " ^ " symbol characterizes lattice operators). Here $\hat{P}_T$ is a gauge-invariant probe built with gauge fields $V_\mu(t,x)$ satisfying a discretized form of the gradient flow, like (3.116). It has been proved that the operator $\mathrm{tr}\{\hat{L}_\mu(0,x)\hat{F}_{\rho\mu}\}$ renormalizes multiplicatively. Then a renormalized operator can be introduced

$$(\tilde{T}_{0\rho})_R = Z_\delta \hat{L}_\mu(0,x)\hat{F}_{\rho\mu} \tag{3.221}$$

such that the following limits are finite

$$\lim_{a \to 0} \langle P_T(\tilde{T}_{0\rho})_R \rangle = \lim_{a \to 0} Z_\delta \langle \hat{\delta}_{x,\rho}\hat{P}_T \rangle = \langle \delta_{x,\rho}P_T \rangle. \tag{3.222}$$

As the operator $\tilde{T}_{0\rho}$ is RG invariant in the continuum, then the renormalization of the corresponding discretized version is finite. This means that Z_δ depends on the lattice spacing only through the bare coupling [24]

$$Z_\delta = 1 + \mathcal{O}(g_0^2) \tag{3.223}$$

According to the analysis of section (2.5), the lattice-renormalized EMT is defined as

$$(\hat{T}_{\mu\nu})_R = \sum_{i=1}^{n} Z_i \left(\hat{T}_{\mu\nu}^{(i)} - \langle \hat{T}_{\mu\nu}^{(i)} \rangle \right), \tag{3.224}$$

the coefficients Z_i to be identified as the renormalization constants. In principle, a mixing with the identity has to be consider (as in the equation above), however this term does not contribute to the lattice TWI, its lattice derivative being zero. The lattice TWI is given by

$$\langle [\partial_\mu(\hat{T}_{\mu\nu})_R + R_\nu](x)\hat{P}_T \rangle = -Z_\delta \langle \hat{\delta}_{x,\rho}\hat{P}_T \rangle, \tag{3.225}$$

where the r.h.s. is already known to converge to the correct continuum limit. On the l.h.s., the restoration of translation invariance is ensured by the following conditions:

- the limit

$$\lim_{a \to 0} \langle \partial_\mu(\hat{T}_{\mu\nu})_R \hat{P}_T \rangle = \langle P_T \partial_\mu T_{\mu\rho} \rangle, \tag{3.226}$$

  is finite and regular at the space-time point x (as no contact terms are generated);

- the contribution of the operator $R_\nu(x)$ (which is finite), vanishes at any space-time point x

$$\lim_{a \to 0} \langle R_\nu(x)\hat{P}_T \rangle = 0 \tag{3.227}$$

Putting all together, up to subleading corrections in the lattice spacing:

$$Z_\delta \langle \hat{\delta}_{x,\rho}\hat{P}_T \rangle = -\langle \hat{P}_T \partial_\mu(\hat{T}_{\mu\rho})_R(x) \rangle, \tag{3.228}$$

$$Z_\delta \langle \hat{X}_T a^d \sum_y \hat{\delta}_{y,\rho}\hat{\phi}(T,x) \rangle = \langle \hat{X}_T \partial_\rho \hat{\phi}(T,x) \rangle + \mathcal{O}\left(e^{-\frac{\bar{r}^2}{4T}} \right). \tag{3.229}$$

Equations (3.228-3.229) can be straightforwardly used to numerically determine the renormalization constants Z_i and Z_δ for any finite value of the lattice spacing.

---

[24]It should be mentioned that things will become even simpler when the scalar theory in 3 dimensions is considered. In this case it shall be proven that Z_δ is exactly 1.

Determination of Z_i/Z_δ

Equation (3.228) can be employed to measure the ratios Z_i/Z_δ. Using n different gauge-invariant probes at positive flow time (n being the number of constants Z_i) the following system

$$\sum_{\alpha=1}^{n} \langle \hat{\Phi}^{(\beta)}(t,x) \partial_\mu (\hat{T}^{(\alpha)}_{\mu\rho})_R(x) \rangle k_\alpha = -\langle \hat{\delta}_{x,\rho} \hat{\Phi}^{(\beta)}(t,x) \rangle \tag{3.230}$$

can be solved with respect $k_\alpha = Z_\alpha/Z_\delta$. Here local probes at positive flow time have been chosen

$$\hat{P}_t = \hat{\Phi}(t,x), \tag{3.231}$$

and are positioned at the same space-time point as the lattice EMT. The smearing properties of the flow prevent the emergence of contact terms and allow to enhance the signal since the correlators in (3.230) involve operators coalescing on the boundary theory. A further improvement is obtained using vector-like probes

$$\hat{P}_t = \hat{\Phi}_\rho(t,x), \tag{3.232}$$

and summing equation (3.230) over the all lattice directions[25]

$$\sum_{\alpha=1}^{n} \underbrace{\sum_\rho \langle \hat{\Phi}^{(\beta)}_\rho(t,x) \partial_\mu (\hat{T}^{(\alpha)}_{\mu\rho})_R(x) \rangle}_{M^{\beta\alpha}(t,x)} k_\alpha = -\underbrace{\sum_\rho \langle \hat{\delta}_{x,\rho} \hat{\Phi}^{(\beta)}_\rho(t,x) \rangle}_{v^\beta(t,x)}. \tag{3.233}$$

The system defined by (3.233) has a non trivial solution if

1. The probes are chosen such that not all their variations $v^\beta(t,x)$ are zero.

2. The matrix $M^{\beta\alpha}(t,x)$ has rank n.

If these two conditions are satisfied, then, for each flow time t, a vector of renormalization constants $k_{\alpha,t}$ can be defined. The difference between solutions at different flow times will be explained in detail in the following chapter.

Determination of Z_δ

Once the ratios $k_\alpha = Z_\alpha/Z_\delta$ have been determined, the multiplicative factor Z_δ needs to be measured. The latter can be numerically evaluated using equation (3.229). There are several way this identity can be used [34]. For the pure gauge case the following formulation has been adopted

$$Z_\delta \langle a^4 \sum_{y_0 \in \boldsymbol{D}} \hat{\delta}_{y_0,0} \hat{\Phi}(t, L_0/2 - 1)) \rangle_{O-SF} = \langle \partial_{0S} \hat{\Phi}(t, L_0/2 - 1)) \rangle_{O-SF} + \mathcal{O}\left(e^{-\frac{\bar{r}^2}{4t}}\right). \tag{3.234}$$

Here, the suffix $O-SF$ defines open-Schrödinger functional boundary conditions [60] for the direction $\mu = 0$. The global translation is applied along the time direction, integrating its local version within the domain

$$\boldsymbol{D} = \{x \in (L_0/2 - 1) - d \leq x_0 \leq (L_0/2 - 1) + d\}. \tag{3.235}$$

The distance $\bar{r}^2$ that controls the exponential suppression is just $d \leq L_0/2 - 1$. If periodic boundary conditions were applied on the time direction and the integration carried over the all time extension, then the r.h.s. of (3.234) would have vanished. For the direction along which the translation is applied, it is necessary to engineer boundary conditions such that no translational symmetry is generated. The $O-SF$ setup represents a possible choice.

---

[25]This prevents the terms in equation (3.233) to vanish in the continuum, as only scalar quantities produce non-zero expectation values.

Chapter 4

Yang-Mills theory in 4 dimensions

4.1 Introduction

This chapter deals with the determination of the lattice-renormalized EMT in Yang-Mills theory. A brief introduction to the theory is given, followed by the description of the EMT in the continuum. Then, the numerical setup is explained in detail. Results coming from simulations are reported and discussed.

4.2 Yang-Mills theory in a nutshell

Yang-Mills theory is a gauge theory based on the $SU(N)$ group, or, more generally, any compact, semi-simple Lie group. Its fundamental degrees of freedom are represented by gauge fields $A_\mu(x)$. The latter are defined as elements of the $\mathfrak{su}(N)$ algebra and describe the dynamic of gauge bosons. The classical action of the theory is defined as[1]

$$S = -\frac{2}{g_0^2} \int d^d x \, \text{tr}\{F_{\mu\nu} F_{\mu\nu}\},\tag{4.1}$$

while the quantized theory is described by the following path integral

$$\mathcal{Z}[J] = \int D[A] \exp\left(-S - \frac{2}{g_0} \int d^d x \, \text{tr}\{J_\mu A_\mu\}\right),\tag{4.2}$$

which can be used to compute gauge-invariant correlation functions of gauge fields. Once a gauge fixing has been applied [56], the perturbative analysis of Yang-Mills theory can be carried out re-scaling the gauge field

$$A_\mu \to g_0 A_\mu,\tag{4.3}$$

and expanding the path integral (4.2) up to a given order in the bare coupling g_0. The latter is the only parameter that controls the theory. In the perturbative regime, Yang-Mills theory exhibits a single RG fixed point, i.e. the Gaussian one. For the latter, the bare coupling g_0 represents a marginally relevant direction. At finite cut-off, the continuum limit of the theory is obtained properly tuning g_0 towards the Gaussian point while keeping physical quantities unchanged. The lattice formulation of the theory, along with its perturbative and non perturbative studies, have been thoroughly developed during the last four decades [11, 41, 42, 61] and will not be discussed here .

---

[1]The same convention of section (3.2) has been adopted to define the generators of the $\mathfrak{su}(N)$ algebra.

4.2.1 Lattice and continuum EMT

The classical EMT in pure Yang-Mills theory is given by

$$T_{\mu\nu} = -\frac{2}{g_0^2}\text{tr}\left\{F_{\mu\tau}F_{\nu\tau} - \frac{\delta_{\mu\nu}}{4}F_{\lambda\tau}F_{\lambda\tau}\right\}. \tag{4.4}$$

It can be decomposed as

$$T_{\mu\nu} = T_{\mu\nu}^{(2)} + T_{\mu\nu}^{(0)} \tag{4.5}$$

where the components

$$T_{\mu\nu}^{(2)} = -\frac{2}{g_0^2}\text{tr}\left\{F_{\mu\tau}F_{\nu\tau}\right\} \qquad\qquad \text{Spin 2,} \tag{4.6}$$

$$T_{\mu\nu}^{(0)} = \frac{\delta_{\mu\nu}}{2g_0^2}\text{tr}\left\{F_{\lambda\tau}F_{\lambda\tau}\right\} \qquad\qquad \text{Spin 0,} \tag{4.7}$$

$$\tag{4.8}$$

transform according two different irreducible representations of the $SO(4)$ group.

Using a regularization that preserves translational invariance, it can be proved [18] that the renormalized EMT coincides with the bare one if the following definition

$$(T_{\mu\nu})_R = T_{\mu\nu} - \langle T_{\mu\nu}\rangle, \tag{4.9}$$

is adopted. As already pointed out in chapter (3), the VEV does not contribute to the translation WI. However, it has to be included when dilatation invariance is under study. When only translation WI are concerned, $T_{\mu\nu}$ does not renormalize at all, i.e. it is a RG-invariant quantity.

On the lattice, the operator mixing that defines the renormalized EMT can be read off from (2.158), excluding the matter content. The contributing operators are classified according to irreducible representations of the hypercubic group[2]

- Singlet

$$\hat{T}_{\mu\nu}^{(1)} = \frac{\delta_{\mu\nu}}{2g_0^2}\text{tr}\left\{\sum_{\rho\lambda}\hat{F}_{\lambda\rho}\hat{F}_{\lambda\rho}\right\} \quad\simeq\quad \alpha\begin{pmatrix} 1 & & & \\ & 1 & & \\ & & 1 & \\ & & & 1 \end{pmatrix}, \tag{4.10}$$

- Triplet

$$\hat{T}_{\mu\nu}^{(3)} = -\frac{2}{g_0^2}\delta_{\mu\nu}\text{tr}\left\{\sum_{\rho}\hat{F}_{\mu\rho}\hat{F}_{\nu\rho} - \frac{1}{4}\sum_{\rho\lambda}\hat{F}_{\lambda\rho}\hat{F}_{\lambda\rho}\right\} \quad\simeq\quad \begin{pmatrix} \alpha & & & \\ & \beta & & \\ & & \gamma & \\ & & & -(\alpha+\gamma+\beta) \end{pmatrix} \tag{4.11}$$

- Sextet

$$\hat{T}_{\mu\nu}^{(6)} = -\frac{2}{g_0^2}(1-\delta_{\mu\nu})\text{tr}\left\{\sum_{\rho}\hat{F}_{\mu\rho}\hat{F}_{\nu\rho}\right\}, \quad\simeq\quad \begin{pmatrix} 0 & \alpha & \beta & \gamma \\ \alpha & 0 & \delta & \epsilon \\ \beta & \delta & 0 & \eta \\ \gamma & \epsilon & \eta & 0 \end{pmatrix} \tag{4.12}$$

The lattice-renormalized EMT can be written as

$$(T_{\mu\nu})_R = Z_1\left[\hat{T}_{\mu\nu}^{(1)} - \langle\hat{T}_{\mu\nu}^{(1)}\rangle\right] + Z_3\hat{T}_{\mu\nu}^{(3)} + Z_6\hat{T}_{\mu\nu}^{(6)}, \tag{4.13}$$

---

[2]In order to avoid ambiguities, summations over repeated indices, if any, have been explicitly written.

where the VEV of $\hat{T}_{\mu\nu}^{(1)}$ does not contribute to the translation WI.

In the continuum, the EMT is a RG-invariant quantity, provided its VEV has been properly subtracted. As a consequence, the renormalization constants of the lattice EMT have to be finite and can depend on the lattice spacing only through the bare coupling g_0. At one loop in perturbation theory, their expressions are [50]

$$Z_1 = \frac{\beta_0}{2}g_0^2, \tag{4.14}$$

$$Z_3 = 1 + 0.24068g_0^2, \tag{4.15}$$

$$Z_6 = 1 - 0.03008g_0^2. \tag{4.16}$$

β_0 being the leading coefficient of the β function. More generally, these constants allow an expansion of the form

$$Z_{3,6} = 1 + \sum_{j=1}^{\infty} (z_{3,6})_j g_0^{2j}, \tag{4.17}$$

$$Z_1 = \sum_{j=1}^{\infty} (z_1)_j g_0^{2j}, \tag{4.18}$$

$$\tag{4.19}$$

where the coefficients $(z_{1,3,6})_j$ are numerical factors evaluated in perturbation theory. It should be noticed that the contribution coming from $\hat{T}_{\mu\nu}^{(1)}$ is expected to vanish as $a \to 0$, while those related to $\hat{T}_{\mu\nu}^{(3,6)}$ mix together in order to reproduce the correct EMT in the continuum.

4.3 Numerical setup

The only, directly measurable quantities are the ratios $Z_{1,3,6}/Z_\delta$ (which solve the translation WI (3.233)) and the Z_δ factor (3.234). All the numerical effort has been devoted to precisely measure these quantities and determine $Z_{1,3,6}$. The specific setup used for solving equations (3.233) and (3.234) will be explained in detail. In subsection (4.3.3), a description of the numerical algorithms used to generate gauge configurations, as well as evolve them along the flow, is provided. Afterwards, the parameters used to simulate the theory will be displayed. Finally, the outcome of numerical simulations is presented. A comparison with results obtained with other available methods is discussed.

4.3.1 Lattice TWI

To determine the ratios $Z_{1,3,6}/Z_\delta$, at least three vector-like probes at positive flow time are necessary. The simplest choice is represented by

$$\hat{\Phi}_\mu^{(\alpha)}(t,x) = \partial_\nu {}_S \hat{T}_{\mu\nu}^{(\alpha)}|_{U(x)=V(t,x)} \quad \alpha = \{1,3,6\}. \tag{4.20}$$

Then, the ratios can be determined as the solution of the following square system

$$\sum_{\alpha=1}^{3} \underbrace{\sum_{\rho,\mu} \langle \hat{\Phi}_\rho^{(\beta)}(t,x) \partial_\mu (\hat{T}_{\mu\rho}^{(\alpha)})_R(x) \rangle}_{M^{\beta\alpha}(t,x)} k_\alpha = -\underbrace{\sum_\rho \langle \hat{\delta}_{x,\rho} \hat{\Phi}_\rho^{(\beta)}(t,x) \rangle}_{v^\beta(t,x)}. \tag{4.21}$$

The quality of the signal can be improved averaging (4.21) over the spatial directions

$$\sum_{\alpha=1}^{3} \underbrace{L^{-3} \sum_{\vec{x}} \sum_{\rho,\mu} \langle \hat{\Phi}_{\rho}^{(\beta)}(t,\vec{x},x_0) \partial_{\mu}(\hat{T}_{\mu\rho}^{(\alpha)})_R(\vec{x},x_0) \rangle \, k_{\alpha}}_{M^{\beta\alpha}(t,x_0)} = \underbrace{-L^{-3} \sum_{\vec{x}} \sum_{\rho} \langle \hat{\delta}_{\vec{x},x_0,\rho} \hat{\Phi}_{\rho}^{(\beta)}(t,\vec{x},x_0) \rangle}_{v^{\beta}(t,x_0)}, \quad (4.22)$$

however, no average can be taken along the 0 direction, since asymmetric boundary conditions have been used. To reduce boundary effects coming from $x_0 = \{0, L_0 - 1\}$, the operators above have been positioned at $\bar{x}_0 = L_0/2 - 1$.

$$L^{-3} \Sigma_{\underline{x}} < \partial_{\nu}(T_{\nu\rho})^{(3)}(x) \Phi_{\rho}^{(3)}(t,x) >$$
$$x_0 = (L_0 - 1)/2$$
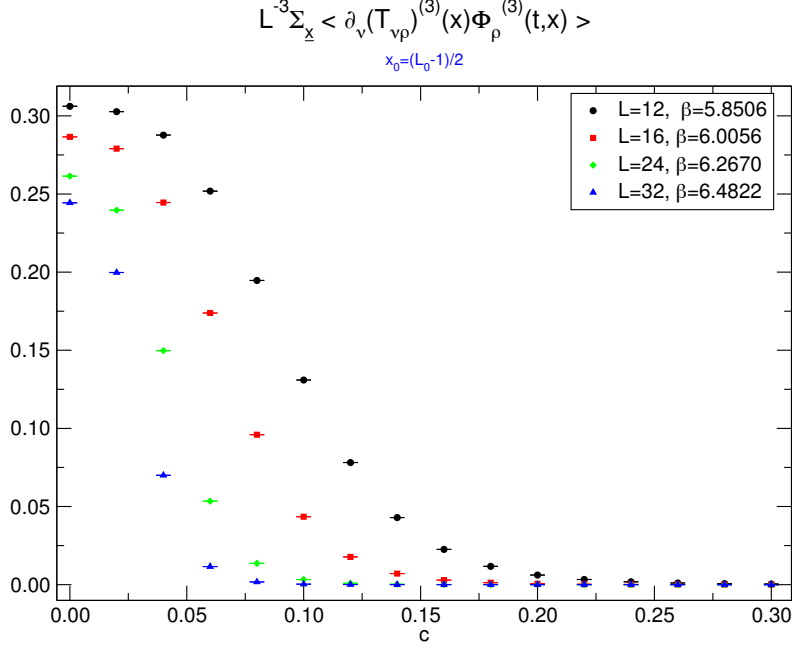
Figure 4.1: Statistical estimates of terms appearing on the l.h.s. of (4.22). Measurements have been taken for different lattices, the β parameter in the legend being defined as $\beta = 6/g_0^2$. The set of values (L,β) defines a line of constant physics. Averages have been taken over Monte Carlo histories, using proper methods in order to take into account the auto-correlation. Data have been displayed with respect the smearing ratio $c = \sqrt{8t}/L$. It should be noticed how the effects of the contact term at $t = 0$ are still quite significant at small flow times.

The numerical strategy can be divided in few steps:

1. representative ensembles of gauge fields are generated employing a proper Monte Carlo algorithm;

2. using a suitable integrator, each configuration is evolved along the flow for several (discrete) values of the flow time[3];

3. for every flow time, the operators appearing in (4.22) are computed using boundary and bulk gauge fields;

---

[3]As it will be shown in the following, the length of the flow time window is crucial in order to reduce lattice artefacts.

4. the elements describing $M^{\beta\alpha}(t, \bar{x}_0)$ and $v^\beta(t, \bar{x}_0)$ are estimated averaging over their corresponding Monte Carlo histories (figures 4.1-4.2).
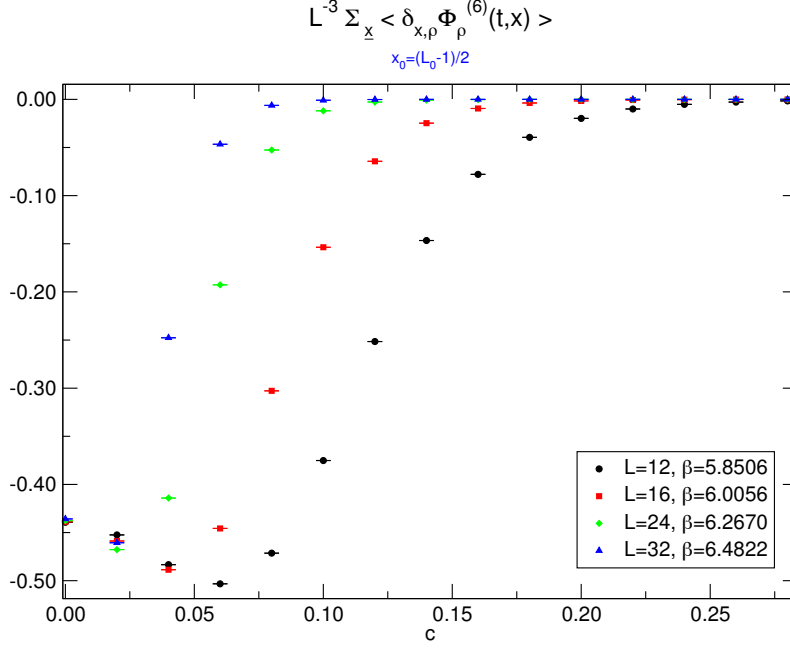
Figure 4.2: Statistical estimates of terms appearing on the r.h.s. of (4.22). Measurements have been taken for different lattices, the β parameter in the legend being defined as $\beta = 6/g_0^2$. The set of values (L, β) define a line of constant physics. Averages have been taken over Monte Carlo histories, using proper methods in order to take into account the auto-correlation. Data have been displayed with respect the smearing ratio $c = \sqrt{8t}/L$. It should be noticed how the effects of the contact term at $t = 0$ are still quite significant at small flow times.

For any value of the flow time t, (4.22) describes a (square) linear system with statistical noise, whose solutions can be numerically estimated. The probes in (4.20) constitute a minimal set necessary to solve the TWI. In this case, operators with the lowest possible mass dimension ($[\Phi_\nu] = 5$) have been employed. This choice is motivated by the fact that numerical signal usually (but not always) gets poorer as the dimension of the probe increases. This is more an empirical fact, not supported by theoretical studies[4]. A priori, it is impossible to know which probes provide the best signal. A possible solution to this problem could be using an arbitrary large basis of probes. One could engineer $n \gg 3$ gauge-invariant operators, combine them to devise different types of square systems and study their numerical outcome. With a proper selection procedure, one could extract the subset of probes which provides the less noisy system, and use it to estimate the ratios $Z_{1,3,6}/Z_\delta$ for all the lattices simulated. With a large enough basis, it is more likely to find the right combination of operators which can significantly improve the signal[5].

However, preliminary studies showed that already the simplest strategy (3 probes, square system) is computationally very expensive. Most of the computation time is spent in the evolution of

---

[4]A qualitative argument can be given using RG ideas. It is known that operators with mass dimension greater than four are irrelevant to the Gaussian fixed point. As a consequence, they do not participate in the description of UV physics. In the continuum, expectation values involving such operators will be then strongly suppressed.

[5]As it will be shown in chapter (5), this method works effectively well for the scalar theory.

configurations and of the Jacobian operator along the flow. The former are necessary for evaluating probes at positive flow time, while the latter is used to compute the variation

$$\hat{\delta}_{x,\rho}\hat{\Phi}^{(\beta)}(t,y). \tag{4.23}$$

A more quantitative idea of the costs can be gained looking at table (4.1).

L	conf. generation (sec)	flow evolution (sec)	obs. computation (sec)
12	0.873	2.61×10^3	2.68×10^3
16	0.240	1.36×10^3	1.39×10^3
24	1.17	6.78×10^3	6.85×10^3
32	0.436	9.66×10^3	9.81×10^3

Table 4.1: Computation times for different set of lattices (first column). Second column shows the time needed to generate a single configuration. Third column displays the total time required to evolve gauge fields and Jacobian. Fourth column contains the times needed to compute elements that form equation (4.22)-(4.26). Even if smaller, the $L = 12$ lattice cannot be parallelized as effectively as the $L = 16$ case. This explains why $t_{12} > t_{16}$.

Here, the time needed to evolve fields and Jacobian over the entire flow-time window is definitely quite large (a factor 10^3 bigger than the time spent to generate a configuration). Measurements have been taken keeping the following ratio

$$c = \frac{\sqrt{8t}}{L}, \tag{4.24}$$

fixed for all the lattices, with

$$c_{max} = 0.3. \tag{4.25}$$

As a consequence, the flow-time window gets wider with the number of lattice points. This has the effect of making measurements more and more expensive when continuum limit is approached.

Having considered these circumstances, a choice has been done to obtain enough precise results in a reasonable amount of time, and the simplest possible strategy (3 probes, square system) has been adopted.

4.3.2 Z_δ

The multiplicative factor Z_δ has been measured using the identity (3.234)

$$Z_\delta \langle a^4 \sum_{y_0 \in \boldsymbol{D}} \hat{\delta}_{y_0,0}\hat{\Phi}(t, L_0/2 - 1) \rangle_{O-SF} = \langle \partial_{0S}\hat{\Phi}(t, L_0/2 - 1) \rangle_{O-SF} + \mathcal{O}\left(e^{-\frac{\bar{r}^2}{4t}}\right), \tag{4.26}$$

where the probe $\hat{\Phi}(t, x_0)$ is obtained as a spatial average of a local probe $\hat{\Phi}(t, x)$. The integration domain is defined as

$$\boldsymbol{D} = \{(L_0/2 - 1) - d \le x_0 \le (L_0/2 - 1) + d\}. \tag{4.27}$$

In principle, any gauge-invariant probe $\hat{\Phi}(t, x_0)$ could be employed. To have good enough estimates of Z_δ, it is necessary to maximize the probe derivative along the direction $\mu = 0$. The nature of the boundary conditions plays a key role in singling out the right operator. When $O - SF$ boundary conditions are adopted, the best candidate probe is the (spatially averaged) Polyakov loop along

spatial directions.

$$\hat{\Phi}(t, L_0/2 - 1) = W(t, L_0/2 - 1), \tag{4.28}$$

$$W(t, L_0/2 - 1) = L^{-3} \sum_{j=1}^{3} W_j(t, L_0/2 - 1), \tag{4.29}$$

$$W_i(t, L_0/2 - 1) = \text{tr}\{ \prod_{x_i=0}^{L_i-1} V(t, \vec{x}, L_0/2 - 1)\}, \tag{4.30}$$

where periodic boundary conditions have been imposed for $\mu = 1, 2, 3$.
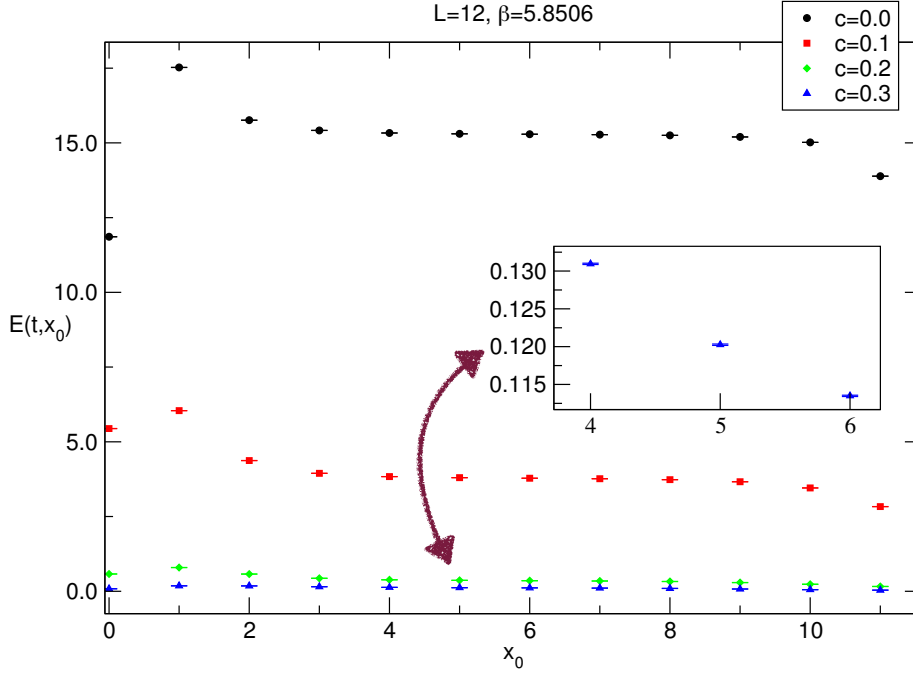
Figure 4.3: Spatial average of energy density at positive flow time. Data are displayed as functions of the position along the $\mu = 0$ direction, for different values of the smearing radius $c = \sqrt{8t}/L$.

This choice can be quantitatively motivated making comparisons with other candidate probes. Figure (4.3) shows the estimates of the following quantity

$$E(t, x_0) = L^{-3} \sum_{\vec{x}} E(t, \vec{x}, x_0) = -2L^{-3} \sum_{\vec{x}} \langle \text{tr}\{\hat{G}_{\mu\nu}\hat{G}_{\mu\nu}\}(t, \vec{x}, x_0)\rangle, \tag{4.31}$$

which is the spatial average of the energy density at positive flow time. Data are plotted as functions of x_0, for different, fixed values of the flow time. Inside the interval $[0, L_0 - 1]$, the derivative of $E(t, x_0)$ changes sign. This means that $\partial_0 E(t, x_0)$ vanishes at some point $x_0^* \in [0, L_0 - 1]$. Moreover, around $x_0 = L_0/2 - 1$, $E(t, x_0)$ (zoomed area) is varying really slowly ($\sim -11\%$ from $x_0 = 4$ to $x_0 = 6$, for $c = 0.3$). As a consequence, its derivative, measured at $x_0 = L_0/2 - 1$, is going to be very small.
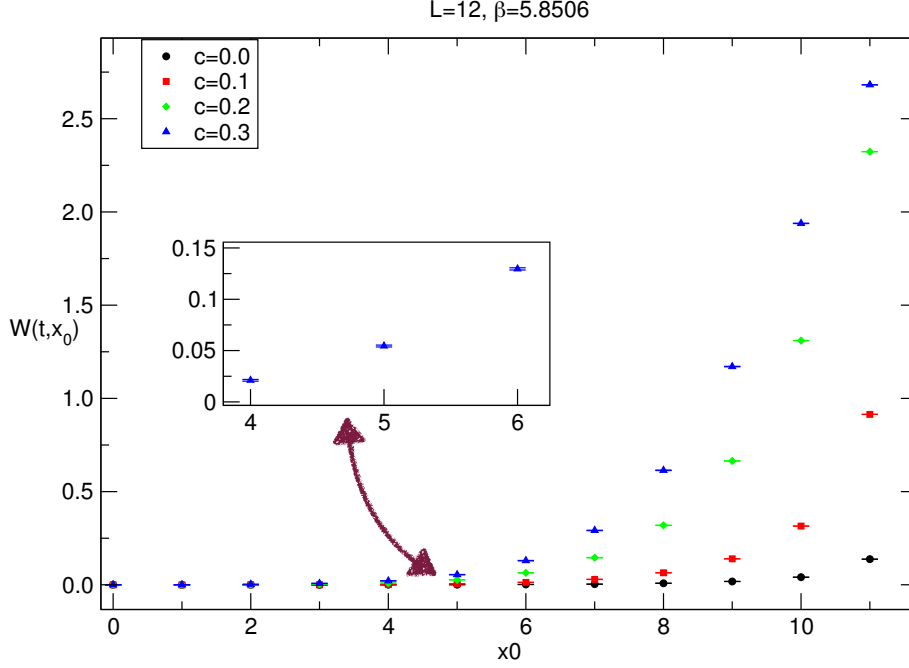
Figure 4.4: Spatial average of the Polyakov line at positive flow time. Data are displayed as functions of the position along the $\mu = 0$ direction, for different values of the smearing radius $c = \sqrt{8t}/L$.

On the other hand, figure (4.4) displays the values of the (spatially-averaged) Polyakov line $W(t, x_0)$. The derivative of $W(t, x_0)$ is monotonic inside the interval $[0, L_0 - 1]$ and varies more rapidly around $x_0 = L_0/2 - 1$ ($\sim 400\%$ from $x_0 = 4$ to $x_0 = 6$, for $c = 0.3$). Using the data displayed above, the symmetric derivatives of the two quantities at $x_0 = L_0/2 - 1$ can be compared

c	0.0	0.1	0.2	0.3
$\partial_{0S} W(t, L_0/2 - 1)$	0.0007(2)	0.0059(3)	0.0274(7)	0.0543(9)
$\partial_{0S} E(t, L_0/2 - 1)$	$-0.021(5)$	$-0.02702(41)$	$-0.01459(15)$	$-0.00873(8)$

Table 4.2: Symmetric derivatives comparisons.

As it will be shown in the following, the renormalization coefficients can be suitably extracted in a flow-time region that runs from $c = 0.2$ to $c = 0.3$. Looking at the data in (4.2), it can be noticed that the Polyakov line provides the larger derivative inside this interval.

Similar comparisons have been made with other gauge-invariant probes. The final outcome is that $W(t, x_0)$ is the best candidate for the measurement of Z_δ. For the latter, equation (4.26) becomes

$$Z_\delta = \frac{\langle \partial_{0S} W(t, L_0/2 - 1) \rangle \rangle_{O-SF}}{\langle a \sum_{y_0=L_-}^{L_+} \hat{\delta}_{y_0,0} W(t, L_0/2 - 1) \rangle \rangle_{O-SF}} + \mathcal{O}\left(e^{-\frac{d^2}{4t}}\right), \tag{4.32}$$

where $L_\pm = L_0/2 - 1 \pm d$.

The constant Z_δ can be measured for several values of the radius d. The latter has to be large enough to suppress the exponential contribution in (4.32). As a consequence, small lattices (in terms of number of points) cannot be adopted.

4.3.3 Simulation setup

Geometrical setup

The setup adopted for numerical simulations consisted of a hypercubic lattice with periodic boundary conditions along the spatial directions and $O - SF$

$$F_{0k}(x)|_{x_0=0} = 0, \tag{4.33}$$

$$A_k(x)|_{x_0=L_0} = 0 \tag{4.34}$$

for the temporal extension. Simulations have been done using a modified version of openQCD, which employs a hybrid Monte Carlo algorithm (HMC) [62] to generate gauge field configurations. With respect its original version, the modified code includes routines for the computation of the elements that compose equations (4.22) and (4.32).

Simulation parameters

Renormalization constants have to be measured along a renormalized trajectory (also called line of constant physics). Such a line is characterized by a series of lattices coupled to a specific value of the bare coupling. The latter, in the spirit of Wilsonian RG, has to be tuned in order to keep physical quantities (like a hadron mass, or a length scale) fixed as the number of lattice points changes. Once the tuning has been accomplished, the path towards the continuum limit is obtained moving from the coarsest lattice to the finest one. This *scale setting* procedure is necessary whenever physical quantities are measured and their continuum values extrapolated. In this case, a line of constant physics has been provided by the following set

L	12	16	24	32
β	5.8506	6.0056	6.2670	6.4822

Table 4.3: Lattice setup.

which has been used by L. Giusti and M. Pepe to measure the renormalized EMT [38]. Using shifted boundary conditions, the authors measured the renormalization constants in the infinite volume limit, solving specific thermal WIs. For a set of renormalization constants measured in two different volume schemes (finite vs. infinite) the following ratio

$$\frac{Z_{i,FLOW,L}}{Z_{i,SHIFTED}}, \quad i = \{1,3,6\}, \tag{4.35}$$

admits an analytic expansion in powers of the lattice spacing[6]

$$\frac{Z_{i,FLOW,L}}{Z_{i,SHIFTED}} = 1 + \sum_{j=1}^{\infty} (c_i)_j \left(\frac{a}{L}\right)^{2j} \qquad i = \{1,3,6\}, \tag{4.36}$$

for small values of a. Equation (4.36) represents the perfect tool to check the consistency of the method adopted in this work.

---

[6]The original Symanzik expansion contains also logarithms, which are here neglected.

Before starting with the measurements, the HMC parameters had been properly tuned to guarantee the best efficiency on all the lattices of (4.3). The evolution along the flow has been implemented using a 3rd order Runge-Kutta algorithm, following the formulation in [21]. The integration step had to be adjusted to make systematic errors, due to discretization of flow time, negligible.

Measurements

Numerical simulations have been carried out on a BlueGeneQ supercomputer using a large number of replicas[7] to increase the statistics. Consecutive measurements have been separated by several Monte Carlo trajectories in order to reduce auto-correlation effects.

L	β	Replicas	M.D. steps	Traj. per measure	$Z_{1,3,6}/Z_\delta$	Z_δ
12	5.8506	128	5	500	96000	29440
16	6.0056	16	5	500	52248	18488
24	6.2670	16	5	500	30088	9144
32	6.4822	8	5	700	25288	3384

Table 4.4: Simulation parameters. The first two columns denotes the number of lattice points and the corresponding bare coupling β. The third column shows how many replicas have been employed for each lattice, while the fourth contains the number of *molecular dynamics* steps used in the HMC algorithm. Fifth column displays the number of configurations generated between two consecutive measurements. The last two columns contain the number of total measurements for $Z_{1,3,6}/Z_\delta$ and Z_δ

The asymmetry between measurements of $Z_{1,3,6}/Z_\delta$ and Z_δ in (4.4) is motivated by the following facts. The first is that Z_δ can be measured quite precisely with a smaller statistics than the one required for $Z_{1,3,6}/Z_\delta$. The second is that the routine used to compute terms in (4.32) requires a lot of computation time, and it should be deactivated as soon as Z_δ is measured with enough precision. To optimize the simulations, it has been decided to disable the computation of the elements in (4.32) as soon as the precision on Z_δ was about .5%[8]. On the other hand, evaluation of the observables in (4.22) has been kept active to obtain more data for $Z_{1,3,6}/Z_\delta$.

Choice of the flow times

The width of the flow time window, as well as the number of flow times, has been determined after few numerical investigations.

---

[7]With replica, a copy of the same type of run (same lattice, bare parameters and flow times) but different start configuration is intended.

[8]For $c = \sqrt{8t}/L = 0.2$ on each lattice.
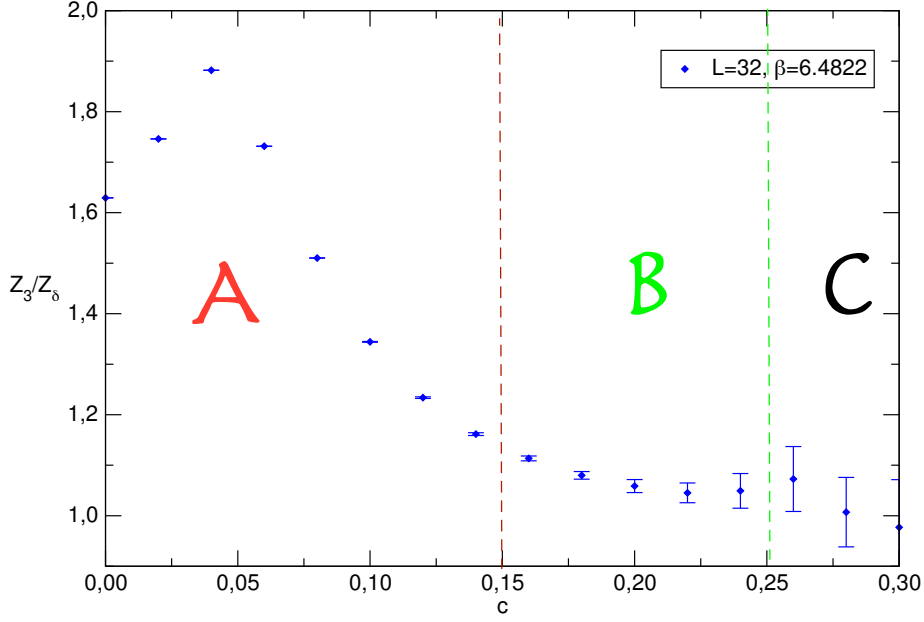
Figure 4.5: Example of how the EMT renormalization constants behave with the flow time. In this case, the ratio Z_3/Z_δ, measured on the finest lattice, has been considered.

At zero flow time, the TWI are affected by a contact term arising from the coalescence of probe and energy momentum tensor. At positive flow time, one would ideally distinguish three different regions, as in figure (4.5). The first one is a small flow time window characterized by large lattice artefacts (region A), representing the remnant of the divergence at $t = 0$: these artefacts are supposed to vanish when continuum limit is approached. As the flow time increases, these effects get quite reduced and data start to vary slowly with t. Here the constants $Z_{1,3,6}/Z_\delta$ are still measured with good precision (region B): this is the second region of flow times, where the values of the coefficients $Z_{1,3,6}/Z_\delta$ could be extracted. Finally, a big flow time window should follow (region C), where the solution of the system would get more and more noisy due to signal depletion. The length of the flow time window has to be enough to contain the first two kind of regions. The last region should be discarded, since it is reached at the cost of large simulation times and poor statistical signal. Moreover, the smearing radius c cannot be too large, otherwise boundary contributions at $x_0 = \{0, L_0 - 1\}$ will come into play. These terms generate $\mathcal{O}(a)$ scaling violations when continuum limit is approached, and worsen the natural $\mathcal{O}(a^2)$ convergence of gauge theories.

For the set of lattices in (4.3), the following window

$$c = \{0.0, 0.02, 0.04, 0.06, 0.08, ..., 0.3\}, \quad c = \frac{\sqrt{8t}}{L} \tag{4.37}$$

represented the optimal flow-time interval for carrying out measurements in a reasonable amount of time.

4.4 Results

In this section all the numerical results will be presented and discussed. In section (4.4.5) the constants $Z_{1,3,6}$ will be compared with those measured by L.Giusti and M. Pepe [38].

4.4.1 $Z_{1,3,6}/Z_\delta$

In the following, the values of $Z_{1,3,6}/Z_\delta$ are displayed as functions of the flow time, for the set of lattices given in (4.3). For any fixed flow time, a set of renormalization constants is defined. The latter describe a lattice-renormalized EMT such that

$$\langle \partial_{\mu S}(\hat{T}_{\mu\nu})_R \hat{P}_T \rangle \underset{a\to 0}{\to} \langle \partial_\mu \hat{T}_{\mu\nu} P_T \rangle + \mathcal{O}(a^2), \tag{4.38}$$

$$Z_\delta \langle \hat{\delta}_{x,\rho} \hat{P}_T \rangle \underset{a\to 0}{\to} \langle \delta_{x,\rho} P_T \rangle + \mathcal{O}(a^2). \tag{4.39}$$

Renormalization constants extracted at different flow times will generate different $\mathcal{O}(a^2)$ corrections in the above limits. A suitable set of constants should provide the smallest possible scaling violations when continuum limit is approached. As explained in subsection (4.3.3), these optimal sets can be determined exploring the flow time window in figures (4.8)-(4.6)-(4.7).

- The $0.0 < c < 0.2$ region is characterized by large lattice artefacts, especially for $L = \{12, 16\}$. These artefacts are a remnant of the $t = 0$ contact term. They can be identified as a^2/t terms and are supposed to vanish in the continuum. At fixed lattice spacing, the size of these effects can be qualitatively identified with the width of the peaks displayed in the plots. As expected, these peaks shrink and move towards smaller flow times when continuum limit is approached. At zero lattice spacing, they should reconstruct the $t = 0$ divergence.
  In this region of flow times, the extraction of renormalization constants is not recommended, the size of scaling violations to physical quantities being quite large ($\mathcal{O}(a^4)$ or higher).

- For $c \geq 0.2$, contact term effects are reduced (especially for $L = \{24, 32\}$) and only $(a/L)^2$ artefacts would remain. Ideally, data should display a plateau, since the renormalization constants do not depend on the flow time. Actually this does not happen, because remnants of the $t = 0$ divergence are not totally suppressed. The latter can be totally removed only flowing the probes at really large flow times. However, this comes at the price of longer simulations and poorer signal. Moreover, for $c > 0.26$, the precision on some of the renormalization constants is already quite poor. As a consequence, measurements at larger flow times would require larger statistics, which are computationally expensive.

For these reasons, the $0.2 \leq c \leq 0.3$ region seemed to be the most suitable interval for extracting the renormalization constants.

Among the all measured quantities, Z_3/Z_δ proves to be the most accurate one (figure (4.6)). Data are precisely measured up to $c \leq 0.24$, then precision drops down. For $c \geq 0.12$, ordered sequences, from the coarsest lattice to the finest one, become quite clear (circled area in figure (4.6)).
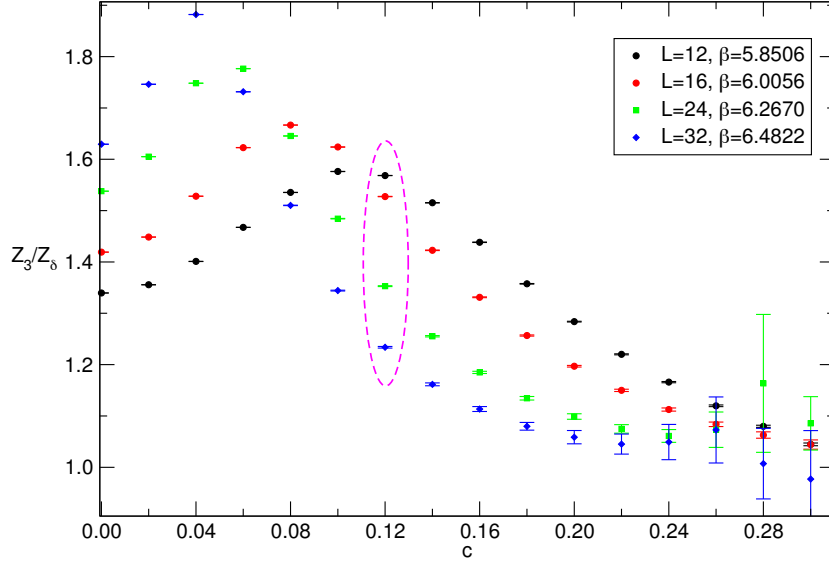
Figure 4.6: Plot of Z_3/Z_δ as function of the ratio $c = \sqrt{8t}/L$.

For Z_6/Z_δ (figure (4.7)), contact term effects are still quite important (up to $c \leq 0.18$ for $L = 32$), and ordered sequences are manifest only for $c \geq 0.2$. As for Z_3/Z_δ, numerical precision worsens for $c \geq 0.26$. Moreover, the solution of translation WI here seems to become quite unstable. This is a clear signal that a larger number of measurements is required.

Remnants of the contact term affects Z_1/Z_δ (figure (4.8)) up to $c \leq 0.14$ (on the finest lattice). Data show a continuum-like order already for $c \geq 0.8$. However, in the region of interest ($c \geq 0.2$), this order gets lost due to signal depletion (zoomed area in figure (4.8)). The main problem is that the ratio Z_1/Z_δ is a quite small quantity[9]. A quantitative idea can be obtained using the one loop expression of Z_1 (4.14)

L	β	Z_1
12	5.8506	0.037
16	6.0056	0.035
24	6.2670	0.032
32	6.4822	0.03

Table 4.5: Z_1 at one-loop in perturbation theory.

for the set of lattices (4.3). From table (4.5), it can be inferred that Z_1/Z_δ is a quantity of order 10^{-2} or smaller. This means that it can be precisely measured only with a really large statistics.

---

[9]In the continuum, $Z_1/Z_\delta = 0$.

117
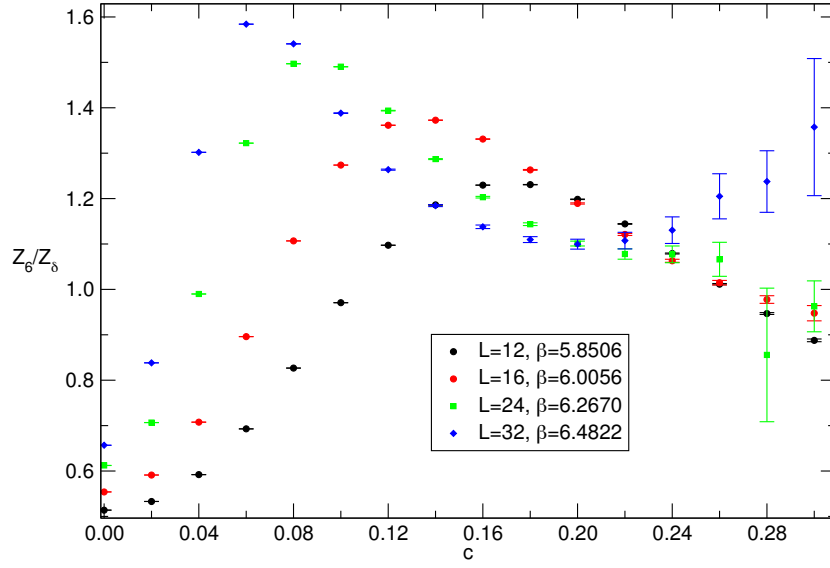
Figure 4.7: Plot of Z_6/Z_δ as function of the ratio $c = \sqrt{8t}/L$.
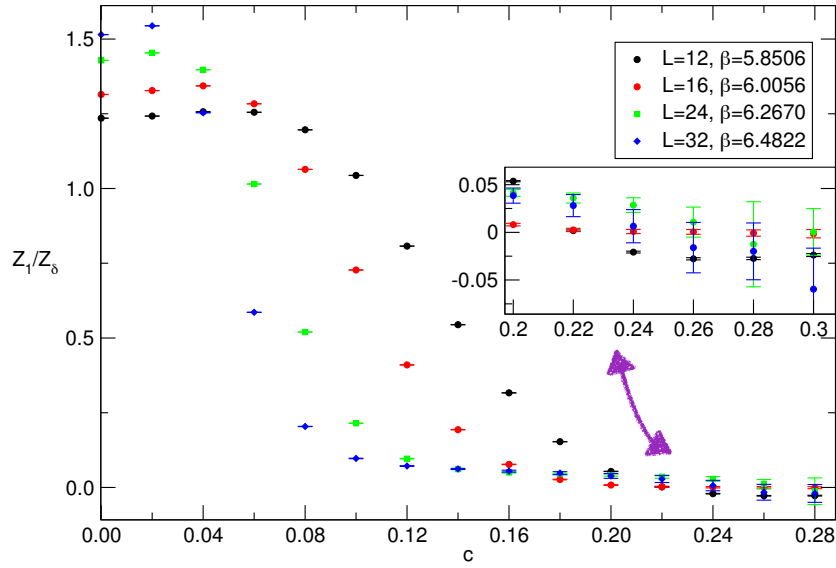
Figure 4.8: Plot of Z_1/Z_δ as function of the ratio $c = \sqrt{8t}/L$. The zoomed area focuses on the flow time window where lattice artefacts should be most reduced.

4.4.2 Z_δ

In this section, the measurement of the multiplicative factor Z_δ is discussed. An idea of how this quantity has been extracted is provided by figure (4.9). Here, data have been plotted as functions of the flow time for fixed values of the radius d, which defines the integration domain around a local translation

$$Z_\delta = \frac{\langle \partial_{0S} W(t, L_0/2 - 1) \rangle\rangle_{O-SF}}{\langle a \sum_{y_0=L_-}^{L_+} \hat{\delta}_{y_0,0} W(t, L_0/2 - 1) \rangle\rangle_{O-SF}} + \mathcal{O}\left(e^{-\frac{d^2}{4t}}\right), \tag{4.40}$$

where $L_\pm = L_0/2 - 1 \pm d$. As for the case of translation WI, the ratio above generates a contact term at zero flow time. As the probe gets evolved, two different regions can be identified.

- For values of c smaller than 0.08, the signal is quite noisy[10]. The reason behind this behaviour is that contact term effects are still quite dominant, and large cancellations occur in the ratio above. This causes loss of precision and huge statistical errors.

- When $c \geq 0.08$, numerical estimates become stable, and their precision grows as the flow time increases. For any values of the radius d, measurements of Z_δ seem to be compatible up to $c \leq 0.12$. Then deviations appear. The latter are caused by the growth of the exponential corrections

$$\mathcal{O}\left(e^{-\frac{d^2}{4t}}\right), \tag{4.41}$$

with the flow time. These deviations gets suppressed as the integration radius d increases. Indeed, for $d = \{(L_0/2 - 2), (L_0/2 - 1)\}$, these effects are totally negligible, figure (4.10).
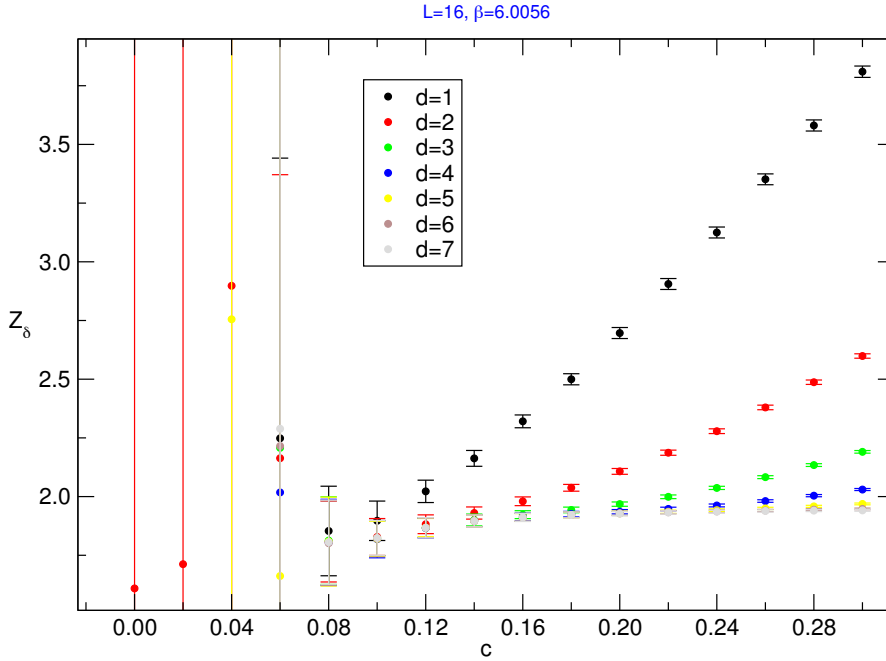
Figure 4.9: Plot of Z_δ as function of the ratio $c = \sqrt{8t}/L$. Different data sets are characterized by different radius d of integration.

---

[10]This behaviour has been observed also on the other lattices of (4.3).
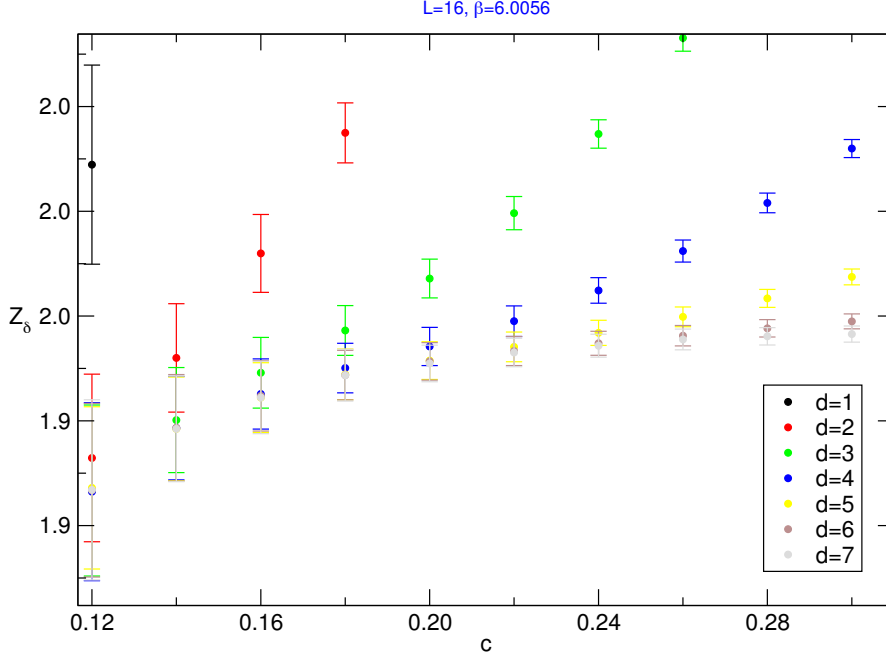
Figure 4.10: Zoom on the $c \geq 0.12$ region. Different data sets are characterized by different radius d of integration. It should be noticed how deviations becomes negligible, within error bars, for $d = \{6, 7\}$

A similar behaviour has been observed also for the other lattices in (4.3). The only difference among them consists in the value of the flow time at which deviations appear. For finer lattices, usually these effects become evident at larger flow times[11].

For any lattice spacing , the values of Z_δ have been extracted using data sets labelled by the largest integration radius (4.6). This ensured numerical estimates to be quite safe from any spurious exponential correction of the form (4.41).

L	β	d_{max}/a
12	5.8506	5
16	6.0056	7
24	6.2670	11
32	6.4822	15

Table 4.6: Maximum integration radius used for measuring Z_δ. The formula $d_{max} = L_0/2 - 1$ has been adopted. For finer lattices, only 7 radiuses have been used ($L_0/2 - 1, ..., L_0/2 - 7$) to make the computation of terms in (4.32) less expensive.

Having fixed the radius d to its maximum value, each measurement at $c > 0.18$ is a good candidate for estimating Z_δ (figure (4.11)). The outcomes of these measurements are all displayed in table (4.7). The reference value for Z_δ has been extracted at $c = 0.2$ (circled area in figure (4.11)). This particular value of the flow time seems to be a good compromise to obtain an enough precise

---

[11]$c = 0.20$ for $L = 24$ and $c = 0.26$ for $L = 32$

estimate without enhancing exponential corrections. The selected value can be used for the straight evaluation of $Z_{1,3,6}$, as it will be shown in the next subsection.
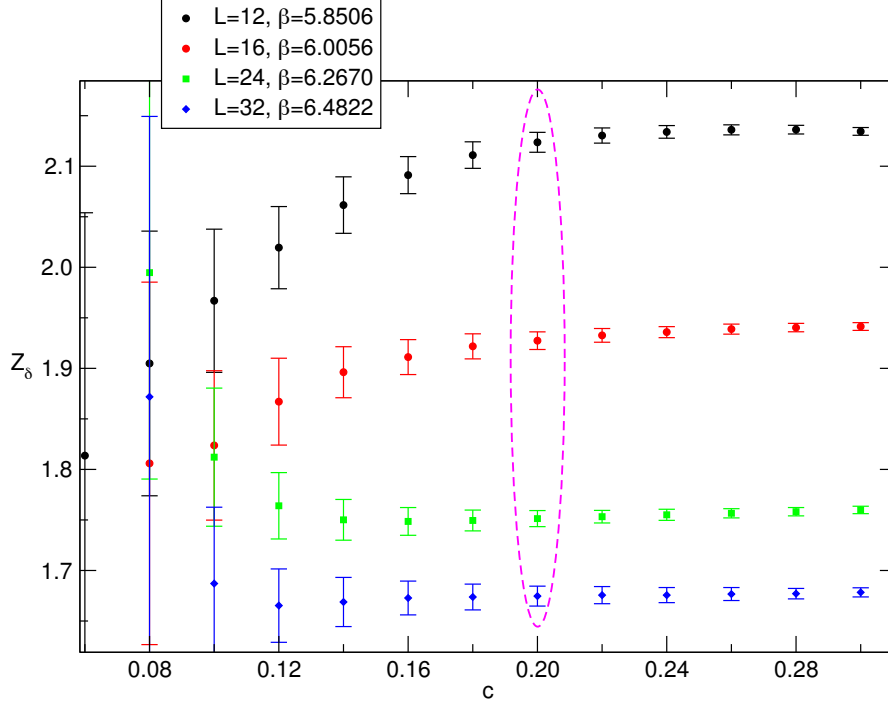
Figure 4.11: Estimates of Z_δ in terms of the ratio $c = \sqrt{8t}/L$. For all the lattices in (4.3), the data set labelled by d_{max} has been selected.

Z_δ						
L	$c = 0.2$	$c = 0.22$	$c = 0.24$	$c = 0.26$	$c = 0.28$	$c = 0.3$
12	2.1236(98)	2.1304(75)	2.1339(63)	2.1360(50)	2.1361(43)	2.1344(38)
16	1.9274(87)	1.9326(68)	1.9358(55)	1.9388(50)	1.9403(42)	1.9414(39)
24	1.7513(79)	1.7533(62)	1.7551(55)	1.7566(46)	1.7582(41)	1.7600(37)
32	1.6747(99)	1.6757(85)	1.6757(75)	1.6767(64)	1.6771(52)	1.6784(45)

Table 4.7: Values of Z_δ for $0.2 \leq c \leq 0.3$, for all the lattices employed in the simulations. For each lattice, the data set labelled by d_{max} has been considered. The coloured column highlights the reference values chosen for Z_δ.

4.4.3 $Z_{1,3,6}$

In this subsection, numerical results for $Z_{1,3,6}$ (figures (4.12)-(4.13)-(4.14)) are shown.
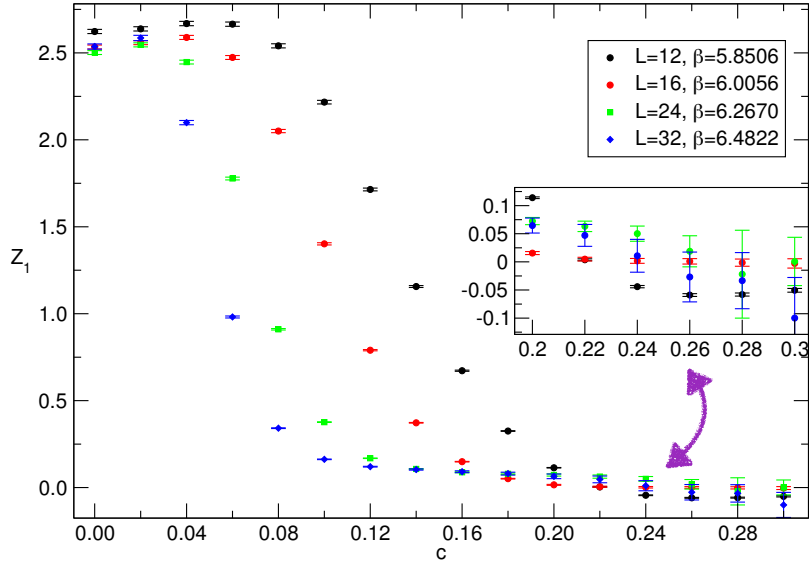
Figure 4.12: Plot of Z_1 as function of the ratio $c = \sqrt{8t}/L$. The zoomed area focuses on the flow time window where lattice artefacts should be most reduced.
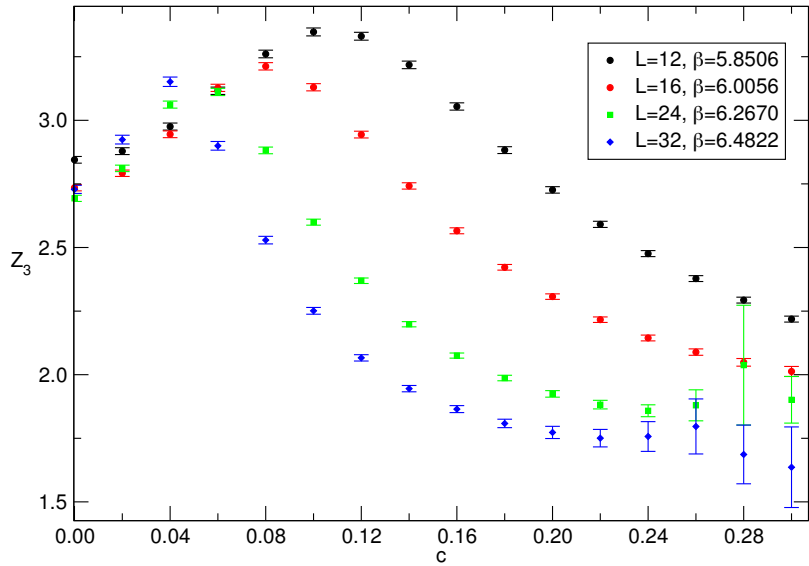
Figure 4.13: Plot of Z_3 as function of the ratio $c = \sqrt{8t}/L$.
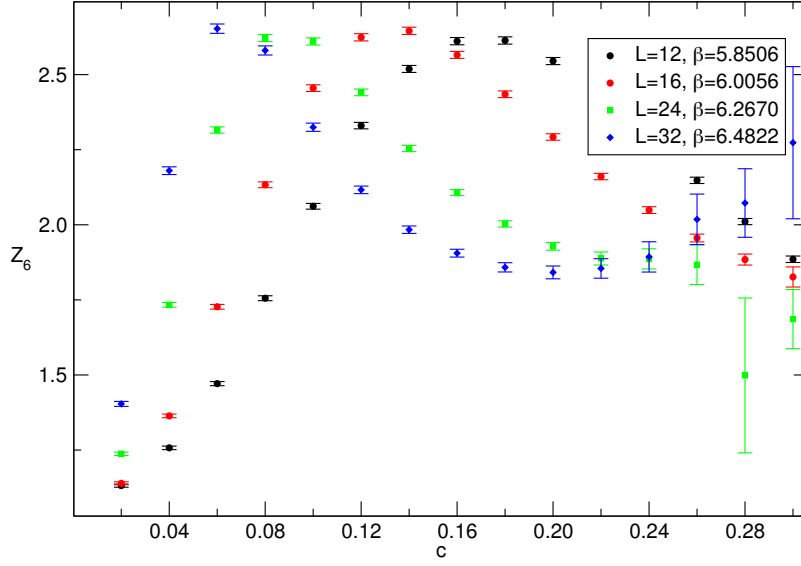
Figure 4.14: Plot of Z_6 as function of the ratio $c = \sqrt{8t}/L$.

From the solution of the TWI, other two interesting quantities have been determined. These are given by the following ratios

$$r_1 = \frac{Z_1}{Z_6}, \tag{4.42}$$

$$r_3 = \frac{Z_3}{Z_6}, \tag{4.43}$$

which are shown in figure (4.15) and (4.16).

In the region of interest ($0.2 \leq c \leq 0.3$), r_1 shows a behaviour similar to that of Z_1/Z_δ and Z_1. This is not so unexpected, since r_1 is a small quantity of the same order of magnitude of Z_1. As a consequence, it can be precisely measured only if a large statistic is employed.

The situation is different for r_3, which shows some interesting features.
For $0.2 \leq c \leq 0.3$, the values of such ratio seem to be really close to one. The statement undoubtedly holds for the finer lattices $L = \{24, 32\}$ where the values of r_3 are compatible with $r_3 = 1$ within the errors. For $L = \{12, 16\}$, deviations from r_3 becomes larger, but this is not surprising, since for these lattices the remnants of the $t = 0$ divergence are still quite strong. As before, coarse lattices provides enough precise data in the entire range of flow times, while for the finer ones the precision drops down for $c \geq 0.26$[12]. Data suggest that lattice artefacts affecting r_3 are highly reduced in the region of interest ($c \geq 0.2$), especially on the finest lattices. This is a quite remarkable feature, which plays a key role when comparisons with other available results are made.

---

[12]This is usually expected, since simulations on coarse lattices allow to obtain quite high statistics in a "small" amount of computation time.
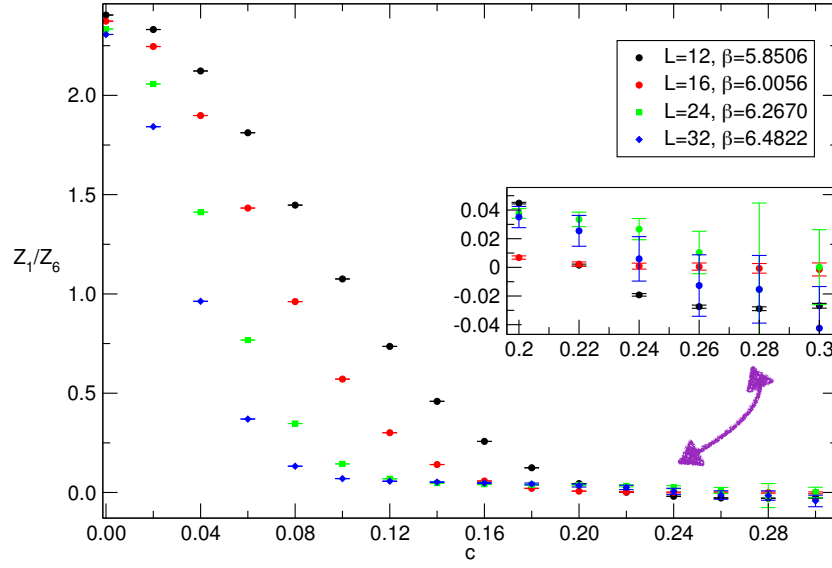
Figure 4.15: Plot of Z_1/Z_6 as function of the ratio $c = \sqrt{8t}/L$. The zoomed area focuses on the flow time window where lattice artefacts should be most reduced.
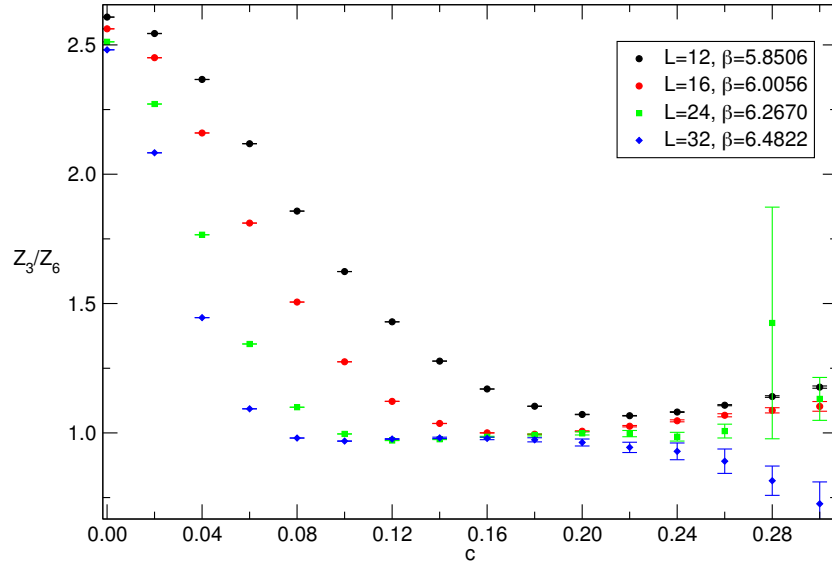
Figure 4.16: Plot of Z_3/Z_6 as function of the ratio $c = \sqrt{8t}/L$.

4.4.4 $Z_{1,3,6}$: tree-level improvement

Along with the original data, a tree-level improvement has been applied. Removing terms that come from the tree-level expansion of translation WI *could* reduce[13] the lattice artefacts affecting the measurement of $Z_{1,3,6}$. Hopefully, this procedure could extend the region in which $Z_{1,3,6}$ are extracted towards smaller flow times.

Tree-level contributions are removed in the following way:

- terms that enter in the definition of the tree-level translation WI are computed;

- having measured, and extracted Z_δ, the following (square) system is solved[14]

$$\sum_{\beta=1,3,6}\left[\sum_{\rho\sigma}\langle\hat{T}_{\mu\rho}^{[\beta]}(x)\partial_{\mu_s}\hat{\Phi}_\rho^{(\alpha)}(t,x)\rangle\right]Z_\beta - Z_\delta\sum_\rho\langle\hat{\delta}_{x,\rho}\hat{\Phi}_\rho^{(\alpha)}(t,x)\rangle =$$
$$= \sum_{\beta=3,6}\left[\sum_{\rho\sigma}\langle\hat{T}_{\mu\rho}^{[\beta]}(x)\partial_{\mu_S}\hat{\Phi}_\rho^{(\alpha)}(t,x)\rangle_{\text{tree}}\right] - \sum_\rho\langle\hat{\delta}_{x,\rho}\hat{\Phi}_\rho^{(\alpha)}(t,x)\rangle_{\text{tree}}$$

with respect to $Z_{1,3,6}$.

On the r.h.s. the sum is restricted only to two terms since

$$Z_{3,6} = 1, \tag{4.44}$$
$$Z_1 = 0, \tag{4.45}$$

at tree-level. The effectiveness of an improvement can be appreciated when the lattice spacing is not too small. As a consequence, the method has been initially probed on the coarsest lattices ($L = \{12, 16\}$). Numerical results are shown in figures (4.17)-(4.18)(4.19). Unfortunately, the effect of this procedure is only to modify the shape of data at very small flow times. Here, lattice artefacts are quite huge and there is no interest in extracting the value of the constants.

(a)   **(b)**
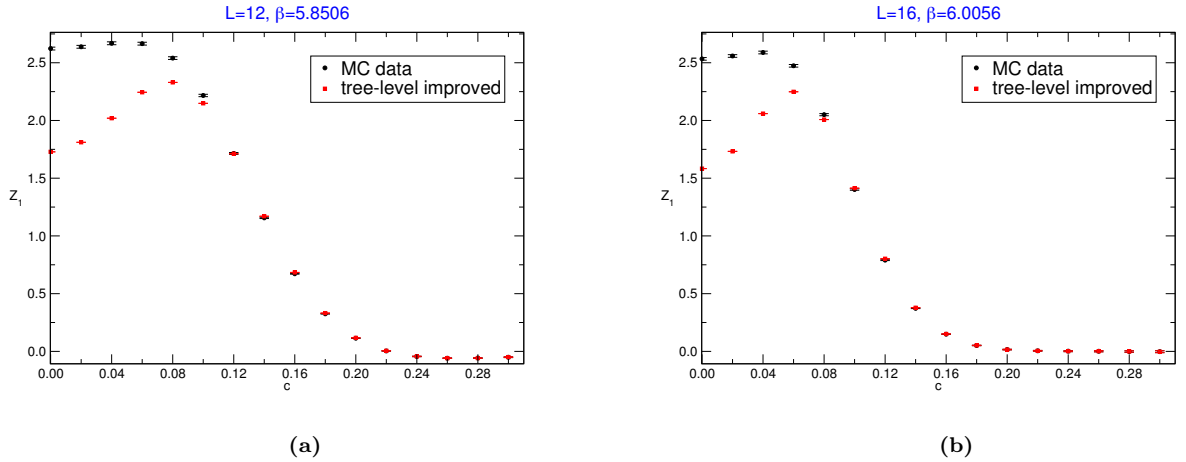
Figure 4.17: Tree-level improved Z_1 for $L = \{12, 16\}$

---

[13]A proper improvement à la Symanzik would require the removal of tree-level contributions coming from boundary and bulk action, as well as lattice EMT and translation WI.

[14]In order to lighten the formulas, average over spatial directions has not been written.
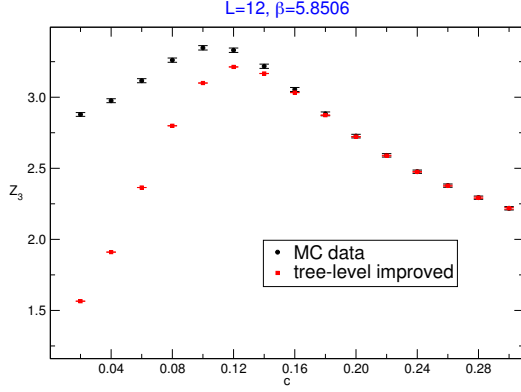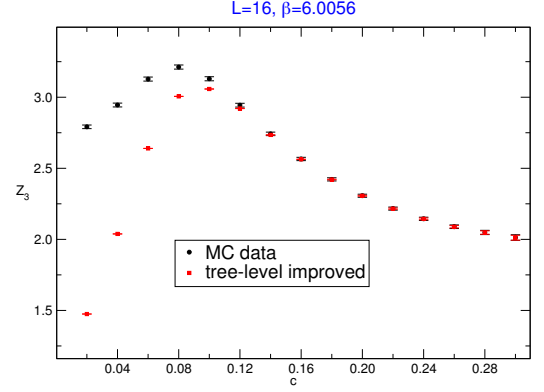
Figure 4.18: Tree-level improved Z_3 for $L = \{12, 16\}$
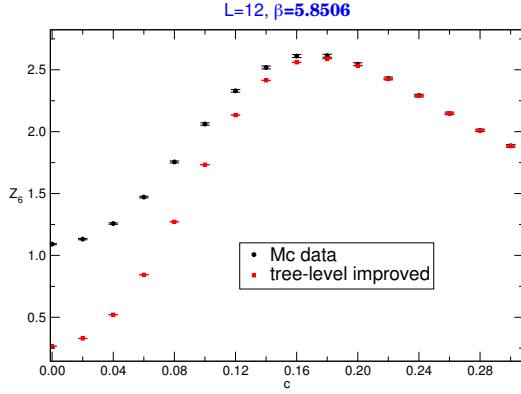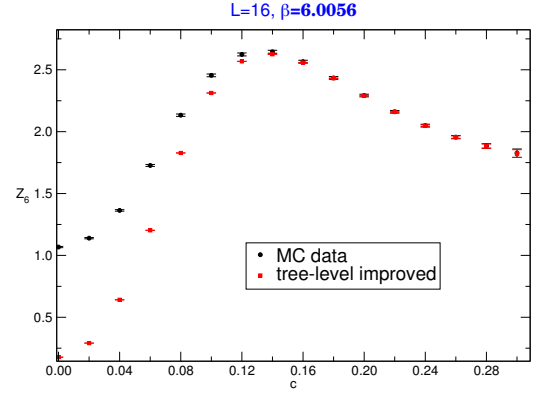
Figure 4.19: Tree-level improved Z_6 for $L = \{12, 16\}$

4.4.5 Comparisons

The quality, and the effectiveness, of the strategy adopted has to be tested. Usually, a comparison with other (possibly established) methods represents a good test. Meaningful comparisons can only be done taking the continuum limit of some reference observable. The latter could be any kind of dimensionless quantity that allows an analytic expansion in powers of the lattice spacing[15]. In this case, the continuum limit of the following ratio

$$R_{i,L} = \frac{Z_{i,FLOW,L}}{Z_{i,SHIFTED}}, \quad i = \{3, 6\} \tag{4.46}$$

has been studied.

---

[15] A simple example could be a dimensionless combination of physical quantities related to the renormalized EMT.

The numerator consists of the renormalization constants $Z_{3,6}$ measured through the gradient flow. The denominator describes the same quantities measured by L. Giusti and M.Pepe, using *shifted boundary conditions* (SBC). The description of this specific setup will not be discussed here[16]. The key point is that SBC allow to extract $Z_{3,6}$ in the infinite volume limit, while the Wilson Flow method (WF) is defined at finite volume. As a consequence, the ratio (4.46) can be expanded in the following way

$$R_{i,L} = \frac{Z_{i,FLOW,L}}{Z_{i,SHIFTED}} = 1 + \sum_{j=1}^{\infty} (c_i)_j \left(\frac{a}{L}\right)^{2j} \qquad i = \{3,6\}, \tag{4.47}$$

as continuum limit is approached. A consistent match between the two methods is achieved if their extrapolated ratios are compatible with

$$\lim_{a \to 0} R_{i,L} = 1, \quad i = \{3,6\}, \tag{4.48}$$

within statistical errors. The extrapolations have been carried out using values of $Z_{3,6}$ extracted from the region $0.2 \leq c \leq 0.3$. At fixed flow time, the ratios (4.46) have been fitted using the following expansion

$$R_{i,L} = \frac{Z_{i,FLOW,L}}{Z_{i,SHIFTED}} = A + B \left(\frac{a}{L}\right)^2, \tag{4.49}$$

using two different sets of lattices

$$L = \{12 \to 32\}, \quad L = \{16 \to 32\}, \tag{4.50}$$

to obtain insights of the systematic errors. Examples of the fit (4.49) can be found in figures (4.20)-(4.21)-(4.22) for $R_{3,L}$ and (4.24)-(4.25)-(4.26) for $R_{6,L}$. Each plot displays

- values of the ratios (4.46) along with their statistical errors;
- fitting curves for the lattice intervals (4.50) and related reduced χ^2 ;
- values of continuum limit extrapolations (zoomed area).

Possible $\mathcal{O}(a)$ effects coming from the $x_0 = \{0, L_0 - 1\}$ boundaries have been investigated. In this case, data have been fitted using the following expansion

$$R_{i,L} = \frac{Z_{i,FLOW,L}}{Z_{i,SHIFTED}} = A + B \left(\frac{a}{L}\right) + C \left(\frac{a}{L}\right)^2, \tag{4.51}$$

for the largest interval in (4.50). The values of the fitting parameters B and C proved to be zero within their statistical uncertainties. This result suffices to confirm that the smearing radius c is not large enough to make measurements sensitive to boundary effects.

The fit procedure of $R_{3,L}$ seems to be the most reliable one. The reduced χ^2 is always smaller than 1 and continuum extrapolations are compatible within error bars. The latter are precisely determined for $0.2 \leq c \leq 0.24$, then their precision worsen. This is caused by the increase of statistical noise on Z_3/Z_δ at large flow times ($c \geq 0.26$).
Continuum limit extrapolations are displayed in figure (4.23) as functions of the flow time. For $0.2 \leq c \leq 0.24$ they deviate from

$$\lim_{a \to 0} R_{3,L} = 1 \tag{4.52}$$

by several (> 3) standard deviations. At larger flow times results seem to be more compatible with their expected value, but this phenomenon is faked by the growth of statistical errors.

---

[16]The interested reader can find all the details in [37, 38].
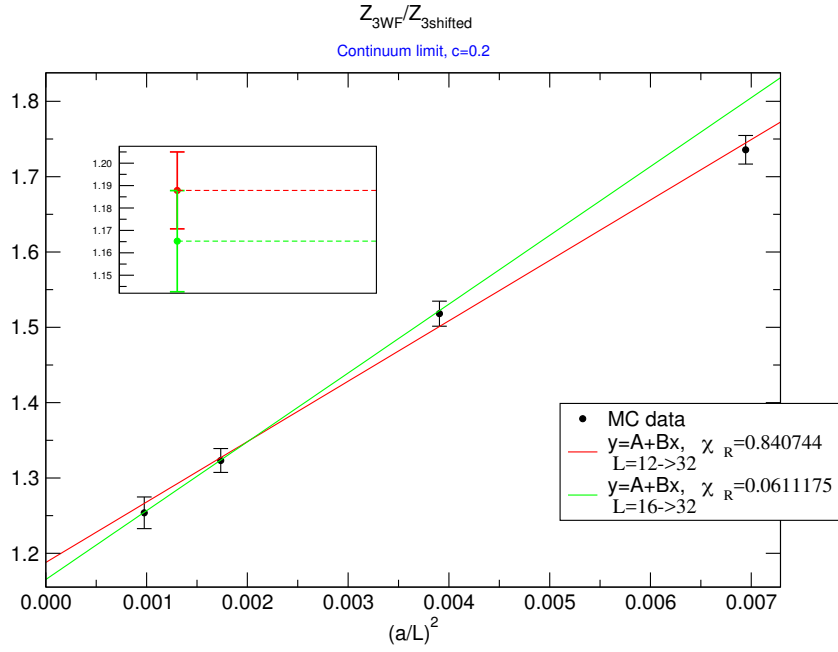
Figure 4.20: $Z_{3WF}/Z_{3shifted}$ ratio at fixed flow time. Data are displayed as functions of the number of lattice points. The zoomed area focuses on the $a = 0$ extrapolations.
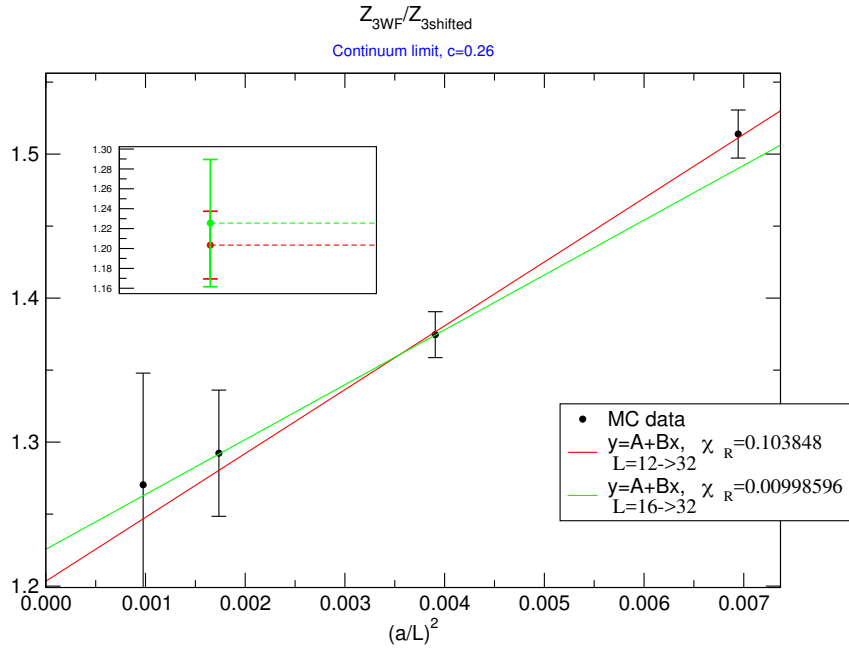
Figure 4.21: $Z_{3WF}/Z_{3shifted}$ ratio at fixed flow time. Data are displayed as functions of the number of lattice points. The zoomed area focuses on the $a = 0$ extrapolations.

Figure 4.22: $Z_{3WF}/Z_{3shifted}$ ratio at fixed flow time. Data are displayed as functions of the number of lattice points. The zoomed area focuses on the $a = 0$ extrapolations.
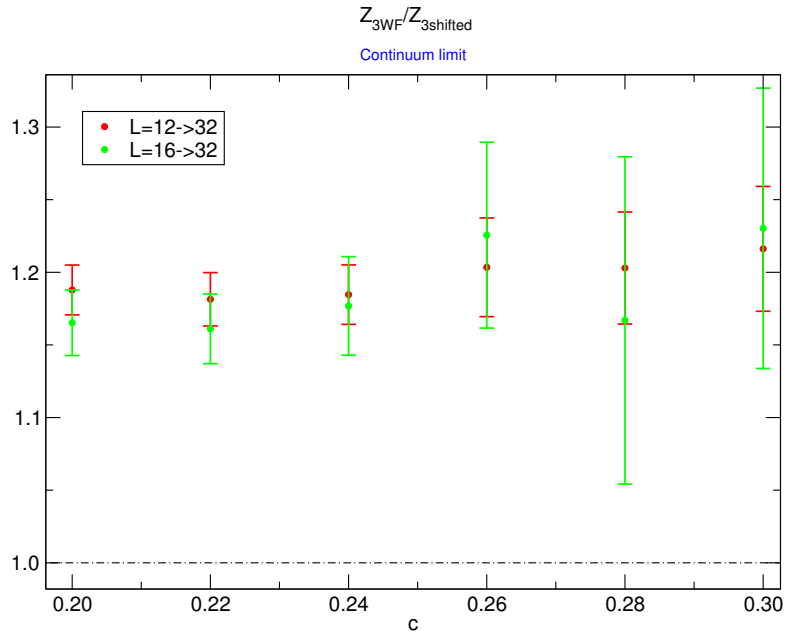
Figure 4.23: Continuum extrapolations of the ratio $Z_{3WF}/Z_{3shifted}$ as functions of the flow time.

$R_{6,L}$ does not yield enough reliable results as for the case of $R_{3,L}$. It has been shown in section

(4.4.1) how measurements of Z_6/Z_δ were plagued by large lattice artefacts and significant noise. This behaviour is reflected in the fitting procedure of $R_{6,L}$, the latter being less reliable and stable. The reduced χ^2 is always greater than 1 and grows as the flow time increases. Continuum limit extrapolations are always compatible within few standard deviations (figure (4.27)).

Both $R_{3,L}$ and $R_{6,L}$ show a consistent mismatch between the values of $Z_{3,6}$ measured through the gradient flow and those measured using SBC. Quantitatively, the deviations of $R_{3,6,L}$ from the expected continuum value can be read off from table (4.8).

$L = \{12 \rightarrow 32\}$				
c	$1 - R_{3,L}$	$\chi^2_{R,3}$	$1 - R_{6,L}$	$\chi^2_{R,6}$
0.2	0.188(17)	0.84	0.188(12)	6.86
0.22	0.181(18)	0.39	0.180(16)	1.50
0.24	0.185(20)	0.10	0.184(19)	2.58
0.26	0.203(34)	0.10	0.169(24)	5.85
0.28	0.2023(39)	0.51	0.153(33)	5.49
0.3	0.216(43)	0.52	0.153(48)	2.78
$L = \{16 \rightarrow 32\}$				
0.2	0.165(23)	0.06	0.151(17)	2.85
0.22	0.161(24)	0.01	0.175(24)	2.94
0.24	0.177(34)	0.06	0.232(32)	1.56
0.26	0.226(64)	0.01	0.319(53)	2.86
0.28	0.167(11)	0.95	0.389(100)	4.11
0.3	0.230(97)	1.04	0.219(106)	5.38

Table 4.8: Deviation of the ratios $R_{3,6,L}$ from their expected, continuum value. The third and fifth columns display the values of the reduced χ^2.

It is important to understand what could be the cause of these deviations. Actually, two distinct sources of errors can be singled out.

The first one could be attributed to lattice artefacts. The latter could be still quite large and substantially affect the outcome of the fit procedure. Should it be the case, then it could still be possible to improve the numerical strategy using two, different (also combinable) methods.

1. Finer lattices could be added to the set (4.3), and make continuum extrapolations more precise. This is the simplest type of improvement, however it comes at the price of longer simulation times. Indeed, fine lattices contain lots of lattice points, and this has the effect to slow down both the update procedure as well as the flow time evolution. In section (4.4.1) it has been shown how precision on fine lattices drops down as the flow time becomes large. On these lattices, reliable estimates could be provided only with a large amount of computation time. A priori, nothing forbids to follow this path. However, a numerically effective strategy should provide enough precise results in a *reasonable* amount of time. If this is not the case, then the strategy is not effective and should be abandoned.

2. A global tree-level improvement can be applied. This would mean removing (lattice) tree-level contributions from boundary and bulk action, renormalized EMT and translation WI. This strategy seems more feasible in terms of computation times. However, it does not always guarantee the reduction of lattice artefacts[17].

---

[17]Tree-level improvements are not effective if lattice artefacts are sourced by one-(or higher)-loop contributions.
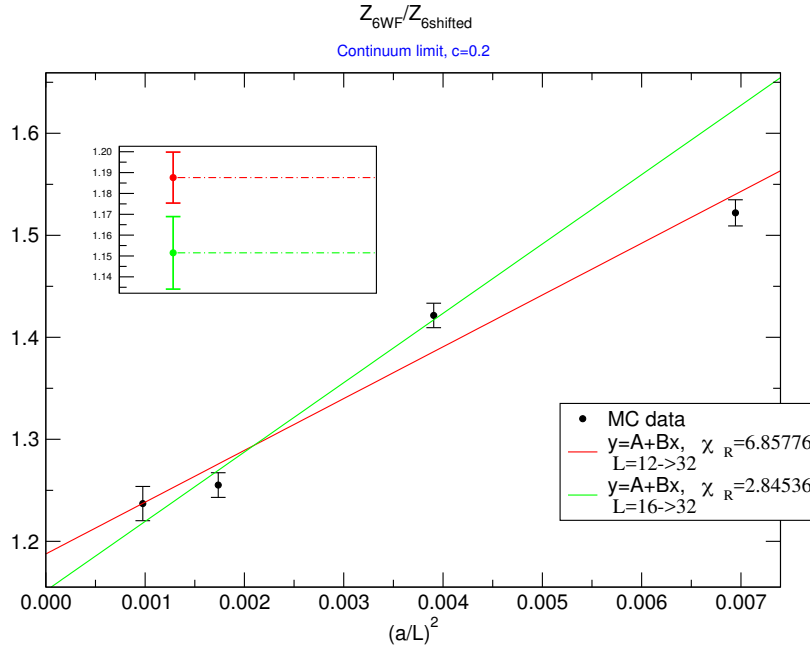
Figure 4.24: $Z_{6WF}/Z_{6shifted}$ ratio at fixed flow time. Data are displayed as functions of the number of lattice points. The zoomed area focuses on the $a = 0$ extrapolations.
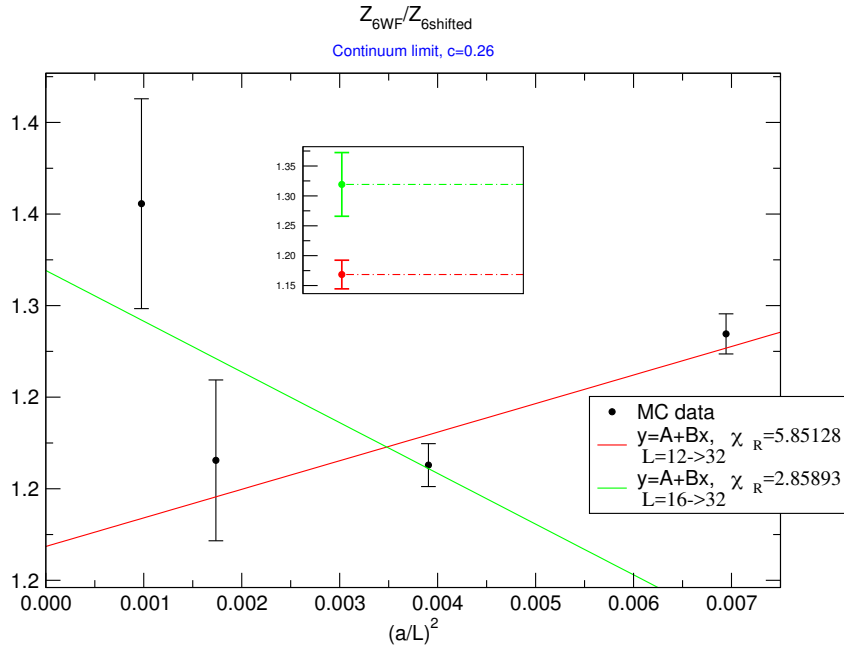
Figure 4.25: $Z_{6WF}/Z_{6shifted}$ ratio at fixed flow time. Data are displayed as functions of the number of lattice points. The zoomed area focuses on the $a = 0$ extrapolations.
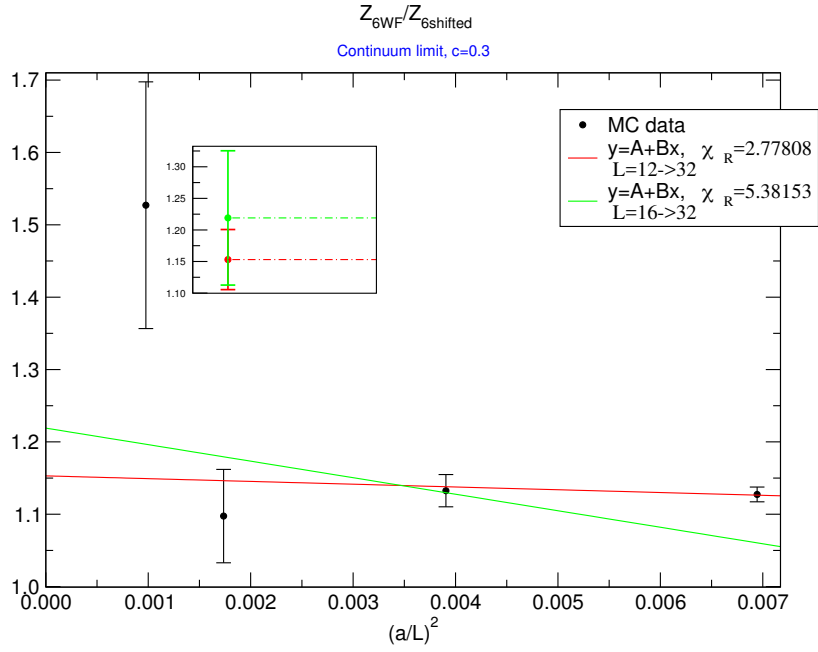
Figure 4.26: $Z_{6WF}/Z_{6shifted}$ ratio at fixed flow time. Data are displayed as functions of the number of lattice points. The zoomed area focuses on the $a = 0$ extrapolations.
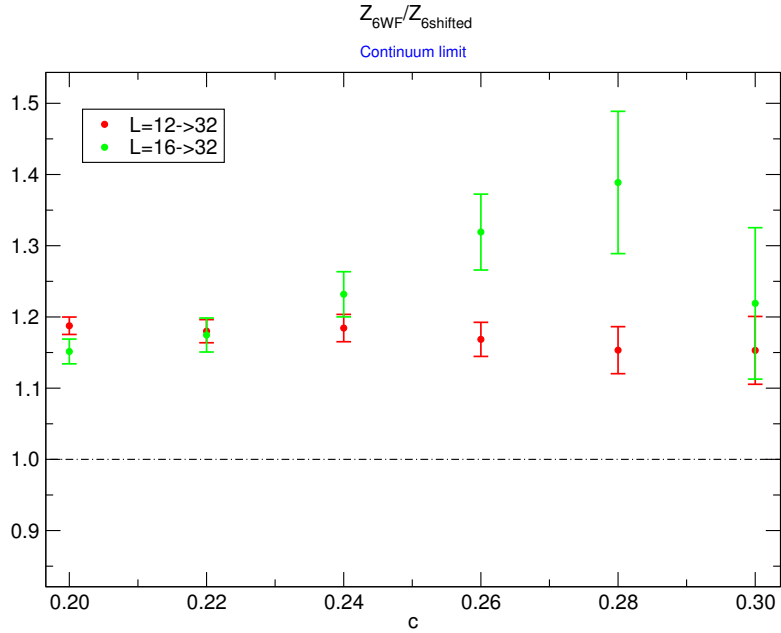
Figure 4.27: Continuum extrapolations of the ratio $Z_{6WF}/Z_{6shifted}$ as functions of the flow time.

The other[18], possible source of problems could be related to the determination of Z_δ. From figures (4.23) and (4.27), it could be argued that the sets of constants $Z_{3,6,WF}$ and $Z_{3,6,shifted}$ differ just for an overall constant factor

$$R_{3,L} = 1.196(30), \quad L = \{12 \to 32\}, \tag{4.53}$$
$$= 1.188(69), \quad L = \{16 \to 32\}, \tag{4.54}$$
$$R_{6,L} = 1.171(28), \quad L = \{12 \to 32\}, \tag{4.55}$$
$$= 1.246(66), \quad L = \{16 \to 32\}, \tag{4.56}$$

within statistical errors. To support this statement, the following ratio

$$r_{3,L} = \frac{r_{3,WF,L}}{r_{3,shifted}}, \tag{4.57}$$

has been studied using the same expansion as in equation (4.49). Fits for the ratio (4.57) are displayed in figures (4.28)-(4.29)-(4.30). The reduced χ^2 is always greater than 1 and grows with the flow times due to loss of numerical precision. It is interesting to study the continuum extrapolations (figure (4.31)) for each flow time. For the largest interval in (4.50), their values are quite precisely determined and seem to be compatible with $r_{3,L} = 1$. In the worst case, they differ from the expected value of just two standard deviations. The situation becomes worse when the study is restricted to the interval ($L = \{16 \to 32\}$). At large flow times deviations are consistent as well as the statistical error. This is clearly sourced by the loss of precision on Z_6/Z_δ. Nonetheless, the extrapolations are all compatible with one.

$L = \{12 \to 32\}$			$L = \{16 \to 32\}$		
c	$1 - r_{3,L}$	χ^2_{R,r_3}	c	$1 - r_{3,L}$	χ^2_{R,r_3}
0.20	0.007(11)	2.70	0.20	0.019(14)	3.03
0.22	0.016(14)	1.92	0.22	0.003(22)	2.52
0.24	0.025(17)	3.34	0.24	0.033(27)	0.79
0.26	0.039(17)	4.03	0.26	0.048(40)	2.55
0.28	0.028(28)	6.87	0.28	0.239(78)	1.45
0.30	0.006(43)	6.49	0.30	0.154(101)	8.73

Table 4.9: Deviation of the ratio $r_{3,L}$ from the expected, continuum value. The third column displays the values of the reduced χ^2.

Data in tables (4.9) show that more precise estimates are necessary, especially for $c \geq 0.26$. However, these results clearly signal that the difference between $Z_{3,6,WF}$ and $Z_{3,6,shifted}$ could be just an overall normalization. It has to be understood how such normalization is generated. Clearly it can only be related to the determination of Z_δ. This does not necessary imply that the method adopted in this work is wrong[19]. However, further theoretical, and numerical, studies will be necessary to understand the validity and applicability of equation (4.32) to measure Z_δ[20].

---

[18]Actually, a third source of problems could simply be the lack of a reasonably large statistics, especially on finer lattices. The statement is surely true for both ratios at large flow times. However, results for $R_{3,L}$ are quite precise for $c = 0.2, ...0.24$ and show clear deviations from their expected continuum value.

[19]*Possible* issues *could* be hidden in the way SBC are employed to measure the renormalized EMT.

[20]The problem seems to affect only Yang-Mills theory. When the scalar case is considered (5), this issue disappears, since $Z_\delta = 1$ at finite lattice spacing.
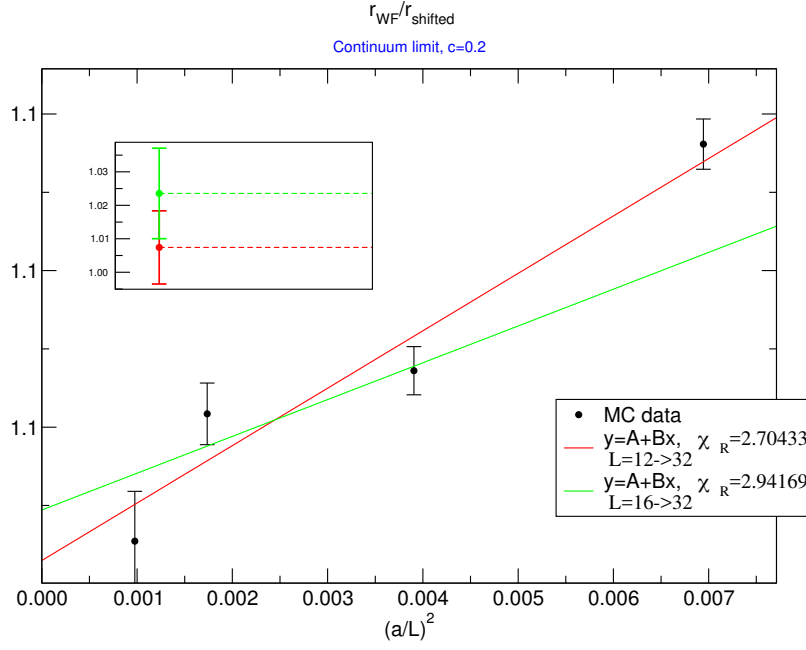
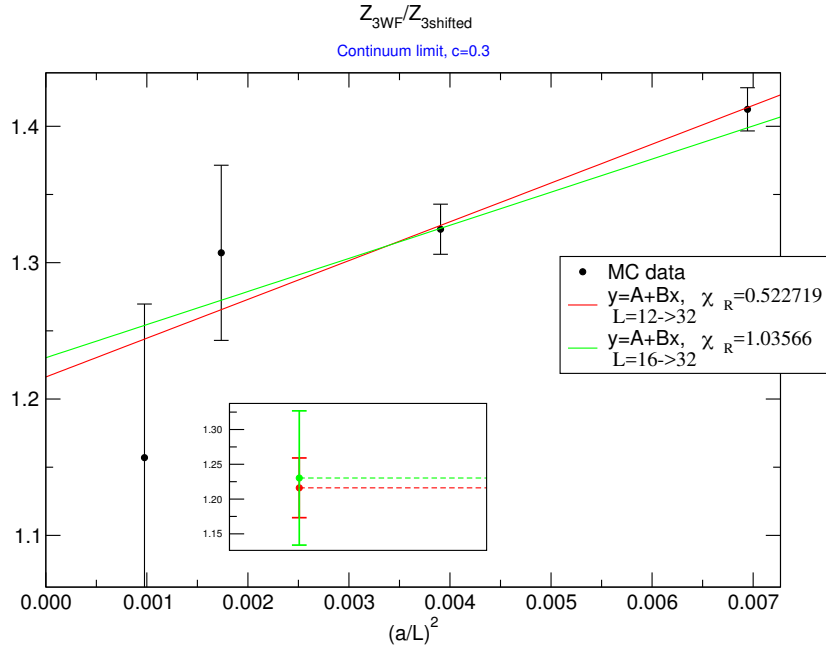**Figure 4.28:** $r_{3WF}/r_{3shifted}$ ratio at fixed flow time. Data are displayed as functions of the number of lattice points. The zoomed area focuses on the $a = 0$ extrapolations.
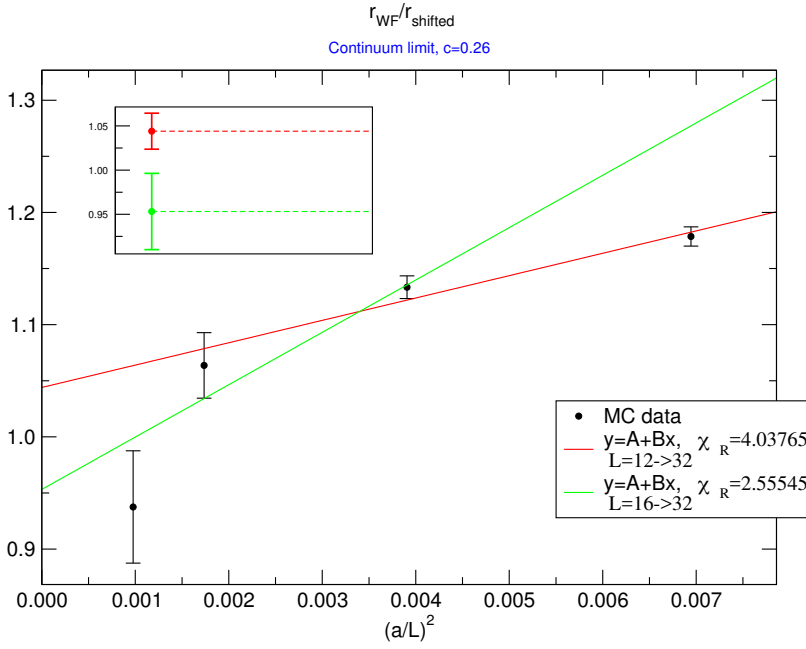
Figure 4.29: $r_{3WF}/r_{3shifted}$ ratio at fixed flow time. Data are displayed as functions of the number of lattice points. The zoomed area focuses on the $a = 0$ extrapolations.
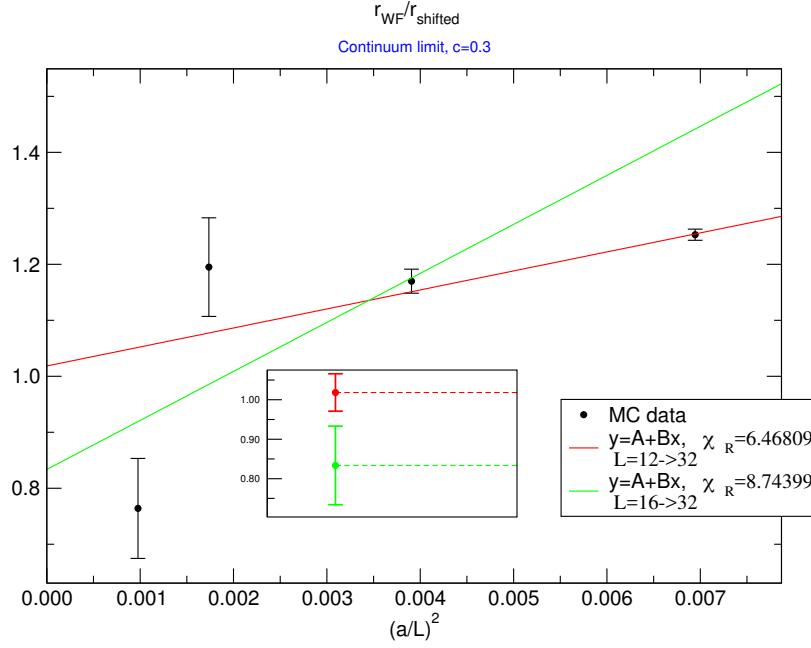
Figure 4.30: $r_{3WF}/r_{3shifted}$ ratio at fixed flow time. Data are displayed as functions of the number of lattice points. The zoomed area focuses on the $a = 0$ extrapolations.
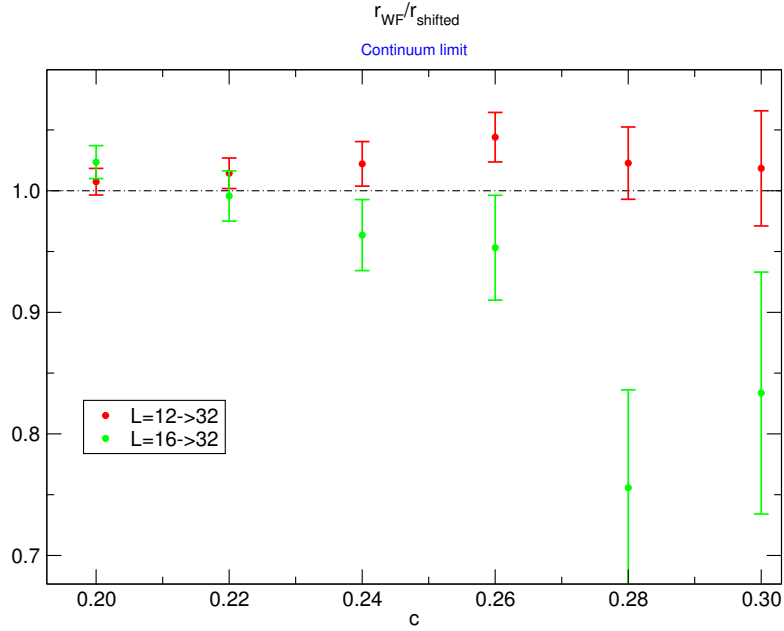
Figure 4.31: Continuum extrapolations of the ratio $r_{3WF}/r_{3shifted}$ as functions of the flow time.

Chapter 5

Scalar field theory in 3 dimensions

5.1 Introduction

In this chapter, the renormalization of the lattice EMT in scalar theory is discussed in detail. In 3 space-time dimensions, the theory exhibits two distinct RG fixed points, as it will be shown in subsections (5.2.1)-(5.2.2). These two points lie on a critical surface, whose projection onto the subspace of the relevant couplings is defined as the critical line (cfr. subsection (1.3.1)). In subsection (5.2.3), the latter is precisely located through a numerical study of the phase diagram of the theory. Then, a brief description of the renormalized EMT using continuum and lattice regularization follows (section (5.3)). In section (5.4), a method to renormalize the scalar EMT using probes at positive flow times is presented. The strategy follows the guide lines of chapter (3), with some modification for what concerns the gradient flow formulation. Finally, the numerical setup for measuring the renormalized EMT is described (5.5). The outcome of numerical simulations is presented and discussed, along with some fundamental checks that probe the goodness of the strategy adopted.

5.2 Scalar field theory

Scalar field theory has been already presented in chapter (1.2), for $D = 4$ space-time dimensions

$$ S = \int d^4x \left(\frac{1}{2} \partial_\rho \phi \partial_\rho \phi + \frac{m_0^2}{2} \phi^2 + \frac{\lambda_0}{4!} \phi^4 \right). \tag{5.1} $$

In four dimensions, the only available fixed point is the Gaussian one, which is UV *repulsive*. As a consequence, the theory does not have a continuum limit. A different scenario appears when the number of dimensions is lowered from 4 to 3. In this case, two different RG fixed points appear. The first is a UV fixed point (Gaussian) and define a proper continuum limit for the theory. The second one is an IR fixed point (Wilson-Fisher) and determines the behaviour of the theory at large distances. In the following sections, a brief description of these two points is presented, along with the set of relevant couplings that characterize them.

5.2.1 Gaussian fixed point

The RG group flows for a Z_2 invariant scalar theory have been determined in chapter (1.2). Using the effective potential approximation, the flows are described by the following differential equation

(crf. equation (1.55))

$$\Lambda \frac{dg_{2n}}{d\Lambda} = (n(d-2) - d)g_{2n} - a\Lambda^{n(d-2)} \frac{d^{2n}}{d\phi^{2n}} \log[\Lambda^2 + V''(\phi)]\bigg|_{\phi=0}. \tag{5.2}$$

For $d = 3$, the evolution of relevant and marginal couplings can be determined by the set of equations

$$\Lambda \frac{dg_2}{d\Lambda} = -2g_2 - \frac{ag_4}{1 + g_2}, \tag{5.3}$$

$$\Lambda \frac{dg_4}{d\Lambda} = -g_4 + \frac{3ag_4^2}{(1 + g_2)^2} - \frac{ag_6}{1 + g_2}, \tag{5.4}$$

$$\Lambda \frac{dg_6}{d\Lambda} = -\frac{30ag_4^3}{(1 + g_2)^3} + \frac{15ag_4g_6}{(1 + g_2)^2}, \tag{5.5}$$

where $a = (2\pi)^{-2}$. Around the Gaussian point, the linearized RG flows take the following form

$$\Lambda \frac{d\delta g_2}{d\Lambda} = -2\delta g_2 - a\delta g_4, \tag{5.6}$$

$$\Lambda \frac{d\delta g_4}{d\Lambda} = -\delta g_4 - a\delta g_6, \tag{5.7}$$

$$\Lambda \frac{d\delta g_6}{d\Lambda} = 0. \tag{5.8}$$

where $\delta g_{2n} = (g_{2n} - g_{2n}^*)$, $g_{2n}^* = 0$. The critical exponents at the Gaussian fixed point are determined by the eigenvalues of the linearized evolution matrix

$$L = - \begin{pmatrix} 2 & a & 0 \\ 0 & 1 & a \\ 0 & 0 & 0 \end{pmatrix}. \tag{5.9}$$

The set of eigenvectors

$$c_1 = \delta g_2 + a\delta g_4 + \frac{a^2}{2}\delta g_6, \tag{5.10}$$

$$c_2 = \delta g_4 + a\delta g_6, \tag{5.11}$$

$$c_3 = \delta g_6, \tag{5.12}$$

satisfy the decoupled equations

$$\Lambda \frac{dc_1}{d\Lambda} = -2, \tag{5.13}$$

$$\Lambda \frac{dc_2}{d\Lambda} = -1, \tag{5.14}$$

$$\Lambda \frac{dc_3}{d\Lambda} = 0. \tag{5.15}$$

As expected from naïve dimensional analysis, g_6 is a marginal direction when RG flows are linearized around the Gaussian point. Hence, the behaviour of the sextic coupling is determined by higher order terms in the Taylor expansion. Keeping the next-to-leading order contribution, the RG flow of g_6 becomes

$$\Lambda \frac{dg_6}{d\Lambda} = +15a\delta g_4 \delta g_6. \tag{5.16}$$

If only theories with positive quartic coupling are considered, then the sextic coupling decreases when the cut-off a^{-1} is lowered; hence g_6 is marginally irrelevant and will not be included in the

Lagrangian. For what concerns the continuum limit of the theory, only the couplings g_2 and g_4 need to be tuned. Around the Gaussian fixed point, the scalar theory can be described by the following minimal action

$$S = \int d^3x \left(\frac{1}{2} \partial_\rho \phi \partial_\rho \phi + \frac{m_0^2}{2} \phi^2 + \frac{\lambda_0}{4!} \phi^4 \right). \tag{5.17}$$

This information is crucial since it provides the minimal set of parameters that are necessary to run lattice simulations.

5.2.2 Wilson-Fisher fixed point

To determine other, non-trivial fixed points is usually a difficult task. However, some insights can be obtained if the RG flows are studied using the ϵ *expansion* method [9]. In this case, the number of dimensions takes non-integer values, and is controlled by a small parameter $\epsilon = 4 - d$. Flows are determined through a perturbative expansion in ϵ, and the existence of, possibly new, fixed points is investigated. Hopefully, what is established for small ϵ will be qualitatively true for physically interesting cases ($\epsilon = 1, 2...$). Expanding the RG flows (1.55) in powers of the couplings and ϵ allows to determine a new fixed point in the space of theories

$$g_2^* = -\frac{\epsilon}{6} + ..., \quad g_4^* = \frac{\epsilon}{3a} + ..., \quad g_{2n>4}^* = \epsilon^n + ... \quad . \tag{5.18}$$

which is called the Wilson-Fisher fixed point. The latter is physically acceptable only if $\epsilon > 0$, otherwise the couplings g_{2n}^* are all negative and the potential of the theory would not be bounded from below, leading to instability. In the neighbourhood of the fixed point, the linearized RG flows become

$$\Lambda \frac{d\delta g_2}{d\Lambda} = \left(\frac{\epsilon}{3} - 2 \right) \delta g_2 - b \left(1 + \frac{\epsilon}{6} \right) \delta g_4, \tag{5.19}$$

$$\Lambda \frac{d\delta g_4}{d\Lambda} = \epsilon \delta g_4, \tag{5.20}$$

$$\tag{5.21}$$

with

$$b = \frac{1}{(4\pi)^2} \left[1 + \frac{\epsilon}{2} \log(4\pi e^{-\gamma_E}) \right] + \mathcal{O}(\epsilon^2). \tag{5.22}$$

Here, only the (g_2, g_4) subspace has been considered. In this case, the set of eigenvectors

$$c_1 = \delta g_2, \tag{5.23}$$

$$c_2 = -b(3 + \frac{\epsilon}{2})\delta g_2 + 2(3 + \epsilon)\delta g_4, \tag{5.24}$$

$$\tag{5.25}$$

satisfies the decoupled system of equations

$$\Lambda \frac{dc_1}{d\Lambda} = \left(-2 + \frac{\epsilon}{3} \right) c_1, \tag{5.26}$$

$$\Lambda \frac{dc_2}{d\Lambda} = \epsilon c_2, \tag{5.27}$$

$$\tag{5.28}$$

Therefore, at this fixed point, only the mass coupling c_1 is relevant. The RG flows in the (g_2, g_4) subspace for small $\epsilon > 0$ are sketched below:
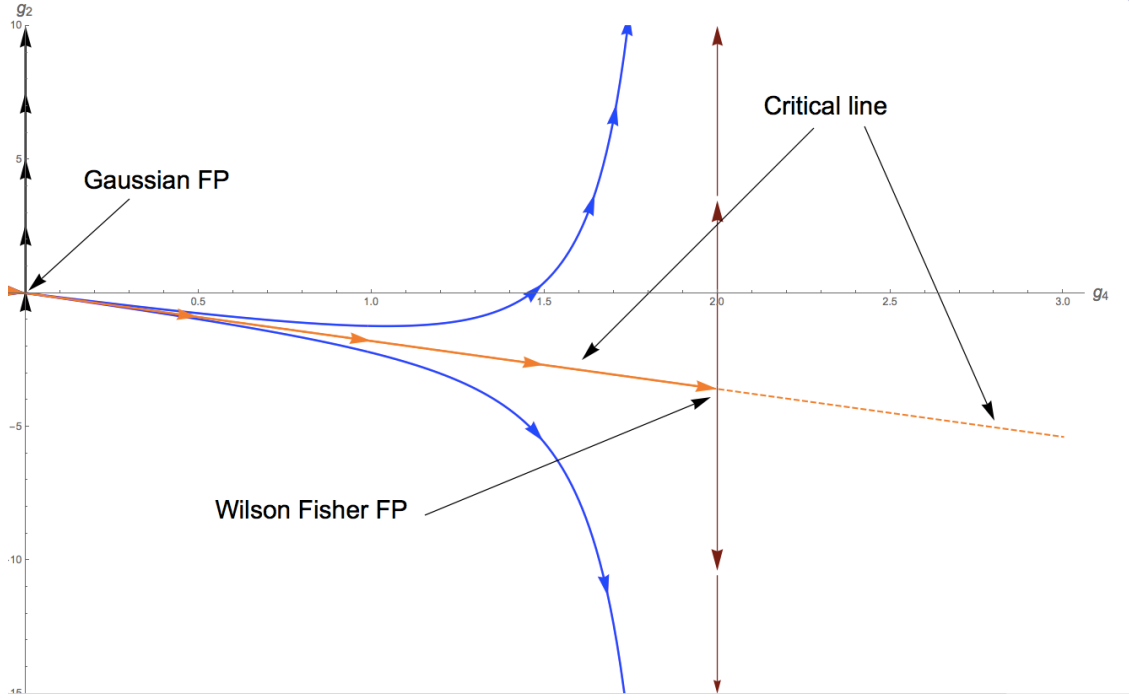
Figure 5.1: RG flows of the scalar field theory in $d = 3$ space-time dimensions.

Here, the Gaussian and Wilson-Fisher fixed points are shown. Since all the other couplings are irrelevant for $d = 3$, only the flows in the (g_2, g_4) subspace are shown. As already mentioned before, the critical surface intersects this subspace in the line that joins the two fixed points. Only RG flows with a UV continuum limit have been displayed. It has to be stressed that the results above hold in the regime of small ϵ. However, the Wilson-Fisher point has been shown to exist also for $\epsilon = 1$. In the language of statistical physics, it is said to lie in the universality class of the Ising Model. Having a good qualitative picture of the RG flows, it is possible to describe the different continuum limits of the scalar field theory in 3 space-time dimensions. Continuum theories are just parametrized by the mass and quartic couplings g_2 and g_4, while the irrelevant couplings g_{2n} have some specific value fixed by g_2 and g_4. Different continuum scenarios are available in figure (5.1):

- The $g_4 = 0$ line is a free, massive theory;

- The red lines starting from the Wilson-Fisher fixed point are massive interacting theories that become the Ising model conformal field theory in the UV;

- The subspace of the critical line emanating from the Gaussian point is a massless interacting theory that interpolates between a free theory in the UV and the Ising model CFT in the IR;

- The two blue lines represent massive interacting field theories, which become asymptotically free in the UV. Theories below the critical line develop a non vanishing VEV, causing the Z_2 symmetry to be spontaneously broken (cfr. section (1.3.1)).

This work focused on the renormalization of the lattice EMT in the unbroken phase of the theory, where no VEV is developed (RG flows above the critical line). To simulate the theory in

the right thermodynamic phase, it has been necessary to first locate the position of the critical line. The latter has been located with the help of numerical investigations to characterize the phase diagram of the theory. In the following session, all the details regarding the numerical study and the related outcomes will be explained.

5.2.3 Phase diagram

A non perturbative study of the phase diagram has been carried out performing Monte Carlo simulations. The discretization of the theory has been already described in section (1.3) for 4 space-time dimensions and will not be repeated here for the $d = 3$ case. The scalar model has been simulated using the algorithm described in [63], alternating local Metropolis updates and Swendsen Wang cluster updates of the embedded Ising Model. The details of the implementation will be presented in section (5.5). Here, all the attention is focused on the determination of the phase diagram of the theory. The critical line has been localized studying the peaks of the following susceptibility

$$\chi = \left\langle \left(\sum_x \phi(x) \right)^2 \right\rangle - \left\langle \left| \sum_x \phi(x) \right| \right\rangle^2 , \tag{5.29}$$

as functions of the parameters of the theory. Having fixed the quartic coupling $\hat{\lambda}_0$[1], the position of the peaks has been determined performing several simulations at different values of the bare mass $\hat{m}_0$. Then, the data have been reweighted to further values of $\hat{m}_0$ using multi-histogram technique. The reweighting procedure helped to improve the localization of the peaks.
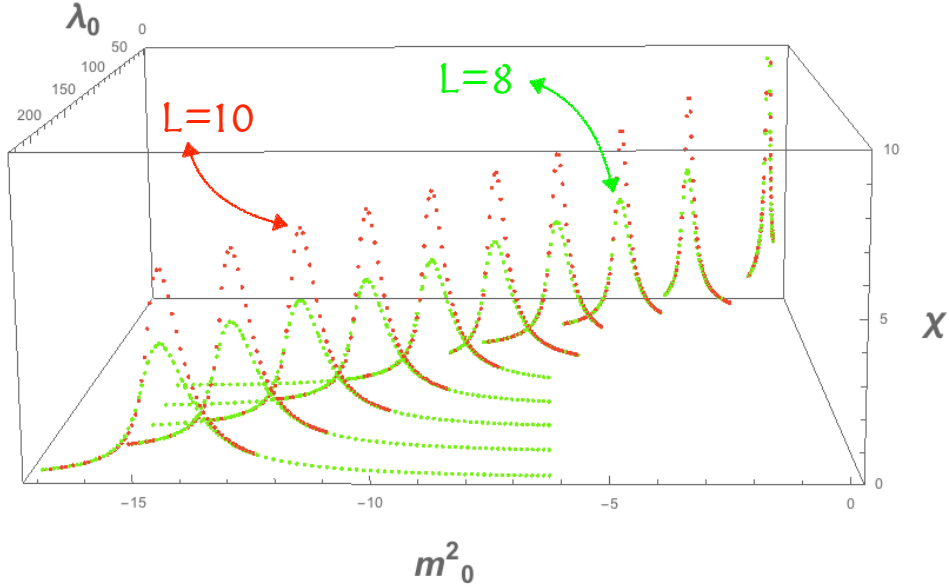
Figure 5.2: Peaks of the susceptibility as functions of $\hat{\lambda}_0$ and (negative) $\hat{m}_0^2$. Here, two different physical volumes have been shown. Errors have not been displayed in order to make the picture clearer.

---

[1]Hatted parameters are properly rescaled with the cut-off a^{-1} in order to be kept dimensionless.

Simulations have been carried out on different physical volumes. For each $\hat{\lambda}_0$, a pseudo-critical mass $\hat{m}_c(L)$ has been defined as the coupling where the peak of the specific heat (5.29) is located at fixed volume. The behaviour of $\hat{m}_c(L)$ has been subjected to a finite size scaling analysis

$$\hat{m}_c(L) = \hat{m}_c(\infty) + m_1 L^{-\frac{1}{\nu}} + ..., \tag{5.30}$$

where the dots denote sub-leading corrections to the scaling of $\hat{m}_c(L)$. Here, the critical exponent ν has been set to the following value

$$\nu = 0.62893(39), \tag{5.31}$$

found in [64]. Equation (5.30) has been adopted to estimate the value of $\hat{m}_c(\infty)$. As an illustration of the adopted method, a specific case ($\hat{\lambda}_0 = 150$) will be discussed in detail. At fixed quartic coupling, the specific heat (5.29) has been measured spanning large intervals of the bare mass parameter $\hat{m}_0$ (figure (5.2)). Estimates of this quantity are displayed in picture (5.3)

(a)

(b)
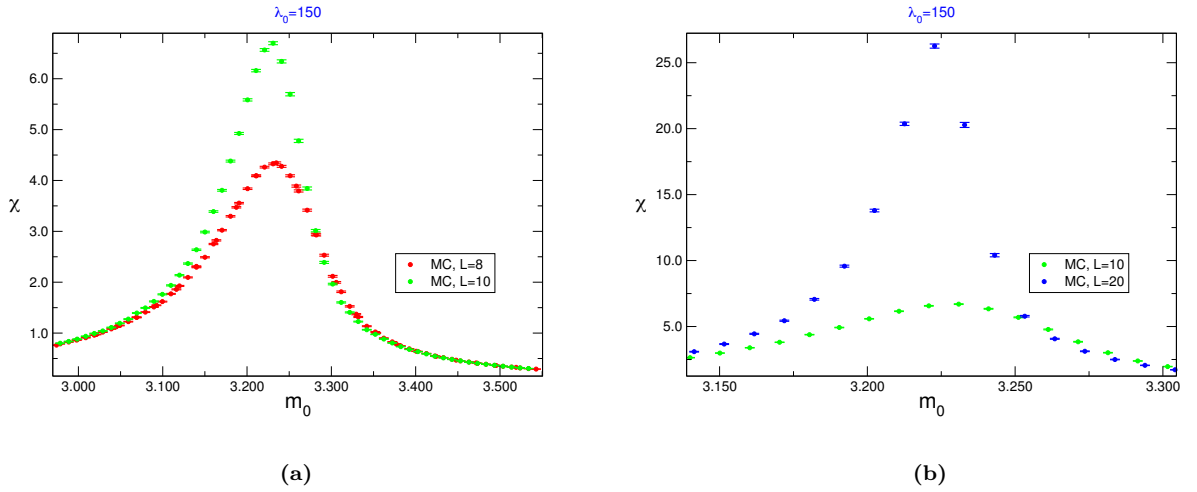
Figure 5.3: Susceptibility at $\hat{\lambda}_0 = 150$. Here, two different volume sets ($L = \{8, 10\}$, $L = \{10, 20\}$) have been considered.

To precisely determine the value of $\hat{m}_0$ that maximizes χ, a multihistogram reweighting procedure [65] has been applied. The latter has been implemented inside a narrow region around the peaks of the specific heat (figure (5.4)). The maximum χ_{max} and its precise position have been determined through a numerical maximization procedure. Their values are displayed in tables (5.2-5.1). The quality of the results has been checked studying the scaling behaviour of $\chi(L)_{max}$. At criticality, the specific heat diverges with the physical volume according to the following scaling law

$$\chi_{max}(L) = \chi_1 L^{(2-\eta)}(1 + \chi_2 L^{-\omega}), \tag{5.32}$$

where the exponents

$$\eta = 0.03627(10), \quad \omega = 0.832(6) \tag{5.33}$$

have been taken from [66]. It should be noticed that also a sub-leading term has been included in (5.32). To check the correct scaling of $\chi_{max(L)}$, the coefficients $\chi_{1,2}$ have been fitted keeping η and ω fixed, for all the values of $\hat{\lambda}_0$. Example of such fit can be found in figure (5.5).
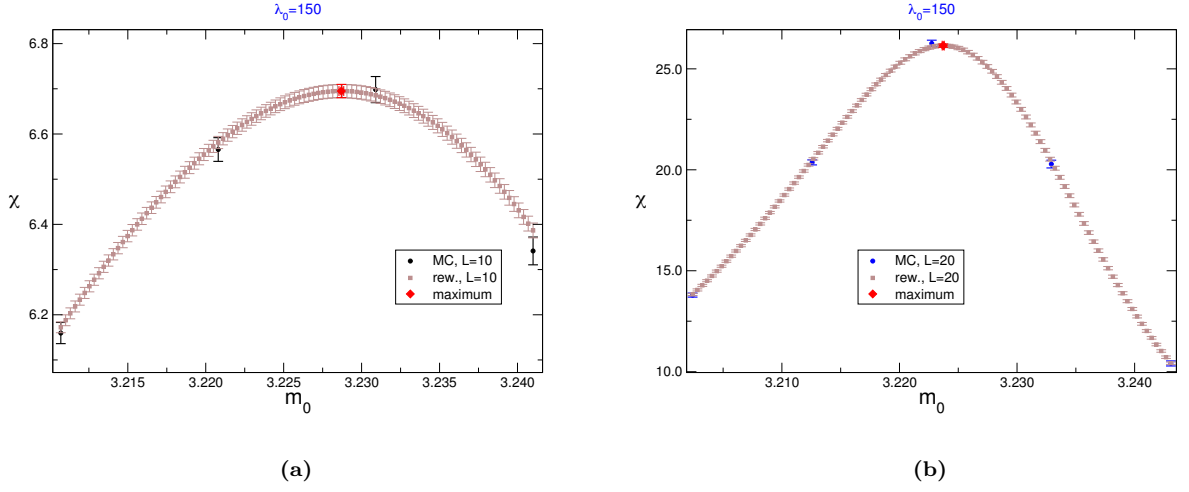
Figure 5.4: Estimates of the specific heat coming from Monte Carlo simulations and reweighting procedure at fixed volume. The reweighting has been applied considering a small interval of bare masses centred around the hypothetical peaks.

$\hat{\lambda}_0 = 26.5$			$\hat{\lambda}_0 = 51$		
L	$\hat{m}_c(L)$	$\chi_{max}(L)$	L	$\hat{m}_c(L)$	$\chi_{max}(L)$
8	1.5944(1)	5.678(8)	8	2.0926(2)	5.012(9)
10	1.5888(1)	8.501(10)	10	2.0883(1)	7.629(13)
20	1.5812(1)	30.902(91)	20	2.0819(1)	28.496(117)
28	1.5798(1)	58.612(252)	28	2.0806(1)	54.351(263)
$\hat{\lambda}_0 = 75.5$			$\hat{\lambda}_0 = 100$		
L	$\hat{m}_c(L)$	$\chi_{max}(L)$	L	$\hat{m}_c(L)$	$\chi_{max}(L)$
8	2.4553(1)	4.715(9)	8	2.7493(2)	4.524(9)
10	2.4510(1)	7.203(12)	10	2.7460(1)	7.004(15)
20	2.4456(1)	27.502(123)	20	2.7405(1)	26.787(107)
28	2.4444(1)	52.688(256)	28	2.7394(1)	51.965(252)
$\hat{\lambda}_0 = 125$			$\hat{\lambda}_0 = 175$		
L	$\hat{m}_c(L)$	$\chi_{max}(L)$	L	$\hat{m}_c(L)$	$\chi_{max}(L)$
8	3.0060(2)	4.425(6)	8	3.4358(2)	4.268(8)
10	3.0027(1)	6.805(13)	10	3.4324(2)	6.602(13)
20	2.9975(1)	26.388(85)	20	3.4274(1)	25.840(80)
28	2.9965(1)	50.845(231)	28	3.4264(1)	49.753(213)
$\hat{\lambda}_0 = 200$			$\hat{\lambda}_0 = 225$		
L	$\hat{m}_c(L)$	$\chi_{max}(L)$	L	$\hat{m}_c(L)$	$\chi_{max}(L)$
8	3.6220(2)	4.201(8)	8	3.7940(2)	4.155(7)
10	3.6189(2)	6.507(16)	10	3.7912(1)	6.468(14)
20	3.6136(1)	25.517(84)	20	3.7862(1)	25.507(74)
28	3.6126(1)	49.546(221)	28	3.7849(1)	48.976(198)

Table 5.1: Estimates of $\chi_{max}(L)$ and $\hat{m}_c(L)$ at fixed lambda.

$\hat{\lambda}_0 = 0.5$			$\hat{\lambda}_0 = 1$		
L	$\hat{m}_c(L)$	$\chi_{max}(L)$	L	$\hat{m}_c(L)$	$\chi_{max}(L)$
10	0.2740(13)	32.760(661)	10	0.3736(5)	24.557(193)
20	0.2578(4)	99.715(2054)	20	0.3562(3)	71.763(937)
25	0.2551(2)	142.139(2460)	25	0.3542(2)	104.377(1012)
30	0.2533(2)	185.638(2241)	30	0.3529(1)	142.647(1796)
$\hat{\lambda}_0 = 2$			$\hat{\lambda}_0 = 3$		
L	$\hat{m}_c(L)$	$\chi_{max}(L)$	L	$\hat{m}_c(L)$	$\chi_{max}(L)$
10	0.5097(2)	18.414(57)	10	0.6108(6)	15.535(160)
20	0.4941(1)	56.682(293)	20	0.5969(1)	49.647(302)
25	0.4917(1)	81.291(500)	25	0.5948(1)	72.965(381)
30	0.4908(1)	112.686(1132)	30	0.5938(1)	97.859(741)
$\hat{\lambda}_0 = 4$			$\hat{\lambda}_0 = 5$		
L	$\hat{m}_c(L)$	$\chi_{max}(L)$	L	$\hat{m}_c(L)$	$\chi_{max}(L)$
10	0.6935(5)	14.085(134)	10	0.7672(4)	13.062(93)
20	0.6818(1)	45.428(264)	20	0.7552(1)	42.698(220)
25	0.6801(1)	66.505(279)	25	0.7537(1)	62.776(225)
30	0.6793(1)	94.074(938)	30	0.7530(1)	88.048(609)

Table 5.2: Estimates of $\chi_{max}(L)$ and $\hat{m}_c(L)$ at fixed lambda.
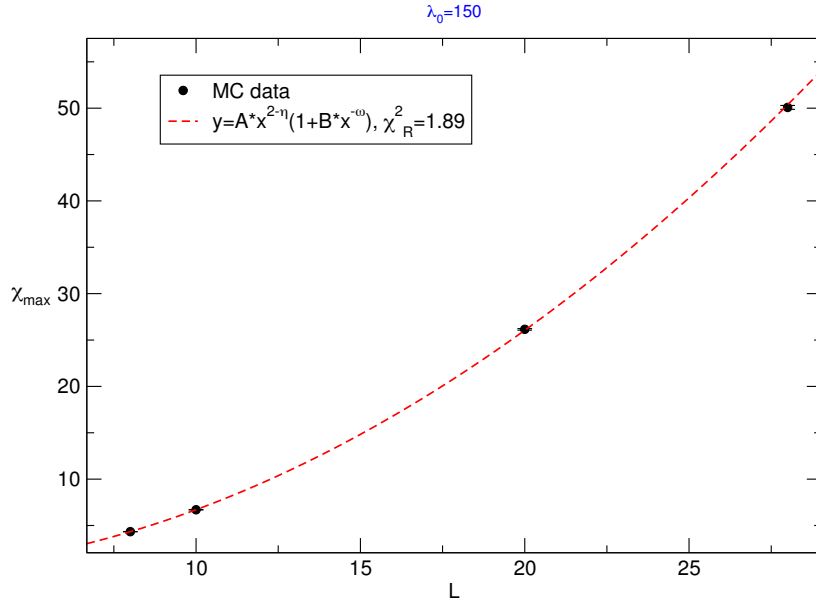
Figure 5.5: Fit of $\chi_{max}(L)$ for $\hat{\lambda}_0 = 150$. Monte Carlo data are displayed in black color.

For almost each $\hat{\lambda}_0$, the fitting procedure proved to be of good quality (5.3), supporting the idea that the values of $\chi_{max}(L)$ and $\hat{m}_c(L)$ are well-measured quantity.

$\hat{\lambda}_0$	0.5	1.0	2.0	3.0	4.0	5.0	26.5	51.0
χ^2_R	2.523	0.456	1.757	4.890	2.631	1.680	1.491	0.140

$\hat{\lambda}_0$	75.5	100.0	125.0	150.0	175.0	200.0	225.0
χ^2_R	0.848	1.890	1.149	1.881	0.835	0.371	2.355

Table 5.3: Reduced *chi-square* from the fit 5.32. Beside the $\hat{\lambda}_0 = 3.$ case, all the other fit procedures seem to produce quite reliable results.

The peak position, $\hat{m}_c(L)$, has been fitted using equation (5.30), keeping the value of the exponent ν fixed at its central value. The critical bare mass has been determined fitting the infinite volume extrapolation $\hat{m}_c(\infty)$. An example of such fit can be found in figure (5.6). Almost the infinite volume fits proved to be of quite good quality, and allowed to extract the value of $\hat{m}_c(\infty)$ (tables 5.4-5.5-5.6). Each couple of values $(\hat{\lambda}_0, \hat{m}_c)$ has been employed to locate the critical line on the plane of relevant couplings (figure (5.7)).
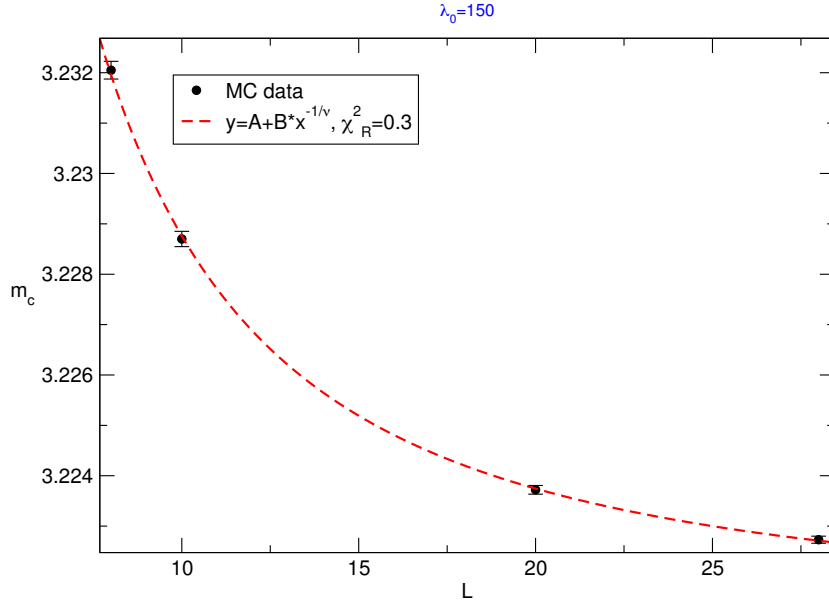
Figure 5.6: Finite size scaling for the bare, critical mass $\hat{m}_c(L)$. Monte Carlo data are displayed in black color.

$\hat{\lambda}_0$	0.5	1.0	2.0	3.0	4.0
$\hat{m}_c(\infty)$	0.24893(34)	0.34838(20)	0.48686(26)	0.59023(15)	0.67622(15)
χ^2_R	0.99	1.49	5.21	1.28	1.59

Table 5.4: Fitted values of $\hat{m}_c(\infty)$ and corresponding reduced χ^2.

$\hat{\lambda}_0$	5.0	26.5	51.0	75.5	100.0
$\hat{m}_c(\infty)$	0.75058(19)	1.57757(6)	2.07873(7)	2.44286(8)	2.73779(8)
χ^2_R	2.70	5.81	0.92	0.04	0.19

Table 5.5: Fitted values of $\hat{m}_c(\infty)$ and corresponding reduced χ^2.

$\hat{\lambda}_0$	125.0	150.0	175.0	200.0	225.0
$\hat{m}_c(\infty)$	2.99496(7)	3.22124(7)	3.42490(8)	3.61110(8)	3.78346(9)
χ^2_R	0.06	0.28	0.41	0.25	7.23

Table 5.6: Fitted values of $\hat{m}_c(\infty)$ and corresponding reduced χ^2.
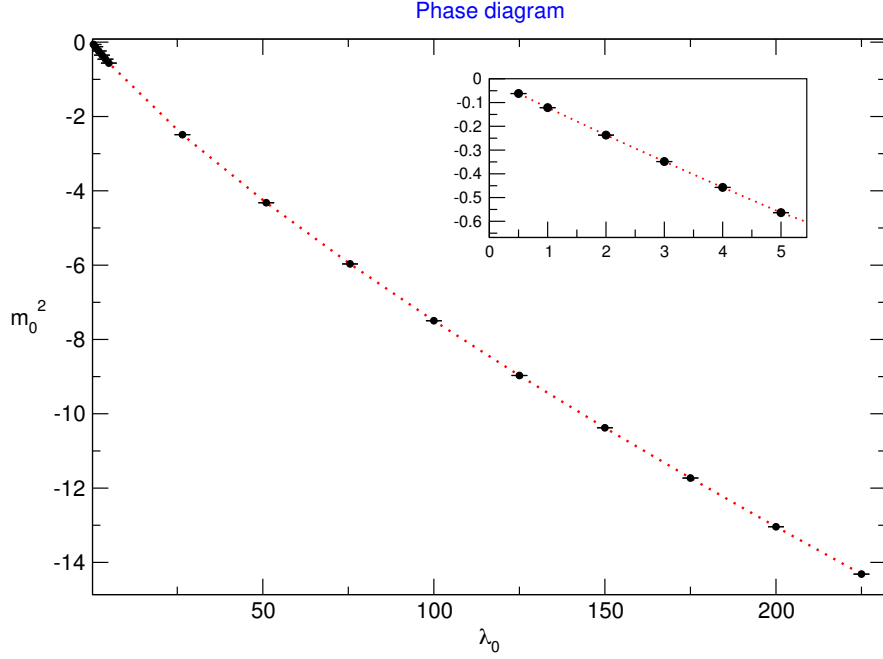
Figure 5.7: Plot of the phase diagram determined through Monte Carlo simulations. The zoomed area focuses on small values $\hat{\lambda}_0$.

Having characterized the phase diagram, it is possible to define renormalized trajectories in the correct thermodynamic phase of the theory.

5.2.4 Super-renormalizability

Before starting with the formulation of the lattice EMT, another fundamental property of the perturbative theory has to be discussed: *super-renormalizability*. In 3 space-time dimensions, for a

scalar theory with quartic interactions, the superficial degree of divergence of a diagram is given by

$$S = 3L - 2I, \tag{5.34}$$

where L is the number of loops and I the number of internal lines. On the other hand, the number of loops can be written as

$$L = I - V + 1, \tag{5.35}$$

while the number of internal lines can be expressed as

$$I = 2V - \frac{E}{2}, \tag{5.36}$$

V and E being the number of vertices and external legs respectively. Combining these three relations, it is possible to express the superficial degree of divergence just in terms of E and V only

$$S = 3 - V - \frac{E}{2}. \tag{5.37}$$

The last equation shows that the theory is super-renormalizable and contains only two divergent diagrams with two external legs and one and two vertices respectively, as shown in figure (5.38).

$$\tag{5.38}$$

The one-loop contribution has the following form

$$\hat{\Pi}(p^2) = -\frac{\lambda_0}{2} \int_{-\pi}^{\frac{\pi}{a}} \frac{d^3 k}{(2\pi)^3} \frac{1}{\hat{k}^2 + m_0^2} \tag{5.39}$$

$$= -\frac{\hat{\lambda}_0}{2} \int_{-\pi}^{\frac{\pi}{a}} \frac{d^3 l}{(2\pi)^3} \frac{1}{4 \sum_{\mu=1}^{3} \sin^2(l_\mu/2) + \hat{m}_0^2}$$

$$= -\frac{\hat{\lambda}_0}{2} Z_0$$

where the numerical value of the integral for $\hat{m}_R^2 = 0$ has been denoted by Z_0. It can be easily evaluated numerically, yielding $Z_0 = 0.252731$. At one loop, the renormalized mass is defined as

$$m_R^2 = m_0^2 + \frac{\lambda_R}{2a} Z_0, \tag{5.40}$$

where mass dimensions have been restored. So, in three dimensions, at one loop, the mass has just a linear additive divergence. Since the only divergent diagrams have two external legs, there is no need of a counterterm for the quartic coupling λ_0. This means that

$$\lambda_0 Z_\phi^2 = \lambda_R \tag{5.41}$$

up to possible finite renormalizations (here, $Z_\phi = 1 + \mathcal{O}(\lambda_0^2)$ is the field renormalization constant). This has important consequences when lattice simulations are set up. As already mentioned before,

the theory has two relevant parameters at the Gaussian fixed point. Therefore, the theory is specified fixing the value of two physical parameters, e.g. m_R and λ_R. The continuum limit is then approached when physical, dimensionful parameters are small in units of the UV cut-off

$$m_R \ll a^{-1}, \quad \lambda_R \ll a^{-1}, \tag{5.42}$$

Since λ_0 can only undergo a finite multiplicative renormalization, the continuum limit can be obtained taking the limit $\hat{\lambda}_0 \to 0$, the physical value of λ_R setting the value of the lattice spacing. To fix a specific theory, the bare mass needs to be tuned as $\hat{\lambda}_0$ is varied, in order to keep constant the following physical ratio

$$\rho = \frac{\lambda_R}{m_R}. \tag{5.43}$$

5.3 EMT in scalar field theory

The renormalization of the EMT in scalar theories has been already discussed in sections (2.4) and (2.6.1) for $d = 4$ space-time dimensions. Here, it will be discussed for the $d = 3$ case, using two different types of regulators. The first one is dimensional regularizations, which is known to preserve translational invariance. The second one is the lattice regularization that, as thoroughly explained in section (2.5), explicitly violates invariance under translations.

5.3.1 Continuum formulation

In terms of renormalized parameters, the one-loop Lagrangian in 3 dimensions is

$$\mathcal{L}_R = \frac{1}{2}\partial_\mu\phi_R\partial_\mu\phi_R + \frac{m_R^2}{2}\phi_R^2 + \frac{\lambda_R}{4!}\phi^4 - \frac{\delta m^2}{2}\phi_R^2, \tag{5.44}$$

where the subscript R denotes renormalized quantities. At one-loop, the value of Z_ϕ and Z_λ is just one. The mass counterterm δm^2 is determined computing the propagator self-energy and imposing the following renormalization conditions

$$\Pi(p^2)|_{p^2=m_R^2} = 0, \tag{5.45}$$

$$\frac{d}{dp^2}\Pi(p^2)|_{p^2=m_R^2} = 0, \tag{5.46}$$

from which it can be inferred that $(D = 3 - \epsilon)$

$$\delta m^2 = \frac{\lambda_R}{2}\frac{1}{(4\pi)^{D/2}}\frac{\Gamma\left(1-\frac{D}{2}\right)}{(m_R^2)^{1-\frac{D}{2}}} \underset{\epsilon \to 0}{=} -\frac{\lambda_R m_R}{8\pi}. \tag{5.47}$$

This is a specific feature of dimensional regularization: *linear divergences are set automatically to zero*. For this reason, at one loop, the mass just acquires a finite, additive renormalization.

In terms of renormalized fields and parameters, the energy momentum tensor is described by the following formula

$$T_{\mu\rho} = \partial_\mu\phi_R\partial_\rho\phi_R - \delta_{\mu\rho}\mathcal{L}_R. \tag{5.48}$$

As customary with composite operators, insertions of the above tensor inside renormalized correlators could generate further divergences that need to be subtracted. At tree-level, insertions of $T_{\mu\rho}$ in two and four-point correlation functions take the following form

$$\langle \tilde{\phi}(p_1)\tilde{T}_{\mu\rho}(q)\tilde{\phi}(p_2) \rangle = \frac{\delta^3(q+p_1+p_2)}{(p_1^2+m_R^2)(p_2^2+m_R^2)}\left[-p_{1\mu}p_{2\rho} - p_{1\rho}p_{2\mu} - \delta_{\mu\rho}(-p_1p_2+m_R^2)\right], \tag{5.49}$$

$$\langle \tilde{\phi}(p_1)\tilde{\phi}(p_2)\tilde{T}_{\mu\rho}(q)\tilde{\phi}(p_3)\tilde{\phi}(p_4) \rangle = -\lambda_R\frac{\delta^3(q+p_1+p_2+p_3+p_4)}{(p_1^2+m_R^2)(p_2^2+m_R^2)(p_3^2+m_R^2)(p_4^2+m_R^2)}, \tag{5.50}$$

From the above set of equations, the corresponding vertex functions are given by

$$\Gamma^{(2)}_{\mu\rho}(q; p_1, p_2) = \left[-p_{1\mu}p_{2\rho} - p_{1\rho}p_{2\mu} - \delta_{\mu\rho}(-p_1 p_2 + m_R^2) \right], \tag{5.51}$$

$$\Gamma^{(4)}_{\mu\rho}(q; p_1, p_2, p_3, p_4) = -\lambda_R, \tag{5.52}$$

where total momentum conservation is intended. For the theory under consideration, the divergent diagrams, by power counting, are listed in figure (5.8)
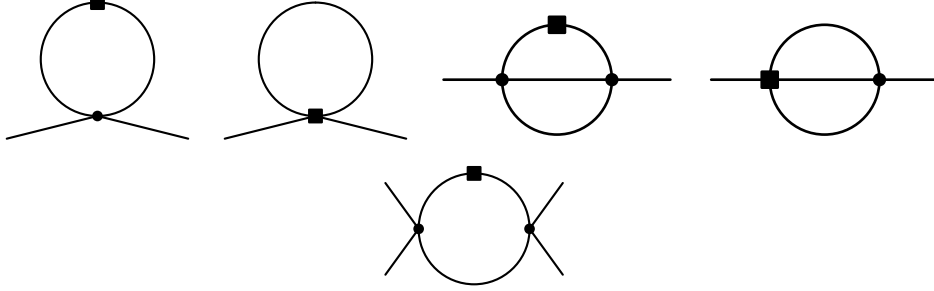
Figure 5.8: Insertions of the EMT that result in divergences into 2- and 4-point functions. The full square denotes the insertion of the EMT, while the bullet represents the interaction vertex proportional to λ_R. The first two diagrams represent the contribution to the insertion in a two-point function at one loop. In the first diagram only the terms in the EMT with two fields contribute, while in the second diagram the terms in the EMT with four fields yield a non zero contribution. The third and fourth diagrams in the first line yield the insertion of the EMT in a two-point function at two loops. Finally, the diagram in the second line yields the contribution of the insertion of the EMT in a four-point function at one loop. In this case, only the terms in the EMT that contain two powers of the field ϕ_R need to be considered.

The second diagram in figure (5.8) represents the contribution of the quartic interaction contained in the EMT. It can be easily shown that such contribution is cancelled by the tree-level insertion of the mass counterterm

$$\Gamma^{(2)}_{\mu\rho}(q; p_1, p_2)_{\phi^4} + \Gamma^{(2)}_{\mu\rho}(q; p_1, p_2)_{\delta m^2} = \underset{-\frac{\lambda_R}{4!}\phi_R^4}{\text{⌢}} + \underset{\frac{\delta m^2}{2}\phi_R^2}{\text{⎯⎯}} = 0. \tag{5.53}$$

At one-loop, linear divergent contributions just come from the first diagram in figure (5.8): these are generated from insertions of derivative terms of the EMT. The explicit expression of such term is given by

$$\begin{aligned}
\underset{\partial^2}{\text{⌢}} &= -\lambda_R \int_l \frac{l_\mu(l+k)_\rho - \frac{\delta_{\mu\rho}}{2}l(l+k)}{(l^2 + m_R^2)[(l+k)^2 + m_R^2]} \\
&\sim -\lambda_R \int_l \frac{l_\mu l_\rho - \frac{\delta_{\mu\rho}}{2}l^2}{(l^2 + m_R^2)^2} + \text{convergent terms} \tag{5.54}
\end{aligned}$$

where only non vanishing terms have been retained on the last line. Clearly, the above divergence is proportional to the operator ϕ^2. However, linear divergences disappear when dimensional regularization is adopted. Hence, the EMT does not need to be renormalized at one loop level. As a consequence, the renormalized EMT will be simply given by

$$(T_{\mu\rho})_R = \partial_\mu \phi_R \partial_\rho \phi_R - \delta_{\mu\rho}\left(\frac{1}{2}\partial_\sigma \phi_R \partial_\sigma \phi_R + \frac{(m_R^2 - \delta m^2)}{2}\phi_R^2 + \frac{\lambda_R}{4!}\phi_R^4\right). \tag{5.55}$$

At 2-loop level, only logarithmic divergences arise, which are also proportional to ϕ^2. Hence, the renormalized EMT is obtained absorbing divergences into the coefficient coupled to ϕ^2. Since the theory is superrenormalizable, there are no other divergent insertions of the EMT. Therefore, only a non trivial renormalization of the ϕ^2 operator is actually expected. Here, a remark needs to be done. The above renormalized operator only satisfies translation WI in the $\epsilon \to 0$ limit. However, any kind of operator of the form

$$(\Theta_{\mu\rho})_R = (T_{\mu\nu})_R + \alpha(\partial_\mu \partial_\rho - \delta_{\mu\rho}\Box)\phi_R^2, \tag{5.56}$$

satisfies the same WI as well. Hence, a one parameter family of renormalized operators can be determined. The value of α can be fixed only by requiring $(\Theta_{\mu\rho})_R$ to satisfy dilatation WI as the regulators is removed. In the classical theory, α can be easily determined requiring $\Theta_{\mu\rho}$ to satisfy the following identity

$$\partial_\mu D_\mu = \Theta_{\mu\mu}, \tag{5.57}$$

where D_μ is the dilatation current. With a simple calculation along the lines of (2.4), it can be easily shown that $\alpha = -1/8$ (appendix (B)) yields the correctly improved EMT that fulfils (5.57).

5.3.2   Lattice formulation

When a lattice regulator is adopted, translational invariance is broken and its restoration is only guaranteed in the continuum limit. In section (2.5), it has been explained how a properly renormalized EMT can be formulated, in order to recover translational symmetry when the lattice spacing goes to zero. Here, a one-loop perturbative calculation along the lines of (5.3.1) will be considered, to determine the divergences that need to be subtracted. The naïvely discretized EMT is given by

$$T_{\mu\rho} = \partial_{\mu S}\phi_R \partial_{\rho S}\phi_R - \delta_{\mu\rho}\left(\frac{1}{2}\partial_{\lambda S}\phi_R \partial_{\lambda S}\phi_R + \frac{m_R^2 - \delta m^2}{2}\phi_R^2 + \frac{\lambda_R}{4!}\phi_R^4\right), \tag{5.58}$$

where $\delta m^2 = \frac{\lambda_R}{2a}Z_0$ is the mass additive renormalization. As for the case of dimensional regularization, the only non trivial renormalization comes from the first diagram of figure (5.8). Here again, divergences are generated only by derivative terms contained in the EMT

$$\overset{\partial^2}{\underset{}{\bigcirc\!\!\!-\!\!\!-}} \quad = \quad -\lambda_R \int_{-\frac{\pi}{a}}^{\frac{\pi}{a}} \frac{d^3l}{(2\pi)^3} \frac{\bar{l}_\mu(\overline{l+k})_\rho - \frac{\delta_{\mu\rho}}{2}\bar{l}(\overline{l+k})}{(\hat{l}^2 + m_R^2)[(\widehat{l+k})^2 + m_R^2]}, \tag{5.59}$$

where the lattice momentum functions

$$\bar{l}_\mu = \frac{1}{a}\sin l_\mu a, \quad \bar{l}^2 = \sum_{\mu=1}^3 \bar{l}_\mu^2, \tag{5.60}$$

$$\hat{l}_\mu = \frac{2}{a}\sin\frac{l_\mu a}{2}, \quad \hat{l}^2 = \sum_{\mu=1}^3 \hat{l}_\mu^2, \tag{5.61}$$

are generated by the use of symmetric and forward derivative respectively. The coefficient coupled to the linear divergence can be extracted once the integral is written in lattice units

$$\begin{aligned}
\overset{\partial^2}{\underset{\bullet}{\bigcirc}} \quad = \quad & -\frac{\lambda_R}{a}\int_{-\pi}^{\pi}\frac{d^3z}{(2\pi)^3}\frac{\bar{z}_\mu\overline{(z+ak)}_\rho - \frac{\delta_{\mu\rho}}{2}\bar{z}\overline{(z+ak)}}{(\hat{z}^2+am_R^2)[\widehat{(z+ak)}^2+am_R^2]} \\
\sim \quad & -\frac{\lambda_R}{a}\int_{-\pi}^{\pi}\frac{d^3z}{(2\pi)^3}\frac{\bar{z}_\mu\bar{z}_\rho - \frac{\delta_{\mu\rho}}{2}\bar{z}^2}{(\hat{z}^2)^2} \\
= \quad & \frac{\lambda_R}{6a}\delta_{\mu\rho}\int_{-\pi}^{\pi}\frac{d^3z}{(2\pi)^3}\frac{\bar{z}^2}{(\hat{z}^2)^2} \\
= \quad & \frac{\lambda_R}{6a}\delta_{\mu\rho}W_0 \tag{5.62}
\end{aligned}$$

$$\tag{5.63}$$

where $W_0 = 0.0215161$. On the firs line, a change of variables $l = z/a$ has been done, while on the second one the continuum limit of the integrand has been taken. This linear divergence can be absorbed through a redefinition of the bare mass coupling

$$m_0^2 \to -Z_3 = m_0^2 + \frac{\lambda_R}{6a}W_0, \tag{5.64}$$

where Z_3 denotes the renormalization constant of the operator ϕ^2. The above relation allows to evaluate the following dimensionless ratio

$$-\frac{Z_3}{m_0^2} = 1 + \frac{\frac{\lambda_R}{6a}W_0}{m_R^2 - \frac{\lambda_R Z_0}{2a}} \underset{a\to 0}{=} 1 - \frac{W_0}{3Z_0} \sim 0.83, \tag{5.65}$$

which can be used as a reference value when the renormalization constant Z_3 is measured non perturbatively. The lattice renormalized EMT is then defined as

$$T_{\mu\rho} = \partial_{\mu S}\phi_R\partial_{\rho S}\phi_R - \delta_{\mu\rho}\left(\frac{1}{2}\partial_{\lambda S}\phi_R\partial_{\lambda S}\phi_R + \frac{m_R^2+k-\delta m^2}{2}\phi_R^2 + \frac{\lambda_R}{4!}\phi_R^4\right), \tag{5.66}$$

where $k = \frac{\lambda_R}{6a}W_0$.

5.4 EMT from the gradient flow

In this section, the gradient flow for a scalar theory in 3 dimensions is proposed. Then, following the guide lines of (3.2), it is used to formulate translation WI probed by observables built along the flow. The latter will provide an effective strategy to renormalize the lattice EMT of the theory.

5.4.1 Gradient flow for scalar field theory

In pure Yang-Mills, the form of the flow equation is strongly constrained by gauge symmetry. To be more specific, the flow equation has to preserve gauge covariance. For the scalar theory under study, only the Z_2 symmetry has to be preserved. This clearly leaves a lot of freedom in the way the gradient flow can be formulated. Surely, the easiest way to evolve scalar fields along the flow is through a simple gaussian smearing

$$\dot{\varphi}(t,x) = \Box\varphi(t,x), \quad \varphi(t,x)|_{t=0} = \phi(x). \tag{5.67}$$

In this case, the solution of the flow equation is given by

$$\varphi(t,x) = \int d^dx\, K_t(x-y)\phi(y), \tag{5.68}$$

with the heat kernel defined as

$$K_t(x - y) = \int_p e^{ip(x-y)} e^{-p^2 t}. \tag{5.69}$$

This specific solution does not have a tree-like expansion as for the pure gauge case.

The renormalization properties of correlation functions built with flowed fields can be still studied in terms of a $(D + 1)$-dimensional field theory defined by the following action

$$S = S_{boundary} + S_{bulk}, \tag{5.70}$$

$$S_{boundary} = \int d^d x \left[\frac{1}{2} \partial_\mu \phi \partial_\mu \phi + \frac{m_0^2}{2} \phi^2 + \frac{\lambda_0}{4!} \phi^4 \right], \tag{5.71}$$

$$S_{bulk} = \int_0^\infty dt \int d^d x L(t, x)(\partial_t - \Box)\varphi(t, x). \tag{5.72}$$

Beside the boundary four-vertex and propagator, two new elements need to be added

- $\varphi\varphi$ flow propagator

$$\langle \tilde{\varphi}(t, p)\tilde{\varphi}(s, q) \rangle = (2\pi)^d \delta^d(p + q)\tilde{D}(p)\tilde{K}_{t+s}(p), \tag{5.73}$$

- $L\varphi$ flow propagator

$$\langle \tilde{\varphi}(t, p)\tilde{L}(s, q) \rangle = (2\pi)^d \delta^d(p + q)\theta(t - s)\tilde{K}_{t-s}(p), \tag{5.74}$$

where $\tilde{K}_t(p)$ and $\tilde{D}(p)$ represent the momentum-space heat kernel and boundary propagator respectively. As for the case of pure gauge theory, an implicit coupling between the Lagrange multiplier L and the boundary field ϕ can be ruled out through the following decomposition

$$\varphi(t, x) = \int d^d y K_t(x - y)\varphi(y) + b(t, x). \tag{5.75}$$

The first term in the equation above drops out from the bulk action, just leaving the b field, which satisfies homogeneous boundary conditions. The latter is used to define the φL contraction. The Feynman rules for this theory are quite simple (figure (5.9)). It has to be noticed that no
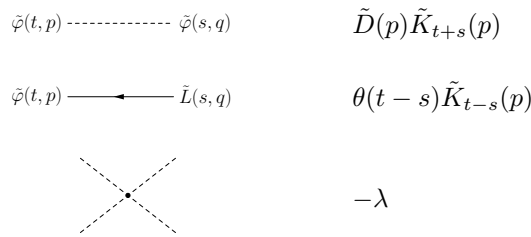
Figure 5.9: Feynman rules in D+1 dimension with the gradient flow.

vertices connecting flow lines with boundary lines exist. This means that loops in diagrams involve just boundary field contractions. Since no flow vertices are generated, flow-line loops cannot be created. As for the case of gauge theory, no divergence can be created in the bulk even if the fields coalesce on the same point at the boundary[2]. The only possible divergences come from the

---

[2]As an example, the renormalization properties of the following correlation function

$$\langle \varphi(x, t)\varphi(x, s) \rangle = \int_p \tilde{D}(p)\tilde{K}_{t+s}(p), \tag{5.76}$$

boundary. However, this divergences are generated *only* by loop contractions of boundary fields and are absorbed when bare parameters are rewritten in terms of renormalized ones. As a consequence, correlation functions of the $(D+1)$-dimensional theory are UV finite by construction.

In this case, the simplest form of the flow equation has been used. It is interesting to verify the UV finiteness of bulk correlation functions when a different flow action is employed. For example, one could use the following form of gradient flow

$$\dot{\varphi}(t,x) = -\left.\frac{\delta S}{\delta \phi}\right|_{\phi=\varphi},$$
$$S = \int d^d x \left[\frac{1}{2}\partial_\mu\phi\partial_\mu\phi + \frac{m_0^2}{2}\phi^2 + \frac{\lambda_0}{4!}\phi^4\right], \tag{5.78}$$

$$\tag{5.79}$$

which is obtained from the boundary $\lambda\phi^4$ action. As for Yang-Mills theory, the solution can be defined in a closed form as

$$\varphi(t,x) = \int d^d y \left[K_{t,m_0}(x-y)_{\mu\nu}\phi(y) - \frac{\lambda_0}{3!}\int_0^t ds K_{t-s,m_0}(x-y)_{\mu\nu}\varphi^3(s,y)\right], \tag{5.80}$$
$$K_{t,m_0}(x) = e^{-m_0^2 t}K_t(x), \tag{5.81}$$

and the existence of flow vertices is guaranteed by non linear contributions in the flow field. Again, the renormalization of bulk correlation functions can be studied in terms of the following $(D+1)$-dimensional theory

$$S = S_0 + S_{bulk}, \tag{5.82}$$
$$S_0 = \int d^d x \left[\frac{1}{2}\partial_\mu\phi\partial_\mu\phi + \frac{m_0^2}{2}\phi^2 + \frac{\lambda_0}{4!}\phi^4\right], \tag{5.83}$$
$$S_{bulk} = \int_0^\infty dt \int d^d x L(t,x)\left[\partial_t - \left(\Box - m_0^2 - \frac{\lambda_0}{3!}\varphi(t,x)^2\right)\right]\varphi(t,x). \tag{5.84}$$

If dimensional regularization is adopted, it can be shown that no flow-line loops exist. Nevertheless, the existence of flow vertices allows to build loops containing boundary lines and at least one flow-line. In analogy with the previous cases, one could study the renormalization properties of the theory and check where divergences come from and how they can be removed. One would naïvely expect divergences to arise at the boundary and, should this be the case, to be absorbed by boundary counterterms. However, this is not the case. The flow described in (5.78) defines a flow vertex and a flow propagator that contain couplings of the boundary theory. If the latter renormalize in a non trivial way, then new *bulk divergences* appear. These cannot be absorbed by any counterterm at the boundary. To renormalize the $(D+1)$-dimensional theory, one needs to add *bulk counterterms* that properly cancel the new divergences. For the theory described by (5.82), this amounts to remove the mass term from the bulk action[3] . Then, further study is needed to detect divergences at zero flow time. Two possible scenarios are available.

can be studied, using dimensional regularization. In this case, the whole renormalization process involves just a boundary propagator $\tilde{D}(p)$,

$$\tilde{D}(p)\tilde{K}_{t+s}(p) = \frac{e^{-(t+s)p^2}}{m_0^2 + p^2 - \Pi(p^2)} \tag{5.77}$$

dressed with a Gaussian smearing function. It should be clear that, once the theory is written in terms of renormalized quantities, the above correlation function is automatically UV finite.

[3] In 4 space-time dimensions, also the cubic interaction must be removed. For this theory, another possible, non-trivial, flow action has been recently proposed by Fujikawa [25].

1. Divergences appear at zero flow time, but they cancel out once the boundary theory is expressed in terms of renormalized couplings. Moreover, no $t = 0$ counterterm containing the L field is needed to renormalize expectation values. Then correlation functions built along the flow are UV finite.

2. Boundary divergences disappear only if also specific counterterms with the Lagrange multiplier are used. The latter has to be determined order by order in perturbation theory. In this case, the good properties that usually characterize bulk correlation functions are totally spoiled. This suggests to change the form of the gradient flow.

The above example tells that not all the flow actions are good candidates to define UV finite bulk correlation functions. Even if the lack of symmetries enlarges the spectrum of possible actions, then renormalizability conditions make it narrower. Surely, it would be interesting to study flows that differ from the trivial Gaussian smearing. However, the gradient flow is just a tool, useful when it shows finiteness properties that can be easily proved. For this reason, only the Gaussian flow described by (5.67) has been considered.

5.4.2 EMT from the gradient flow

To formulate a set of WI like those derived in section (3.3), the effect of a local translation on probes at positive flow time has to be understood. For the scalar theory under study, a local infinitesimal translation has the following form

$$
\begin{aligned}
\delta_\alpha \phi(x) &= \\
&= \int d^d y \, \alpha_\rho(y) \delta_{y,\rho} \phi(x) \\
&= \int d^d y \, \alpha_\rho(y) \delta^d(x - y) \partial_\rho \phi(x) \\
&:= \alpha_\rho(x) \partial_\rho \phi(x).
\end{aligned}
\tag{5.85}
$$

To this transformation, the following EMT is related

$$
T_{\mu\rho} = \partial_\mu \phi \partial_\rho \phi - \delta_{\mu\rho} \mathcal{L}.
\tag{5.86}
$$

For a generic, Z_2 invariant observable, the diffeomorphism (5.85) becomes

$$
\begin{aligned}
\delta_\alpha P &= \int d^d x \, \alpha_\rho(x) \delta_{x,\rho} P \\
&:= \int d^d x \, \alpha_\rho(x) \frac{\delta P}{\delta \phi(x)} \partial_\rho \phi(x),
\end{aligned}
\tag{5.87}
$$

and a corresponding translation WI can be written down as

$$
\langle \delta_{x,\rho} P \rangle = -\langle P \partial_\mu T_{\mu\rho} \rangle.
\tag{5.88}
$$

Translations: probes at positive flow time

On a probe at positive flow time, the action of (5.85) takes the following form

$$
\begin{aligned}
\delta_{x,\rho} P_T &= \\
&= \int d^d y \, \frac{\delta P_T}{\delta \varphi(T, y)} \frac{\delta \varphi(T, y)}{\delta \phi(x)} \partial_\rho \phi(x) \\
&:= \int d^d y \, \frac{\delta P_T}{\delta \varphi(T, y)} J(T, y; 0, x) \partial_\rho \phi(x).
\end{aligned}
\tag{5.89}
$$

As for the case of Yang-Mills theory, the effect of a local translation is propagated from the boundary to the bulk by the Jacobian matrix. The latter can be determined solving the following differential equation

$$\partial_t J(t, x; s, y) = \Box J(t, x; s, u)$$
$$J_{\mu\nu}(t^+, x; t, y) = \delta^d(x - y),$$
$$J_{\mu\nu}(t, x; s, y) = 0 \quad t < s, \tag{5.90}$$

which has been obtained linearizing (5.67). Here, boundary conditions ensure forward propagation in flow time. The solution of (5.90) is easily computed

$$J(t, x; s, y) = \theta(t - s) \int_p e^{ip(x-y)} \tilde{K}_{t-s}(p). \tag{5.91}$$

The main difference with the pure gauge case is that the Jacobian coincides exactly with the free φL propagator. In momentum space, it decays exponentially like a Gaussian function

$$J(t, x; s, y) = \theta(t - s) \frac{e^{-\frac{|x-y|^2}{4(t-s)}}}{[4\pi(t-s)]^{d/2}} \tag{5.92}$$

Combined with (5.92), equation (5.89) tells that local translations on the boundary can be smoothly propagated at $t > 0$, integrating boundary fields over a smearing radius of $\sqrt{6t}$[4].

Renormalization of $\delta_{x,\rho} P_T$

To devise translation WI for probes at positive flow time, the renormalization properties of $\delta_{x,\rho} P_T$ need to be determined. Following the same steps of subsection (3.3.4), it can be easily shown that

$$\langle \delta_{x,\rho} P_T \rangle = \langle P_T \tilde{T}_{0\rho} \rangle, \tag{5.93}$$

where $\tilde{T}_{0\rho} = L(0, x) \partial_\rho \phi(x)$. Also for scalar theory, the renormalization of $\delta_{x,\rho} P_T$ can be studied analyzing a *local* operator, built with L and ϕ fields. A generic form of the observable P_T could be given by

$$P_T = \prod_{i=1}^{n} \Phi_i(T, x), \tag{5.94}$$

where each $\Phi_i(T, x_i)$ represents a Z_2-invariant, local observable built with φ fields and their derivatives. It is known that local operators of the bulk theory do not need to be renormalized. The only possible divergences are hidden in the operator $\tilde{T}_{0\rho}$. The latter has the following properties

- It has mass dimension 4.

- It is Z_2 invariant.

Any operator with mass dimension ≤ 4 sharing the same properties could mix with $\tilde{T}_{0\rho}$. The absence of gauge symmetry allows several terms to be included

$$L\partial_\rho \phi, \quad \phi \partial_\rho L, \quad \phi^2 \partial_\rho \phi, ... \tag{5.95}$$

However, no flow vertex is generated by the solution of (5.67). Hence, no loops can be created when $\tilde{T}_{0\rho}$ is inserted inside correlation functions. As a consequence, no divergence is generated and the operator $\tilde{T}_{0\rho}$ does not renormalize at all. This result holds also when a lattice regulator is adopted,

---

[4]Here, the specific $d = 3$ case has been considered.

since the discretized $(D + 1)$-dimensional theory preserves the same renormalization properties of its continuum counterpart. In terms of renormalized operators, a possible translation WI can be written as

$$\langle \delta_{x,\rho} P_T \rangle = -\langle P_T \partial_\mu (T_{\mu\rho})_R \rangle. \tag{5.96}$$

Also in this case, equation (5.96) can be derived from a generalized TWI for the $(D+1)$-dimensional theory, as it will be shown in the next subsection.

Translation WI at positive flow time

The flow equation is invariant under global translations. Hence, the equivalence between the two following actions holds

- Evolving from the boundary theory and then translate the bulk fields at a given flow time t.

- Translating the boundary fields and then evolve them up to flow time t in the bulk.

This argument allows to define a family of transformations parametrized by the flow time

$$\bar{\delta}_{t,\alpha} P = \int d^d x \, \alpha_\rho(x) \bar{\delta}_{t,x,\rho} P = \int d^d x \, \alpha_\rho(x) \frac{\delta P}{\delta \varphi(t,x)} \partial_\rho \varphi(t,x), \tag{5.97}$$

where the differential operator $\bar{\delta}_{t,x,\rho}$ depends locally on φ fields that satisfy the flow equation. Again, it is possible to show that

$$\langle \bar{\delta}_{t,x,\rho} P_T \rangle = \langle P_T \tilde{T}_{0\rho}(t,x) \rangle, \tag{5.98}$$

the operator $\tilde{T}_{0\rho}(t,x)$ being now computed at positive flow time. As for the pure gauge case, the action of the operator $\bar{\delta}_{t,x,\rho}$ assumes two different forms

$$\bar{\delta}_{t,x,\rho} \Phi(T,y) = \frac{\delta \Phi(T,y)}{\delta \varphi(T,x)} \partial_\rho \varphi(T,x) \quad \text{for } T = t, \tag{5.99}$$

$$\bar{\delta}_{t,x,\rho} \Phi(T,y) = \int d^d z \frac{\delta \Phi(T,y)}{\delta \varphi(T,z)} J(T,z;t,x) \partial_\rho \varphi(t,x) \quad \text{for } T > t, \tag{5.100}$$

Equations (5.100) show how the operator $\bar{\delta}_{t,x,\rho}$ generates a local translation on hyper-planes at fixed $t > 0$. A global version of the previous transformations is given by

$$\int_V d^d x \, \bar{\delta}_{t,x,\rho} \Phi(T,y) = \partial_\rho \Phi(T,x) \quad \text{for } T = t, \tag{5.101}$$

$$\int_V d^d x \, \bar{\delta}_{t,x,\rho} \Phi(T,y) = \partial_\rho \Phi(T,x) + \mathcal{O}\left(e^{-\frac{r^2}{4(T-t)}}\right) \quad \text{for } T > t, \tag{5.102}$$

where the integration domain is a sphere V with radius r, centred in x. The result on the second line has been already proved in (3.3) for Yang-Mills theory, and it can be shown to hold also for the scalar theory under study.

The operator $\bar{\delta}_{t,\alpha}$ depends only on bulk fields, and therefore it does not require any renormalization. Associated with it, for each flow time t, there is a new EMT and a corresponding bulk TWI can be formulated. Exploiting the space-time symmetries of the $(D + 1)$-dimensional theory, the new EMT can be written in terms of local operators at positive flow time. First, one has to

define local translations in $(D+1)$ dimensions

$$\delta_\alpha \varphi(t,x) = \int_0^\infty ds \int d^d y \alpha_R(s,y)\delta_{s,y,R}\varphi(t,x)$$
$$= \int_0^\infty ds \int d^d y \alpha_R(s,y)\delta(t-s)\delta^d(x-y)\partial_R\varphi(t,x)$$
$$:= \alpha_R(t,x)\partial_R\varphi(t,x),, \tag{5.103}$$

$$\delta_\alpha L(t,x) = \int_0^\infty ds \int d^d y \alpha_R(s,y)\delta_{s,y,R}L(t,x)$$
$$= \int_0^\infty ds \int d^d y \alpha_R(s,y)\delta(t-s)\delta^d(x-y)\partial_R L(t,x)$$
$$:= \alpha_R(t,x)\partial_R L(t,x), \tag{5.104}$$

with $\alpha_0(0,x) = 0$ and $R, M = 0, 1, ..., D,$. The direction 0 identifies the flow time extension. For a probe that does not depend on the Lagrange multiplier, the corresponding variation will be

$$\delta_\alpha P = \int_0^\infty dt \int d^d x \alpha_R(t,x)\delta_{t,x,R}P$$
$$:= \int_0^\infty dt \int d^d x \alpha_R(t,x)\frac{\delta P}{\delta\varphi(t,x)}\partial_R\varphi(t,x). \tag{5.105}$$

The difference between the operator $\delta_{t,x,R}$ and $\bar\delta_{t,x,\rho}$ has been precisely described in section (3.3) and will not be repeated here again.

From the transformation induced by $\delta_{t,x,R}$, an EMT at any positive flow time can be defined

$$\delta_\alpha S_{fl} = \int_0^\infty dt \int d^d x \tilde T_{MR}(t,x)\partial_M\alpha_R(t,x), \tag{5.106}$$

$$\tilde T_{0R} = L\partial_R\varphi, \tag{5.107}$$

$$\tilde T_{\nu R} = \partial_\nu L\partial_R\varphi - L\partial_\nu\partial_R\varphi, \tag{5.108}$$

From the set of transformations (5.103) and (5.104) the following WI can be derived

$$\langle\delta_{t,x,\rho}P\rangle = -\langle P\partial_M\tilde T_{MR}(t,x)\rangle. \tag{5.109}$$

For a probe P_T depending on bulk fields at flow time $T > t$, the l.h.s of the previous equation vanishes, leaving the identity

$$\langle P_T\partial_t\tilde T_{0R}(t,x)\rangle = -\langle P_T\partial_\mu\tilde T_{\mu R}(t,x)\rangle. \tag{5.110}$$

Only the case $R = \rho$ is considered here. It has to be noticed that both sides of the equation are finite at positive flow time. Equation (5.110) leads to a set of WI for the family of transformations (5.100). This can be verified integrating (5.110) with respect the flow time in an interval $(0,t)$. The problem is that at $t = 0$ an extra contribution arises from the fact that boundary fields are transformed along with the bulk ones. Moreover equation (5.110) is valid for bare fields at finite cut-off. As long as the flow time is non-zero, this equation does not exhibit divergences in the $\epsilon \to 0$ limit. Therefore, the cut-off gets removed at positive flow time, then equation (3.185) is integrated in an interval (t_0, t)

$$\langle P_T\tilde T_{0\rho}(t,x)\rangle = \langle P_T\tilde T_{0\rho}(t_0,x)\rangle - \langle P_T\partial_\mu\int_{t_0}^t ds\tilde T_{\mu\rho}(s,x)\rangle, \tag{5.111}$$

and then the $t_0 \to 0^+$ limit is taken. The l.h.s. of the above equation can be written as

$$\langle P_T\tilde T_{0\rho}(t,x)\rangle = \langle\bar\delta_{t,x,\rho}P_T\rangle, \tag{5.112}$$

and is used to take the the limit of the first term on the r.h.s.

$$\lim_{t_0 \to 0^+} \langle P_T \tilde{T}_{0\rho}(t_0, x) \rangle = \langle \delta_{x,\rho} P_T \rangle = -\langle P_T \partial_\mu T_{\mu\rho}(x) \rangle. \tag{5.113}$$

Collecting all the pieces together, a translation WI for the operator $\bar{\delta}_{t,x,\rho}$ can be written as

$$\langle \bar{\delta}_{t,x,\rho} P_T \rangle = -\langle P_T \partial_\mu \bar{T}_{\mu\rho}(t, x) \rangle, \tag{5.114}$$

$$\bar{T}_{\mu\rho}(x) = T_{\mu\rho}(x) + \int_0^t ds \tilde{T}_{\mu\rho}(s, x). \tag{5.115}$$

This TWI can be reduced to equation (5.96) at $t = 0$ only if the integral appearing in (3.190) is finite. The finiteness of the integral is ensured by the fact that insertions of $\tilde{T}_{\mu\rho}(s, x)$ cannot produce loop at positive flow time since flow vertices do not exist. Hence, the $t \to 0^+$ limit in (5.114) can be safely taken, finally giving

$$\langle \delta_{x,\rho} P_T \rangle = -\langle P_T \partial_\mu T_{\mu\rho}(x) \rangle. \tag{5.116}$$

As for the case of Yang-Mills theory, the renormalized EMT in scalar theory can be determined using a numerical strategy based on (5.116).

In analogy with the case of translations, it can be easily proven that also dilatation WI for flowed probes can be formulated. For the integrated trace of the EMT, they take the following form

$$\langle \left[2T \frac{d}{dT} + d_\Phi \right] \Phi(T, x) \rangle = \langle \Phi(T, x) \int d^d y T_{\mu\mu}(y) \rangle. \tag{5.117}$$

The above result can be easily proved following the approach adopted in (3.3).

5.5 Numerical setup

Equation (5.116) can be used to devise translation WI probed by observables at positive flow time. These identities can be used to non perturbatively determine a renormalized EMT on the lattice. The latter has to be defined in terms of a proper operator mixing

$$(\hat{T}_{\mu\nu})_R = \sum_{i=1}^n Z_i \left[\hat{T}_{\mu\nu}^{(i)} - \langle \hat{T}_{\mu\nu}^{(i)} \rangle \right]. \tag{5.118}$$

For a Z_2-invariant scalar theory, the number of mixing operators could be considerably large

$$\hat{T}_{\mu\nu} = Z_1 \partial_\mu \phi \partial_\nu \phi + Z_2 \phi \partial_\mu \partial_\nu \phi + \delta_{\mu\nu} \left(Z_3 \sum_\rho \partial_\rho \phi \partial_\rho \phi + Z_4 \partial_\mu \phi \partial_\mu \phi + ... \right), \tag{5.119}$$

however, the perturbative analysis of subsection (5.3.2) shows that divergences can only be created by terms proportional to ϕ^2. The latter is the only operator that renormalizes in a non trivial way. This result is a consequence of superrenormalizability, and severely restricts the number of mixing operators. To be more precise, only four operators need to be considered

$$(\hat{T}_{\mu\nu})_R = \frac{Z_1}{2} \partial_{\mu S} \phi \partial_{\nu S} \phi + \delta_{\mu\nu} \left(\frac{Z_2}{2} \sum_\rho \partial_{\rho S} \phi \partial_{\rho S} \phi + \frac{Z_3}{2} \phi^2 + \frac{Z_4}{4!} \phi^4 \right). \tag{5.120}$$

To avoid $\mathcal{O}(a)$ scaling violations, the symmetric lattice derivative has been adopted in (5.120). Unlike ϕ^2, the other three operators are supposed to not renormalize at all. This provides quite

stringent constraints on the coefficients $Z_{1,2,4}$. More precisely, the following results

$$Z_1 = 2, \tag{5.121}$$

$$Z_2 = -1, \tag{5.122}$$

$$\frac{Z_4}{\lambda_0} = -1, \tag{5.123}$$

are expected to hold within statistical errors. On the other hand, Z_3 renormalizes non trivially. Due to superrenormalizability, it is affected by radiative corrections just up to $\mathcal{O}(\lambda_0^2)$. In subsection (5.3.2), its value at one loop has been determined and can be qualitatively used as a reference value

$$\frac{Z_3}{m_0^2} = -0.83 + \mathcal{O}(\lambda_0^2), \tag{5.124}$$

where $\mathcal{O}(\lambda_0^2)$ corrections are supposed to be small.

5.5.1 Lattice TWI

All the numerical effort has been devoted to precisely measure the coefficients $Z_{1,2,3,4}$, using equation (5.116). To obtain non vanishing expectation values, vector probes have been chosen and a sum over all directions has been applied. To maximize the signal, probes and EMT have been positioned at the same space-time point, and a volume average has been taken

$$\sum_{\alpha=1}^{4} \underbrace{L^{-3} \sum_{\vec{x}} \sum_{\rho,\mu} \langle \hat{\Phi}_\rho^{(\beta)}(t,\vec{x}) \partial_\mu (\hat{T}_{\mu\rho}^{(\alpha)})_R(\vec{x}) \rangle}_{M^{\beta\alpha}(t)} Z_\alpha = -\underbrace{L^{-3} \sum_{\vec{x}} \sum_{\rho} \langle \hat{\delta}_{\vec{x},\rho} \hat{\Phi}_\rho^{(\beta)}(t,\vec{x}) \rangle}_{v^\beta(t)}, \tag{5.125}$$

where $\hat{\Phi}_\rho^{(\beta)}$ is a generic probe that transforms as a vector in the continuum limit. Unlike the pure gauge case, no multiplicative Z_δ factor has to be measured. This allowed to apply periodic boundary conditions to all the lattice extensions, and to take rigid volume averages. This point is crucial, since averaging over the volume can considerably enhance the signal.

As for Yang-Mills theory, the numerical strategy can be divided in few steps:

1. representative ensembles of scalar fields are generated employing a proper Monte Carlo algorithm;

2. using a suitable integrator, each configuration is evolved along the flow for several (discrete) values of flow time;

3. for every flow time, the operators appearing in (5.125) are computed using boundary and bulk scalar fields;

4. the elements describing $M^{\beta\alpha}(t)$ and $v^\beta(t)$ are estimated averaging over their corresponding Monte Carlo histories (figure 5.10).
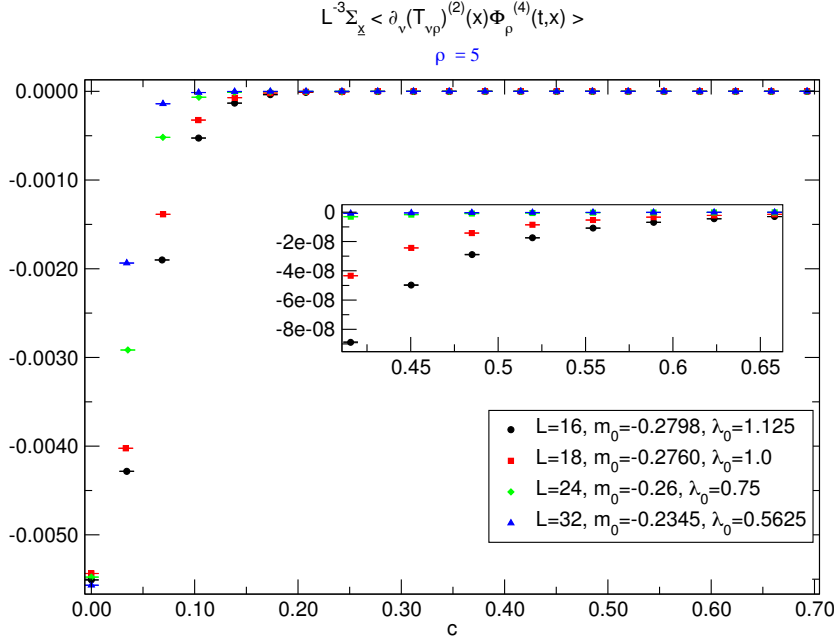
Figure 5.10: Statistical estimates of terms appearing on the r.h.s. of (5.125). Measurements have been taken for different lattices, for a given renormalized trajectory. The latter is defined by the values (L, λ_0, m_0) in the legend box. Averages have been taken over Monte Carlo histories, using proper methods in order to take into account of the auto-correlation. Data have been displayed with respect the smearing ratio $c = \sqrt{6t}/L$. The zoomed area focuses on a small interval of large flow times.

For any value of the flow time t, equation (5.125) describes a linear system with statistical noise, whose solutions can be numerically estimated.

In Yang-Mills theory, a minimal set of three probes, with the smallest possible mass dimension, has been chosen. Hence, the corresponding square system has been solved. This choice has been motivated by high computational costs, and the necessity of producing results in a reasonable amount of time. However, nothing guarantees this setup to be the optimal one for measuring the renormalization constants.

Indeed, it is hard to know a priori which kind of probes provide a well conditioned system over a wide range of flow times. To give a more quantitative idea, the condition number of $M^{\alpha\beta}(t)$ is plotted in figure (5.11) as a function of the flow time, for different sets of probes. It is quite clear that the condition number, as the quality of the solution, strongly depends on the flow time and the chosen set of probes. This suggests that a different strategy should be adopted. A more efficient way to extract the renormalization constants might be to generate a large number of probes to be combined in several different subsets of 4 operators: then an optimal setup can be determined looking for the subset whose corresponding square system provides the best numerical signal[5].

In principle, an infinite number of probes, sharing the right symmetry properties, could be generated. This is clearly not feasible, and an upper bound on this number has to be produced. In this case, only vector-like probes[6] with mass dimension $d_\Phi \leq d^*$ have been included, the value of

---

[5]Due to computational costs, it would be impossible to apply the same strategy in Yang-Mills theory. However, a scalar theory in 3 dimensions is far more cheap to simulate and, due to the simple form of the flow equation (5.67), it provides dramatically precise results within a reasonable amount of time.

[6]The probes must transform as four vectors in the continuum, such that their contribution to (5.125) does not

d^* having been determined after few numerical studies.
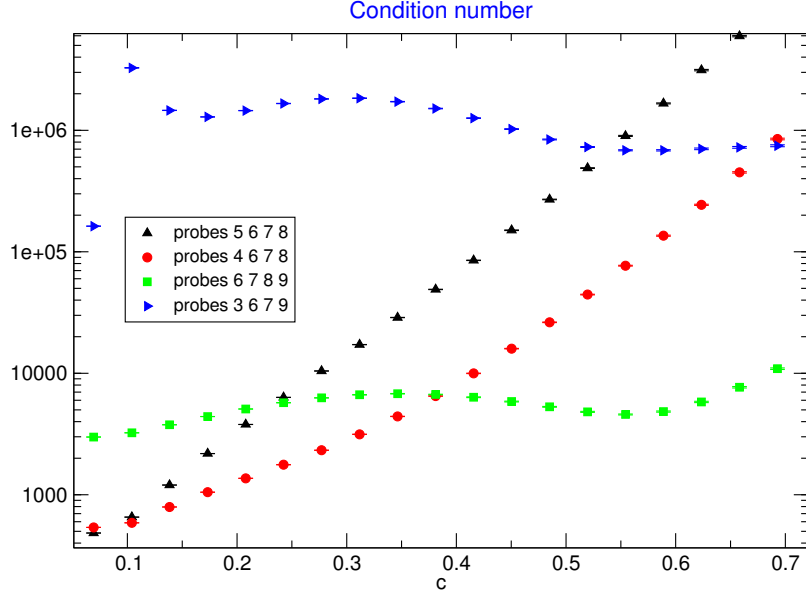
Figure 5.11: Condition number for $\hat{\lambda}_0 = 0.75, (m_0)^2 = -(0.26)^2$ on a $L = 24$ lattice. Data have been plotted as functions of the ratio $c = \sqrt{6t}/L$, using different sets of probes. Each set of probes defines a specific square (4×4) system. The probe numbers correspond to the operators in table (5.7)

.

In table (5.7), probes up to mass dimension $d^* = 5$ are displayed.

Label	Operator	Mass dimension
1	$(\partial_\mu \varphi)\varphi$	2
2	$(\partial_\mu \partial_\rho \partial_\rho \varphi)\varphi$	3
3	$(\partial_\rho \partial_\rho \varphi)(\partial_\mu \varphi)$	3
4	$(\partial_\mu \partial_\rho \varphi)(\partial_\rho \varphi)$	3
5	$(\partial_\mu \varphi)\varphi^3$	4
6	$(\partial_\mu \partial_\rho \partial_\rho \varphi)\varphi^3$	5
7	$(\partial_\rho \partial_\rho \varphi)(\partial_\mu \varphi)\varphi^2$	5
8	$(\partial_\mu \partial_\rho \varphi)(\partial_\rho \varphi)\varphi^2$	5
9	$(\partial_\rho \varphi)(\partial_\rho \varphi)(\partial_\mu \varphi)\varphi$	5
10	$(\partial_\mu \varphi)\varphi^5$	4
11	$(\partial_\mu \varphi)\varphi^7$	5

Table 5.7: Vectorial probes up to mass dimension 5.

Few numerical studies proved that the set (5.7) suffices to provide quite precise numerical results[7]. Probes have been automatically generated and included inside the simulation code, along

---

vanish when the lattice spacing goes to zero.

[7]Measurements with $d^* > 5$ sets have been also carried out, without any substantial improvement from the $d^* = 5$ case.

with their variation

$$\delta_{x,\rho} P_T. \tag{5.126}$$

In this way, linear systems have been easily tested using a large number of different P_Ts. This testing procedure is crucial, since statistical errors on final results strongly depend on the set of adopted operators. This should be clear from figure (5.11), where the condition number changes of several orders by changing a single probe.

For each lattice of a given renormalized trajectory, a study of the *best square system* has been done. The procedure can be described in few steps:

1. a set of 4 probes is selected, and the corresponding matrix $M^{\alpha\beta}(t)$ and variation vector $v^{\beta}(t)$ are computed;

2. TWI are numerically solved for all the flow times. Estimates of renormalization constants and condition number are produced;

3. the set of probes is changed and points (1-2) are repeated for all the possible 4×4 square system that can be created.

The optimal set of 4 probes has been identified by looking for the square system with the smallest condition number. Such optimal set is likely to change with the flow time and the lattice spacing. However, renormalization constants, and corresponding lattice artefacts, are determined properly only if the same set of probes is adopted for all the lattices of a given renormalized trajectory. Hence a selection criterion need to be adopted.

In this case, the optimal set has been determined looking for square systems with the smallest condition number on the finest lattice, for large flow times. It is indeed known that the signal is supposed to worsen as the flow time increases. Choosing a set of probes providing the best signal at large flow times should ensure to have good numerical estimates in the flow time region where renormalization constants are extracted (cfr. subsection (5.5.4)).

5.5.2   Simulation setup

Simulation algorithm

Numerical simulations have been carried out using a cubic lattice with periodic boundary conditions along all directions. As mentioned in section (5.2.3), the algorithm adopted alternates local Metropolis updates with global Swendsen-Wang updates of the embedded Ising model. The latter is introduced defining a set of discrete variables s_x, representing the sign of the fundamental fields

$$\phi_x = |\phi_x| s_x. \tag{5.127}$$

In terms of these variables, the scalar action takes the following form

$$S(s, |\phi|) = \sum_x \left\{ \sum_{\mu=1}^{d} \left(|\phi_x| \, |\phi_{x+\mu}| \, s_x s_{x+\mu} \right) + \frac{d + \hat{m}_0^2}{2} \phi^2 + \frac{\hat{\lambda}_0}{4!} \phi^4 \right\}. \tag{5.128}$$

with $d = 3$ for the theory under study. At fixed magnitude $| \phi_x |$, the action defines an embedded Ising model where the coupling between nearest neighbours $\beta_{x,x+\mu}$ is given by

$$\beta_{x,x+\mu} = |\phi_x| \, |\phi_{x+\mu}| \,. \tag{5.129}$$

The embedded Ising model can be updated using the Swendsen-Wang cluster algorithm where the probability to create a bond is

$$P_{x,x+\mu} = 1 - e^{-\beta_{x,x+\mu}(1+s_x s_{x+\mu})} = 1 - e^{-(|\phi_x||\phi_{x+\mu}| + \phi_x \phi_{x+\mu})}. \tag{5.130}$$

After the bond are created, the clusters are identified and flipped with 50% probability. Metropolis updates have been alternated with cluster updates with a ratio in the range $2 - 20$. The latter has been tuned depending on how close to the phase transition simulations were carried out. This algorithm is particularly effective in reducing the dynamical critical exponent near the phase transition (the authors of [63] found $z \sim 0.29$). Indeed, in this work, negligible auto-correlations have been found for every set of simulations. The Wilson flow defined in (5.67) can be integrated exactly using equation (5.68). However this is not efficient since the last equation is very expensive to evaluate. In place of the exact solution, a numerical integration routine based on the fourth order Runge-Kutta method has been implemented. The systematic error due to this approximation is very small, orders of magnitude smaller than the statistical errors.

5.5.3 Simulation parameters

As described in section (5.2.4), the theory is controlled by two relevant couplings, and can be determined by specifying the value of two physical parameters, e.g. m_R and λ_R. The continuum limit is approached when physical dimensionful parameters are small with respect the UV cut-off. Since the quartic coupling just undergoes a finite multiplicative renormalization, the bare value λ_0 can be used to set the scale of the theory. For the same reason, the dimensionless ratio

$$\rho = \frac{\lambda_0}{m_R} \tag{5.131}$$

is a RG-invariant quantity and can be used to label renormalized trajectories in the plane of relevant couplings (λ_0, m_0). The renormalized mass is defined via the renormalization condition specified in (5.3.1) and can be computed non-perturbatively using the following equation

$$(am_R)^2 = \frac{(ap)^2 \langle |\tilde{\phi}(p)|^2 \rangle}{\langle |\tilde{\phi}(0)|^2 \rangle - \langle |\tilde{\phi}(p)|^2 \rangle}, \tag{5.132}$$

where $p = (\frac{2\pi}{a}, 0, 0)$ is the smallest non-zero momentum and $\tilde{\phi}$ is the Fourier transform of the fundamental fields variables

$$\tilde{\phi}(p) = \sum_x e^{ipx} \phi(x). \tag{5.133}$$

Renormalized trajectories have been determined in the following way. The lattice spacing is changed with $\hat{\lambda}_0 = \lambda_0 a$ while the physical volume of the system $V = (L)^3$ is kept constant. At the same time, the value of the bare mass $\hat{m}_0$ is adjusted in order to keep ρ constant along the whole trajectory. In this strategy, statistical errors are generated only from the determination of the renormalized mass m_R, which can be computed with high precision[8]. Three renormalized trajectories have been determined, corresponding to $\rho = 1.5, 5, 10$ (5.8). For each trajectory, the physical volume has been kept large enough, in order to avoid finite size effects.

---

[8]In this work, the relative error on m_R has been found always smaller than 0.5%.
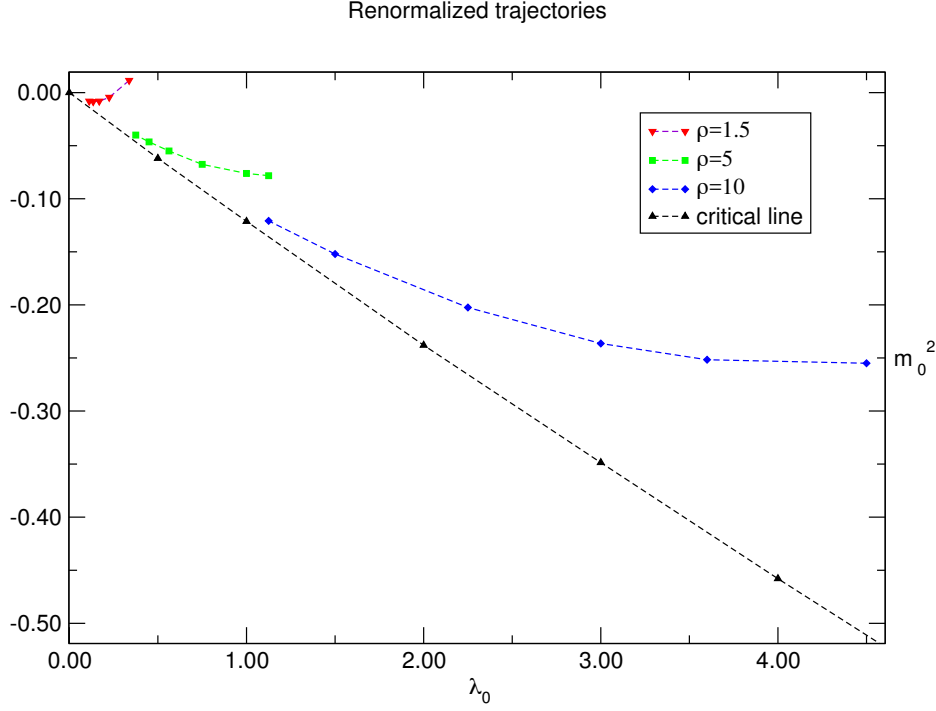
Figure 5.12: Renormalized trajectories for different values of the parameter ρ along with the critical line. Here, dashed lines are used only to guide the eye.

$\rho = 1.5$			$\rho = 5$			$\rho = 10$		
L	$\hat{\lambda}_0$	$\hat{m}_0^2$	L	$\hat{\lambda}_0$	$\hat{m}_0^2$	L	$\hat{\lambda}_0$	$\hat{m}_0^2$
16	0.3317	0.011449	16	1.1250	-0.078288	8	4.5	-0.255025
24	0.225	-0.004489	18	1.0000	-0.076176	10	3.6	-0.251703
32	0.16875	-0.0081	24	0.7500	-0.0676	12	3.0	-0.2364
40	0.13500	-0.008464	32	0.5625	-0.0549902	16	2.25	-0.2025
48	0.11250	-0.0081	40	0.4500	-0.0464402	24	1.5	-0.1521
			48	0.3750	-0.04	32	1.125	-0.120843

Table 5.8: Renormalized trajectories

5.5.4 Measurements

Simulations have been carried out for all the trajectories in (5.8)[9], using computing facilities of Plymouth and Edimburgh university. For each lattice, the observables entering in (5.125) have been measured using a blocking procedure[10] to reduce the effects of autocorrelation. Measurements

---

[9]Finest lattices $L = \{40, 48\}$ have not been included for $\rho = 1.5$ and $\rho = 5$. Notwithstanding the computing cheapness of scalar theories, these lattices required too long times to get measurements quite rapidly, and have been discarded.

[10]Depending on the lattice, each measure has been obtained averaging over a block of $100 \sim 1000$ measures

have been taken over a wide range of flow times, using several replicas[11].

$\rho = 1.5$			
L	Replicas	Meas. per replica	Block
16	160	25000	250
24	800	25000	1000
32	800	5000	1000
$\rho = 5$			
L	Replicas	Meas. per replica	Block
16	100	10000	100
18	800	5000	1000
24	160	25000	250
32	800	5000	1000
$\rho = 10$			
L	Replicas	Meas. per replica	Block
8	50	80000	80
10	400	10000	2000
12	800	25000	250
16	50	80000	80
24	200	20000	200
32	800	5000	100

Table 5.9: Summary of the statistic produced. Given a fixed value of ρ, the first column denotes the corresponding set of lattices. Second column shows the number of replicas produced for a given lattice. The total number of measurements per replica is displayed inside the third column, while the average block is specified by data in fourth column. For each replica, the number of effective measurements is obtained taking the ratio between third and fourth column.

Choice of the flow times

Numerical studies in Yang-Mills theory allowed to get an insight about the width of the flow time window.

---

[11]With replica, a copy of the same type of run (same lattice, bare parameters and flow times) but different start configuration is intended.
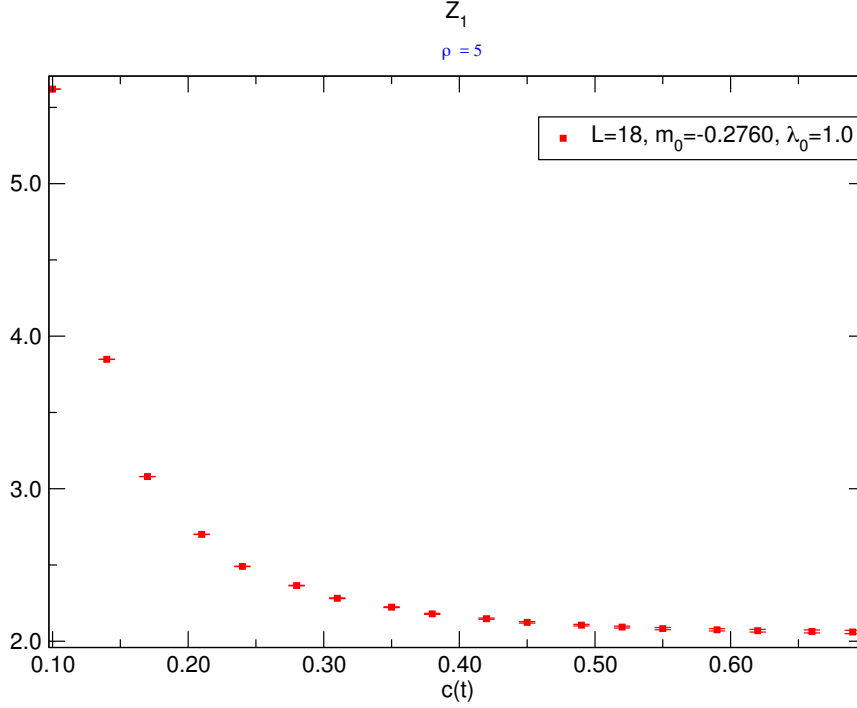
Figure 5.13: Example of how the EMT renormalization constants behave with the flow time. In this case, the constant Z_1, measured on one of the lattices of the $\rho = 5$ trajectory, has been considered. It should be noticed that data can be precisely measured over the entire range of flow times.

As already explained in (4.3.3), TWI are affected by a contact term at zero flow time, the latter being caused by the coalescence of probe and energy momentum tensor. At positive flow time, three different regions can be distinguished. The first one is a small flow time window characterized by large a^2/t artefacts, representing the remnant of the divergence at $t = 0$: these artefacts are supposed to vanish when continuum limit is approached. As the flow time increases, these effects get quite reduced and only $(a/L)^2$ artefacts are supposed to remain. Data start to vary slowly with t, and the constants $Z_{1,2,3,4}$ are still measured with good precision: this is the second region of flow times, where the values of the coefficients $Z_{1,2,3,4}$ could be extracted. Finally, a big flow time window should follow, where the solution of the system would get more and more noisy due to signal depletion. The flow time window has to be large enough to contain the first two kind of regions. The last region should be discarded, since it is reached at the cost of large simulation times and poor statistical signal. For the set of lattices in (5.8), the following window

$$c = \{0.0, 0.07, 0.10, 0.14, 0.17, 0.21, 0.24, 0.28, 0.31, 0.35, \tag{5.134}$$

$$0.38, 0.42, 0.45, 0.49, 0.52, 0.55, 0.59, 0.62, 0.66, 0.69\}, \tag{5.135}$$

$$c = \frac{\sqrt{6t}}{L} \tag{5.136}$$

represented the optimal flow-time interval for carrying out measurements in a reasonable amount of time. Here, a difference with the pure gauge case should be highlighted. Scalar theories are cheap to simulate, and allow to consider quite large flow time windows, definitely larger than the case of Yang-Mills theory. This becomes quite clear looking at figure (5.13). Here, data have been

166

measured with high precision over the entire flow time window, which proved to be more than two times larger than the one used in pure gauge.

5.6 Results

In this section, numerical results are reported. The renormalization constants $Z_{1,2,3,4}$ have been measured for all the trajectories described in (5.8). Then, their continuum limit has been checked using the following constraints

$$Z_1 = 2, \tag{5.137}$$

$$Z_2 = -1, \tag{5.138}$$

$$\frac{Z_3}{|m_0^2|} = +0.83 + \mathcal{O}(\lambda_0^2), \tag{5.139}$$

$$\frac{Z_4}{\lambda_0} = -1, \tag{5.140}$$

As an example, the $\rho = 10$ trajectory will be discussed in here in detail. Results coming from the analysis of all the trajectories will be then resumed in appendix (C).

5.6.1 $Z_{1,2,3,4}$

The renormalization constants have been measured using the method described in (5.5.1). For the $\rho = 10$ trajectory, the optimal probe set has been determined using the $L = 32$ lattice (the finest one), looking for the system with smallest condition number at large flow times. The following probes[12]

$$\hat{\Phi}_\mu^{(6)}(t,x) = \sum_\rho (\partial_{\mu S} \partial_{\rho S} \partial_{\rho S} \varphi(t,x)) \varphi^3(t,x), \tag{5.141}$$

$$\hat{\Phi}_\mu^{(7)}(t,x) = \sum_\rho (\partial_{\rho S} \partial_{\rho S} \varphi(t,x))(\partial_{\mu S} \varphi) \varphi^2(t,x), \tag{5.142}$$

$$\hat{\Phi}_\mu^{(8)}(t,x) = \sum_\rho (\partial_{\mu S} \partial_{\rho S} \varphi(t,x))(\partial_{\rho S} \varphi) \varphi^2(t,x), \tag{5.143}$$

$$\hat{\Phi}_\mu^{(9)}(t,x) = \sum_\rho (\partial_{\rho S} \varphi(t,x))(\partial_{\rho S} \varphi(t,x))(\partial_{\mu S} \varphi(t,x)) \varphi(t,x), \tag{5.144}$$

turned to be the right candidates to perform an optimized numerical analysis along the whole renormalized trajectory. Renormalization constants have been measured for all the lattices and are here displayed (figures (5.14-5.15-5.16-5.17)). A quite large time interval ($c = 0.2 \rightarrow 0.7$) has been considered, to show the behaviour of the constants in an interesting region of flow times, disregarding the values of $c < 0.2$.

---

[12]Symmetric lattice derivative has been employed, in order to avoid $\mathcal{O}(a)$ scaling violations.
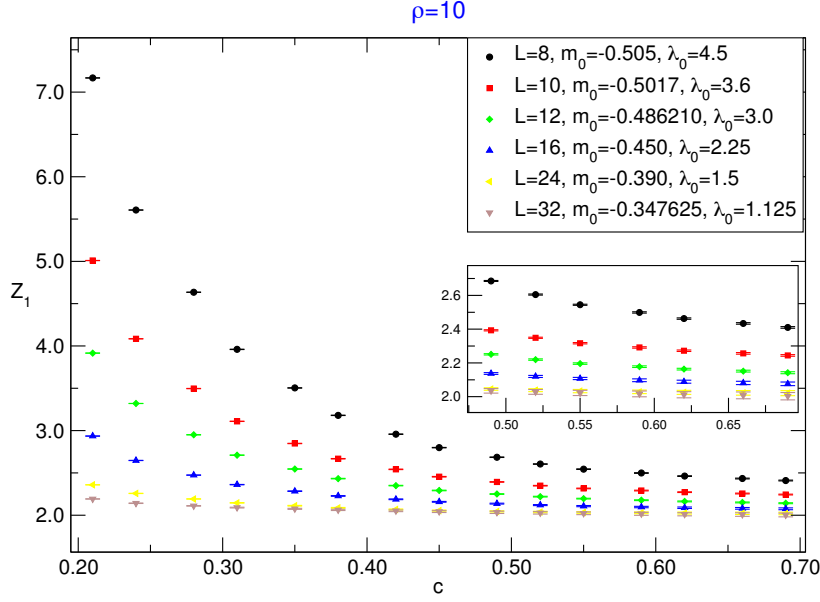
Figure 5.14: Plot of Z_1 as function of the ratio $c = \sqrt{6t}/L$. The zoomed area focuses on the flow time window where lattice artefacts should be most reduced.

Among the all constants, Z_1 proved to be the most precise quantity. It has been well measured over the entire range of flow times, even at small ones (figure (5.14)). Estimates are quite precise, and their precision remains good as the flow time increases (1% for the finest lattice at the largest flow time). This suggests that no signal depletion is affecting this constant, as opposed to what happens in pure Yang-Mills. For $c \geq 0.38$ contact terms mildly affect the measurements, especially on coarse lattices. Over the entire range of flow times data display clear continuum limit sequences, from the coarsest lattice to the finest one.

Precise measurements have been obtained also for Z_2 (figure (5.15)), even if cut-off effects seem to affect this quantity more consistently. The shape of the data signals that a^2/t effects are quite strong, especially on coarse lattices ($L = \{8, 10, 12\}$). Measurements on finer lattices ($L = \{16, 24, 32\}$) are less affected by these artefacts. However, they clearly show significant deviations from the expected continuum value, especially for $L = \{16, 24\}$. This could be caused by consistent $(a/L)^2$ effects.

Figures (5.16) and (5.17) show the two dimensionless ratios

$$r_3 = \frac{Z_3}{|m_0^2|}, \quad r_4 = \frac{Z_4}{\lambda_0}, \tag{5.145}$$

whose expected continuum values are given by (5.139) and (5.140). They have been determined with less precision than $Z_{1,2}$[13]. However, they proved to be less affected by a^2/t artefacts, especially for $c \geq 0.42$. For large flow times ($c \geq 0.52$) data show overlap within few standard deviations. This could be caused by small cut-off effects or lack of precision at large flow times. Fit procedures to extract the continuum values of $r_{3,4}$ supported the latter hypothesis.

---

[13]For both ratios, relative precision drops from 3.5% on the coarsest lattice to 26% on the finest one. In this case, the largest flow time has been considered.
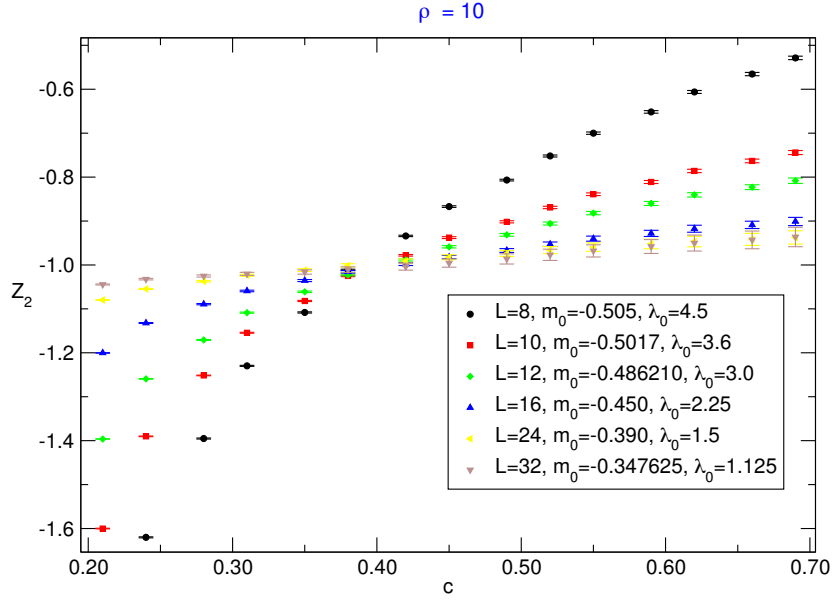
Figure 5.15: Plot of Z_2 as function of the ratio $c = \sqrt{6t}/L$.
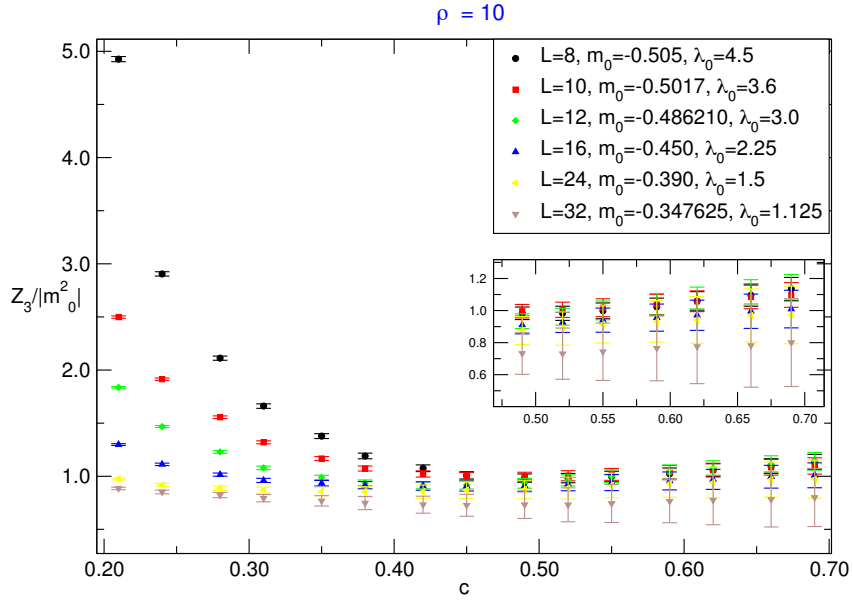
Figure 5.16: Plot of $Z_3/|m_0^2|$ as function of the ratio $c = \sqrt{6t}/L$. The zoomed area focuses on the flow time window where lattice artefacts should be most reduced.
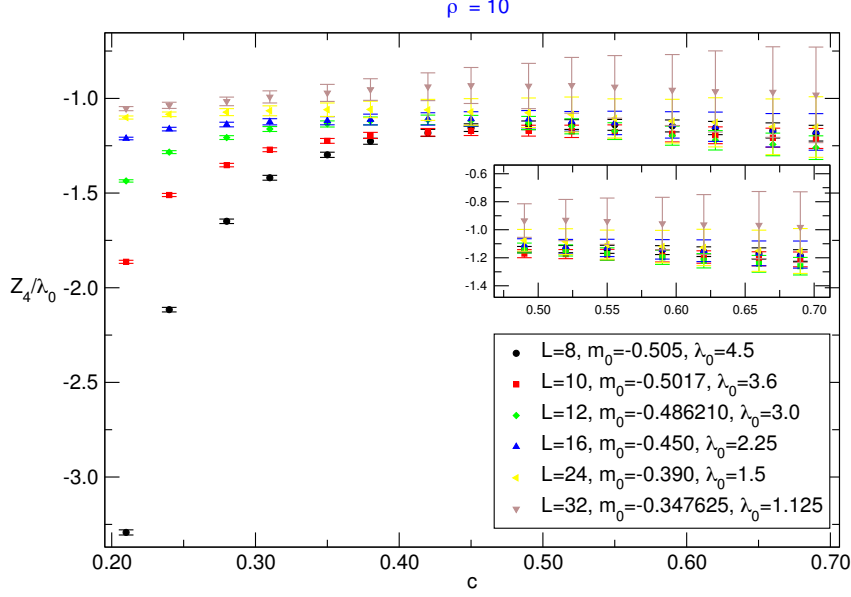
Figure 5.17: Plot of Z_4/λ_0 as function of the ratio $c = \sqrt{6t}/L$. The zoomed area focuses on the flow time window where lattice artefacts should be most reduced.

Previous plots show that a set of renormalization constants can be consistently extracted for $c \geq 0.38$. To each flow time corresponds a specific set of constants, which defines a renormalized lattice EMT such that

$$\langle \partial_{\mu\,S}(\hat{T}_{\mu\nu})_R \hat{P}_T \rangle \underset{a\to 0}{\to} \langle \partial_\mu T_{\mu\nu} P_T \rangle + \mathcal{O}(a^2), \tag{5.146}$$

The effectiveness of the method has been tested fitting the continuum values of $Z_{1,2}$, $Z_3/|m_0^2|$ and Z_4/λ_0 for the entire $c \geq 0.38$ interval. In this case, two types of polynomial fit have been considered

$$r_i = A + B\left(\frac{a}{L}\right)^2 + C\left(\frac{a}{L}\right)^4 \quad i = \{1, 2, 3, 4\},, \tag{5.147}$$

$$r_i = A + B\left(\frac{a}{L}\right)^2 \quad i = \{1, 2, 3, 4\},. \tag{5.148}$$

Where $r_{1,2} = Z_{1,2}$, and $r_{3,4}$ are just given by (5.139) and (5.140). The fits (5.147)-(5.148) have been applied to the entire set of lattices, in order to determine the size of leading $\mathcal{O}((a/L)^2)$ and higher order $\mathcal{O}((a/L)^4)$ scaling violations to continuum quantities.

As an example, fits of $r_{1,2,3,4}$ at $c = 0.45$ are shown below (figures (5.18-5.19-5.20-5.21)).

For each renormalization constant, only fit procedures with reasonable reduced χ^2 and fit parameters have been considered.

When coarse lattices are included ($L = \{8, 10\}$), Z_1 (figure (5.18)) is well described by the expansion (5.147). The reduced χ^2 varies slowly when the coarsest lattice is discarded, proving the stability of the fit. When smaller lattice subsets are considered, only equation (5.148) provides quite reliable results.

As can be seen from figure (5.18), all continuum limit extrapolations are compatible within few sigmas. Their deviations provide an insight of the systematic introduced by the expansions (5.147-5.148).

170
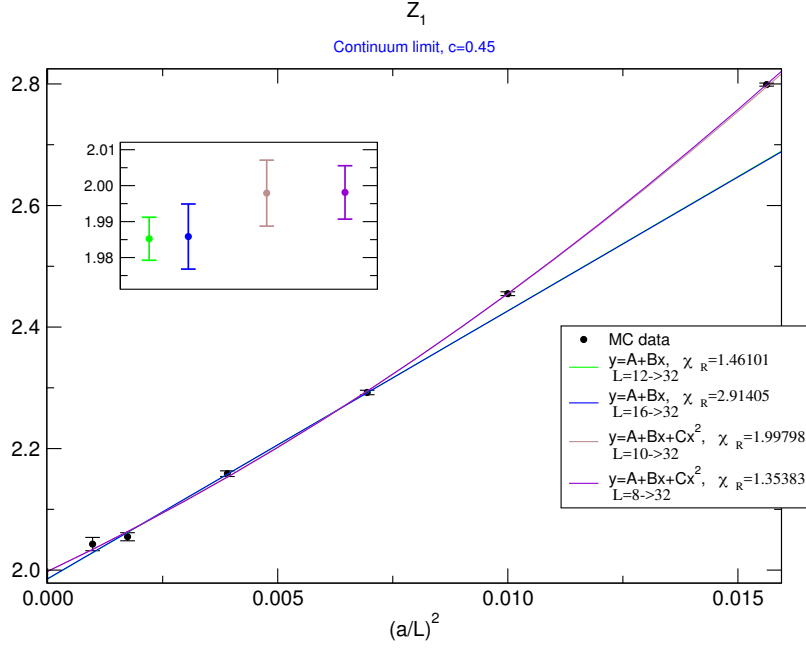
Figure 5.18: Z_1 at fixed flow time. Data have been displayed as functions of the number of lattice points. The zoomed area focuses on the $a = 0$ extrapolations.

Things are different for Z_2 (figure (5.19)). For this specific value of the flow time, a quadratic fit in $(a/L)^2$ makes sense only if the coarsest lattice $L = 8$ is considered. For other lattice subsets, this kind of expansion produced fit parameters B and C that were always compatible with zero within errors.
In this case, only linear fits of the form (5.148) provided a reasonable result[14]. This behaviour could be already hinted from figure (5.15), where, beside $L = 8$, all the data are almost overlapping at $c = 0.45$. As the flow time increases, this behaviour is expected to change, as can be seen from figure (5.15). For large enough flow times, the linear approximation is quite likely to fail, and the expansion (5.147) will have to be adopted.
Finally, fits for $Z_3/|\hat{m}_0^2|$ and $Z_4/\hat{\lambda}_0$ can be observed in figures (5.20)-(5.21).
For all the lattices of the $\rho = 10$ trajectory, the expansion (5.147) proved to be not good for describing the dependence of these ratios on the lattice spacing. Indeed, both slope and curvature coefficients result zero within error bars. This is surely caused both by data overlap in the interesting flow time region (cfr. figures (5.16)-(5.17)) as well as not so small errors on fine lattices.
In this case, a linear expansion in $(a/L)^2$ is preferred to study how $r_{3,4}$ approach the continuum limit.
Even if the intercept A can be estimated with good precision, the slope coefficient is not determined quite precisely. Indeed, figures (5.20)-(5.21) suggest that data could be fitted almost with a constant relation. Again, this is probably caused by data overlap and lack of enough numerical precision on fine lattices. To obtain a better knowledge of $\mathcal{O}(a^2)$ effects in the scaling region, the error bars would need to be reduced, especially on fine lattices[15].

---

[14]It should be said that on fine lattices ($16 \to 32$) a fit to a constant would be more appropriate (the slope B is zero within the errors. This is sourced by lack of precision on fine lattices).

[15]At flow times smaller than $c = 0.45$, non zero values of the slope can still be estimated when the full set of lattices is considered for the fit procedure. Things gets worse when smaller lattice subsets are adopted.
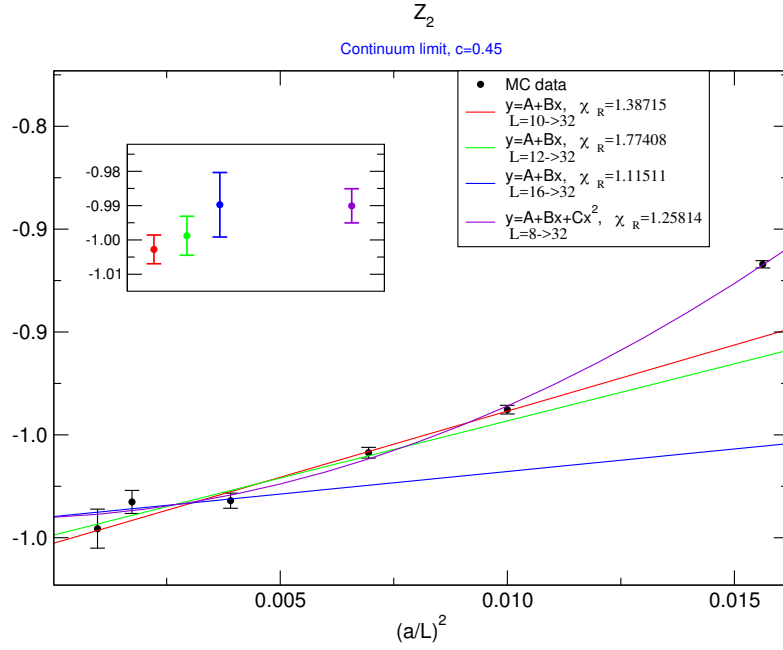
Figure 5.19: Z_2 at fixed flow time. Data have been displayed as functions of the number of lattice points. The zoomed area focuses on the $a = 0$ extrapolations.
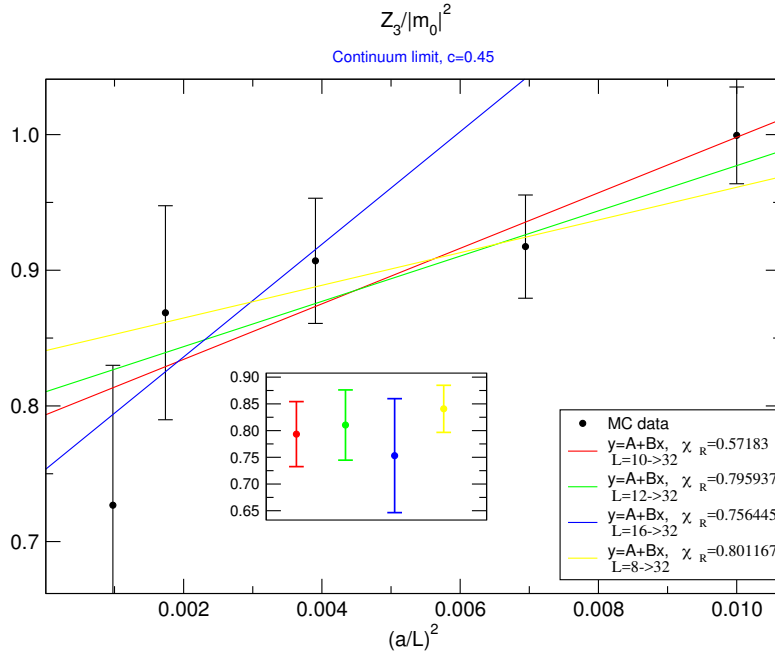
Figure 5.20: $Z_3/|m_0^2|$ at fixed flow time. Data have been displayed as functions of the number of lattice points. The zoomed area focuses on the $a = 0$ extrapolations.
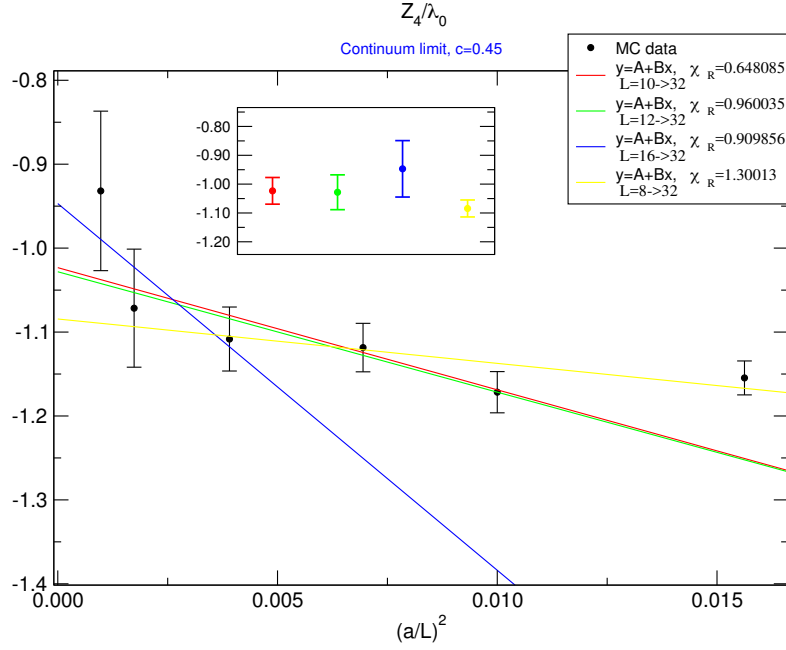
Figure 5.21: Z_4/λ_0 at fixed flow time. Data have been displayed as functions of the number of lattice points. The zoomed area focuses on the $a = 0$ extrapolations.

Continuum limit extrapolations of $Z_{1,2}$, $Z_3/|\hat{m}_0^2|$ and $Z_4/\hat{\lambda}_0$ are reported in figures (5.22-5.23-5.24-5.25). Each plot shows the estimates of continuum values as functions of the flow time, for different types of fitting procedure. Only fits with a reasonable χ^2 have been considered.

Continuum extrapolations of Z_1 coming from different fits are all compatible within few standard deviations (figure (5.22)). More important, they are compatible with the constraint (5.137). The quadratic fit (5.147) applied to the largest lattice set ($L = 8 \to 32$) proved to be effective for almost the entire range of flow times. The statement holds also for the linear fit procedure applied to the smallest lattice set ($L = 16 \to 32$). Small deviations from the expected result appear when a linear fit is applied to the ($L = 12 \to 32$) subset. Deviations enlarges when coarser lattices are included ($L = 10 \to 32$). However, also the corresponding χ^2 grows ($\chi^2 \geq 2, \chi^2 \geq 3$) signalling that the quality of the fit is worsening.

A less nice behaviour is obtained for Z_2 (figure (5.22)). At large flow times, some of the extrapolations deviate from the expected continuum value of at least two standard deviation. This could be caused by still large cut-off effects, as could be also argued looking at figure (5.15). As mentioned before, quadratic fits become important when the flow time increases. At small flow times, data are quite overlapped, and linear fits on fine lattice sets becomes less reliable, as it has already been explained for $Z_3/|\hat{m}_0^2|$ and $Z_4/\hat{\lambda}_0$.

Continuum estimates of $Z_3/|\hat{m}_0^2|$ and $Z_4/\hat{\lambda}_0$ are displayed in figures (5.24-5.25). Both quantities can be estimated with linear fits. At small time, the latter proved to be more effective, especially including coarse lattices. At large flow times, linear fits become less reliable, due to data overlap. Probably, more statistics is needed to reduce the error bars. All results coming from different fits are all compatible with their expected continuum value.

173
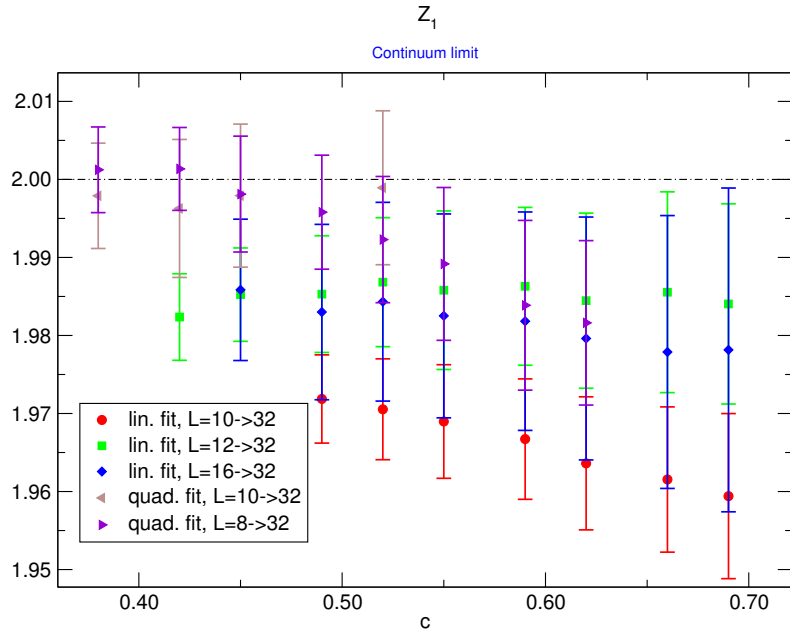
Figure 5.22: Continuum extrapolations of Z_1 as functions of the flow time.
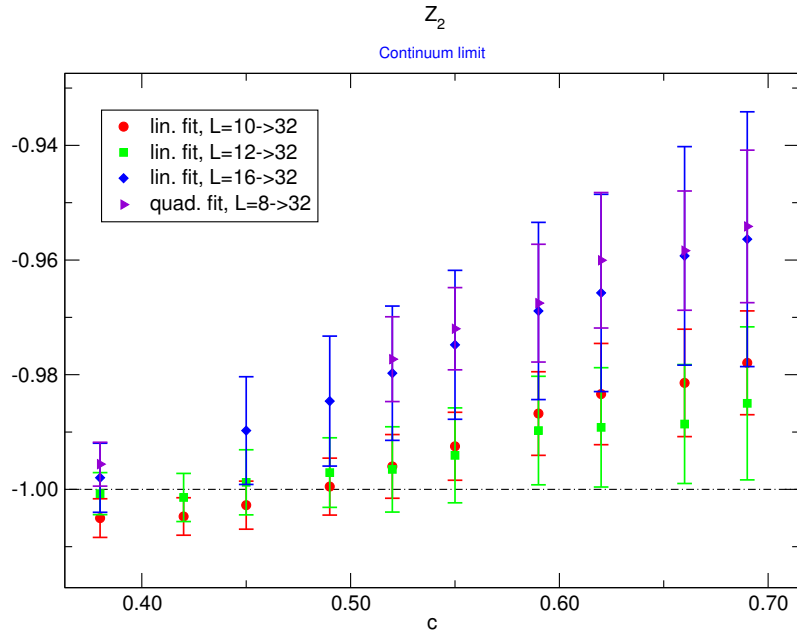
Figure 5.23: Continuum extrapolations of Z_2 as functions of the flow time.
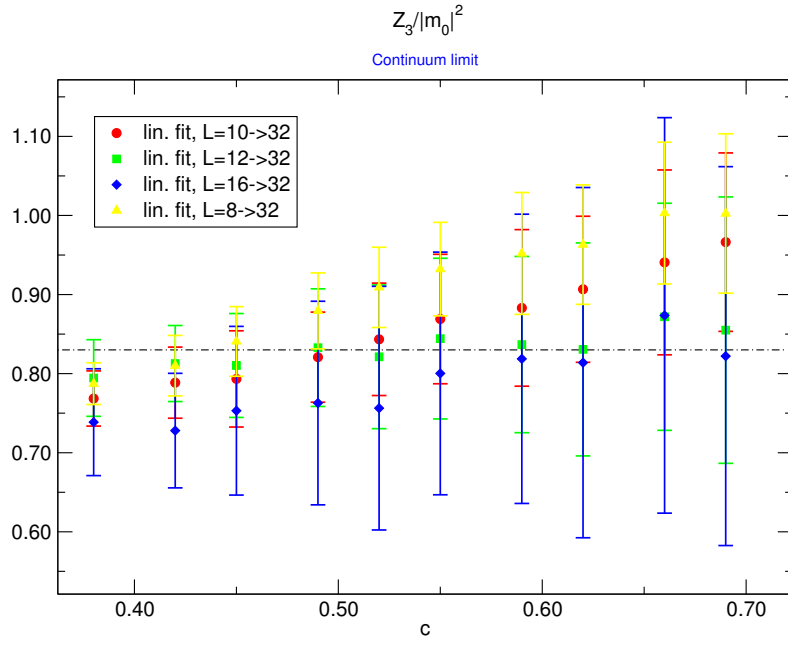
Figure 5.24: Continuum extrapolations of $Z_3/|m_0^2|$ as functions of the flow time.
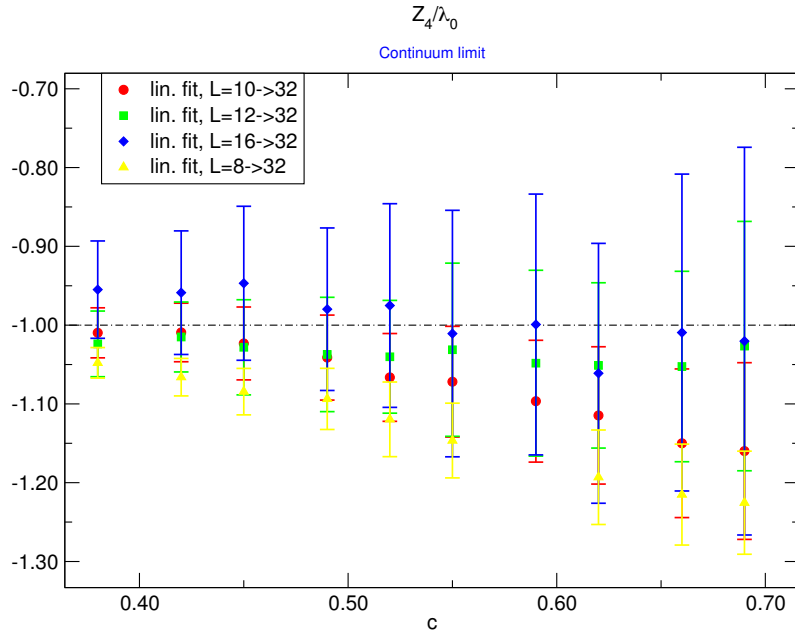
Figure 5.25: Continuum extrapolations of Z_4/λ_0 as functions of the flow time.

Chapter 6

Conclusions

In this work, a new method to numerically determine the lattice renormalized energy-momentum tensor has been tested. The method is based on probing translation and dilatation WI with operators built with the gradient flow. The natural UV finiteness of these operators allow the new WI to be free from any kind of contact term. The absence of the latter makes this set of identities a potentially good candidate to renormalize the EMT in non perturbative numerical studies[1]. The method has been initially devised only for pure gauge theories [34], while in this work it has been extended to the specific case of a $\lambda\phi^4$ theory in 3 dimensions[2].

The EMT is a fundamental quantity for different aspects of particle physics. It is the generator of Poincaré, dilatation and conformal transformations. It thus carries information concerning physical quantities associated with those spacetime symmetries. When finite temperature studies are concerned, expectation values of the EMT provide direct access to thermodynamic quantities, like energy, pressure and entropy density. These quantities are necessary to determine the equation of state of hot, dense systems, like the *quark-gluon plasma* (QGP). This specific state of matter describes the early stages of the universe and is currently under the lens of perturbative and non perturbative studies[3]. Also in this case, the EMT momentum tensor has a key role in providing useful informations; indeed, two-point correlators of this operator yield quantitative estimates of the sheer viscosity, a transport coefficient used to characterize the fluid dynamics of the QGP.

In the last four decades, several attempts have been made to extend the knowledge of fundamental particles and their interactions beyond the current Standard Model (SM). Many different *beyond Standard Model* (BSM) theories have been proposed, whose low energy limit could be recast into the actual SM. Some of these BSM formulations include a new, strongly interacting sector that calls for an IR fixed point inside its phase diagram [67]. To precisely locate such fixed point, non perturbative studies are needed. Hence, the lattice formulation is necessary to characterize these type of BSM theories. In the last years, the location of the IR fixed point has been investigated using two different numerical approaches, based on measuring the running coupling or the spectrum of the theory.

Knowledge of the fully non perturbative EMT provides a third alternative method. The trace of the EMT is the order parameter of dilatation and conformal symmetry. Hence, it can be used to investigate the restoration of these symmetries, to which a fixed point of the RG should correspond. Thus, there are enough motivations to compute the EMT with the lattice regularization, a most well established, non perturbative formulation of quantum field theory.

---

[1] Actually, this new type of identities allow to renormalize the original translation and dilatation WI of the theory.

[2] In collaboration with L. Del Debbio, S. Ehret, R. Pellegrini and Antonio Rago.

[3] The QGP can be actually reproduced in heavy ion collision experiments.

In this work, the renormalized EMT has been determined within two different theoretical frameworks: a $SU(3)$ Yang-Mills theory and a scalar $\lambda\phi^4$ theory in 3 dimensions.

In pure Yang Mills theory, the renormalized EMT is characterized by a mixing of three operators[4]. To each operator corresponds a (finite) renormalization constant that needs to be determined. Moreover, a multiplicative factor Z_δ, coupled to the operator that generates naïvely discretized translations, has to be fixed. All these quantities have been numerically determined using WI probed by observables built along the flow. In this case, the method provides reasonably precise results only at the price of large computation times, especially when fine lattices are considered. To avoid a^2/t artefacts, probes should be flowed at quite large flow times. However, at these times, the signal worsen and a larger statistics is needed to compensate for signal depletion. Long computation times are caused by the evolution of gauge fields along the flow, and can be reduced only by accessing to more powerful computing facilities[5]. This technical issue could seriously compromise the application of the method to more realistic theories, like those including fermionic matter.[6] Numerical results have been compared with the renormalization constants measured using shifted boundary conditions. In this case, a discrepancy between the two methods has been detected. To better understand the source of such discrepancy, further theoretical, and numerical, studies are needed.

A different outcome is obtained when the scalar theory in 3 dimensions is considered. In this case, the renormalized EMT is characterized by four different renormalization constants, and no multiplicative Z_δ factor has to be determined. The only non trivial renormalization is encoded in the constant coupled to the ϕ^2 operator. This result is sourced by the superrenormalizability of the theory, and provides quite stringent constraints to be used for testing the method. Scalar theories are really cheap to simulate, and allow to accumulate considerably large statistics in small amounts of time. This feature allowed to measure the renormalization constants with good numerical precision. Their values at finite lattice spacing have been determined for three different renormalized trajectories. For each trajectory, continuum extrapolations have been checked with perturbative results, supporting the correctness of the method.
The scalar theory is physically less interesting than Yang-Mills theory. However, it proves to be a good model for precisely checking the validity of the adopted method. Moreover, it gives room for other interesting applications.

The first one is directly related to the investigation of BSM theories. In 3 dimensions, the scalar theory exhibits an IR fixed point, called Wilson Fisher fixed point. The latter could be located through a numerical strategy based on the renormalized EMT. Being computationally cheap, the scalar theory provides a unique framework in which this new method can be thoroughly studied. From this first application, useful informations about finite size effects and signal-to-noise ratio could be extracted and used when physically interesting theory are concerned.

Another interesting application comes from the study of the early Universe, the period usually associated with inflation, using holographic models. Within the holographic framework, the early Universe is described by a three dimensional QFT. Conventional inflation is included in this framework as s strongly coupled quantum field theory. Hence, a lattice formulation of such theory could provide quantitative knowledge about the inflation period. In its simplest, not-fully realistic form, the inflation is represented by a scalar $\lambda\phi^4$ theory. In this case, knowledge of the renormalized EMT provides access to physical quantities (power spectrum) that could be directly compared with experimental results.

---

[4]This is true whenever the VEV of the operator is subtracted.

[5]Or faster algorithms for evolving the gauge fields.

[6]Among the all physically interesting theories, pure Yang Mills is supposed to be the cheapest one to simulate.

Appendix A

Bulk EMT

The following flow equation

$$S_{fl} = -2 \int_0^\infty dt \int d^d x \, \text{tr}\{L_\mu(G_{0\mu} - D_\nu G_{\nu\mu})\}, \tag{A.1}$$

$$G_{0\mu} = \dot{B}_\mu - D_\mu B_0, \tag{A.2}$$

is invariant under local gauge transformations in $(D+1)$ dimensions. Under the local variations

$$\delta_\alpha B_M = \alpha_R G_{RM}, \tag{A.3}$$

$$\delta_\alpha L_\mu = \alpha D_R L_\mu, \tag{A.4}$$

the action changes according to

$$\delta S_{fl} = -2 \int_0^\infty dt \int d^d x \, \text{tr}\{\alpha_R D_R L_\mu(G_{0\mu} - D_\nu G_{\nu\mu}) + L_\mu[\delta_\alpha(G_{0\mu}) - \delta_\alpha(D_\nu G_{\nu\mu})]\}. \tag{A.5}$$

The first term in equation (A.5) can be written as

$$
\begin{aligned}
\text{tr}\{\alpha_R D_R L_\mu(G_{0\mu} - D_\nu G_{\nu\mu})\} = \text{tr}\{ & -\partial_R \alpha_R L_\mu(G_{0\mu} - D_\nu G_{\nu\mu}) \\
& - \alpha_R L_\mu \partial_R(G_{0\mu} - D_\nu G_{\nu\mu}) \\
& - \alpha_R[L_\mu, B_R](G_{0\mu} - D_\nu G_{\nu\mu})\},
\end{aligned}
\tag{A.6}
$$

up to a total derivative that does not contribute to the integral in δS_{fl}. Then, the following identity can be used

$$\text{tr}\{[A,B]C\} = \text{tr}\{A[B,C]\}, \tag{A.7}$$

to rewrite equation (A.6) as

$$
\begin{aligned}
\text{tr}\{\alpha_R D_R L_\mu(G_{0\mu} - D_\nu G_{\nu\mu})\} = \text{tr}\{ & -\partial_R \alpha_R L_\mu(G_{0\mu} - D_\nu G_{\nu\mu}) \\
& - \alpha_R L_\mu D_R(G_{0\mu} - D_\nu G_{\nu\mu})\}.
\end{aligned}
\tag{A.8}
$$

The first line in (A.8) does not contribute inside correlation functions, because the integration over the Lagrange multiplier imposes the flow equation. As a consequence, it is legitimate to write

$$\text{tr}\{\alpha_R D_R L_\mu(G_{0\mu} - D_\nu G_{\nu\mu})\} = \text{tr}\{-\alpha_R L_\mu D_R(G_{0\mu} - D_\nu G_{\nu\mu})\}. \tag{A.9}$$

The variations of the second term in (A.5) are

- $\delta_\alpha(G_{0\mu})$

$$\begin{aligned}
\delta_\alpha(G_{0\mu}) &= D_0 \delta_\alpha B_\mu - D_\mu \delta_\alpha B_0 \\
&= \dot{\alpha}_R G_{R\mu} - \partial_\mu \alpha_R G_{R0} + \alpha_R (D_0 G_{R\mu} + D_\mu G_{0R}) \\
&= \dot{\alpha}_R G_{R\mu} - \partial_\mu \alpha_R G_{R0} + \alpha_R D_R G_{0\mu},
\end{aligned} \tag{A.10}$$

where the Bianchi Identity

$$D_R G_{MN} + D_M G_{NR} + D_N G_{RM} = 0 \tag{A.11}$$

has been used.

- $\delta_\alpha(D_\nu G_{\nu\mu})$

$$\delta_\alpha(D_\nu G_{\nu\mu}) = D_\nu \delta_\alpha G_{\nu\mu} + \alpha_R [G_{R\nu}, G_{\nu\mu}], \tag{A.12}$$

where

$$\begin{aligned}
\delta_\alpha G_{\nu\mu} &= D_\nu \delta_\alpha B_\mu - D_\mu \delta_\alpha B_\nu \\
&= \partial_\nu \alpha_R G_{R\mu} - \partial_\mu \alpha_R G_{R\nu} + \alpha_R (D_\nu G_{R\mu} + D_\mu G_{\nu R}) \\
&= \partial_\nu \alpha_R G_{R\mu} - \partial_\mu \alpha_R G_{R\nu} + \alpha_R D_R G_{\nu\mu}.
\end{aligned} \tag{A.13}$$

Using this result, and the following identity

$$(D_N D_R - D_R D_N) G_{NM} = [G_{NR}, G_{NM}], \tag{A.14}$$

it can be shown that

$$\begin{aligned}
\delta_\alpha(D_\nu G_{\nu\mu}) &= \partial_\nu \partial_\nu \alpha_R G_{R\mu} - \partial_\nu \partial_\mu \alpha_R G_{R\nu} \\
&\quad + \partial_\nu \alpha_R (D_R G_{\nu\mu} + D_\nu G_{R\mu}) - \partial_\mu \alpha_R D_\nu G_{R\nu} \\
&\quad + D_R D_\nu G_{\nu\mu},
\end{aligned} \tag{A.15}$$

and

$$\begin{aligned}
\mathrm{tr}\{L_\mu[\delta_\alpha(G_{0\mu}) - \delta_\alpha(D_\nu G_{\nu\mu})]\} = \mathrm{tr}\{L_\mu[&-\partial_\nu \partial_\nu \alpha_R G_{R\mu} + \partial_\nu \partial_\mu \alpha_R G_{R\nu} \\
&- \partial_\nu \alpha_R (D_R G_{\nu\mu} + D_\nu G_{R\mu}) + \partial_\mu \alpha_R D_\nu G_{R\nu} \\
&+ \dot{\alpha}_R G_{R\mu} - \partial_\mu \alpha_R G_{R0} + \alpha_R D_R (G_{0\mu} - D_\nu G_{\nu\mu})]\}.
\end{aligned} \tag{A.16}$$

The last term on the last line cancels exactly equation (A.9).

Collecting all the pieces together, the variation of the flow action takes the following form

$$\begin{aligned}
\delta S_{fl} = -2 \int_0^\infty dt \int d^d x\, \mathrm{tr}\{L_\mu[&-\partial_\nu \partial_\nu \alpha_R G_{R\mu} + \partial_\nu \partial_\mu \alpha_R G_{R\nu} \\
&- \partial_\nu \alpha_R (D_R G_{\nu\mu} + D_\nu G_{R\mu}) \\
&+ \partial_\mu \alpha_R (D_\nu G_{R\nu} - G_{R0}) \\
&+ \dot{\alpha}_R G_{R\mu}]\}.
\end{aligned} \tag{A.17}$$

The third line can still be manipulated imposing the flow equation

$$\begin{aligned}
\partial_\mu \alpha_R L_\mu (D_\nu G_{R\nu} - G_{R0}) &= \partial_\mu \alpha_0 L_\mu D_\nu G_{0\nu} - \partial_\mu \alpha_\sigma L_\mu (D_\nu G_{\nu\sigma} - G_{0\sigma}) \\
&= -\partial_\mu \alpha_R \delta_{R0} L_\mu D_\nu G_{\nu 0},
\end{aligned} \tag{A.18}$$

$$\tag{A.19}$$

giving the variation of the action as

$$\delta S_{fl} = -2\int_0^\infty dt \int d^d x \text{tr}\{L_\mu[\dot{\alpha}_R G_{R\mu} - \partial_\mu \alpha_R \delta_{R0} D_\nu G_{\nu 0}$$
$$- \partial_\nu \partial_\nu \alpha_R G_{R\mu} + \partial_\nu \partial_\mu \alpha_R G_{R\nu}$$
$$- \partial_\nu \alpha_R \underbrace{(D_R G_{\nu\mu} + D_\nu G_{R\mu}}_{2D_\nu G_{R\mu} - D_\mu G_{R\nu}})]\}. \tag{A.20}$$

Using integration by parts and the formula (A.7) one finds

$$-2\int_0^\infty dt \int d^d x \text{tr}\{L_\mu[-\partial_\nu \partial_\nu \alpha_R G_{R\mu} + \partial_\nu \partial_\mu \alpha_R G_{R\nu} - \partial_\nu \alpha_R (2D_\nu G_{R\mu} - D_\mu G_{R\nu})]\} =$$
$$= -2\int_0^\infty dt \int d^d x \partial_\mu \alpha_R \text{tr}\{-L_\nu D_\mu G_{R\nu} + D_\mu L_\nu G_{R\nu} + D_\nu L_\nu G_{R\mu}\}, \tag{A.21}$$

and finally[1]

$$\delta S_{fl} = -2\int_0^\infty dt \int d^d x[\dot{\alpha}_R \text{tr}\{L_\mu G_{R\mu}\}$$
$$+ \partial_\mu \alpha_R \text{tr}\{-L_\nu D_\mu G_{R\nu} + D_\mu L_\nu G_{R\nu} + D_\nu L_\nu G_{R\mu} - \delta_{R0} D_\nu G_{\nu 0}\}]$$
$$= \int_0^\infty dt \int d^d x \tilde{T}_{MR} \partial_M \alpha_R \tag{A.22}$$

The components of the bulk EMT are then given by

$$\tilde{T}_{0R} = -2\text{tr}\{L_\mu G_{R\mu}\}, \tag{A.23}$$
$$\tilde{T}_{\mu R} = 2\text{tr}\{L_\nu D_\mu G_{R\nu}\} - 2\text{tr}\{D_\mu L_\nu G_{R\nu}\} - 2\text{tr}\{D_\nu L_\nu G_{\mu R}\} + 2\delta_{R0}\text{tr}\{L_\mu D_\nu G_{\nu 0}\}. \tag{A.24}$$

---

[1] A $\nu \leftrightarrow \mu$ redefinition is necessary for some of the terms.

Appendix B

Improved scalar EMT in 3 dimensions

In their work, Coleman et al. [17] shows that the scalar field theory is dilatation invariant if the following condition is satisfied

$$- D\mathcal{L} + d_\varphi \frac{\partial \mathcal{L}}{\partial \varphi} \varphi + (1 + d_\varphi)\Pi_\mu \partial_\mu \varphi = 0, \tag{B.1}$$

where $\mathcal{L}$ is the classical Lagrangian density, $\Pi_\mu = \frac{\partial \mathcal{L}}{\partial(\partial_\mu \varphi)}$ and $d_\varphi = [\varphi]$. Usually, a massless action of the form

$$S = \int d^D x \left[\frac{1}{2} \partial_\mu \varphi \partial_\mu \varphi + \frac{g}{\alpha} \varphi^{\frac{2D}{D-2}} \right], \tag{B.2}$$

satisfies the condition (B.1): the corresponding dilatation current is given by

$$D^\mu = x_\rho T^{\mu\rho} + V^\mu, \tag{B.3}$$

where $V^\mu = d_\varphi \Pi_\mu \varphi$ is the so called field virial: the conservation law of the current is

$$\partial_\mu D^\mu = T^\mu_\mu + \partial_\mu V^\mu. \tag{B.4}$$

As already explained in (2.4), if $V^\mu = \partial_\alpha \sigma^{\alpha\mu}$, an improved EMT can be built to relate conservation of dilatation current to the cancellation to the trace of such EMT

$$\Theta_{\mu\nu} = T_{\mu\nu} + \frac{1}{2} \partial^\lambda \partial^\rho X_{\lambda\rho\mu\nu}, \tag{B.5}$$

where

$$X_{\lambda\rho\mu\nu} = \delta_{\lambda\rho}\sigma^+_{\mu\nu} - \delta_{\lambda\mu}\sigma^+_{\nu\rho} - \delta_{\lambda\nu}\sigma^+_{\mu\rho} + \delta_{\mu\nu}\sigma^+_{\lambda\rho} - \frac{1}{3}\delta_{\lambda\rho}\delta_{\mu\nu}\sigma^+_{\alpha\alpha} + \frac{1}{3}\delta_{\lambda\mu}\delta_{\nu\rho}\sigma^+_{\alpha\alpha}, \tag{B.6}$$

and

$$\sigma^\pm_{\mu\nu} = \frac{1}{2}(\sigma_{\mu\nu} \pm \sigma_{\nu\mu}). \tag{B.7}$$

In this case, the field virial has the following form

$$V^\mu = d_\varphi \partial^\mu \varphi \varphi = \partial_\alpha \left(\frac{d_\varphi}{2} \delta_{\mu\alpha} \varphi^2 \right), \tag{B.8}$$

which means that it is possible to build the following improved tensor $\Theta_{\mu\nu}$

$$\Theta_{\mu\nu} = T_{\mu\nu} + \frac{d_\varphi}{2} \left(1 - \frac{D}{6} \right) \left[\delta_{\mu\nu}\partial^2 - \partial_\mu \partial_\nu \right] \varphi^2. \tag{B.9}$$

However, this kind of improvement works only for $D = 3$ and $D = 4$; indeed, taking equation (B.5) and plugging it inside eq (B.4), one obtains

$$\partial_\mu V^\mu = \Theta_\mu^\mu + \frac{d_\varphi}{2}\left[1 - \left(1 - \frac{D}{6}\right)(D-1)\right]\partial^2\varphi, \tag{B.10}$$

that is

$$\left[1 - \left(1 - \frac{D}{6}\right)(D-1)\right] = 0 \rightarrow D = \{3, 4\}. \tag{B.11}$$

Only two solutions are admitted for D: to each of these solutions corresponds a specific improved EMT

$$T^{\mu\rho}(x) = \partial^\mu\varphi\partial^\rho\varphi - \delta^{\mu\rho}\mathcal{L} - \frac{1}{6}\left[\partial^\mu\partial^\rho - \delta^{\mu\rho}\Box\right]\varphi^2 \quad, \quad D = 4, \tag{B.12}$$

$$T^{\mu\rho}(x) = \partial^\mu\varphi\partial^\rho\varphi - \delta^{\mu\rho}\mathcal{L} - \frac{1}{8}\left[\partial^\mu\partial^\rho - \delta^{\mu\rho}\Box\right]\varphi^2 \quad, \quad D = 3 \tag{B.13}$$

Appendix C

Numerical results for $\lambda\phi^4$ theory

C.0.1 Results: $\rho = 10$

Z_1

$A + Bx : 8- > 32$			
c	A	B	χ^2_R
0.38	1.9028(27)	80.3(3)	153.51
0.42	1.9187(31)	65.4(3)	78.39
0.45	1.9298(36)	54.8(3)	40.99
0.49	1.9378(40)	47.2(4)	21.21
0.52	1.9419(47)	41.9(4)	13.10
0.55	1.9453(54)	38.0(5)	8.12
0.59	1.9476(55)	35.0(5)	5.17
0.62	1.9485(58)	32.7(5)	3.71
0.66	1.9502(60)	30.7(6)	2.71
0.69	1.9500(69)	29.3(6)	2.08

$A + Bx + Cx^2 : 8- > 32$				
c	A	B	C	χ^2_R
0.38	2.0012(55)	51.2(13)	1547(64)	1.82
0.42	2.0013(53)	41.5(14)	1261(72)	1.79
0.45	1.9981(74)	35.8(17)	991(84)	1.35
0.49	1.9958(73)	31.6(17)	804(84)	1.08
0.52	1.9923(81)	28.7(18)	677(92)	1.02
0.55	1.9892(98)	26.7(21)	569(104)	1.23
0.59	1.9839(109)	25.6(23)	478(111)	1.28
0.62	1.9816(105)	24.3(22)	418(110)	1.47
0.66	1.9765(114)	24.1(26)	334(134)	1.53
0.69	1.9717(131)	24.2(28)	245(133)	1.59

$A + Bx : 10- > 32$			
c	A	B	χ^2_R
0.38	1.9607(38)	70.0(5)	17.16
0.42	1.9667(46)	57.0(6)	9.01
0.45	1.9706(44)	47.9(6)	5.74
0.49	1.9719(57)	41.7(7)	3.86
0.52	1.9705(65)	37.4(8)	3.57
0.55	1.9690(73)	34.2(9)	3.37
0.59	1.9667(77)	32.0(10)	2.88
0.62	1.9636(85)	30.4(11)	2.78
0.66	1.9615(93)	29.0(12)	2.54
0.69	1.9594(106)	28.1(13)	2.29

$A + Bx + Cx^2 : 10- > 32$				
c	A	B	C	χ^2_R
0.38	1.9979(68)	52.9(25)	1402(202)	2.50
0.42	1.9963(88)	44.0(33)	1058(261)	2.47
0.45	1.9979(92)	36.1(31)	955(236)	2.00
0.49	1.9952(109)	31.5(38)	818(295)	1.60
0.52	1.9989(99)	25.4(38)	958(310)	1.22
0.55	2.0002(117)	21.7(42)	992(331)	1.11
0.59	1.9977(149)	19.4(56)	992(439)	0.84
0.62	1.9961(134)	17.2(46)	1033(362)	0.73
0.66	2.0003(160)	13.9(54)	1176(406)	0.62
0.69	1.9967(199)	13.7(63)	1096(462)	0.59

$A + Bx : 12->32$			
c	A	B	χ^2_R
0.38	1.9783(46)	65.2(9)	4.96
0.42	1.9824(55)	53.0(10)	2.43
0.45	1.9852(60)	44.2(11)	1.46
0.49	1.9853(75)	38.3(14)	0.85
0.52	1.9868(83)	33.6(15)	0.54
0.55	1.9858(102)	30.2(17)	0.40
0.59	1.9863(101)	27.6(18)	0.22
0.62	1.9845(112)	25.7(19)	0.13
0.66	1.9855(129)	23.8(21)	0.10
0.69	1.9840(128)	22.8(22)	0.07

$A + Bx + Cx^2 : 12->32$				
c	A	B	C	χ^2_R
0.38	1.9995(89)	51.9(52)	1532(594)	5.08
0.42	1.9904(100)	48.4(54)	490(607)	4.17
0.45	1.9877(119)	42.9(65)	139(733)	2.86
0.49	1.9819(139)	40.8(76)	-304(858)	1.70
0.52	1.9861(143)	34.0(77)	-51(857)	1.06
0.55	1.9806(183)	34.0(101)	-434(1143)	0.63
0.59	1.9751(211)	33.8(112)	-667(1234)	0.36
0.62	1.9787(231)	29.8(122)	-455(1346)	0.14
0.66	1.9795(217)	27.2(120)	-365(1347)	0.09
0.69	1.9768(256)	26.8(155)	-429(1772)	0.02

$A + Bx : 16->32$			
c	A	B	χ^2_R
0.38	1.9879(73)	61.2(23)	6.32
0.42	1.9870(75)	51.1(24)	4.52
0.45	1.9858(91)	44.1(30)	2.91
0.49	1.9830(112)	39.2(34)	1.58
0.52	1.9843(127)	34.6(40)	0.98
0.55	1.9825(131)	31.7(41)	0.56
0.59	1.9818(140)	29.4(48)	0.27
0.62	1.9796(156)	27.9(51)	0.11
0.66	1.9779(175)	26.8(56)	0.07
0.69	1.9782(207)	25.2(67)	0.01

Z_2

$A + Bx : 8->32$			
c	A	B	χ^2_R
0.38	-1.0201(21)	0.3(2)	16.25
0.42	-1.0230(22)	5.4(2)	16.12
0.45	-1.0233(27)	9.7(2)	15.09
0.49	-1.0240(31)	13.5(3)	14.86
0.52	-1.0245(34)	17.0(3)	14.28
0.55	-1.0242(42)	20.3(4)	14.34
0.59	-1.0259(54)	23.5(5)	14.57
0.62	-1.0267(55)	26.3(5)	14.62
0.66	-1.0304(57)	29.1(5)	14.60
0.69	-1.0339(59)	31.6(5)	14.91

$A + Bx + Cx^2 : 8->32$				
c	A	B	C	χ^2_R
0.38	-0.9956(38)	-6.3(9)	339(43)	1.19
0.42	-0.9924(41)	-2.4(9)	394(48)	1.14
0.45	-0.9901(50)	1.1(12)	434(58)	1.26
0.49	-0.9843(58)	3.5(14)	501(69)	1.53
0.52	-0.9773(74)	5.3(17)	582(81)	2.10
0.55	-0.9720(72)	7.3(16)	645(80)	2.71
0.59	-0.9675(103)	9.0(22)	718(105)	2.83
0.62	-0.9600(118)	9.8(25)	817(115)	3.17
0.66	-0.9584(104)	11.4(25)	876(125)	3.41
0.69	-0.9541(133)	11.9(30)	980(149)	3.37

$A + Bx : 10-> 32$			
c	A	B	χ^2_R
0.38	-1.0050(34)	-2.1(4)	2.58
0.42	-1.0047(33)	2.5(4)	1.94
0.45	-1.0028(42)	6.4(5)	1.39
0.49	-0.9995(50)	9.8(6)	1.17
0.52	-0.9960(56)	12.8(7)	1.05
0.55	-0.9925(59)	15.4(7)	1.20
0.59	-0.9868(73)	17.6(9)	1.24
0.62	-0.9834(88)	19.8(11)	1.30
0.66	-0.9814(94)	22.0(11)	1.51
0.69	-0.9779(91)	23.5(11)	1.48

$A + Bx + Cx^2 : 10-> 32$				
c	A	B	C	χ^2_R
0.38	-0.9963(52)	-5.9(19)	297(146)	1.75
0.42	-0.9961(64)	-0.8(23)	261(179)	1.50
0.45	-0.9954(74)	3.5(26)	231(197)	1.34
0.49	-0.9925(97)	7.2(33)	193(245)	1.37
0.52	-0.9911(106)	11.0(35)	123(262)	1.48
0.55	-0.9902(130)	14.9(43)	36(318)	1.80
0.59	-0.9856(127)	17.1(42)	48(320)	1.87
0.62	-0.9824(161)	19.9(53)	-21(398)	1.96
0.66	-0.9869(169)	24.1(54)	-160(409)	2.24
0.69	-0.9845(182)	25.9(62)	-173(466)	2.18

$A + Bx : 12-> 32$			
c	A	B	χ^2_R
0.38	-1.0007(37)	-3.2(7)	1.86
0.42	-1.0014(42)	1.7(8)	1.93
0.45	-0.9988(57)	5.6(10)	1.77
0.49	-0.9971(61)	9.2(10)	1.68
0.52	-0.9965(74)	12.9(13)	1.55
0.55	-0.9941(83)	16.0(14)	1.66
0.59	-0.9897(95)	18.3(18)	1.68
0.62	-0.9892(104)	21.0(20)	1.65
0.66	-0.9886(104)	23.6(18)	1.89
0.69	-0.9850(133)	25.0(23)	1.84

$A + Bx + Cx^2 : 12-> 32$				
c	A	B	C	χ^2_R
0.38	-0.9955(79)	-6.2(46)	331(519)	3.50
0.42	-0.9917(93)	-3.5(49)	566(548)	2.66
0.45	-0.9850(115)	-3.0(61)	968(669)	1.60
0.49	-0.9790(133)	-1.4(68)	1204(732)	0.75
0.52	-0.9734(184)	0.2(90)	1380(952)	0.32
0.55	-0.9642(186)	-1.2(93)	1879(983)	0.11
0.59	-0.9602(172)	0.1(96)	2048(1080)	0.04
0.62	-0.9492(248)	-1.1(127)	2403(1374)	0.09
0.66	-0.9461(300)	-1.1(149)	2720(1578)	0.02
0.69	-0.9420(281)	-1.3(150)	2967(1661)	0.06

$A + Bx : 16-> 32$			
c	A	B	χ^2_R
0.38	-0.9980(60)	-4.2(19)	3.20
0.42	-0.9940(78)	-0.9(25)	2.18
0.45	-0.9897(94)	2.2(27)	1.12
0.49	-0.9846(113)	4.6(33)	0.44
0.52	-0.9797(117)	6.9(36)	0.13
0.55	-0.9748(130)	8.7(40)	0.03
0.59	-0.9689(155)	10.3(46)	0.02
0.62	-0.9657(172)	12.3(56)	0.08
0.66	-0.9593(191)	12.7(58)	0.15
0.69	-0.9564(222)	13.8(65)	0.22

$Z_3/|m_0|^2$

$A + Bx : 8->32$			
c	A	B	χ^2_R
0.38	0.7873(263)	26.6(27)	1.07
0.42	0.8101(382)	18.0(37)	0.94
0.45	0.8407(441)	12.0(43)	0.80
0.49	0.8794(480)	7.9(46)	0.63
0.52	0.9091(507)	6.0(47)	0.56
0.55	0.9322(591)	5.4(54)	0.50
0.59	0.9520(770)	5.9(64)	0.46
0.62	0.9632(756)	8.1(69)	0.48
0.66	1.0030(897)	7.2(84)	0.41
0.69	1.0025(1008)	9.5(97)	0.39

$A + Bx + Cx^2 : 8->32$				
c	A	B	C	χ^2_R
0.38	0.7748(435)	30.6(102)	-231(545)	1.37
0.42	0.7708(603)	30.2(143)	-671(743)	0.96
0.45	0.7764(760)	30.7(190)	-990(991)	0.60
0.49	0.8034(788)	28.5(180)	-1060(926)	0.32
0.52	0.8075(932)	33.5(221)	-1414(1165)	0.20
0.55	0.8056(1100)	39.1(270)	-1687(1393)	0.18
0.59	0.8373(1278)	40.0(299)	-1818(1519)	0.16
0.62	0.8460(1481)	41.9(354)	-1854(1795)	0.21
0.66	0.8626(1504)	43.3(362)	-1823(1918)	0.22
0.69	0.8527(1531)	48.3(328)	-2003(1656)	0.28

$A + Bx : 10->32$			
c	A	B	χ^2_R
0.38	0.7686(348)	29.4(44)	1.29
0.42	0.7886(450)	22.8(59)	0.90
0.45	0.7934(609)	20.5(78)	0.57
0.49	0.8208(569)	17.7(75)	0.31
0.52	0.8434(711)	16.4(87)	0.26
0.55	0.8690(818)	15.7(109)	0.28
0.59	0.8831(990)	18.2(129)	0.28
0.62	0.9067(924)	16.9(127)	0.37
0.66	0.9407(1169)	17.2(150)	0.36
0.69	0.9663(1129)	16.2(152)	0.40

$A + Bx + Cx^2 : 10->32$				
c	A	B	C	χ^2_R
0.38	0.7974(625)	16.8(226)	1008(1810)	1.76
0.42	0.8025(776)	16.8(297)	462(2354)	1.33
0.45	0.8065(927)	18.9(363)	-54(2990)	0.84
0.49	0.7915(1149)	28.0(427)	-787(3368)	0.44
0.52	0.8031(1455)	35.3(518)	-1601(4005)	0.30
0.55	0.7844(1508)	48.8(536)	-2553(4181)	0.22
0.59	0.7901(1694)	60.4(612)	-3521(4795)	0.17
0.62	0.7408(1741)	84.9(599)	-5446(4758)	0.18
0.66	0.7964(1873)	71.5(666)	-4151(5276)	0.18
0.69	0.7430(2206)	103.6(827)	-6843(6550)	0.13

$A + Bx : 12->32$			
c	A	B	χ^2_R
0.38	0.7945(484)	21.9(89)	1.30
0.42	0.8128(481)	16.6(87)	1.13
0.45	0.8103(657)	16.7(126)	0.80
0.49	0.8329(744)	15.3(138)	0.47
0.52	0.8213(908)	20.7(175)	0.36
0.55	0.8443(1015)	22.2(189)	0.28
0.59	0.8367(1114)	30.5(210)	0.19
0.62	0.8306(1346)	36.3(241)	0.13
0.66	0.8719(1436)	33.7(271)	0.15
0.69	0.8550(1684)	41.9(298)	0.10

$A + Bx + Cx^2 : 12->32$				
c	A	B	C	χ^2_R
0.38	0.6923(768)	89.4(414)	-7764(4704)	0.55
0.42	0.6759(970)	96.6(495)	-8906(5328)	0.58
0.45	0.7335(1459)	68.5(732)	-5938(7898)	0.65
0.49	0.7365(1609)	71.1(821)	-6124(8970)	0.46
0.52	0.7666(1588)	56.5(892)	-3948(10176)	0.43
0.55	0.7841(2081)	56.7(1124)	-3715(12337)	0.42
0.59	0.8205(2534)	38.8(1266)	-1123(13908)	0.35
0.62	0.8214(2713)	48.9(1406)	-1707(15515)	0.26
0.66	0.8407(2905)	50.3(1529)	-1724(17315)	0.27
0.69	0.8461(3076)	47.4(1603)	-577(17465)	0.20

$A + Bx : 16- > 32$			
c	A	B	χ^2_R
0.38	0.7386(675)	46.7(221)	0.83
0.42	0.7280(724)	48.4(236)	0.83
0.45	0.7531(1067)	41.5(304)	0.76
0.49	0.7629(1287)	38.4(363)	0.56
0.52	0.7564(1540)	45.0(466)	0.46
0.55	0.8003(1534)	35.9(458)	0.46
0.59	0.8187(1829)	32.4(551)	0.39
0.62	0.8139(2214)	43.4(666)	0.27
0.66	0.8736(2500)	32.8(817)	0.29
0.69	0.8222(2396)	51.0(748)	0.20

Z_4/λ_0

$A + Bx : 8- > 32$			
c	A	B	χ^2_R
0.38	-1.0479(194)	-12.3(18)	1.85
0.42	-1.0660(238)	-8.2(22)	1.63
0.45	-1.0844(295)	-5.3(28)	1.30
0.49	-1.0936(388)	-4.0(34)	1.01
0.52	-1.1196(474)	-2.1(40)	0.84
0.55	-1.1465(474)	-0.7(40)	0.72
0.59	-1.1609(558)	0.0(45)	0.63
0.62	-1.1930(600)	1.6(48)	0.61
0.66	-1.2151(641)	2.0(56)	0.53
0.69	-1.2254(654)	2.4(60)	0.50

$A + Bx + Cx^2 : 8- > 32$				
c	A	B	C	χ^2_R
0.38	-0.9883(384)	-27.9(85)	805(442)	1.32
0.42	-0.9842(430)	-29.2(92)	1042(450)	0.97
0.45	-0.9957(664)	-28.7(145)	1181(710)	0.62
0.49	-0.9960(715)	-30.6(158)	1368(774)	0.33
0.52	-1.0042(796)	-32.0(183)	1490(911)	0.24
0.55	-1.0161(908)	-32.5(204)	1573(1010)	0.21
0.59	-1.0340(961)	-33.4(227)	1670(1157)	0.20
0.62	-1.0814(1184)	-25.8(256)	1374(1239)	0.27
0.66	-1.0575(1359)	-35.6(296)	1818(1449)	0.25
0.69	-1.0539(1607)	-37.1(331)	1853(1575)	0.30

$A + Bx : 10- > 32$			
c	A	B	χ^2_R
0.38	-1.0097(318)	-18.2(40)	1.24
0.42	-1.0093(372)	-16.9(49)	0.96
0.45	-1.0233(463)	-14.6(59)	0.65
0.49	-1.0412(540)	-12.7(71)	0.40
0.52	-1.0663(557)	-10.8(67)	0.36
0.55	-1.0718(702)	-12.2(90)	0.37
0.59	-1.0965(773)	-10.0(97)	0.36
0.62	-1.1146(871)	-9.6(113)	0.43
0.66	-1.1500(944)	-7.7(113)	0.42
0.69	-1.1598(1122)	-7.8(144)	0.46

$A + Bx + Cx^2 : 10- > 32$				
c	A	B	C	χ^2_R
0.38	-1.0145(480)	-15.8(160)	-193(1278)	1.88
0.42	-0.9929(683)	-23.1(236)	479(1781)	1.41
0.45	-0.9957(817)	-25.0(281)	775(2149)	0.91
0.49	-0.9997(985)	-26.9(331)	1018(2471)	0.50
0.52	-1.0080(1269)	-34.9(423)	1890(3182)	0.37
0.55	-0.9729(1305)	-46.3(449)	2588(3432)	0.31
0.59	-1.0058(1430)	-48.3(514)	3051(3962)	0.19
0.62	-0.9723(1682)	-65.7(540)	4432(4049)	0.17
0.66	-0.9779(2016)	-69.8(653)	4747(4800)	0.17
0.69	-0.9785(1837)	-71.9(610)	4787(4617)	0.14

$A + Bx : 12-> 32$			
c	A	B	χ^2_R
0.38	-1.0238(417)	-14.6(73)	1.75
0.42	-1.0150(444)	-15.2(82)	1.41
0.45	-1.0281(604)	-14.3(105)	0.96
0.49	-1.0372(725)	-15.1(127)	0.60
0.52	-1.0402(716)	-16.5(138)	0.45
0.55	-1.0312(1099)	-21.7(196)	0.34
0.59	-1.0483(1179)	-21.4(219)	0.23
0.62	-1.0511(1049)	-24.8(176)	0.17
0.66	-1.0525(1208)	-28.3(207)	0.17
0.69	-1.0266(1583)	-34.0(268)	0.15

$A + Bx + Cx^2 : 12-> 32$				
c	A	B	C	χ^2_R
0.38	-0.9150(685)	-80.7(375)	7359(4228)	0.74
0.42	-0.8840(1015)	-92.9(548)	8615(6091)	0.75
0.45	-0.8921(1177)	-89.1(606)	8109(6602)	0.71
0.49	-0.9365(1300)	-67.6(656)	5812(7241)	0.55
0.52	-0.9555(1740)	-60.8(901)	4749(9813)	0.46
0.55	-0.9513(1877)	-69.0(1021)	5437(11476)	0.47
0.59	-1.0099(2176)	-41.9(1070)	2182(11447)	0.39
0.62	-0.9888(2682)	-66.7(1307)	4740(13833)	0.36
0.66	-0.9920(2587)	-70.5(1276)	5288(13917)	0.38
0.69	-0.9869(2998)	-72.9(1449)	4936(15434)	0.24

$A + Bx : 16-> 32$			
c	A	B	χ^2_R
0.38	-0.9549(618)	-41.9(205)	1.11
0.42	-0.9588(784)	-39.3(248)	1.02
0.45	-0.9469(977)	-43.7(270)	0.91
0.49	-0.9798(1031)	-35.4(317)	0.67
0.52	-0.9751(1292)	-40.5(376)	0.56
0.55	-1.0107(1565)	-31.2(459)	0.54
0.59	-0.9992(1655)	-39.4(504)	0.43
0.62	-1.0612(1649)	-20.7(501)	0.36
0.66	-1.0094(2011)	-44.5(605)	0.34
0.69	-1.0203(2461)	-44.2(739)	0.25

C.0.2 Results: $\rho = 5$

Z_1

$A + Bx : 16-> 32$			
c	A	B	χ^2_R
0.38	2.0068(61)	54.5(20)	1.89
0.42	2.0088(65)	43.1(21)	1.77
0.45	2.0081(78)	35.5(25)	1.52
0.49	2.0062(88)	30.2(28)	1.20
0.52	2.0044(100)	26.2(33)	1.00
0.55	1.9996(104)	24.4(34)	0.85
0.59	2.0008(118)	21.5(37)	0.72
0.62	2.0003(137)	19.2(42)	0.66
0.66	1.9984(135)	18.3(43)	0.60
0.69	1.9977(152)	17.0(49)	0.55

$A + Bx + Cx^2 : 16-> 32$				
c	A	B	C	χ^2_R
0.38	1.9779(160)	80.5(131)	-4895(2365)	0.02
0.42	1.9733(202)	74.5(172)	-5823(3143)	0.07
0.45	1.9728(210)	66.3(176)	-5740(3292)	0.11
0.49	1.9725(229)	60.2(197)	-5699(3686)	0.22
0.52	1.9677(298)	58.4(244)	-5972(4463)	0.35
0.55	1.9608(323)	60.0(267)	-6749(4931)	0.41
0.59	1.9666(372)	51.6(296)	-5570(5379)	0.47
0.62	1.9627(492)	52.1(403)	-6068(7251)	0.48
0.66	1.9688(422)	44.6(340)	-4889(6179)	0.54
0.69	1.9669(568)	44.9(466)	-5176(8504)	0.57

190

$A + Bx : 18- > 32$			
c	A	B	χ^2_R
0.38	2.0000(76)	58.6(31)	0.87
0.42	1.9980(99)	48.6(40)	0.40
0.45	1.9969(111)	41.3(46)	0.21
0.49	1.9939(112)	36.3(47)	0.07
0.52	1.9913(136)	32.9(54)	0.01
0.55	1.9898(133)	29.9(57)	0.01
0.59	1.9894(161)	27.4(65)	0.04
0.62	1.9884(191)	25.2(78)	0.13
0.66	1.9823(235)	26.4(95)	0.13
0.69	1.9861(223)	24.0(98)	0.16

Z_2

$A + Bx : 16- > 32$			
c	A	B	χ^2_R
0.38	-1.0157(50)	0.5(16)	2.21
0.42	-1.0180(58)	6.0(18)	2.00
0.45	-1.0185(65)	10.4(20)	1.63
0.49	-1.0177(78)	14.2(24)	1.23
0.52	-1.0151(87)	16.8(29)	1.00
0.55	-1.0185(105)	21.2(33)	0.91
0.59	-1.0144(128)	22.6(41)	0.92
0.62	-1.0138(124)	25.2(39)	0.82
0.66	-1.0119(140)	26.3(44)	0.80
0.69	-1.0161(146)	29.2(47)	0.64

$A + Bx + Cx^2 : 16- > 32$				
c	A	B	C	χ^2_R
0.38	-0.9954(130)	-18.6(105)	3652(1918)	0.09
0.42	-0.9895(155)	-19.4(126)	4744(2308)	0.14
0.45	-0.9859(173)	-18.5(136)	5449(2486)	0.14
0.49	-0.9867(226)	-13.0(192)	5095(3553)	0.11
0.52	-0.9841(253)	-11.2(216)	5282(4132)	0.10
0.55	-0.9737(315)	-16.2(258)	6793(4754)	0.06
0.59	-0.9668(318)	-19.1(269)	7776(5013)	0.06
0.62	-0.9618(442)	-21.3(359)	8780(6582)	0.09
0.66	-0.9663(436)	-15.4(348)	7913(6313)	0.04
0.69	-0.9603(535)	-19.1(443)	9052(8136)	0.02

$A + Bx : 18- > 32$			
c	A	B	χ^2_R
0.38	-1.0102(54)	-2.8(22)	0.51
0.42	-1.0093(77)	1.4(32)	0.29
0.45	-1.0088(78)	5.5(33)	0.23
0.49	-1.0075(94)	9.1(37)	0.12
0.52	-1.0050(100)	11.6(41)	0.10
0.55	-1.0034(154)	14.2(61)	0.13
0.59	-1.0015(155)	16.2(60)	0.12
0.62	-0.9990(181)	18.0(72)	0.24
0.66	-1.0008(234)	20.0(90)	0.17
0.69	-1.0009(214)	21.8(89)	0.17

$Z_3/|m_0|^2$

$A + Bx : 16-> 32$			
c	A	B	χ^2_R
0.38	0.6576(901)	36.3(313)	1.80
0.42	0.6139(1050)	46.2(354)	1.46
0.45	0.5654(1457)	63.7(515)	1.26
0.49	0.5291(1556)	79.7(581)	0.96
0.52	0.4871(2004)	103.1(703)	0.76
0.55	0.4919(2111)	106.1(766)	0.64
0.59	0.5330(2284)	102.7(798)	0.48
0.62	0.5164(3017)	121.1(1038)	0.38
0.66	0.5100(2771)	132.4(1002)	0.32
0.69	0.4375(3265)	160.9(1108)	0.31

$A + Bx + Cx^2 : 16-> 32$				
c	A	B	C	χ^2_R
0.38	1.0132(2401)	-304.8(1901)	67630(35062)	0.68
0.42	1.0613(2665)	-383.8(2293)	85904(44424)	0.13
0.45	1.0942(3827)	-422.1(3321)	94561(63499)	0.04
0.49	1.0736(4049)	-430.1(3523)	98404(68368)	0.09
0.52	1.1110(6180)	-462.8(5185)	108458(98729)	0.19
0.55	1.1861(6704)	-516.6(5838)	118601(111345)	0.25
0.59	1.1095(8214)	-445.5(7100)	111383(134804)	0.34
0.62	1.0580(8899)	-362.9(7838)	91866(147559)	0.31
0.66	1.0049(8917)	-312.5(7668)	85061(146867)	0.31
0.69	0.9052(10656)	-222.3(9562)	68733(185154)	0.34

$A + Bx : 18-> 32$			
c	A	B	χ^2_R
0.38	0.7313(1107)	-3.2(469)	2.37
0.42	0.7049(1173)	-6.3(473)	1.11
0.45	0.6869(1511)	-11.0(659)	0.64
0.49	0.6829(1754)	-4.9(733)	0.24
0.52	0.7162(2476)	-19.9(1134)	0.06
0.55	0.7638(2977)	-30.9(1306)	0.05
0.59	0.6390(3305)	35.7(1406)	0.05
0.62	0.7004(3683)	18.0(1612)	0.02
0.66	0.6653(4231)	41.6(1828)	0.06
0.69	0.7235(4749)	26.8(2149)	0.07

Z_4/λ_0

$A + Bx : 16->32$			
c	A	B	χ^2_R
0.38	-0.8870(598)	-41.7(192)	1.67
0.42	-0.8453(861)	-51.0(270)	1.29
0.45	-0.8085(847)	-64.6(284)	1.05
0.49	-0.8181(1140)	-64.9(390)	0.81
0.52	-0.7756(1469)	-83.2(479)	0.59
0.55	-0.7767(1691)	-92.5(551)	0.52
0.59	-0.7756(1680)	-92.3(578)	0.39
0.62	-0.7776(2054)	-101.2(658)	0.30
0.66	-0.7797(2232)	-107.5(719)	0.26
0.69	-0.7880(2806)	-109.3(918)	0.23

$A + Bx + Cx^2 : 16->32$				
c	A	B	C	χ^2_R
0.38	-1.1501(1983)	199.0(1717)	-45938(33066)	1.09
0.42	-1.1668(2337)	236.3(1980)	-55601(37484)	0.27
0.45	-1.1790(2610)	266.4(2188)	-63190(41231)	0.05
0.49	-1.1768(3484)	281.4(3044)	-68678(57874)	0.03
0.52	-1.2316(4365)	320.9(3692)	-76599(69124)	0.08
0.55	-1.1934(4876)	291.1(4126)	-72494(77195)	0.14
0.59	-1.1481(5038)	237.8(4385)	-63033(83545)	0.17
0.62	-1.1426(5164)	205.8(4427)	-55074(84515)	0.26
0.66	-1.1471(6543)	224.2(5506)	-62839(102644)	0.27
0.69	-1.0535(7305)	128.7(6241)	-44541(117145)	0.26

$A + Bx : 18->32$			
c	A	B	χ^2_R
0.38	-0.9414(934)	-14.5(395)	2.52
0.42	-0.9174(1081)	-11.6(437)	1.29
0.45	-0.8647(1188)	-33.0(505)	0.73
0.49	-0.9041(1421)	-18.4(609)	0.28
0.52	-0.9202(1843)	-12.9(774)	0.08
0.55	-0.8857(2318)	-26.2(953)	0.03
0.59	-0.9446(2490)	-12.9(1058)	0.01
0.62	-0.8983(2435)	-37.3(1063)	0.03
0.66	-0.9084(2836)	-41.6(1270)	0.05
0.69	-0.8834(3687)	-49.1(1539)	0.08

C.0.3   Results: $\rho = 1.5$

Z_1

$A + Bx : 16->32$			
c	A	B	χ^2_R
0.38	2.0085(73)	55.6(22)	0.47
0.42	2.0118(94)	44.5(31)	0.26
0.45	2.0140(106)	36.5(31)	0.13
0.49	2.0200(106)	29.3(32)	0.05
0.52	2.0191(140)	25.5(40)	0.04
0.55	2.0221(143)	21.9(43)	0.02
0.59	2.0239(175)	18.7(51)	0.05
0.62	2.0227(204)	17.7(58)	0.04
0.66	2.0212(208)	16.5(64)	0.07
0.69	2.0230(203)	14.4(60)	0.04

Z_2

$A + Bx : 16->32$			
c	A	B	χ^2_R
0.38	-1.0111(60)	-1.8(17)	0.77
0.42	-1.0120(73)	2.5(20)	0.75
0.45	-1.0144(90)	6.6(27)	0.72
0.49	-1.0148(97)	9.9(29)	0.64
0.52	-1.0161(132)	12.7(38)	0.87
0.55	-1.0154(145)	15.1(43)	0.79
0.59	-1.0124(164)	16.1(47)	0.79
0.62	-1.0140(159)	18.2(47)	0.89
0.66	-1.0151(199)	20.5(59)	0.81
0.69	-1.0106(265)	20.2(74)	0.80

$Z_3/|m_0|^2$

$A + Bx : 16->32$			
c	A	B	χ^2_R
0.38	1.1464(7292)	-495.3(2167)	3.32
0.42	1.0970(8506)	-492.6(2385)	3.98
0.45	0.3874(12223)	-324.2(3687)	4.33
0.49	0.4162(15682)	-337.7(4629)	3.83
0.52	-0.3203(15380)	-124.1(4552)	3.67
0.55	-0.7292(19374)	49.3(5505)	2.82
0.59	-1.7061(23725)	341.1(7032)	2.24
0.62	-2.1576(24020)	499.0(7064)	1.82
0.66	-2.8956(28018)	726.0(8286)	1.36
0.69	-2.8520(24640)	783.3(7300)	1.09

Z_4/λ_0

$A + Bx : 16->32$			
c	A	B	χ^2_R
0.38	-0.7884(2530)	-96.4(741)	3.43
0.42	-0.6784(2761)	-119.8(840)	3.43
0.45	-0.5415(3570)	-163.0(1086)	3.22
0.49	-0.4309(4458)	-188.8(1327)	2.61
0.52	-0.1779(3912)	-272.2(1203)	2.14
0.55	0.0552(5495)	-331.5(1693)	1.42
0.59	0.3009(6061)	-420.6(1815)	0.99
0.62	0.3389(6228)	-442.9(2033)	0.62
0.66	0.6339(8993)	-546.0(2678)	0.43
0.69	0.6070(9498)	-540.4(2648)	0.24

Bibliography

[1] P. A. M. Dirac. *The Quantum Theory of the Emission and Absorption of Radiation*. Springer Netherlands, Dordrecht, 1988.

[2] E.C.G. Stueckelberg and A. Petermann. The normalization group in quantum theory. *Helvetica Physica Acta (Switzerland)*, Vol: 24, No. 4, Sep 1951.

[3] M. Gell-Mann and F. E. Low. Quantum electrodynamics at small distances. *Phys. Rev.*, 95:1300–1312, Sep 1954.

[4] Curtis G. Callan. Broken scale invariance in scalar field theory. *Phys. Rev. D*, 2:1541–1547, Oct 1970.

[5] K. Symanzik. Small distance behaviour in field theory and power counting. *Communications in Mathematical Physics*, 18(3):227–246, 1970.

[6] David J. Gross and Frank Wilczek. Asymptotically free gauge theories. i. *Phys. Rev. D*, 8:3633–3652, Nov 1973.

[7] Kenneth G. Wilson. Renormalization group and critical phenomena. i. renormalization group and the kadanoff scaling picture. *Phys. Rev. B*, 4:3174–3183, Nov 1971.

[8] Kenneth G. Wilson. Renormalization group and critical phenomena. ii. phase-space cell analysis of critical behavior. *Phys. Rev. B*, 4:3184–3205, Nov 1971.

[9] Kenneth G. Wilson and J. Kogut. The renormalization group and the ϵ expansion. *Physics Reports*, 12(2):75 – 199, 1974.

[10] Kenneth G. Wilson. The renormalization group: Critical phenomena and the kondo problem. *Rev. Mod. Phys.*, 47:773–840, Oct 1975.

[11] Kenneth G. Wilson. Confinement of quarks. *Phys. Rev. D*, 10:2445–2459, Oct 1974.

[12] M. Lüscher and P. Weisz. Scaling laws and triviality bounds in the lattice ϕ^4 theory. one-component model in the symmetric phase. *Nuclear Physics B*, 290:25 – 60, 1987.

[13] M. Lüscher and P. Weisz. Scaling laws and triviality bounds in the lattice ϕ^4 theory. one component model in the phase with spontaneous symmetry breaking. *Nuclear Physics B*, 295(1):65 – 92, 1988.

[14] M. Lüscher and P. Weisz. Scaling laws and triviality bounds in the lattice ϕ^4 theory (iii). n-component model. *Nuclear Physics B*, 318(3):705 – 741, 1989.

[15] John C Collins. *Renormalization: an introduction to renormalization, the renormalization group, and the operator-product expansion*. Cambridge monographs on mathematical physics. Cambridge Univ. Press, Cambridge, 1984.

[16] Sidney Coleman and Roman Jackiw. Why dilatation generators do not generate dilatations. *Annals of Physics*, 67(2):552 – 598, 1971.

[17] Curtis G Callan, Sidney Coleman, and Roman Jackiw. A new improved energy-momentum tensor. *Annals of Physics*, 59(1):42 – 73, 1970.

[18] Kazuo Fujikawa. Energy-momentum tensor in quantum field theory. *Phys. Rev. D*, 23:2262–2275, May 1981.

[19] Sergio Caracciolo, Giuseppe Curci, Pietro Menotti, and Andrea Pelissetto. The energy-momentum tensor on the lattice: The scalar case. *Nuclear Physics B*, 309(4):612 – 624, 1988.

[20] Sergio Caracciolo, Giuseppe Curci, Pietro Menotti, and Andrea Pelissetto. The energy-momentum tensor for lattice gauge theories. *Annals of Physics*, 197(1):119 – 153, 1990.

[21] Martin Lüscher. Properties and uses of the wilson flow in lattice qcd. *Journal of High Energy Physics*, 2010(8):1–18, 2010.

[22] Martin Lüscher. Future applications of the Yang-Mills gradient flow in lattice QCD. *PoS*, LATTICE2013:016, 2014.

[23] Martin Lüscher and Peter Weisz. Perturbative analysis of the gradient flow in non-abelian gauge theories. *Journal of High Energy Physics*, 2011(2):1–23, 2011.

[24] Martin Lüscher. Chiral symmetry and the Yang–Mills gradient flow. *JHEP*, 04:123, 2013.

[25] Kazuo Fujikawa. The gradient flow in $\lambda\phi^4$ theory. *JHEP*, 03:021, 2016.

[26] Sinya Aoki, Janos Balog, Tetsuya Onogi, and Peter Weisz. Flow equation for the large N scalar model and induced geometries. 2016(8):083B04, 2016.

[27] Martin Lüscher. Step scaling and the Yang-Mills gradient flow. *JHEP*, 06:105, 2014.

[28] Alberto Ramos. The gradient flow running coupling with twisted boundary conditions. *JHEP*, 11:101, 2014.

[29] Zoltan Fodor, Kieran Holland, Julius Kuti, Daniel Nogradi, and Chik Him Wong. The yang-mills gradient flow in finite volume. *Journal of High Energy Physics*, 2012(11):1–17, 2012.

[30] Patrick Fritzsch and Alberto Ramos. The gradient flow coupling in the Schrödinger Functional. *JHEP*, 10:008, 2013.

[31] Hiroshi Suzuki. Energymomentum tensor from the YangMills gradient flow. *PTEP*, 2013:083B03, 2013. [Erratum: PTEP2015,079201(2015)].

[32] Masakiyo Kitazawa, Masayuki Asakawa, Tetsuo Hatsuda, Takumi Iritani, Etsuko Itou, and Hiroshi Suzuki. Measurement of thermodynamics using gradient flow. *PoS*, LATTICE2014:022, 2014.

[33] Masayuki Asakawa, Tetsuo Hatsuda, Etsuko Itou, Masakiyo Kitazawa, and Hiroshi Suzuki. Thermodynamics of $SU(3)$ gauge theory from gradient flow on the lattice. *Phys. Rev. D*, 90:011501, Jul 2014.

[34] Luigi Del Debbio, Agostino Patella, and Antonio Rago. Space-time symmetries and the Yang-Mills gradient flow. *JHEP*, 11:212, 2013.

[35] Hiroki Makino and Hiroshi Suzuki. Lattice energymomentum tensor from the YangMills gradient flowinclusion of fermion fields. *Progress of Theoretical and Experimental Physics*, 2014(6), 2014.

[36] Hiroshi Suzuki. Background field method in the gradient flow. *PoS*, LATTICE2015:304, 2016.

[37] M. Pepe and Leonardo Giusti. Non-perturbative renormalization of the energy-momentum tensor in SU(3) Yang-Mills theory. *PoS*, LATTICE2014:322, 2014.

[38] Leonardo Giusti and Michele Pepe. Energy-momentum tensor on the lattice: Nonperturbative renormalization in Yang-Mills theory. *Phys. Rev. D*, 91:114504, Jun 2015.

[39] Timothy J. Hollowood. *Renormalization Group and Fixed Points In Quantum Field Theory*. Springer, London, 2013.

[40] David Skinner. Quantum field theory ii: lecture notes. 2015.

[41] Istvn Montvay and Gernot Mnster. *Quantum fields on a lattice*. Cambridge monographs on mathematical physics. Cambridge Univ. Press, Cambridge, 1994.

[42] J. Smit. Introduction to quantum fields on a lattice: A robust mate. *Cambridge Lect. Notes Phys.*, 15:1–271, 2002.

[43] K. Symanzik. CUTOFF DEPENDENCE IN LATTICE phi^4 in four-dimensions THEORY. In *Cargese Summer Inst.1979:0313*, page 0313, 1979.

[44] Stephen L. Adler. Axial-Vector Vertex in Spinor Electrodynamics. *Phys. Rev.*, 177:2426–2438, Jan 1969.

[45] J. S. Bell and R. Jackiw. A PCAC puzzle: $\pi_0 \to \gamma\gamma$ in the σ model. *Nuovo Cim.*, A60:47–61, 1969.

[46] K. Fujikawa and H. Suzuki. *Path integrals and quantum anomalies*. 2004.

[47] F.J. Belinfante. On the current and the density of the electric charge, the energy, the linear momentum and the angular momentum of arbitrary fields. *Physica*, 7(5):449 – 474, 1940.

[48] Klaus Hepp. Proof of the bogoliubov-parasiuk theorem on renormalization. *Communications in Mathematical Physics*, 2(1):301–326, 1966.

[49] Sergio Caracciolo, Pietro Menotti, and Andrea Pelissetto. Analytic determination at one loop of the energy momentum tensor for lattice QCD. *Phys. Lett.*, B260:401–406, 1991.

[50] Sergio Caracciolo, Pietro Menotti, and Andrea Pelissetto. One loop analytic computation of the energy momentum tensor for lattice gauge theories. *Nucl. Phys.*, B375:195–239, 1992.

[51] K. Symanzik. Continuum Limit and Improved Action in Lattice Theories. 1. Principles and phi^4 Theory. *Nucl. Phys.*, B226:187–204, 1983.

[52] Bernd A. Berg. The Transformations of nonAbelian gauge fields under translations. 2000.

[53] Poul H. Damgaard and Helmuth Hffel. Stochastic quantization. *Physics Reports*, 152(5):227 – 398, 1987.

[54] Jean Zinn-Justin and Daniel Zwanziger. Ward Identities for the Stochastic Quantization of Gauge Fields. *Nucl. Phys.*, B295:297–331, 1988.

[55] Mark Srednicki. *Quantum Field Theory.* Cambridge Univ. Press, Cambridge, 2007.

[56] L.D. Faddeev and V.N. Popov. Feynman diagrams for the yang-mills field. *Physics Letters B*, 25(1):29 – 30, 1967.

[57] J. Zinn-Justin. Renormalization and stochastic quantization. *Nuclear Physics B*, 275(1):135 – 159, 1986.

[58] C Becchi, A Rouet, and R Stora. Renormalization of gauge theories. *Annals of Physics*, 98(2):287 – 321, 1976.

[59] Martin Lüscher. Trivializing maps, the Wilson flow and the HMC algorithm. *Commun. Math. Phys.*, 293:899–919, 2010.

[60] Martin Lüscher. Step scaling and the Yang-Mills gradient flow. *JHEP*, 06:105, 2014.

[61] H. J. Rothe. AN INTRODUCTION TO LATTICE GAUGE THEORIES. 1987.

[62] Simon Duane, A.D. Kennedy, Brian J. Pendleton, and Duncan Roweth. Hybrid monte carlo. *Physics Letters B*, 195(2):216 – 222, 1987.

[63] Richard C. Brower and Pablo Tamayo. Embedded dynamics for φ^4 theory. *Phys. Rev. Lett.*, 62:1087–1090, Mar 1989.

[64] M. Hasenbusch, K. Pinn, and S. Vinti. Critical exponents of the three-dimensional ising universality class from finite-size scaling with standard and improved actions. *Phys. Rev. B*, 59:11471–11483, May 1999.

[65] M. E. J. Newman and G. T. Barkema. *Monte Carlo methods in statistical physics.* Clarendon Press, Oxford, 1999.

[66] Martin Hasenbusch. Finite size scaling study of lattice models in the three-dimensional ising universality class. *Phys. Rev. B*, 82:174433, Nov 2010.

[67] Maurizio Piai. Lectures on walking technicolor, holography and gauge/gravity dualities. *Adv. High Energy Phys.*, 2010:464302, 2010.